

**Illinois Water Resources Center
Annual Technical Report
FY 2017**

Introduction

Illinois water resources are diverse, ranging from Lake Michigan to the Mississippi River to tile drains in agriculture fields. As a result, the Illinois Water Resources Center's outreach and research programs cover a lot of topics, and 2017 was no different. We continued to support the implementation of the Illinois Nutrient Loss Reduction Strategy, working with federal, state, and local governments entities, nonprofits, farmers, industry members, researchers, wastewater treatment professionals, and concerned citizens to decrease the amount of nutrient pollution leaving our state. Through our Annual Small Grants program, we also supported research on green stormwater solutions, road salt contamination of groundwater, nutrient dynamics in restored wetlands, temporal patterns in nutrient uptake in riparian zones, and the ability of wetland mitigation banks to compensate for plant species lost during natural wetland impacts. While the breadth of projects is exciting, the diversity of students and faculty making use of these grants meant that first-generation college students at Northwestern University were trained in research and a new faculty member at the University of Illinois at Urbana-Champaign had an opportunity to begin building a research programs in Illinois. Grants through IWRC supported 33 undergraduate and graduate students during 2017, making this one of the most prolific years in the last decade.

Research Program Introduction

Illinois faces a gamut of water resources challenges, and our research projects reflected that this past year, ranging from the integration of green infrastructure in cities to patterns of nitrate uptake in agricultural buffer zones. Some highlights from this past year include:

- Ashlynn Stillwell and her team at the University of Illinois at Urbana-Champaign used a reliability-based framework to assess the placement of green infrastructure in urban settings. They specifically examined green infrastructure performance, and their models indicated rain gardens should be maintained every three years to prevent clogging. This project also generated future work in understanding where green infrastructure should be placed within existing sewersheds and how to add risk assessment into urban stormwater policy.
- In an effort to address nutrient pollution and water quality in agricultural areas in Illinois, Eric Peterson and his students at Illinois State University asked if nitrate concentrations in shallow groundwater in riparian zones shifted temporally. The project used water samples collected over the course of a year from groundwater wells in a restored prairie riparian zone that received drainage from fertilized agriculture fields. Results indicate that there were changes in nitrate concentrations over a 24-hour period as well as seasonal variation, and much of this pattern is driven by vegetative uptake.
- A cross-disciplinary team from Northwestern University used prairie remnants in the Chicago-area to look at the impacts of road salt on soil and water quality. Aaron Packman, William Miller, and their team of students built a network of sensors to begin developing a model of salt transport in an effort to decrease environmental impacts from road deicing. They found the highest concentrations of road salt chemicals in groundwater wells closest to highways and measured sodium concentrations nearly ten times background concentrations.
- Dr. Michael Lydy and a team of scientists from the U.S. Geological Survey and the U.S. Environmental Protection Agency examined the impacts of holding times when testing sediment toxicity. They found that in some instances contaminate concentrations and toxicity did change with time held, indicating that greater care should be taking in storing samples before testing.

Using bioavailability to assess pyrethroid insecticide toxicity in urban sediments

Basic Information

Title:	Using bioavailability to assess pyrethroid insecticide toxicity in urban sediments
Project Number:	2015IL298G
USGS Grant Number:	G15AS00019
Start Date:	9/1/2015
End Date:	8/31/2018
Funding Source:	104G
Congressional District:	IL012
Research Category:	Water Quality
Focus Categories:	Models, Sediments, Toxic Substances
Descriptors:	None
Principal Investigators:	Michael j Lydy, Amanda D Harwood, Kara Elizabeth Huff Hartz, Samuel A Nutile

Publications

There are no publications.

Progress Report (Year 2) for NIWR 104G:
“Using bioavailability to assess pyrethroid insecticide toxicity in urban sediments”
and
Final Report for Coordination Grant
“Are current sediment bioassays being biased by collecting and holding time procedures?”
Michael Lydy and Kara Huff Hartz
6/1/18

Problem and Research Objectives

The following report summarizes the activities conducted in the Lydy Research lab from 3/1/2017 to 2/28/2018 as part of the NIWR/USGS grant titled “Using bioavailability to assess pyrethroid insecticide toxicity in urban sediments.” The grant aims to study pyrethroid insecticide contamination in urban streams in the northeastern United States. The objective of year 2 of the project was to analyze the data from sediment subsamples collected as part of the Northeast Stream Quality Assessment (NESQA). In particular, the pyrethroid concentrations measured by single-point Tenax will be compared to the pyrethroid concentrations measured by exhaustive chemical extractions and the results from 10-d bioassays with *Hyaella azteca* using the sediments. The pyrethroid data will be summarized as a survey of urban sediments in the northeastern United States and the manuscript is currently in preparation. In addition, we received bioassay data from our collaborators at USGS-Columbia Environmental Research Center (CERC) fall 2017. These data will be related to our Tenax data in order to develop a model that relates bioaccessible pyrethroid concentrations to bioassay results. These data analyses will be completed and summarized in year 3.

A second objective of our 104G project was to resample NESQA sites in order to screen for the development of pyrethroid resistance in field-collected *H. azteca*. However, we ran into two complications which necessitated a delay in the field sampling campaign: 1) the timing of the receipt of samples for the sediment holding time study coincided with potential field campaign; and, 2) the data from invertebrate population surveys from NESQA, which were needed to select field sites, was only partially complete by the summer season. For these reasons, during year 2, we elected to focus on the completion of the sediment holding time project, which was began as part of the NIWR 104G and also supported by a coordination grant titled “Are current sediment bioassays being biased by collecting and holding time procedures?” Samples were received 31 May 2017 and the sample preparation and analysis and bioassays were completed May 2017 through September 2017. The preliminary data collected during year 1 of the 104G was combined with data collected as part of the coordination grant and summarized in a manuscript submitted to Environmental Pollution on 24 April 2018. The manuscript is currently under review.

Because the second objective of year two, i.e., to resample NESQA sites for pyrethroid-resistant *H. azteca*, was delayed to year 3, we instead prepared for a field campaign during year 2. The plan for sampling field-collected *H. azteca* in summer 2018 is discussed below. The final report for the coordination grant is the submitted manuscript, and it is attached as an appendix to this report.

Field Plan

Sites for resistant *H. azteca* assessment were selected by comparing the pyrethroid concentrations, the SIUC 10-d and CERC 28-d *H. azteca* bioassay results, and invertebrate population surveys measured during NESQA in 2016. In addition, historical data were obtained using two databases: National Water Information System (NWIS, <https://nwis.waterdata.usgs.gov/nwis>) and the Water Quality Portal (WQP <https://www.waterqualitydata.us>) to search for additional potential sites. The criteria for site selection were as follows: 1) detectable pyrethroids were found in the Tenax and ASE extracts; 2) at least some sediment toxicity was found as demonstrated by significantly reduced survival or biomass compared to reference sediments in either the 10-d or the 28-d *H. azteca* bioassays; and, 3) the presence of the

amphipods in the biosurveys. The first criteria was included because Weston et al. (2013) showed that development of pyrethroid resistance and pyrethroid exposure co-occur. The second criteria assures that the pyrethroid concentration in sediment would be high enough to affect non-resistant animals and potentially cause selection pressure. The third criteria selects for sites with habitats that are favorable for amphipod populations.

Of the 49 sites that were sampled for toxicity in the NESQA study area, 11 sites met each of the three criteria. Of the 11 sites, nine were selected in the New Jersey, New York, and Connecticut corridor due to proximity (Figure 1), and this sampling is scheduled for June 2018. One site in Albany, NY and one site Rochester, NY met the criteria but were eliminated, because access to additional sites in the same stream system would be limited. In addition to the nine NESQA sites, 19 locations upstream and downstream in the same rivers as the NESQA sites were identified for sampling (Figure 1). These locations were selected because the rivers had a history of pyrethroid detections (as shown by the NWIS or WQP) and the additional sites will provide more opportunities to search for *Hyaella*. *H. azteca* will be targeted by selecting sites with low-flow reaches containing vegetative mats. Amphipods will be sampled using 500 µm dip nets and sorted to remove other invertebrates and unwanted debris. After collection, *Hyaella* will be transferred to moderately hard water in a 1 L high density polyethylene bottle (Uline) which will be aerated for 30 minutes prior to being shipped on ice overnight to SIUC. Upon receipt, the water will be aerated, and the animals allowed to acclimate for 24 h prior to initiating the bioassay.

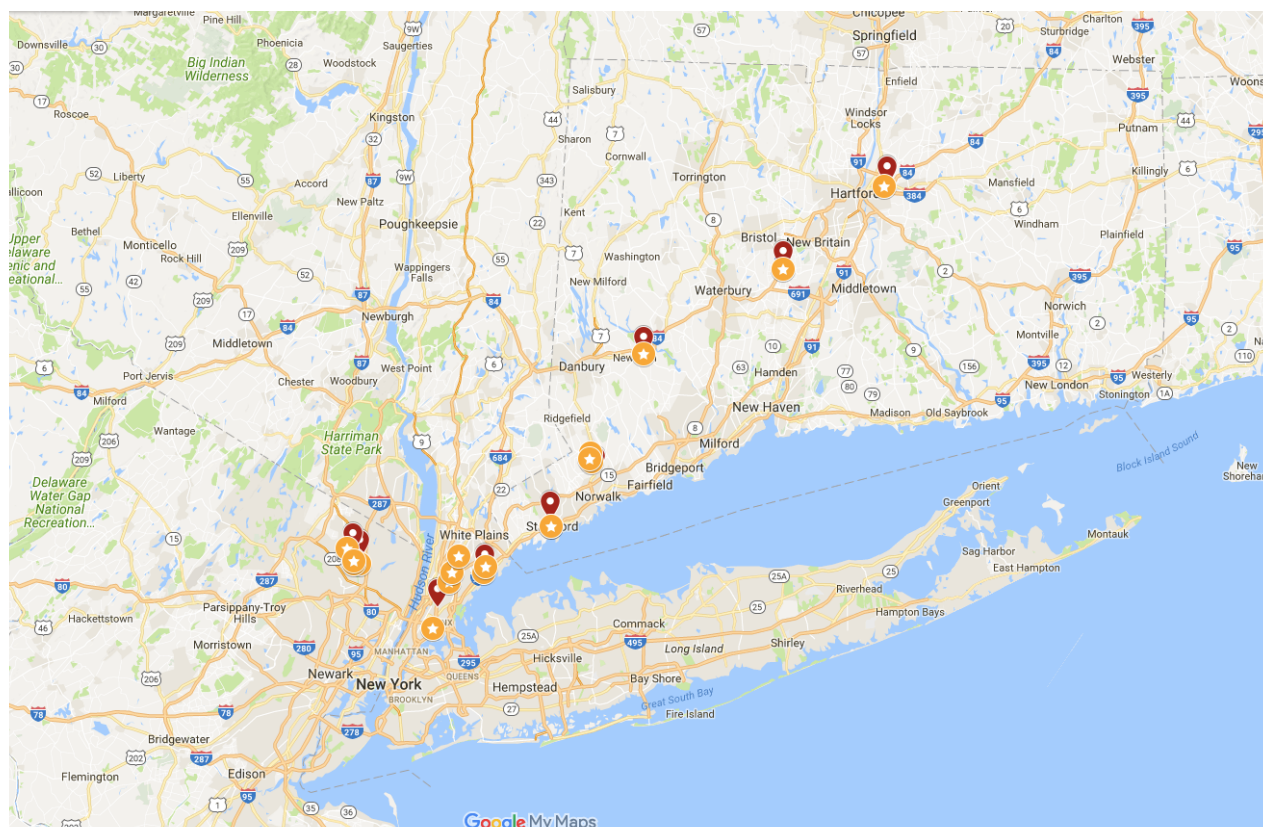


Figure 1: Proposed sites for *H. azteca* sampling June 2018. Red symbols are sites that were sampled as part of the NESQA sampling in 2016. Orange symbols show potential additional sample sites in the same river system.

The goal for the field campaign is to sample 20 sites for *H. azteca* and conduct 96-h single-point toxicity test using 80 animals at each site (40 exposed to 500 ng/L permethrin and 40 animals as a solvent control

to validate the bioassay). Animals that survive the single-point toxicity test will be counted and preserved in ethanol for genetic sequencing to confirm pesticide resistance. Voucher specimens will be retained and used for to confirm species identification. In addition, sediment samples will be collected to confirm presence of pyrethroids and their concentrations at the field sites to support the development of resistance.

Sediment analysis

Sediment will be collected at each site to determine the total pyrethroid concentration using methods previously developed in our laboratory (You et al., 2008; Nutile et al., 2016). Briefly, fine-grained surficial sediment (0-2 cm) will be collected at each site in at least three locations and composited in a stainless steel mixing bowl, sieved to 2 mm, and frozen until extraction. For extraction, 3 g of freeze-dried sediment and 5 g of silica gel will be placed in an accelerated solvent extraction cell along with filler sand and a glass fiber filter. The cell will be spiked with recovery surrogate compounds (50 ng of DBOFB and DCBP). Pyrethroids will be extracted from sediment by pressurized liquid extraction using a Dionex 200 Accelerated Solvent Extraction (ASE) using 1:1 dichloromethane:acetone at 100 °C and 1500 pounds per square inch using two heat-static cycles of 10 minutes each. After extraction, extracts will be cleaned up using Supelclean ENVI-Carb-II/PSA 300/600 mg solid-phase extraction cartridges and 1 g of sodium sulfate (previously dried at 400 °C for 4 h). Extracts will be solvent evaporated to a final volume of 1 mL, and acidified to 0.1 % using acetic acid.

Pyrethroid concentrations (tefluthrin, fenpropathrin, bifenthrin, cyhalothrin, permethrin, cyfluthrin, cypermethrin, esfenvalerate, and deltamethrin) in the sediment extracts will be quantified using an Agilent 7890A gas chromatography equipped with an Agilent 5975A inert XL mass spectrometer (Nutile et al., 2016). Pyrethroids and surrogate concentrations will be determined using internal standard calibration and normalized for dry weight organic carbon. Quality assurance/quality control samples will be analyzed along with the sediment extracts, and will include blank and spiked samples prepared with reference sediment as well as spiked field-collected sediment.

Toxicity testing

Single-point *H. azteca* 96-h toxicity bioassays will follow methods outlined by the USEPA (2000). Briefly, 500 mL (four replicates) of moderately hard water (Ivey et al., 2016), spiked at either 500 ng/L permethrin (concentration determined during Lab Preparation as discussed in the next section), or spiked with acetone (solvent control) will be distributed into 600 mL beakers. A total of 8-10 field-collected organisms will be added to each beaker with two pieces of stainless steel screen, and if possible, they will be sorted by size class (< 1 mm and > 1 mm) to reduce predation. The beakers will be housed in an incubator maintained at 23 °C (\pm 1 °C) and on an 16:8 light:dark cycle. After 96 hours, the test organisms will be assessed, and the number of surviving and affected organisms will be measured. Surviving organisms will be preserved in ethanol for genetic testing and verify species identification. Four sets of QA/QC samples will be added including, juvenile and adult resistant and non-resistant lab cultured *H. azteca*, which will act as negative and positive controls.

Nominal permethrin concentrations will be confirmed by gas chromatography/mass spectroscopy (GC/MS) using similar instrumental methods as sediment analysis. Exposure water will be composited across replicates (100 mL) at time zero and 96 h and salted liquid-liquid extraction will be conducted three times using 10 g NaCl and 50 mL of dichloromethane. The extracts will be combined, solvent change to hexane, dried using a sodium sulfate column, evaporated to 0.5 mL, and acidified to 0.2% using acetic acid. For each batch of samples, one lab blank and three matrix spike samples will be prepared and extracted to demonstrate that the procedures are free from contaminants and to demonstrate quantification accuracy and reproducibility. Also, each sample and blank will be spiked with 25 ng of surrogates (dibromooctafluorobiphenyl and decachlorobiphenyl in hexane) to demonstrate sample recovery.

Lab Preparation and Field Trials

To prepare for the assessment of pyrethroid resistance in field *H. azteca*, we conducted 96-h bioassays using our resistant and non-resistant lab cultures (Muggelberg et al., 2017; Heim et al., 2018). The purpose of this work was to train personnel and also to demonstrate that a single concentration could provide an assessment of pyrethroid resistance. Wild populations collected in California (Weston et al., 2013) had varied responses to pyrethroids, where 96-h bioassays conducted on 7-14 d old animals had cyfluthrin LC50 values (median lethal concentration) that were similar to lab cultures up to a factor of 550 greater. Furthermore, our lab resistant animals typically have permethrin LC50 values that range from 1144 to 1668 ng/L (Heim et al., 2018) and the non-resistant permethrin values that range from 31 to 45 ng/L. For this reason, we chose 500 ng/L permethrin for the single-point exposure concentration, because this value is high enough to be lethal to non-resistant animals, but low enough that the majority of individuals in pyrethroid-resistant field populations would survive the test. In addition, adult *H. azteca* were also tested along with juveniles to determine if the single-point test would be effective for mixed age class populations. Our lab culture of pyrethroid-resistant *H. azteca* had 100% survival (juvenile) and 83% survival (adults) when exposed to 500 ng/L permethrin (nominal) (Table 1). Non-resistant animals showed no survival at either age class, and all animals survived in the solvent control samples. These results suggest that a single-point toxicity bioassay at 500 ng/L can be used to screen for pyrethroid resistance in field animals.

Table 1: Percent survival of lab pyrethroid-resistant and non-resistant *Hyalomma azteca* after exposure to 500 ng/L permethrin (nominal) for 96 h. Average (\pm standard deviation) survival for four replicates, 40 animals exposed.

	% survival (\pm standard deviation) after 96 h	
	500 ng/L permethrin	acetone control (0 ng/L permethrin)
Resistant juvenile	100 \pm 0	98 \pm 5
Resistant adults	83 \pm 10	100 \pm 0
Non-resistant juvenile	0 \pm 0	100 \pm 0
Non-resistant adults	0 \pm 0	98 \pm 5

To prepare for the June field campaign, personnel will be trained during an additional field campaign scheduled for May 2018 in the Cincinnati, OH area. Sites were selected using Midwest Stream Quality Assessment conducted by USGS in 2013 (<https://webapps.usgs.gov/RSQA/#!/region/MSQA>). Additional locations along the same river systems were also selected (Figure 2). In addition to training personnel, the goal for this sampling campaign is to visit the 13 sites shown below and collect animals and sediment wherever *H. azteca* are present (up to 8 sites). Field *H. azteca* and sediment will be collected and processed as described above, and this will provide feedback for our methods that will be incorporated into the June field campaign. In addition, an added benefit of this sampling is the additional assessment for pyrethroid resistance in a different geographical region, which helps define the scope of development of resistance.

Expected Outcomes and Future Work

The success of the summer field campaign likely depends on the ability to find *Hyalomma* in sufficient numbers to conduct bioassays. If sufficient numbers are not available, composites of animals collected at different sites will be made within the same watershed. Recent work in California (Major et al., 2018) has shown that the development of pyrethroid resistance is correlated with rivers and streams with high expected pyrethroid concentrations, thus it's possible that urban streams in the northeastern US and Ohio with sediment pyrethroids also have the potential for the development of pyrethroid resistance in non-target aquatic amphipods. If pyrethroid resistant *H. azteca* are found and confirmed in the northeastern US and Ohio, this finding would suggest that the presence of pyrethroids in sediment drives this genetic change. In addition, this finding would suggest that *H. azteca* in northeastern US and Ohio streams are

vulnerable to potential fitness costs that may co-occur with the development of resistance (Heim et al., 2018).

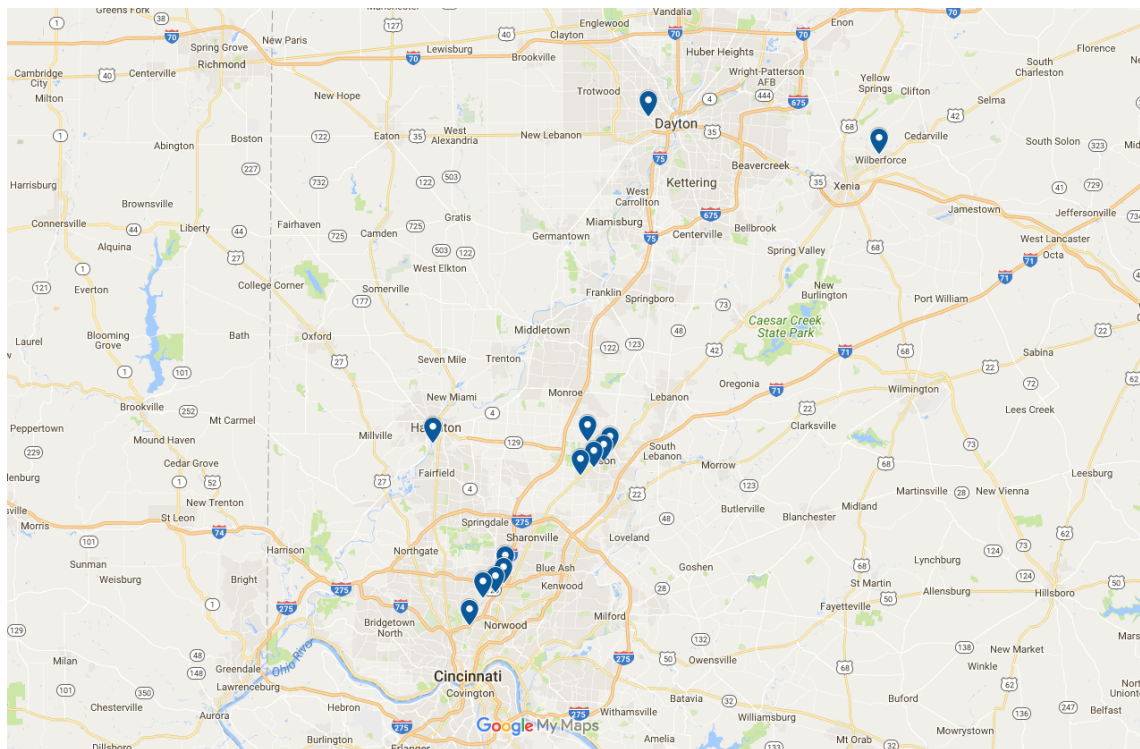


Figure 2: Proposed sites (blue symbols) in Ohio for *H. azteca* sampling in May 2018 training trip.

Students supported and education level (undergrad, MS, PhD)

The 104G project supported three undergraduate and two graduate students. Andrew Derby, Tristin Miller, and Haleigh Sever (undergraduate students) cultured *H. azteca* for bioassays and provided assistance when the experiments were conducted by preparing for experiments (sample receipt, logging, and sub-sampling, glassware and equipment preparation) and data collection. Courtney Y. Fung (MS student) prepared the same-day age *H. azteca* used in the toxicity bioassays, she served as the bioassay lead, bioassays and fTIEs, and provided assistance during sub-sampling. Corie Fulton (MS student) helped conduct the bioassays and provided instrumentation maintenance support. The coordination funding project supported one graduate student Federico Sinche (PhD student) who served as lead for the Tenax extractions and extract cleanup, and he helped conduct the bioassay experiments.

Publications

Data collection and analysis is in progress for this project. One publication has been submitted, and two publications are in progress with aim to submit by December 2018.

1) “Effect of Sample Holding Time on Pyrethroid- and Polychlorinated Biphenyl-Contaminated Sediment Assessments: Application of Single-Point Tenax Extractions” Kara E. Huff Hartz, Federico L. Sinche, Samuel A. Nutile, Courtney Y. Fung, Patrick W. Moran, Peter C. Van Metre, Lisa H. Nowell, Marc Mills, Michael J. Lydy, submitted to *Environmental Pollution*.

2) “Survey of Bioaccessible Pyrethroids and Sediment Toxicity in the Northeast United States Urban and Suburban Streams Target publication: *Environmental Science & Technology*”

3) “Development of Toxicity Tenax Model for Pyrethroid-Contaminated Sediments” Target publication: *Environmental Toxicology and Chemistry*

References Cited

Heim, J.R., Weston, D.P., Major, K., Poynton, H., Huff Hartz, K.E., Lydy, M.J. 2018. Are there fitness costs of pyrethroid resistance in the amphipod, *Hyalella azteca*? *Environmental Pollution* 235: 39-46 doi: 10.1016/j.envpol.2017.12.043.

Ivey CD, Ingersoll CG 2016. Influence of bromide on the performance of the amphipod *Hyalella azteca* in reconstituted waters. *Environ. Chem. Toxicol.* 35(10): 2425-2429.

Major, K. M., Weston, D.P., Lydy, M.J., Wellborn, G.A., Poynton, H.C. 2018. Unintentional exposure to terrestrial pesticides drives widespread and predictable evolution of resistance in freshwater crustaceans. *Evolutionary Applications* 11:748-762 doi: 10.1111/eva.12584.

Muggelberg, L.L., Huff Hartz, K.E., Nutile, S.A., Harwood, A.D., Heim, J.R., Derby, A.P., Weston, D.P., Lydy, M.J. 2017. Do pyrethroid-resistant *Hyalella azteca* have greater bioaccumulation potential compared to non-resistant populations? Implications for bioaccumulation in fish. *Environmental Pollution* 220: 375-382 doi: 10.1016/j.envpol.2016.09.073.

Nutile SA, Harwood AD, Sinche FL, Huff Hartz KE, Landrum PF, Lydy MJ. 2016. The robustness of single-point Tenax extractions of pyrethroids: Effects of the Tenax to organic carbon mass ratio on exposure estimates. *Chemosphere* 171: 308-317.

Weston, D.P., Poynton, H.C., Wellborn, G.A., Lydy, M.J., Blalock, B.J., Sepulveda, M.S., Colbourne, J.K. 2013. Multiple origins of pyrethroid insecticide resistance across the species complex of a nontarget aquatic crustacean, *Hyalella azteca*. *Proceedings of the National Academy of Sciences* 110(41):16532-16537 doi: 10.1073/pnas.1302023110.

[USEPA] US Environmental Protection Agency 2000. Methods for measuring the toxicity and bioaccumulation of sediment-associated contaminants with freshwater invertebrates. EPA600/R-99/064. Washington, DC.

You J, Weston DP, Lydy ML 2008. Quantification of pyrethroid insecticides at sub-ppb levels in sediment using matrix-dispersive accelerated solvent extraction with tandem SPE cleanup. In *Synthetic Pyrethroids* ACS Symposium Series, Vol. 991 Chapter 5, pp 87–113.

Identifying wetland inundation extent and patterns in Illinois

Basic Information

Title:	Identifying wetland inundation extent and patterns in Illinois
Project Number:	2016IL311B
Start Date:	3/1/2016
End Date:	2/28/2018
Funding Source:	104B
Congressional District:	IL-12
Research Category:	Biological Sciences
Focus Categories:	Wetlands, Floods, Ecology
Descriptors:	None
Principal Investigators:	Michael W Eichholz

Publications

There are no publications.

Identifying wetland inundation extent and patterns in Illinois

Category: Biological Sciences

Wetland inundation, habitat availability, wetland resources, water allocation

Michael W. Eichholz, Ph.D.
Avian/Wetland Ecologist, Associate Professor
Southern Illinois University Carbondale
Cooperative Wildlife Research Laboratory
eichholz@siu.edu
(618) 453-6951

Congressional District: IL-12

Problem

Continued increase in human population combined with increasing climatic variability associated with climate change will likely exacerbate future demands on our limited water supply throughout North America. Managing water for wildlife is one of several competing interests for limited water resources. Maximizing efficiency of water use for wildlife will require precise knowledge of wildlife habitat requirements and how those requirements vary throughout the annual cycle. For example, the hydrologic variation of wetlands makes them the most productive habitat in our ecosystem (Mitsch and Gosselink 2000, Batzer and Sharitz 2006). This same hydrologic variation, however, often limits the availability of resources provided by wetlands to wetland-dependent organisms in that wetlands may be dry when organisms are most dependent on them (Batzer and Sharitz 2006). This variation of inundation in wetlands makes accurately developing restoration goals based on the resource needs of wildlife populations difficult.

The National Wetlands Inventory provides an estimate of the total acreage of wetlands, but we are currently unable to estimate the acreage of wetlands that are inundated by water in a given time period. In the upper Midwest region, February-March, May-July and August-September are the most biologically important time periods for waterfowl, breeding wading birds and shorebirds, respectively. Estimates of inundation during those periods will allow for more precise allocation of water to provide habitat for those groups.

The location of inundation is also important if it is to provide resources to those groups. Directly monitoring inundation at all of the state's wetlands via ground survey is unfeasible on a seasonal or annual basis. Traditional remote sensing techniques such as aerial and optical imagery are unable to detect inundation in heavily vegetated areas. Classification error in the NWI can be exaggerated by vegetation cover type, with classifications of forested wetlands often having the highest error (Kudray and Gale 2000). Considering that Illinois has lost over 85% of its historical wetland area, with palustrine wetlands most heavily impacted (Dahl and Allord 1996), it is crucial to develop a method to estimate the availability of remaining wetlands to inundation-dependent species.

By developing models to estimate seasonal wetland inundation at the state level, this study could be used to develop more accurate wetland protection and restoration goals, allowing more efficient use of limited water resources for wildlife. Further, the estimates of wetland inundation obtained may be used as baselines to detect changes in the availability of water resources in wetlands in the future.

Project objectives and scope

This project aims to develop models to estimate wetland inundation for the entire state of Illinois. Two different approaches are being used to reach these ends.

Objective 1 will use ground surveys to estimate the seasonal changes in inundation and NWI error at random sites and then scale those values to the statewide NWI layers. This will provide an estimate of total wetland inundation in the state, specific to wetland type. Objective 1 constitutes a portion of a larger project which is funded by Federal Grant-in-Aid W-184-R-1-4 in

cooperation with IDNR. That project also includes quality assessments of the areas determined to be inundated. Habitat quality will be determined using several metrics including vegetation sampling and stress indicators, and will be analyzed by a Master's student at the University of Illinois under the advisement of Heath M. Hagy, Director of Illinois Natural History Survey's Forbes Biological Station.

Objective 2 will utilize satellite-based synthetic aperture radar (SAR) imagery to detect inundation on a larger scale and use the results from that analysis to model inundation patterns in the state. Unlike optical methods such as Landsat, L-band SAR can penetrate the forest canopy, and C-band SAR can penetrate emergent vegetation. The intensity of the radar return and polarity shifts in the radiation are used to estimate the presence of inundation (Lang et al. 2008). Imagery resolutions range from 3 meters to 100 meters. Funds to purchase imagery for preliminary analyses have been provided by the Upper Mississippi River and Great Lakes Joint Venture. Technical assistance with imagery processing and analysis will be provided by Donald Atwood, Senior Research Scientist at Michigan Tech Research Institute and former Senior Researcher at the Alaska Satellite Facility's SAR archives.

Methods

Sample sites were selected by stratified random sampling, using the 15 natural divisions of IL as the different strata with a Neyman allocation used to weight the number of samples per division. Lake Michigan was excluded due to logistical constraints. Survey sites were then assigned from the NWI using the reverse randomized quadrant-recursive raster (RRQRR) algorithm to create a spatially-balanced sampling pattern. The order in which each survey was conducted was randomized using the Mersenne Twister algorithm, but some exceptions were made to the sampling order due to logistical constraints such as private land access, boat availability, and ice.

Surveys are being conducted in three discrete seasons to coincide with the spring waterfowl migration, the summer marsh and wading bird nesting season and the fall shorebird migration (respectively): mid-February to mid-April, mid-April-June and August-September. Surveys will be conducted at each site once per season. During surveys, a team of 2-3 technicians will utilize GPS units to record the perimeter of all inundated areas that they encounter. Two teams will operate concurrently to maximize coverage: one from INHS and one from SIU. Geo-coded satellite images and field notes will be used with GPS tracks to create thematic maps of inundated and non-inundated areas within the surveyed areas. In 2015, ~90 sites of ~25 hectares each were surveyed in each of the three sampling seasons. We expect similar coverage in future years.

For objective 1, the thematic maps will be compared to NWI polygons using ArcGIS to determine what proportion of each NWI wetland type is inundated in each season and highlight any areas that have inundation, but are omitted in the NWI dataset. Determining these proportions specific to wetland type will allow us to scale the proportional inundation to the remainder of the dataset, providing an estimate of statewide wetland inundation, along with an uncertainty value.

For objective 2, two L-band SAR images taken on August 28th, 2015 were purchased. The images were taken at 6-m resolution and used the maximum number of polarizations (four). Downscaling and removal of polarizations will be conducted to simulate lower resolution/polarimetry options. Thematic maps from wetlands surveyed within one week of the imagery capture will be used to compare the accuracy for each imagery option. This will be weighed along with cost-per-unit-area of the coverage to determine the optimal imagery for further studies. Additional imagery will be purchased in May of 2017 to aid in the development of a classification model. A random forest classification model will be used along with C-band imagery, Landsat imagery, ancillary data, and a portion of the GIS inundation data to parse areas of inundation and non-inundation across the extent of the imagery. A separate subset of the GIS inundation data will be used to assess the accuracy of the classifier for each resolution level.

We were approved for a data grant from the Japanese Aerospace Exploration Agency (JAXA), providing us with up to 50 free images per year, for a total of three years, but they cannot be scheduled *a priori*. We have also been granted access to C-band SAR data through the European Space Agency. Our purchase imagery will be used to develop and evaluate the classification model. These additional free images will be used to increase the extent for estimates of inundation, providing substantial coverage of the state. Seasonal inundation extent and variability will be evaluated using geostatistical methods, allowing an estimation of the average proportion of available wetland area and variation across each of the seasons. The dissertation associated with the project is scheduled to be completed in 2018.

Expected results and significance

The inundation portion of the overall Federal project will support one dissertation, 3-4 peer-reviewed publications and several presentations at regional and national conferences. Presentations on preliminary analyses have already been given at multiple local and national conferences. Additional publications may be produced in synergy with the wetland quality study. Algorithms, models, satellite imagery, and survey data derived from the overall project will be made available to contributing agencies for further analysis and implementation.

Accurate estimates of wetland inundation will help refine estimates of available wetland habitat for WDA. Refined estimates should help correct for the potential overestimation of available habitat that arises when fluctuations in inundation are not considered. By evaluating multiple methods of estimating wetland inundation in Illinois, this project will provide a verified framework for future monitoring. Further, the methods and models developed in this study will potentially allow for wetland inundation to be estimated rapidly and at large spatial scales across the state.

Current status

Approximately 90 sites (~25 ha each) were sampled in 2015, and another 110 were sampled in 2016. Our recently completed spring 2017 samples covered 110 sites, and a similar number will be expected for repeat surveys in spring and autumn of this year. We are continuing to digitize the survey data into a GIS for analysis once field survey is completed. The first 50 free images have been downloaded from JAXA, spanning multiple seasons and years from 2014-2016. We will acquire additional images for that period and will also obtain images for 2017

with our remaining allotment of 100 images. The multi-season, multi-year dataset will allow analyses of patterns of wetland inundation in Illinois during that period.

Participating students

- John O'Connell – Doctoral student at SIU – dissertation on wetland inundation
- Abigail Blake-Bradshaw – Master's student at U of Illinois – thesis on wetland quality
- Micah Miller – Master's Zoology student at SIU – field assistant
- Harley Copple – Senior Zoology student at SIU – field/lab technician
- Shawn Caldwell – Senior Geography student at SIU – field/lab technician
- Travis Preston – Senior Geography student at SIU – field/lab assistant
- Hannah Judge – Junior undergraduate student at SIU – field and GIS assistant
- Alex Bell – Sophomore undergraduate student at SIU – field and GIS assistant
- Several recent graduates employed as field technicians (4 in 2015, 3 in 2016, 2 in 2017)

Literature citations

Batzer, D. P. and R. R. Sharitz 2006. Ecology of Fresh Water and Estuarine Wetlands. University of California Press. Berkeley, CA USA

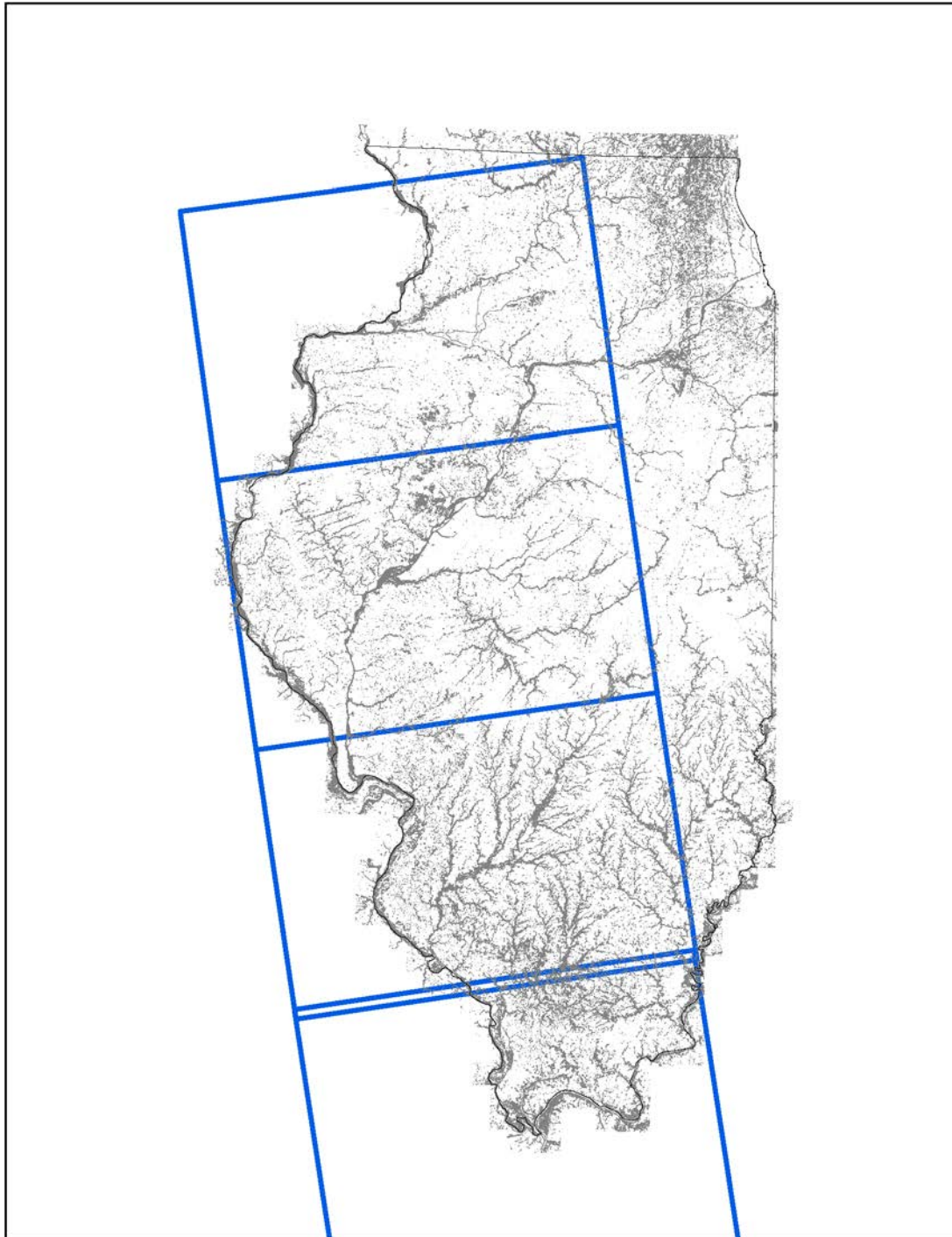
Dahl, T. E., and G. J. Allord. 1996. History of Wetlands in the Conterminous United States. Judy D. Fretwell, John S. Williams, and Phillip J. Redman.(eds.), National Water Summary on Wetland Resources, USGS Water-Supply Paper 2425: 19–26.

Kudray, G. M., and M. R. Gale. 2000. Evaluation of National Wetland Inventory maps in a heavily forested region in the Upper Great Lakes. *Wetlands* 20: 581-587.

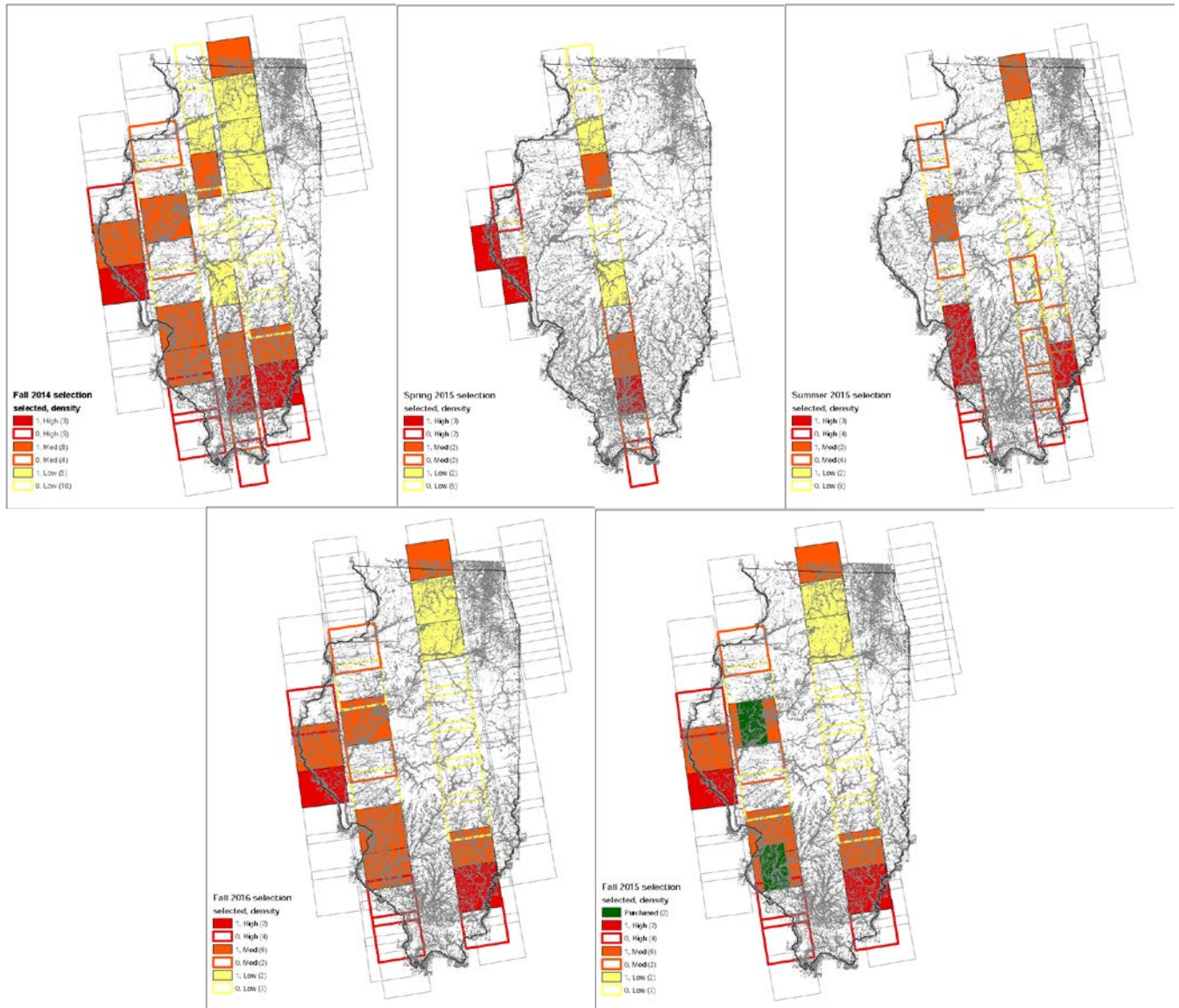
Lang, M. W.; Townsend, P. A.; Kasischke, E. S. 2008. Influence of incidence angle on detecting flooded forests using C-HH synthetic aperture radar data. *Remote Sensing of Environment*. 112:3898-3907

Mitsch, W. J., and J. G. Gosslink 2000. *Wetlands*. John Wiley& Sons, Inc. New York, NY. USA

Appendix A. Extent of Sentinel-1 C-band SAR imagery that is consistently available in the seasons and years of evaluation.



Appendix B. PALSAR-2 L-Band imagery currently downloaded for the focal period. Scenes were selected randomly from each of three strata of available images based on wetland density within the scene. Grey boxes signify scenes that were not selected because they did not overlap much of the state's wetlands or the Sentinel-1 imagery. Colored, hollow boxes represent those that were not randomly selected from the remaining sample. Filled boxes were selected. The maps include the NWI layer for Illinois.



Spatial and temporal modeling of road salts in a watershed with mixed, urban and agricultural, land use

Basic Information

Title:	Spatial and temporal modeling of road salts in a watershed with mixed, urban and agricultural, land use
Project Number:	2016IL313B
Start Date:	3/1/2016
End Date:	2/28/2018
Funding Source:	104B
Congressional District:	IL-103
Research Category:	Water Quality
Focus Categories:	Water Quality, Non Point Pollution, Models
Descriptors:	None
Principal Investigators:	Eric Wade Peterson

Publications

1. Ludwikowski, J., 2016, The transport and fate of chloride within the groundwater of a mixed urban and agricultural watershed, MS Dissertation, Geology, Illinois State University, Normal, IL, 56 p.
2. Chabela, L., 2017, Using 3-D modeling to describe the relationship between peak stage, storm duration, and bank storage and the implications along a meandering stream in central Illinois: Normal, IL, Illinois State University, 57 p.
3. Ludwikowski, J., 2016, The transport and fate of chloride within the groundwater of a mixed urban and agricultural watershed, MS Dissertation, Geology, Illinois State University, Normal, IL, 56 p.
4. Chabela, L., 2017, Using 3-D modeling to describe the relationship between peak stage, storm duration, and bank storage and the implications along a meandering stream in central Illinois: Normal, IL, Illinois State University, 57 p.

Progress Report: Spatial and temporal modeling of road salts in a watershed with urban and agricultural land use

Principal Investigator: Eric W. Peterson

Academic Rank: Professor

University: Illinois State University

Email: ewpeter@ilstu.edu

Phone: 309-438-7865

Research Category: Water quality

Keywords: Deicers; Road Salts; Transport & Fate; Modeling

For Period: March 1, 2016 to February 28, 2017

Submitted: May 12, 2017

Table of Contents

I. Introduction.....	4
II. Research Objectives.....	4
III. Site Description	5
IV. Methodology	5
a. Stream Cl ⁻ concentrations.....	5
b. Numerical Modeling-Watershed.....	5
c. GIS - Regression Modeling.....	7
V. Principle Findings.....	7
a. Stream Cl ⁻ concentrations.....	7
b. Numerical Modeling-Watershed.....	9
i. Flush Scenario Results.....	9
ii. Build-up Scenario Results.....	13
c. GIS – Regression Modeling.....	17
VI. Significance.....	18
VII. Students supported.....	19
VIII. Publications	20
a. MS Thesis	20
b. Peer-Reviewed Academic Journals.....	20
c. Presentations	20
IX. References.....	21

Table of Tables

Table 1: Values used for model parameters.....	6
Table 2: Build-up scenarios: Assigned application rate.....	7
Table 3: Cl ⁻ concentration and Cl ⁻ load data for the sampling locations.....	10
Table 4: Descriptive data for sub basins.....	17
Table 5: Results of initial regression analysis. Bold values.....	17
Table 6: Results of final regression analysis, land use and roads were not used.....	17

Table of Figures

Figure 1: Little Kickapoo Creek watershed showing the proposed sampling sites and the land use for the area.....	5
Figure 2: a) Precipitation (black) and snowfall (red) during the period of sampling. b) Air temperature during the period of sampling. c) Chloride concentrations for the waters at the seven locations. Purple line represents the 230 mg/L threshold and the black dashed lines is in the background concentrations of 10 mg/L. d) chloride load for the locations.	8
Figure 3: Box and whisker plots of a) Mean Cl ⁻ concentrations for each season at the individual locations. Purple line represents the 230 mg/L threshold and the black dashed lines is in the background concentrations of 10 mg/L. b) Mean seasonal concentrations for the locations pooled together. Symbols, # and *, below box and whiskers signify values that are statistically similar.	9
Figure 4: Relationships between water temperature and a) Cl ⁻ concentrations and b) Cl ⁻ load. Purple line represents the 230 mg/L threshold and the black dashed lines is in the background concentrations of 10 mg/L.....	10
Figure 5: Chloride concentration color flood map of model scenario 1 at 1,000 mg/L (A) and 10,000 mg/L (B) application rates. Both panels show models in which road salt was applied for 10 winter seasons; shut off at end of year 10 and then ran at background levels for 50 years after.	11
Figure 6: Model scenario 1 results, wherein road salt was applied for 10 winter seasons and shut off at end of year 10. Reported is the maximum Cl ⁻ concentration (mg/L) at the end of each decade and the background levels (black).	12
Figure 7: Model scenario 1 results, wherein road salt was applied for 10 winter seasons and shut off at end of year 10. Reported is the net mass of Cl ⁻ (Kg/L) at the end of each decade.	12
Figure 8: Build-up model results, wherein road salt was applied for 60 winter seasons. Reported are the maximum Cl ⁻ concentrations (mg/L) at the end of each five-year period.	13
Figure 9: Relationship between the application rate and the maximum Cl ⁻ concentration at the end of the 60-year simulation.	14
Figure 10: Build-up model results, wherein road salt was applied for 60 winter seasons. Reported are the maximum net mass of Cl ⁻ at the end of each five-year period.....	14
Figure 11: Build up scenario results wherein road salt was applied for 60 winter seasons. Shown is the maximum solute residence time (days) and application rate (mg/L).....	15
Figure 12: a) Chloride concentration color flood map of model scenario 2 at the 1,000 mg/L application rate. Shown is the model in which road salt was applied for 60 winter seasons and LKC (white). B) Chloride concentration color flood map of model scenario 2 at the 10,000 mg/L application rate. Shown is the model in which road salt was applied for 60 winter seasons and LKC (blue). White areas indicate concentrations at or below 200 mg/L.	16
Figure 13: a) Observed versus simulated Cl ⁻ concentrations; b) Error in Cl ⁻ concentration at the downstream locations (LKC2-LKC7).....	19

I. Introduction

Chloride (Cl^-) is highly soluble and does not biodegrade, volatilize, precipitate, or adsorb onto mineral surfaces [1, 2]. Thus, Cl^- is extremely mobile, easily transported within surface water or infiltrated into the subsurface. Natural sources of Cl^- include atmospheric deposition, rock weathering, and basin brines [3-5]. During winter months in northern latitudes, deicers, typically composed of a Cl^- salt, are applied to impervious surfaces, roads, walkways, and parking lots, to keep these areas clear of snow and ice [2, 6, 7]. In watersheds where deicers have been employed, natural Cl^- inputs contribute less than 1% of the Cl^- [1, 8], and inputs from agricultural and septic sewer systems only contribute an additional 1% to 3% to the total Cl^- load [8]. The remaining load is attributed to deicers, which serve as a nonpoint source of Cl^- [1, 4, 8]. Annual Cl^- use for road deicing in the US increased from 163,000 tons in 1940 to over 23 million tons in 2005 [9]; six states apply three quarters of the total mass of salt: New York, Ohio, Michigan, Illinois, Pennsylvania, and Wisconsin [10]. In the Chicago area, multiple entities apply over 270,000 tons of road salt, primarily as NaCl , to roads during an average winter [11, 12].

Between 35 to 55% of the applied salt will be transported away via overland flow, with Cl^- concentrations in excess of 1000 mg/L [13], to surface water bodies [14]. Following runoff, streams exhibit acute changes, 20- to 30-fold increases, in Cl^- concentrations [15-20]. The long-term use of deicers has had a chronic impact on streams [21, 22], with reported concentrations increasing 1.5 mg/L per year (Cl^-). Rural watersheds with low density of roadways have seen increases in Cl^- concentrations as a result of deicing applications in urban areas [23, 24]. Cl^- concentrations in the rural streams did not return to baseline levels in summer, even when no salt was being applied. Salt concentrations build up over many years and remain high in the soil and groundwater. Elevated concentrations within the groundwater contribute to elevated baseflow concentrations in streams during the spring and summer [3, 18, 25] and to chronic impacts on groundwater and surface water systems [1, 26, 27].

Between 45% to 65% of applied deicers accumulate in the shallow subsurface waters [2, 15, 28]. Infiltration of runoff from salted roads elevates Cl^- concentrations in roadside soils up to distances of 50 m [29-31], with Cl^- concentrations as high as 13,700 mg/L [20]. Cl^- accumulation in soils and in groundwater subsequently raises the baseflow Cl^- concentrations in surface water bodies during the summer and leads to increases in the baseline salinity of surface waters [32, 33]. In select cases, Cl^- concentrations have increased by 243% over a 47-year period [17], and in other cases, Cl^- concentrations are up to 100 times greater than non-impacted streams [23]. Although acute concentration spikes associated with winter runoff can exceed 1000 mg/L [34], sustained, chronic, concentrations have been rising in streams. For example, the baseflow Cl^- concentration in Highland Creek (Toronto) has increased from 150 mg/L in 1972 to about 250 mg/L in 1995 [21]. Once in ground water, Cl^- can persist for many years [35], and even if deicing applications stopped, it would be decades before the Cl^- concentrations returned to pre-1960 levels in shallow ground water [4, 20].

Although Cl^- has typically been viewed as a benign ion in the environment, exposure to acute (> 1000 mg/L) and chronic (>210 mg/L) Cl^- concentrations can have deleterious effects on aquatic flora [2, 29, 36-49] and fauna [31, 50-52]. Subsequently, the USEPA [53] established a criteria maximum concentration (acute toxicity) of 860 mg/l and a criterion continuous concentration (chronic toxicity) of 230 mg/l for chloride for freshwater aquatic life. As a result of delayed (lagged) Cl^- concentrations in streams, sensitive life stages can be exposed to concentrations long after the winter period of application has occurred [54].

II. Research Objectives

Aquifer salt loading can be quite variable due to diversity of road types, application rates, land use, soil characteristics, and subsurface geology. Cl^- concentrations in the recharging waters can also change with time due to variation in precipitation and application rates. Scarcity of accurate data (i.e. salt application rates) and complexities associated with characterizing the urban hydrologic system lead to difficulties in linking spatial variability with potential impact of this nonpoint source contaminant.

Through this project, we sought to develop models to understand the transport and fate of Cl^- in a watershed. Overall, this study examined spatial and temporal variations in Cl^- concentrations, addressing the following questions:

1. Does road salt applications elevate Cl^- concentrations in a stream throughout the year?
2. Under what conditions will a watershed reach equilibrium between Cl^- inputs and outputs?
3. What is the time interval required for a system to return to background levels of Cl^- once inputs are decreased or ceased?

III. Site Description

The study focuses on Little Kickapoo Creek (LKC), a low gradient, low order, perennial stream that occupies a glacial outwash valley and its watershed (LKCW)(Figure 1). LKC headwaters are in southeast Bloomington, Illinois; Bloomington’s total population is 78,902 and is growing at an annual rate of 3.0% [55]. Upon leaving the urbanized area of Bloomington, LKC flows through a low density suburban setting and then into an agricultural area. The LKC watershed covers a total area of approximately 56 km², from which 1.7 km² is road surface. The land use is 27% urban, 69% agricultural, and 4% forested/ wetland/ surface water areas; classifying the watershed as mixed urban and agricultural. The average annual precipitation for the area (1971-2000) is 95 cm of rain and 56 cm of snowfall [56]. Previous studies have examined and reported the geology, hydrology, and hydrogeology of the area [57-63]. Background stream Cl^- concentrations and groundwater concentrations tend to be less than 10 mg/L

IV. Methodology

a. Stream Cl^- concentrations

Surface water samples were collected every two weeks from seven locations (LKC1-7) along LKC (Figure 1) and analyzed for major anions (Cl^- , SO_4^{2-} , and $\text{NO}_3\text{-N}$) with a Dionex DX-120 Ion Chromatograph housed within the ISU Department of Geography-Geology. Quality assurance (QA) and quality control (QC) were maintained during analysis of each sampling event by running blank, duplicate, and replicate samples. In-situ measurements of dissolved oxygen, specific conductance, and temperature were recorded using a YSI-85. Stream discharge measurements at each location were calculated using the velocity-area method [64], where velocity was measured using an electromagnetic flowmeter. Chloride loads were calculated using the discharge and the Cl^- concentration data. Sampling was conducted from August 2015 to February 2017.

b. Numerical Modeling-Watershed

Groundwater flow was simulated using MODFLOW [65], while MT3D [66] was used to simulate the transport of Cl^- within the system. The model domain of the LKCW was delineated utilizing hydrography data from the National Hydrography Dataset [67]. The domain of the model was limited to the surface water drainage basin for LKC, assuming that the surface water divide serves as a groundwater divide for the shallow groundwater system. At the watershed perimeter, no-flow conditions were assigned to represent the groundwater divide. Along the bottom of the domain, the contact between the glacial materials and Pennsylvanian shale served as a no-flow boundary, restricting flow to two-dimensions. Consistent with previous studies in the area (e.g. [30, 57, 59, 62, 68]) uniform recharge of 3.0×10^{-9} m/s, equivalent to 10% of the average annual precipitation, was applied across the surface of the model domain (Table 1). LKC and the tributaries were treated as a constant head boundary with constant solute conditions. Groundwater flow was assumed to be steady-state, but the solute transport (Cl^-) was transient

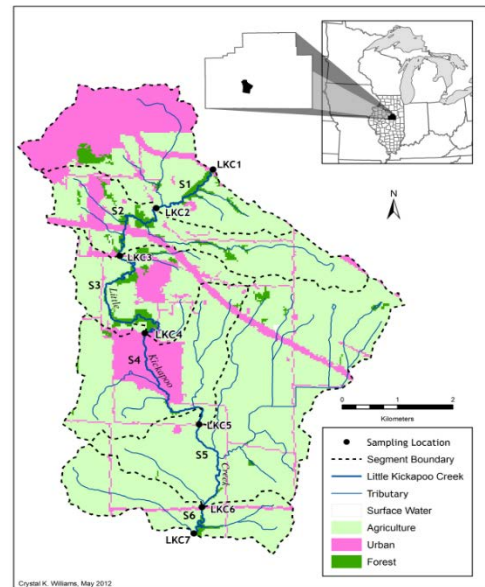


Figure 1: Little Kickapoo Creek watershed showing the proposed sampling sites and the land use for the area.

due to the seasonal depositional rates. Given the geology of the system and the interest in horizontal transport towards the stream, a one-layer model accounting for two-dimensional (2-D) flow through the glacial sediments was developed. The area was discretized into model cells with a dimension of 100 m by 100 m, generating a finite-difference grid with 164 rows, 72 columns, and a total of 7,136 active cells.

Cells were assigned hydraulic conductivities to represent the respective units, either till or outwash. Individually, the till and outwash are represented as homogeneous and isotropic. As a whole, the system is heterogeneous with K values differing between the units. Storage parameters were derived from field work or from reported values in previous studies (Table 1). Aquifer test data from wells located in the modeled area were used to measure storage values for the tills and outwash (Table 1).

Table 1: Values used for model parameters.

Parameter	Value	Source
K – outwash	1.0×10^{-4} m/s	Ackerman, Peterson [68]
K – till	1.0×10^{-8} m/s	Hensel and Miller, 1991
Porosity – outwash	0.25	Ackerman, Peterson [68]
Porosity – till	0.35	Ackerman, Peterson [68]
S_y – outwash	0.021	Field test
S_y – till	0.01	Field test
S_s – outwash	0.0007	Field test
S_s – till	0.00056	Field test
Recharge rate	3.0×10^{-9} m/s	[30, 62, 68]
Cl ⁻ Dispersivity longitude	1.78 m	[69]
Cl ⁻ Dispersivity latitude	1.64 m	[69]
Cl ⁻ concentration – Winter	$\geq 1,000$ mg/L	Lax and Peterson [30]
Cl ⁻ concentration – Winter	10 mg/L	Kelly [70]

Solute transport was simulated under transient conditions with two stress periods; one period represents winter, a time of Cl⁻ application. The second period represents no Cl⁻ application, spring, summer, and fall. Combined, the two periods equal a year, with the winter stress period lasting 84 days and the summer through fall spanning 281 days. For each stress period, the time step is one (1) day. The 84 day winter stress period is based upon the results of an infiltration model [30]. The National Land Cover Database assisted in the classification of cells in the model by revealing urbanized, road, agricultural and forested land use locations. Urbanized and road cells were treated as sources of Cl⁻, with an increased Cl⁻ value that reflects elevated winter concentrations (Table 1); while agricultural and forested areas had constant Cl⁻ concentrations, 10 mg/L, through the whole simulation. Cells identified as roadways and urban areas from the National Transportation Dataset [71] were designated as sources of Cl⁻ due to road salt. To winter simulate conditions similar to those observed in Illinois [30, 72](Table 2), the different scenarios utilized different Cl⁻ levels, all above 1000 mg/L, for the urbanized cells. The 1,000 mg/L is lower than the measured concentrations within infiltration near a road [30] but given the size of the model cells, was determined to be more representative of the input concentration. Non-urban cells were assigned an initial concentration of 10 mg/L simulating background conditions [70], and the recharge maintained a constant 10 mg/L concentration over the duration of the simulation. To accurately model Cl⁻ movement a dispersivity coefficient of 1.78 m for longitude and 1.64 m for latitude was employed [69]. Porosity values of the till and outwash units were 0.25 and 0.35 respectively. Since Cl⁻ is conservative, no retardation factors or reactions were simulated.

Seven scenarios were developed to assess the transport and fate of Cl⁻ in the watershed. Scenarios 1 and 2 simulated 10 cycles (or 10 years) of winter and summer. Beginning in cycle 11, year 11, the simulation of road salt application ceases, and the background Cl⁻ levels are applied consistently to all cells during all stress periods. Scenario 1 used Cl⁻ application rates of 1,000 mg/L whereas Scenario 2 employed 10,000 mg/L. At the end of each decade, the maximum Cl⁻ concentration and net mass values were recorded. Utilizing a basic mass balance equation the amount of Cl⁻ entering and leaving the system was calculated. Scenarios 1 and 2, referred to as the “**Flush Scenarios**”, offer insight into how the watershed flushes out Cl⁻ after 50 years of no application and to determine storage relative to the different application rates.

Table 2: Build-up scenarios: Assigned application rate.

Scenario	Winter Application Rate (mg/L)
3	1,000
4	2,500
5	5,000
6	7,500
7	10,000

Scenarios 3 - 7 simulated a constant, but different, deposition rate across a 60-year span (Table 2). As the application of Cl⁻ occurs over the entire 60 years, Scenarios 3 – 7 are referred to as the “**Build-Up Scenarios**”. The scenarios provided insight to the relationship between Cl⁻ application rate and 1) the accumulation of Cl⁻ mass in the system and 2) the residence time of Cl⁻ in the system. For each year, the residence time was calculated using the Equation (1), presented by Dingman [73]:

$$Tr = \frac{\text{Total Mass solute}}{\text{Mass Out solute}} \tag{Equation 1}$$

c. GIS - Regression Modeling

A GIS model was developed in ArcGIS 10.3 to model concentrations along the stream. The model examined the kilometers of roads in each sub-watershed and land use from the United States Geological Survey. Both the developed high intensity and developed medium intensity were added together to provide the area of urbanization in each sub basin. The developed high intensity and developed medium intensity were chosen because 50-100% of the area represent impervious surfaces, which is where road salts are likely to be applied.

The spatial data and field data were incorporated into a GIS database. The data included Cl⁻ concentration at a given location, Cl⁻ concentration at the most upstream site (LKC1), water day, temperature, sub-watershed drainage area, kilometers of road in sub-watershed, and land cover area per sub basin. A multiple linear regression model was developed to simulate concentrations along LKC and to determine the parameters that were controls on the Cl⁻ concentrations. The multiple linear regression was completed using SPSS. SPSS calculated a coefficient for each variable and p value to show that variable’s significance to the dataset. The coefficients will be multiplied by each respective variable and summed together to predict the chloride concentration at downstream locations. The regression was conducted multiple times, adding and subtracting variables, until each variable was statistically significant ($p < 0.05$).

V. Principle Findings

a. Stream Cl⁻ concentrations

Chloride concentrations ranged from 37.4 mg/L to 460.4 mg/L in the waters of LKC, with the waters possessing similar concentrations across the seven locations (Table 3; Figure 2). The Cl⁻ concentrations are typically below the 230 mg/L Cl⁻ identified as the chronic toxicity threshold established by the USEPA [53]. Chloride load ranged from 1436 Kg/s to 321578 Kg/s (Table 3). Spatially, no differences in concentrations were observed among the locations.

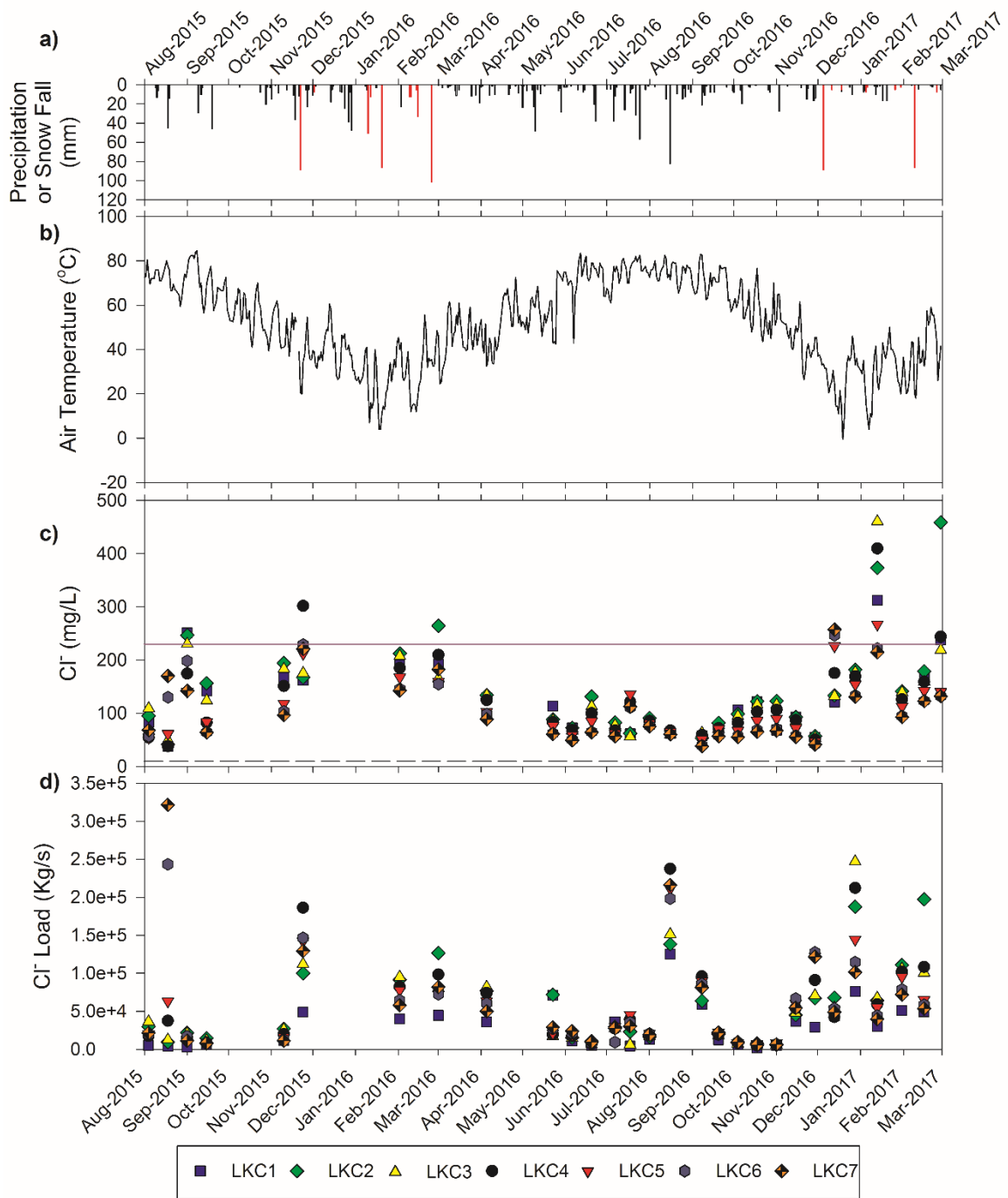


Figure 2: a) Precipitation (black) and snowfall (red) during the period of sampling. b) Air temperature during the period of sampling. c) Chloride concentrations for the waters at the seven locations. Purple line represents the 230 mg/L threshold and the black dashed lines is in the background concentrations of 10 mg/L. d) chloride load for the locations.

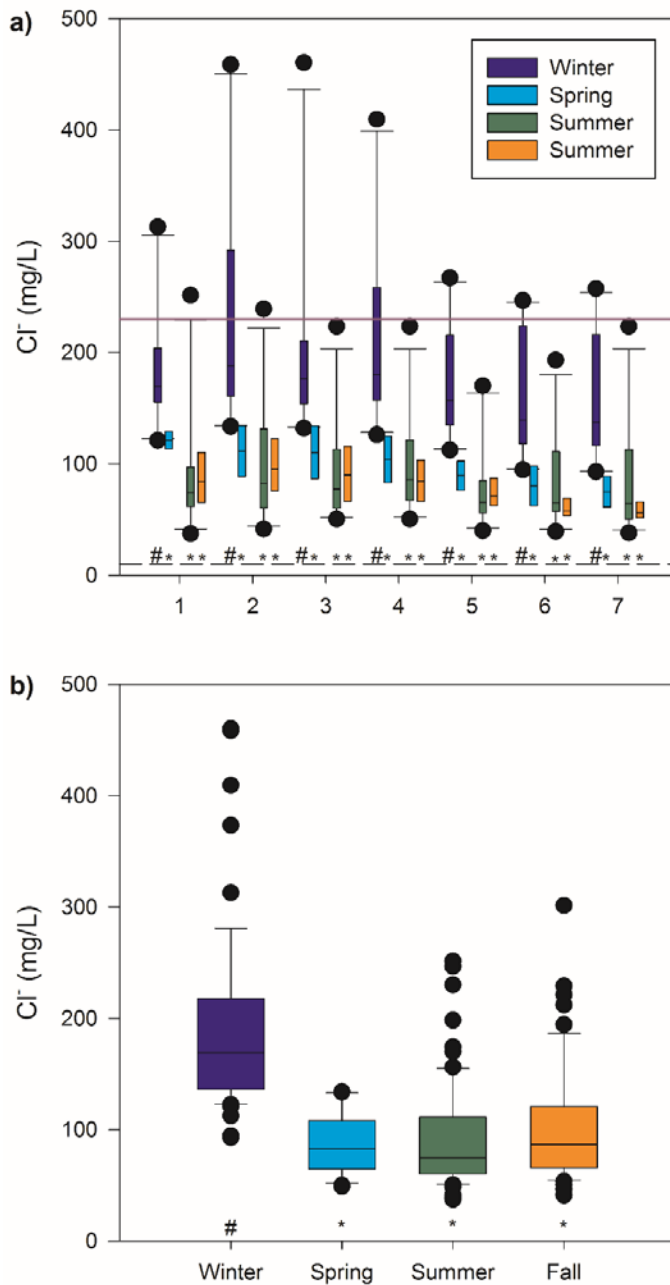


Figure 3: Box and whisker plots of a) Mean Cl⁻ concentrations for each season at the individual locations. Purple line represents the 230 mg/L threshold and the black dashed lines is in the background concentrations of 10 mg/L. b) Mean seasonal concentrations for the locations pooled together. Symbols, # and *, below box and whiskers signify values that are statistically similar.

Chloride concentrations varied temporally, with higher concentrations occurring consistently in the winter. No difference in concentrations among the other seasons was observed [F(3,6)=81.9, p<0.001] (Figure 2 and Figure 3). The highest Cl⁻ concentrations follow snow events (Figure 2c). While the highest Cl⁻ concentrations were observed in the winter, the largest Cl⁻ loads were measured in August (Figure 2d). The high loads in August correspond to precipitation events when discharge was high. Both Cl⁻ concentration (r = -0.585, n = 203, p = 0.001) and Cl⁻ load (r = -0.317, n = 203, p = 0.001) are negatively correlated to water temperature (Figure 4), which serves as a proxy for time of year.

b. Numerical Modeling-Watershed

i. Flush Scenario Results

The flush scenarios simulate road salt application of 1,000 or 10,000 mg/L for 10 winter seasons. After year 10, the application of Cl⁻ is discontinued, and the model simulates 50 additional years with no additional Cl⁻ inputs. In both scenarios, Cl⁻ accumulates within and near roadways and urbanized areas (Figure 5). Some areas, not near the roads or urbanization, show deposition of Cl⁻, with concentrations remaining at the background values. After the Cl⁻ application is ceased, the Cl⁻ dissipates from roadways and urbanized areas into the surrounding aquifer and moves toward LKC. At the end of the 60-year period, Cl⁻ concentrations remain highest along roadways, especially those within areas comprised of till material. Till dominated areas have increased Cl⁻ concentrations and continue to store Cl⁻ despite 50 years of no

application. The 10,000 mg/L rate has more Cl⁻ in storage than the 1,000 mg/L rate due to Cl⁻ loading in the low conductivity tills.

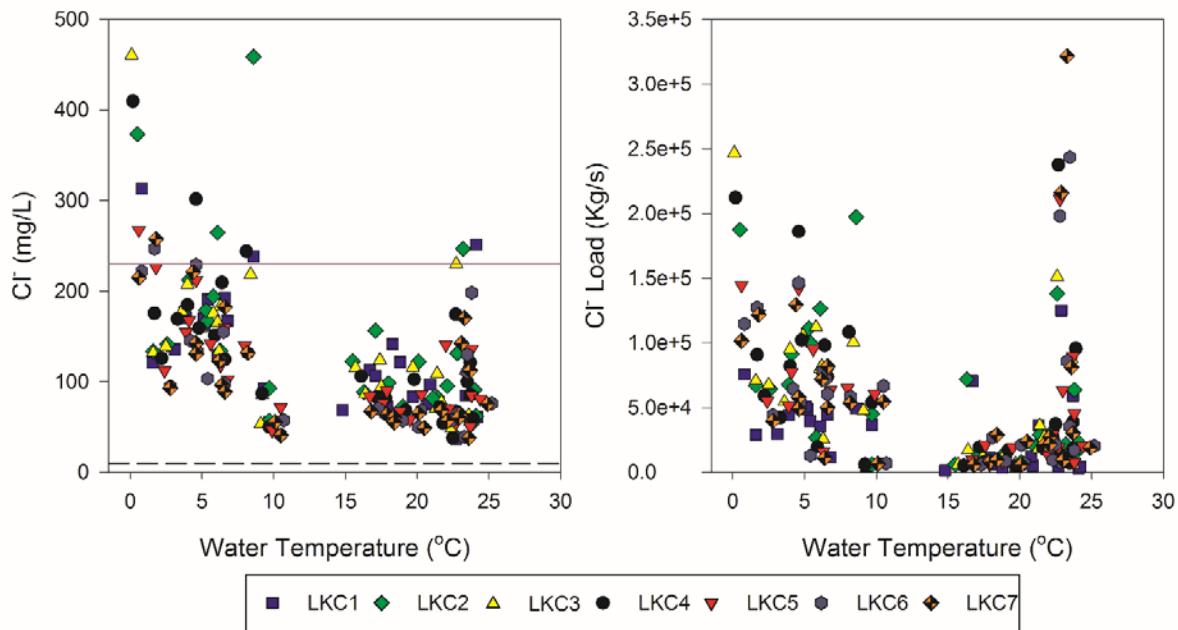


Figure 4: Relationships between water temperature and a) Cl⁻ concentrations and b) Cl⁻ load. Purple line represents the 230 mg/L threshold and the black dashed lines is in the background concentrations of 10 mg/L.

Table 3: Cl⁻ concentration and Cl⁻ load data for the sampling locations.

Sample Location	Cl ⁻ (mg/L)			Cl ⁻ Load (Kg/s)		
	Mean ± StdDev	Minimum	Maximum	Mean ± StdDev	Minimum	Maximum
LKC1	125.8 ± 66.1	37.4	312.9	29970 ± 28829	1437	125122
LKC2	144.8 ± 95.3	41.6	458.6	57041 ± 53750	5964	197303
LKC3	131.3 ± 82.0	48.9	460.3	53116 ± 55199	5912	246859
LKC4	129.5 ± 82.5	37.9	409.6	59030 ± 62906	4784	237348
LKC5	110.0 ± 56.4	46.8	267.2	54260 ± 50679	6272	211077
LKC6	103.7 ± 59.1	39.4	246.8	56711 ± 59774	5980	243400
LKC7	102.9 ± 59.1	38.1	257.5	57592 ± 69405	5614	321579

For each application rate, the peak Cl^- concentration in the system increases, reaching a maximum concentration at year 10 (Figure 6). After year 10, the concentrations decrease following power laws (Figure 6). For the 1,000 mg/P application rate, the peak Cl^- concentrations, 85 mg/L, represents 8.5% of the application rate. When the application rate is 10,000 mg/L, the peak Cl^- concentration at year 10 is 767 mg/L, 7.7% of the application rate (Figure 6). Although the decrease in Cl^- concentration follows a power law, neither system has returned to the background concentration of 10 mg/L by the end of the simulation. Following 50 years of no Cl^- application, the maximum Cl^- concentration was 166 and 25 mg/L for 10,000 and 1,000 mg/L application rates, respectively. Using the appropriate power laws, the 1,000 mg/L and the 10,000 mg/L application rates would return to background concentrations after 237 years and 1658 years, respectively. After the 10 years of Cl^- application, the application of 10,000 mg/L resulted in the storage of 127,000 Kg of Cl^- . The lower application rate produced 11,800 Kg of Cl^- in storage. In accord with the reduction in Cl^- concentration in the waters of the system during the 50 years of no application, the mass of Cl^- in the system decreased. Following exponential decay trends, the mass drops by a little more than half by the simulation end to

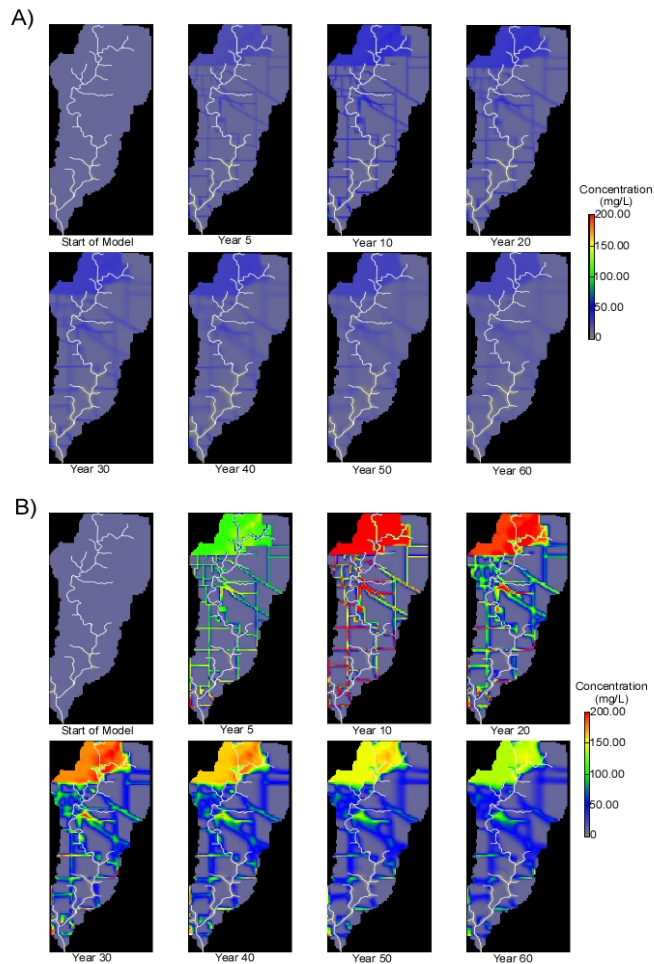


Figure 5: Chloride concentration color flood map of model scenario 1 at 1,000 mg/L (A) and 10,000 mg/L (B) application rates. Both panels show models in which road salt was applied for 10 winter seasons; shut off at end of year 10 and then ran at background levels for 50 years after.

6,200 Kg for the 1,000 mg/L application rate and to 73,500 Kg for the 10,000 mg/L application rate (Figure 7).

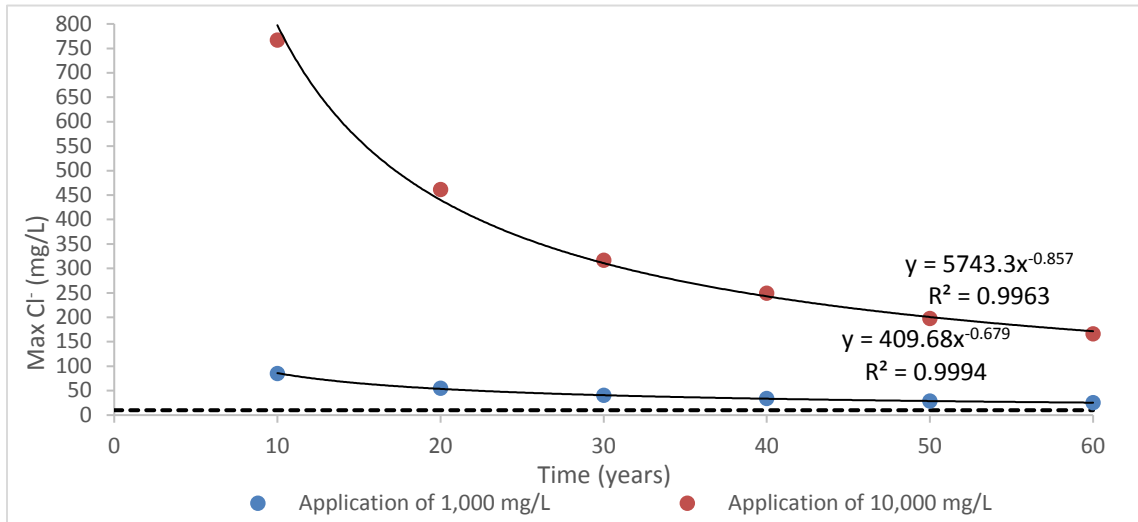


Figure 6: Model scenario 1 results, wherein road salt was applied for 10 winter seasons and shut off at end of year 10. Reported is the maximum Cl⁻ concentration (mg/L) at the end of each decade and the background levels (black).

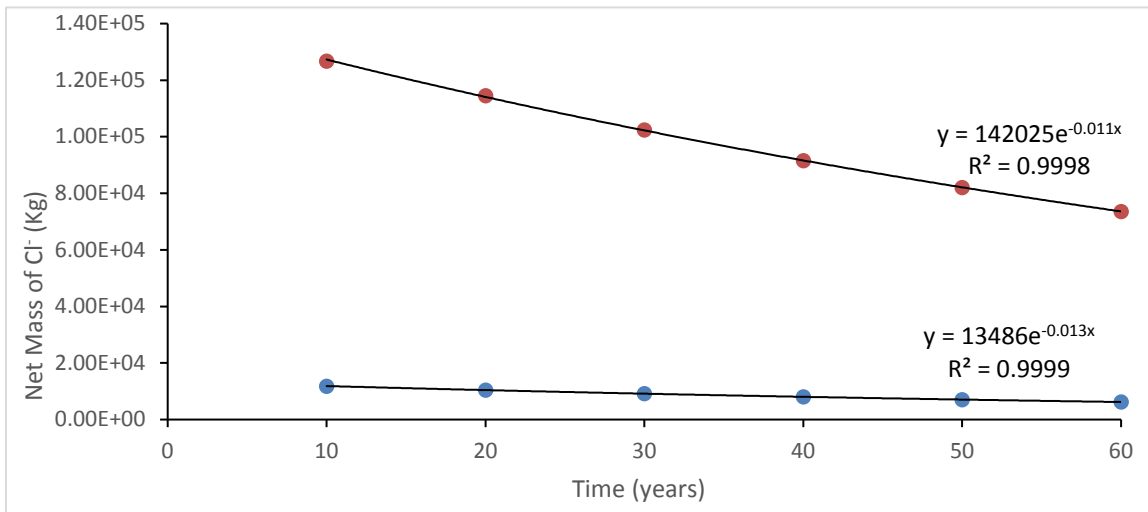


Figure 7: Model scenario 1 results, wherein road salt was applied for 10 winter seasons and shut off at end of year 10. Reported is the net mass of Cl⁻ (Kg/L) at the end of each decade.

Flush models were assigned specific application rates that were applied for 10 winter seasons then shut off. The estimated flush time is relative to application rate with the application rate of 1,000 mg/L having 47% of its mass flush away while the 10,000 mg/L saw 42% flushed away (Figure 6). The 10,000 mg/L rate took 40 years to return to the EPA chronic toxicity level of 230 mg/L (Figure 6). Bester et al. [74] simulated the transport of a Cl⁻ plume in an industrial/urban aquifer setting; model simulations indicated Cl⁻ would flush out of the aquifer after four decades of no application. For both application rates, the simulations show that after 15 years the maximum Cl⁻ concentrations are half of the peak concentrations, similar to [74] (Figure 6).

ii. Build-up Scenario Results

Build-up scenarios simulate a constant road salt application for 60 winter seasons, with each scenario having a specific application rate (Table 2). Similar to the flush scenarios, mass balance data and the maximum Cl⁻ concentrations at five-year intervals were recorded. For each individual application rate, the maximum Cl⁻ level increases every year (Figure 8). Application rates of 7,500 mg/L and 10,000 mg/L show no signs of reaching steady state, but the lower rates appear to be nearing a plateau by the end of the 60-year simulation (Figure 8). The point at which the watershed reaches steady state is relative to the application rate; severe application rates such as 10,000 mg/L show the watershed as continually storing Cl⁻. As the application rate increases so do the Cl⁻ concentrations within the system, a linear relationship between the two is implied (Figure 9). Even after a 60-year period, the maximum Cl⁻ levels are only about 19% of input for all rates.

The net mass of Cl⁻ was also computed for build-up models at the end of each five-year period. From the start to year 60, each simulation shows Cl⁻ mass accumulating annually, with the 1,000 mg/L and 2,500 mg/L rates stabilizing towards the end of the 60 years (Figure 10). At the end of year 60, the net mass is 596,000 Kg for the 10,000 mg/L application rate and 58,000 Kg for the 1,000 mg/L (Figure 10). As expected, increasing road salt application also increases the net mass of Cl⁻ in the system.

Color flood maps of model scenario 2 were constructed to demonstrate the distribution of Cl⁻ across the watershed. Both map's roadways and urbanized areas have the highest concentration of Cl⁻ and the lowest concentrations are found in LKC (Figure 12). Unlike the first set of color flood maps (Figure 5), the spreading and storing of higher concentration water s from the source areas in to the adjacent sediments is illustrated (Figure 12). As LKC represents a point of groundwater discharge, Cl⁻ transport is directed towards LKC. For both application rates, the agricultural lands have the lowest concentrations due to their distance from urban areas and roadways (Figure 12). With both application rates, the Cl⁻

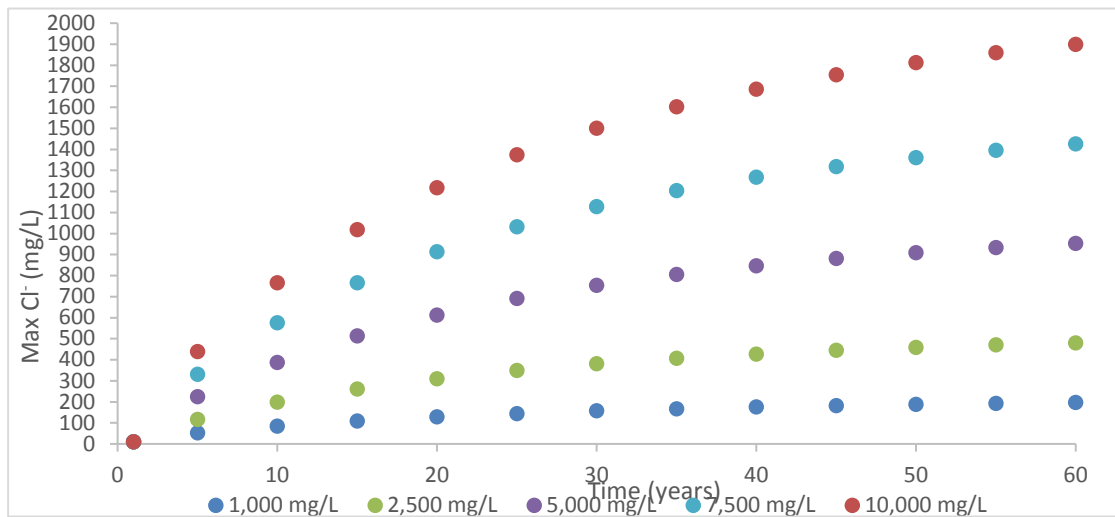


Figure 8: Build-up model results, wherein road salt was applied for 60 winter seasons. Reported are the maximum Cl⁻ concentrations (mg/L) at the end of each five-year period.

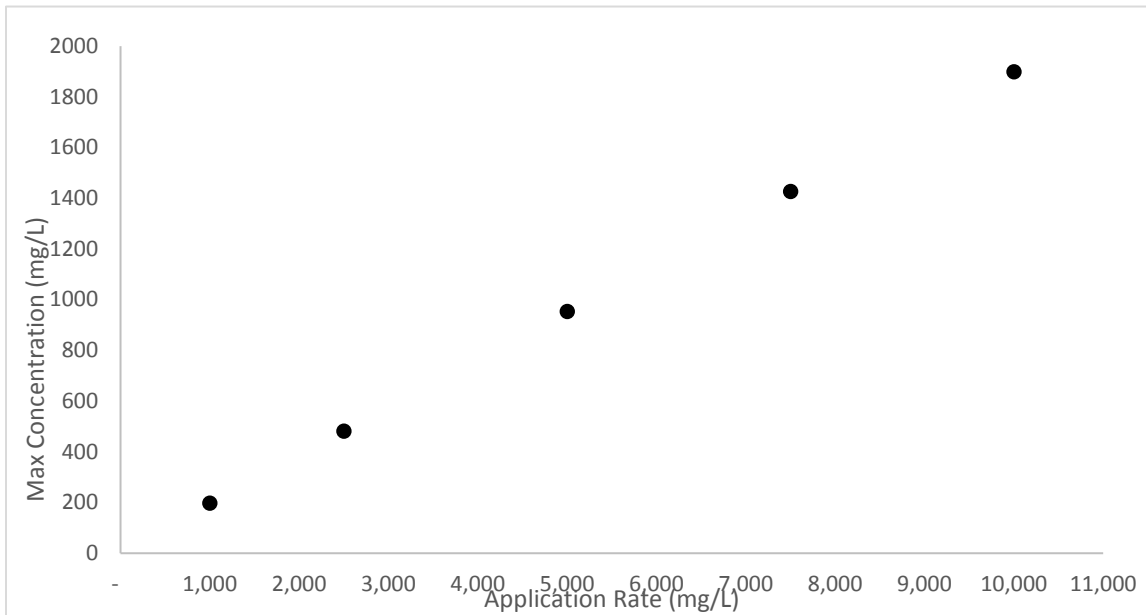


Figure 9: Relationship between the application rate and the maximum Cl⁻ concentration at the end of the 60-year simulation.

concentration increases over time in the agricultural areas (Figure 12). The 10,000 mg/L map uses a different color scale due to reaching concentrations over 200 mg/L only after 10 years of application.

The residence time was calculated every year for each application rate using Equation 1. Application rate and residence time display a positive relationship with a range of 1,123 to 1,288 days for the rates of 1,000 and 10,000 mg/L (Figure 11). The relationship between application rate and Cl⁻ residence time is positive; as the application rate increases so increases the residence time. The Cl⁻ residence time of ~3 years is similar to reported groundwater residence times of 3 years reported in previous studies [75].

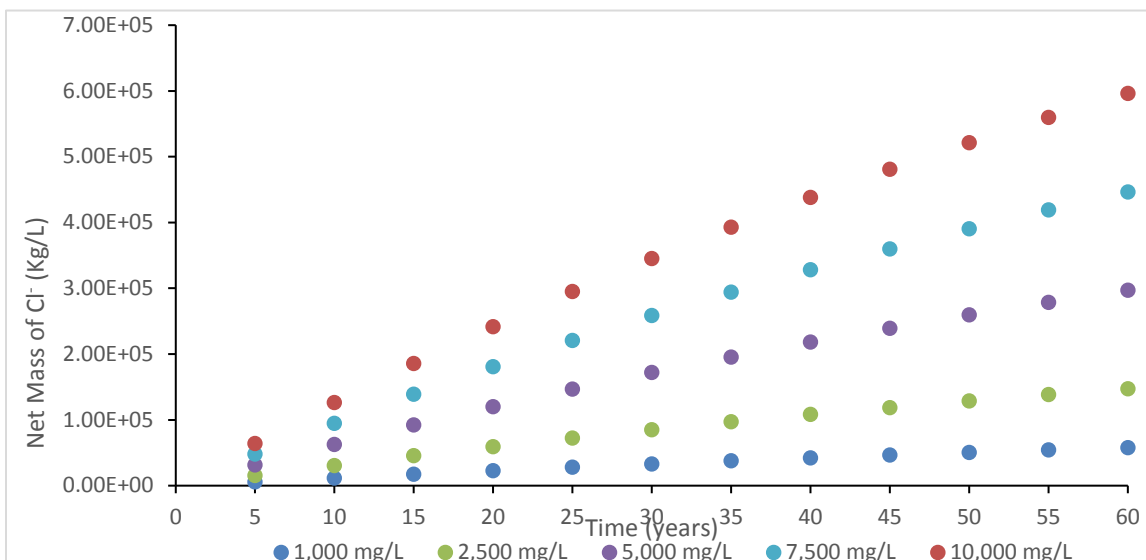


Figure 10: Build-up model results, wherein road salt was applied for 60 winter seasons. Reported are the maximum net mass of Cl⁻ at the end of each five-year period.

Build-up models were assigned application rates that were held constant for 60 years (Table 2). Application rate has a linear relationship with mass accumulation and groundwater concentration of Cl⁻. The maximum Cl⁻ concentration within all simulations rose annually at a rate greater than 1 mg/L (Figure 8), similar to rates reported by [70]. By year 60, maximum Cl⁻ concentrations ranged from 197 mg/L to 1,900 mg/L, which are similar to measured Cl⁻ concentrations in previous studies [70, 72, 76](Figure 8). Alarming, all models except rates of 1,000 mg/L and 2,500 mg/L possessed maximum concentrations that exceeded the MCL after 10 years of Cl⁻ application (Figure 8). The net mass accumulation is dependent upon application rate; final net mass ranges from 58 million metric tons to 596 million metric tons, exhibiting a linear relationship with application rates (Figure 10). Lower rates of 1,000 mg/L and 2,500 mg/L reached steady-state conditions at year 60 contrasting higher rates. For the scenarios examining the lower application rates, estimates of time to reach steady state matches those of previous studies [28, 77]. This study’s simulations reveal that the watershed exhibits a linear relationship between with Cl⁻ storage and application rate, which affects steady-state estimates.

Color flood maps of the watershed display the distribution of Cl⁻ concentrations throughout the watershed (Figure 12). The Cl⁻ concentration is influenced by the land use of that area. The LKC watershed is 27% urbanized and 69% agricultural land use, both of which have associated Cl⁻ concentrations. Urbanized areas (i.e. roadways) exhibit the highest Cl⁻ concentrations, which is analogous with [76]. Agricultural land use have low Cl⁻ concentrations that range from 10 mg/L to 50 mg/L which is supported by previous studies [70, 76](Figure 5 and Figure 12). Lax, Peterson [24] found that during winter months Cl⁻ concentrations in an urban stream range between 65 to 1,350 mg/L and for an agricultural stream between 20 and 60 mg/L. In addition, there is a seasonal variance in which spikes of Cl⁻ are observed in surface waters during winter storm events [25, 34, 70, 78]. Summer Cl⁻ concentrations can also spike due to contaminated groundwater leaching into LKC [58]. However, this

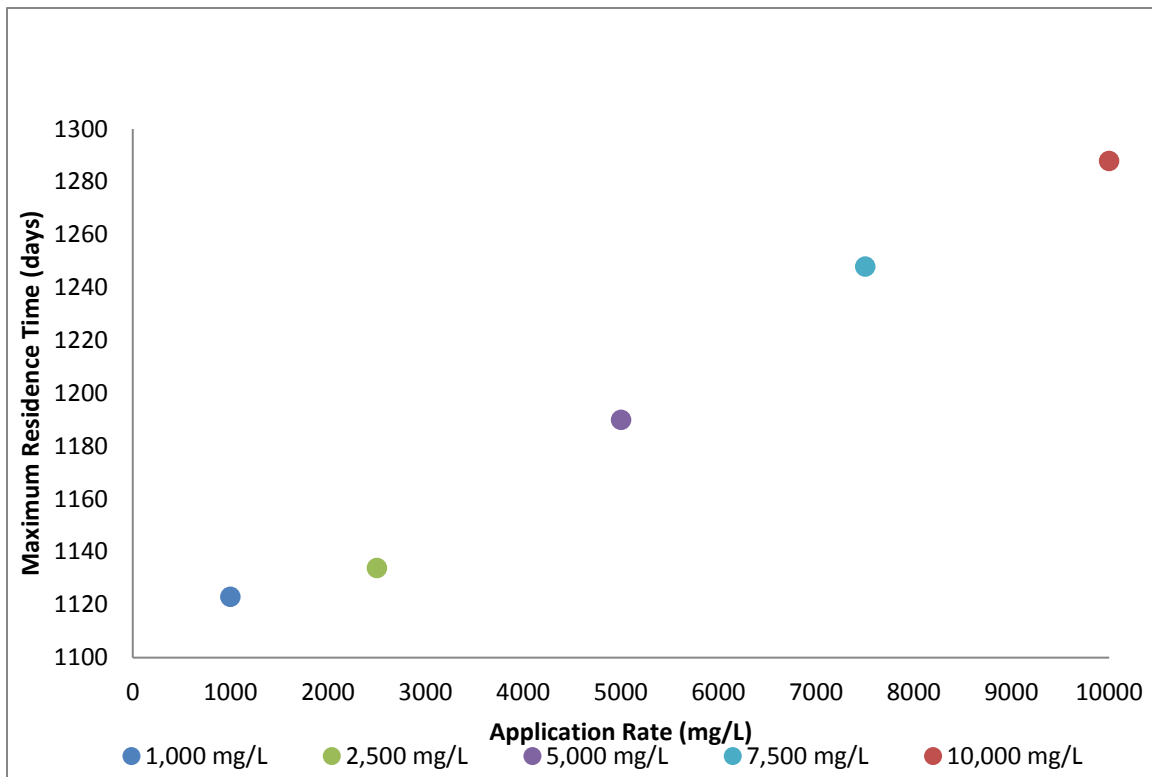


Figure 11: Build up scenario results wherein road salt was applied for 60 winter seasons. Shown is the maximum solute residence time (days) and application rate (mg/L)

solute transport model did not incorporate the transient nature of the stream into the model; rather it examined only the application rates.

Modeling of the watershed revealed 1) the relationship between road salt application rates and mass solute storage and 2) the relationship between road salt application rate and solute residence time. A positive relationship was observed between application rate and mass accumulation. In addition, a positive relationship was observed between application rate and residence time. The time it takes for the watershed to return to safe drinking levels is dependent upon the application rate; as the application rate increases the flush time increases. Steady-state time was also dependent on application rates, wherein a positive relationship was observed.

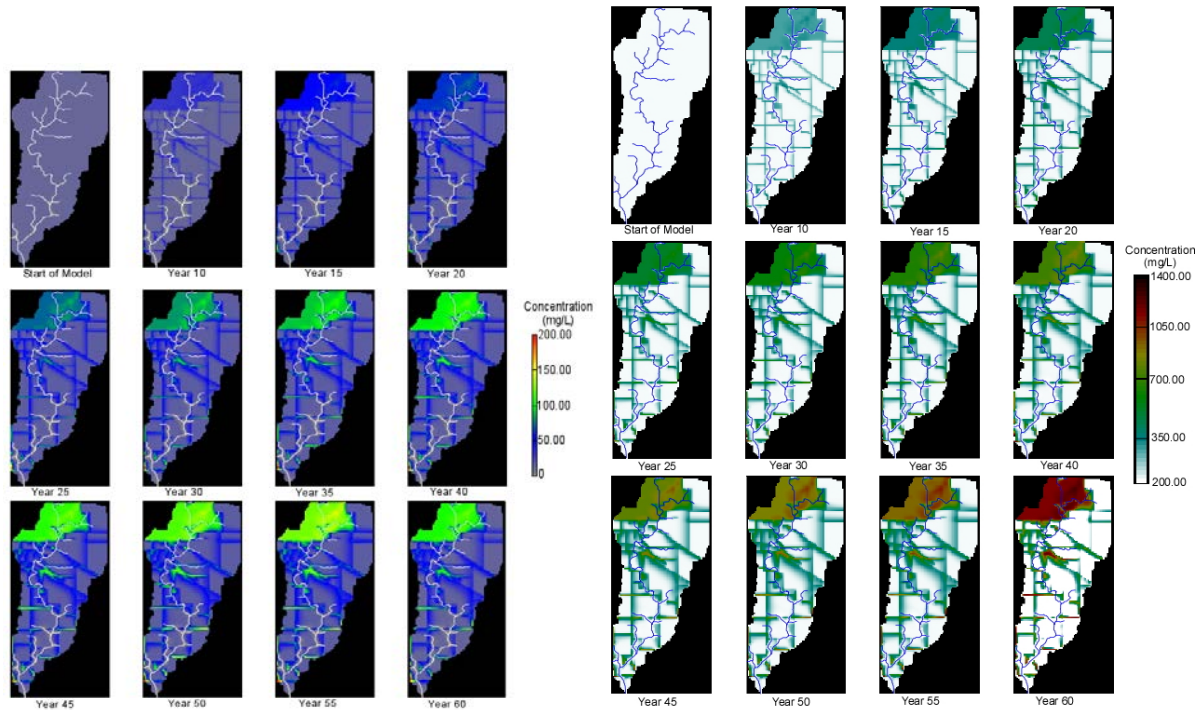


Figure 12: a) Chloride concentration color flood map of model scenario 2 at the 1,000 mg/L application rate. Shown is the model in which road salt was applied for 60 winter seasons and LKC (white). B) Chloride concentration color flood map of model scenario 2 at the 10,000 mg/L application rate. Shown is the model in which road salt was applied for 60 winter seasons and LKC (blue). White areas indicate concentrations at or below 200 mg/L.

The modeling of Cl^- transport in this study reveals the proficiency in which a watershed can store and cleanse road salt. At high application rates, the watershed takes 30 years of no application to return to safe drinking levels, which would not be achievable due to human dependency on deicers. Lower application rates reached steady-state conditions after 60 years of deposition. Presently, watersheds within the Midwest could have reached steady-state conditions with road salt considering application started in the 1960s. Kelly, Panno [75] demonstrated that shallow aquifers within the Chicago metropolitan area have increased in Cl^- concentrations since the 1970s. The Cl^- -contaminated groundwater then feeds local streams wherein we observed elevated surface water Cl^- concentrations through non-salting seasons [75]. The results of this study display that elevated Cl^- concentrations in the groundwater can sustain high surface water concentrations through the non-salting season. Therefore, with a continuance of application in the proceeding winters it is possible that surface water Cl^- concentrations will continue to increase through the decades as shown in Kelly, Panno [75] and [4]. Elevated surface waters and groundwater could lead to detrimental effects on the watershed ecosystem.

c. GIS – Regression Modeling

Urban land cover area and kilometers of roads for each sub basin were determined from the urban land cover datasets and road layers, respectively (Table 4). The drainage area, kilometer of roads, and urban land cover area all increase for each location downstream. The initial regression analysis identified the concentration of Cl⁻ at LKC1, the water day, the water temperature at LKC1, and the drainage area of the sub basin as the significant variables for predicting Cl⁻ concentrations at the downstream locations, with kilometers of road and land use as insignificant (Table 5). Given the lack of significance, the kilometers of road and land use parameters were removed and a final regression analysis was conducted (Table 6). All parameters remained significant, and the final coefficient values remained the same with the exception of drainage area, which increased slightly.

Table 4: Descriptive data for sub basins.

Location (Sub Basin)	Drainage Area (km ²)	Kilometers of Roads (km)	Urban Land Cover (km ²)
LKC1	25.07	174.7	5.71
LKC2	31.50	208.3	7.22
LKC3	36.80	233.7	7.31
LKC4	40.25	261.4	7.36
LKC5	47.58	294.8	7.42
LKC6	55.99	322.3	7.48
LKC7	57.45	330.3	7.48

Table 5: Results of initial regression analysis. Bold values parameters that were not significant.

Parameter	Standard Coefficient	Significance (p-value)
Concentrations at LKC1	0.636	0.000
Water Day	-0.146	0.029
Water temperature LKC1	-0.279	0.001
Roads (km)	-0.0006	0.666
Drainage area (km ²)	0.484	0.033
Urban land cover (km ²)	7.65×10^{-6}	0.402

Table 6: Results of final regression analysis, land use and roads were not used.

Parameter	Standard Coefficient	Significance (p-value)
Concentrations at LKC1	0.632	0.000
Water Day	-0.146	0.028
Water temperature LKC1	-0.281	0.000
Drainage area (km ²)	-0.124	0.032

The linear regression model, generated from the parameter coefficients, simulated chloride concentrations at all locations downstream from LKC1. The model over-predicted the concentrations at LKC4, LKC5, LKC6, and LKC7 and under-predicted the concentrations at LKC2 and LKC3 (Figure 13). Values used to test the models accuracy were not included in the construction of the linear model. The highest errors were associated with the locations farthest downstream from LKC1, LKC6 and LKC7 (Figure 13). Overall, the model produced a mean absolute error (MAE) of 15.39 mg/L.

The regression analysis indicates the only independent variable per sub basin is the drainage area of the sub basin. The regression model did not compensate for any other parameter. Lax [79] identified a relationship between chloride concentrations and land-use and found that land-use was a controlling factor of surface stream quality. Streams with their headwaters originating in urban areas have much higher chloride concentrations than those originating in agricultural areas [79]. The current regression model is not differentiating the upstream areas, which receive most of its water from the impacted urban runoff, from the downstream areas, which receive the majority of its water from groundwater infiltrating from agricultural areas. Dilution is a major controlling factor for chloride concentrations as high stream flow correlates with lower chloride concentrations [78, 80]. The land-use pattern of the watershed may play a role in the predictive use of the regression analysis. Moving downstream, the percentage of urban land use decreases as the drainage area increases. The larger drainage results in greater discharge, with water added from groundwater input [58, 59, 63]. The linear regression model is not compensating for the differences in water added to the stream at the upstream and downstream locations. The baseflow water adding to the upstream locations should have similar concentrations to the upstream locations so little dilution should occur. However, downstream baseflow waters, draining agricultural areas, have lower concentration relative to the waters in the downstream sites. Therefore, the dilution effectively lowers the concentration while maintaining the load, which is seen in the field data (Figure 2).

VI. Significance

Outcomes from these activities present spatial and temporal data for Cl^- within a watershed impacted by deicing agents. Results identify seasonal trends in the concentration of Cl^- in the LKC watershed, with elevated concentrations in the winter. However, periodic spikes during the summer follow precipitation events. The spikes appear to be associated with Cl^- stored within the aquifer system that is released in response to infiltration associated with the precipitation events. The continued use of roads salts will continue to elevate the concentration of Cl^- within the waters. If the application of Cl^- ceased, the watershed would not fully recover within 50 years. Residual Cl^- would remain in the system. The numerical modeling approach provides an initial evaluation; additional modeling incorporating transient flow will be needed to support all future research activities and develop appropriate BMPs for Cl^- applications.

The Illinois State Geological Survey and the Illinois State Water Survey have examined the issue of road salts in the Chicago metropolitan area and the subsequent effects on the Illinois River watershed [5, 13, 36, 70, 80-82]. A pilot GIS model developed to evaluate the transport and fate of Cl^- within Illinois indicated that data are spatially and temporally too variable to accurately assess the problem [83]. Our data indicate suggest a balance between spatial resolution and temporal resolution exists. While our sampling points were closer together, the 2-week time period was too coarse to model accurately the pulse of Cl^- moving through the system. A finer temporal resolution is needed to develop more adequate GIS and flow models.

Increases in road salts use, leading to increases in stream/groundwater chloride concentrations, are fueling the need for useful tools to study chloride fate and transport. Linear regression modeling has been used many times to predict the movement of a contaminant and is used here to predict chloride concentrations downstream. Land cover, representing impervious surfaces, drainage area, and discharge are all controlling factors in chloride concentration downstream, however there must be other factors controlling chloride concentration other than the ones viewed in this study. This study also revealed that there is an impacted area around an urban setting. Chloride concentrations are less diluted upstream due to the chlorides stored and discharging into the upstream sites. More dilution occurs downstream due to the waters discharging into downstream locations are agriculturally derived.

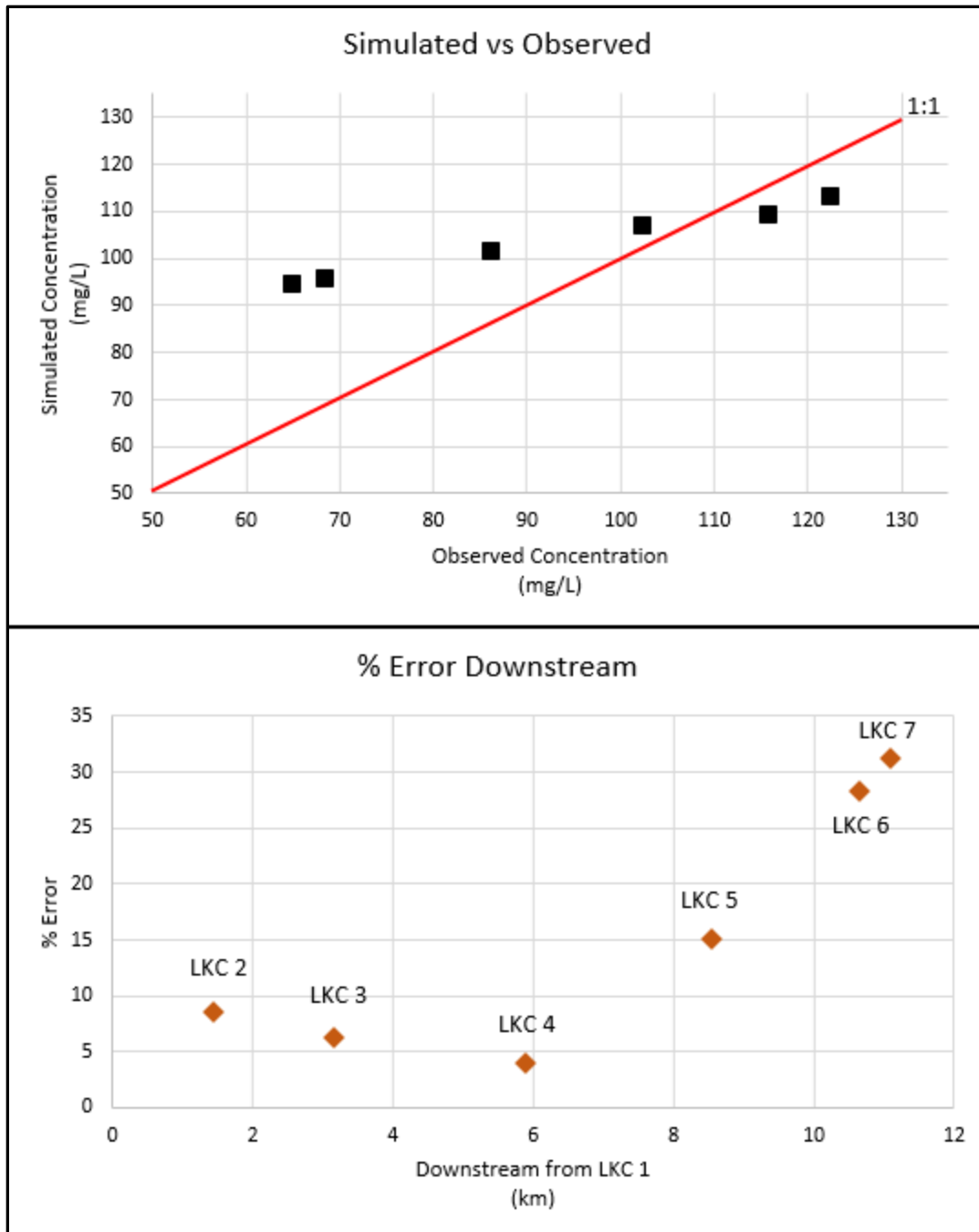


Figure 13: a) Observed versus simulated Cl⁻ concentrations; b) Error in Cl⁻ concentration at the downstream locations (LKC2-LKC7).

VII. Students supported

A total of five students were involved in the project: Graduate students Jessica Ludwowski and Lucas Chabela; Undergraduate students Kyagaba David Lwanga, Alan Jensen; and Clint Updike. Direct support was provided to Mr. Chabela, Mr. Jensen, and Mr. Updike. Ms. Ludwowski and Mr. Lwanga were involved through independent research. Below, I provide a more detailed description of the students' role and status.

Jessica Ludwikowski – MS 2016, Ms. Ludwikowski generated the groundwater flow (MODFLOW) and Cl⁻ transport model (MT3D) for the watershed, which served as her thesis research. Upon graduation, Ms. Ludwikowski began a position as an Environmental Control Engineer with the Cook County Department of Environmental Control.

Lucas Chabela – MS 2017, Mr. Chabela served as the lead student on the project. Mr. Chabela conducted the two-week stream sampling events. In addition to coordinating and collecting the water samples, Mr. Chabela developed a bank-storage model (MODFLOW) to examine Cl⁻ storage along the stream; this project served as his thesis research. Lucas was instrumental in the development of the GIS analysis to model concentrations within the watershed using the water sample data. Lucas is a May 2017 graduate and is in the process of finding employment.

Kyagaba David Lwanga – BS 2016, Mr. Lwanga was involved in water sampling and the initial GIS development. He participated in both the collection of water samples and the analysis of the samples. Upon graduation, Mr. Lwanga took a position as a GIS analyst at ExteNet Systems in Lisle, IL.

Alan Jensen – BS 2016, Upon Mr. Lwanga's graduation, Mr. Jensen began assisting Mr. Chabela in the collection of water samples. As a result of his schedule, Mr. Jensen's involvement was limited to sample preparation, sample collection, and data entry. After graduation, Mr. Jensen began working for Mostardi Platt, an environmental consulting firm in Chicago.

Clint Updike – BS expected 2018, Mr. Updike transitioned into the project as Mr. Jensen was about to graduate. Mr. Updike was involved with sample preparation, sample collection, and data entry. More recently, Mr. Updike began examining the data as part of an independent research project that he will complete during the next academic year. He has plans to present the work at the North-Central GSA meeting in Ames, Iowa in April 2018.

GEO 444 – Applied Groundwater Modeling: The data collected during the project will be incorporated into the curriculum of the Applied Groundwater Modeling course. Students will use the data in two projects: 1) a geostatistical model to assess the temporal trends of the data and 2) a 1-D transient storage model development. While the thesis work by Ms. Ludwikowski and Mr. Chabela provide these answers, the data set is well-suited for student learning. The patterns that are present, the natural variability in the data, and the imperfections in the data provide students an opportunity to examine and to discuss how to incorporate imperfect the data into the models.

VIII. Publications

a. MS Thesis

Ludwikowski, J., 2016, The transport and fate of chloride within the groundwater of a mixed urban and agricultural watershed: Normal, IL, Illinois State University, 56 p.

Chabela, L., 2017, Using 3-D modeling to describe the relationship between peak stage, storm duration, and bank storage and the implications along a meandering stream in central Illinois: Normal, IL, Illinois State University, 57 p.

b. Peer-Reviewed Academic Journals

None at this time. I am developing two papers based upon the MS theses of Ms. Ludwikowski and Mr. Chabela. Additional papers are planned to examine the seasonal variation of Cl⁻ in the watershed.

c. Presentations

Peterson, E.W., and Ludwikowski, J.*, (2016) Transport and fate of chloride within the groundwater of a mixed urban and agricultural watershed, Illinois Water Conference, October 26, 2016.

Chabela, L. P.*, Peterson, E. W., Miller, J.*, (2016) Seasonal variation of chloride inputs from road salt application in a mixed urban/agricultural watershed in central Illinois, Abstract with Programs - Geological Society of America, September 2016, Vol. 48, No. 7, doi: 10.1130/abs/2016AM-287247

Ludwikowski, J.*, and Peterson, E.W., (2016) Transport and fate of chloride within the groundwater of a mixed urban and agricultural watershed, Illinois Groundwater Association, April 20, 2016.

Additional presentations in 2017-2018 are planned at the 2017 annual GSA meeting, the 2018 North-Central GSA meeting, the Illinois Water Conference, and an Illinois Groundwater Association meeting.

IX. References

1. Meriano, M., N. Eyles, and K.W.F. Howard, *Hydrogeological impacts of road salt from Canada's busiest highway on a Lake Ontario watershed (Frenchman's Bay) and lagoon, City of Pickering*. Journal of Contaminant Hydrology, 2009. **107**(1–2): p. 66-81.
2. Environment Canada, *Priority substances list assessment report: Road Salts*, Health Canada, Editor. 2001, Minister of Public Works and Government Services. p. 171.
3. Gardner, K.M. and T.V. Royer, *Effect of Road Salt Application on Seasonal Chloride Concentrations and Toxicity in South-Central Indiana Streams*. J. Environ. Qual., 2010. **39**(3): p. 1036-1042.
4. Kelly, V.R., et al., *Long-term sodium chloride retention in a rural watershed: Legacy effects of road salt on streamwater concentration*. Environmental Science & Technology, 2008. **42**(2): p. 410-415.
5. Panno, S.V., et al., *Characterization and identification of Na-Cl sources in ground water*. Ground Water, 2006. **44**(2): p. 176-187.
6. Locat, J. and P. Gélinas, *Infiltration of de-icing road salts in aquifers: the Trois-Rivières-Ouest case, Quebec, Canada*. Canadian Journal of Earth Sciences, 1989. **26**(11): p. 2186-2193.
7. Marsalek, J., *Road salts in urban stormwater: an emerging issue in stormwater management in cold climates*. Water Science & Technology, 2003. **48**(9): p. 61-70.
8. Novotny, E.V., et al., *Chloride ion transport and mass balance in a metropolitan area using road salt*. Water Resources Research, 2009. **45**(12): p. n/a-n/a.
9. Jackson, R.B. and E.G. Jobbágy, *From icy roads to salty streams*. Proceedings of the National Academy of Sciences of the United States of America, 2005. **102**(41): p. 14487-14488.
10. Kostick, D.S., J.A. Milanovich, and R.R. Coleman, *2005 Minerals Yearbook: Salt*, U.S.G. Survey, Editor. 2007, U.S. Geological Survey. p. 21.
11. Friederici, P., *Salt on earth*. Chicago Wilderness Magazine, Winter, Chicago, 2004.
12. Keseley, S., *Road salt is a slippery subject*. Lake County Health Department and Community Health Center Cattail Chronicles, 2006. **16**(1): p. 4-5.
13. Kelly, W.R., S.V. Panno, and K.C. Hackley. *Impacts of road salt on water resources in the Chicago region*. in 2009 UCOWR conference. 2009. Southern Illinois University, Carbondale, IL.
14. Church, P.E. and P.J. Friesz, *Effectiveness of Highway Drainage Systems in Preventing Road-Salt Contamination of Groundwater: Preliminary Findings*. Transportation Research Record, ed. T.R. Record. Vol. 1420. 1993, Washington, DC Transportation Research Record. 64.
15. Ruth, O., *The effects of de-icing in Helsinki urban streams, Southern Finland*. Water Science and Technology, 2003. **48**(9): p. 33-43.
16. Bäckström, M., et al., *Speciation of Heavy Metals in Road Runoff and Roadside Total Deposition*. Water, Air, and Soil Pollution, 2003. **147**(1-4): p. 343-366.
17. Godwin, K.S., S.D. Hafner, and M.F. Buff, *Long-term trends in sodium and chloride in the Mohawk River, New York: the effect of fifty years of road-salt application*. Environmental Pollution, 2003. **124**(2): p. 273-281.
18. Koryak, M., et al., *Highway Deicing Salt Runoff Events and Major Ion Concentrations along a Small Urban Stream*. Journal of Freshwater Ecology, 2001. **16**(1): p. 125-134.
19. Scott, W.S., *The effect of road deicing salts on sodium concentration in an urban water-course*. Environmental Pollution (1970), 1976. **10**(2): p. 141-153.

20. Howard, K.W.F. and P.J. Beck, *Hydrogeochemical implications of groundwater contamination by road de-icing chemicals*. Journal of Contaminant Hydrology, 1993. **12**(3): p. 245-268.
21. Bowen, G.S. and M.J. Hinton. *The temporal and spatial impacts of road salt on streams draining the Greater Toronto Area*. in *Proceedings of the Groundwater in A Watershed Context Symposium*. 1998. Burlington, Ontario: Ontario Ministry of the Environment and Geological Survey of Canada.
22. Warren, L.A. and A.P. Zimmerman, *The influence of temperature and NaCl on cadmium, copper and zinc partitioning among suspended particulate and dissolved phases in an urban river*. Water Research, 1994. **28**(9): p. 1921-1931.
23. Kaushal, S.S., et al., *Increased salinization of fresh water in the northeastern United States*. Proceedings of the National Academy of Sciences of the United States of America, 2005. **102**(38): p. 13517-13520.
24. Lax, S.M., E.W. Peterson, and S. Van der Hoven, *Quantifying Stream chloride concentrations as a function of land-use*. Water, Air, and Soil Pollution, in review.
25. Perera, N., B. Gharabaghi, and K. Howard, *Groundwater chloride response in the Highland Creek watershed due to road salt application: A re-assessment after 20 years*. Journal of Hydrology, 2013. **479**: p. 159-168.
26. Marsalek, J., et al., *Review of operation of urban drainage systems in cold weather: water quality considerations*. Water Science and Technology, 2003. **48**(9): p. 11-20.
27. Viklander, M., et al., *Urban drainage and highway runoff in cold climates: conference overview*. Water Science and Technology, 2003. **48**(9): p. 1-10.
28. Howard, K.W.F. and J. Haynes, *Groundwater contamination due to road de-icing chemicals--Salt balance implications*. Geoscience Canada, 1993. **20**(1): p. 1-8.
29. Karraker, N.E., J.P. Gibbs, and J.R. Vonesh, *Impacts of Road Deicing Salt on the Demography of Vernal Pool-Breeding Amphibians*. Ecological Applications, 2008. **18**(3): p. 724-734.
30. Lax, S. and E.W. Peterson, *Characterization of chloride transport in the unsaturated zone near salted road*. Environmental Geology, 2009. **58**(5): p. 1041-1049.
31. Miklovic, S. and S. Galatowitsch, *Effect of NaCl and Typha angustifolia L. on marsh community establishment: A greenhouse study*. Wetlands, 2005. **25**(2): p. 420-429.
32. Rosenberry, D.O., et al., *Movement of Road Salt to a Small New Hampshire Lake* Water, Air, & Soil Pollution, 1999. **109**(1-4): p. 179-206 DOI 10.1023/A:1005041632056
33. Siver, P.A., et al., *Historical changes in Connecticut lakes over a 55-year period*. Journal of Environmental Quality, 1996. **25**(2): p. 334-345.
34. Williams, D.D., N.E. Williams, and Y. Cao, *Road salt contamination of groundwater in a major metropolitan area and development of a biological index to monitor its impact*. Water Research, 2000. **34**(1): p. 127-138.
35. Watson, L.R., et al., *Effects of highway-deicer application on ground-water quality in a part of the Calumet Aquifer, Northwestern Indiana*, U.G. Survey, Editor. 2002, US Department of the Interior, US Geological Survey.
36. Panno, S.V., et al., *Impact of urban development on the chemical composition of ground water in a fen-wetland complex*. Wetlands, 1999. **19**(1): p. 236-245.
37. Mayer, T., et al., *Impact of road salts on small urban ponds: Rouge River pond case study*, N.W.R. Institute, Editor. 1999, National Water Research Institute: Burlington, Ontario.
38. Wegner, W. and M. Yaggi, *Environmental Impacts of Road Salt and Alternatives in the New York City Watershed*. Stormwater, 2001. **2**(5): p. http://www.forester.net/sw_0107_environmental.html.
39. Demers, C.L., *Effects of road deicing salt on aquatic invertebrates in four Adirondack streams, in Chemical deicers and the environment*, F.M. D'Itri, Editor. 1992, Lewis Publishing: Boca Raton, Florida.
40. Crowther, R.A. and H.B.N. Hynes, *The effect of road deicing salt on the drift of stream benthos*. Environmental Pollution (1970), 1977. **14**(2): p. 113-126.

41. Molles, M., *Effects of road salting on stream invertebrate communities*. Eisenhower Consortium Bulletin, 1980. **10**: p. 1-9.
42. Hart, B., et al., *A review of the salt sensitivity of the Australian freshwater biota*. Hydrobiologia, 1991. **210**(1-2): p. 105-144.
43. Fay, L. and X. Shi, *Environmental Impacts of Chemicals for Snow and Ice Control: State of the Knowledge*. Water, Air, & Soil Pollution, 2012. **223**(5): p. 2751-2770.
44. Seilheimer, T., et al., *Impact of urbanization on the water quality, fish habitat, and fish community of a Lake Ontario marsh, Frenchman's Bay*. Urban Ecosystems, 2007. **10**(3): p. 299-319.
45. Sanzo, D. and S.J. Hecnar, *Effects of road de-icing salt (NaCl) on larval wood frogs (Rana sylvatica)*. Environmental Pollution, 2006. **140**(2): p. 247-256.
46. Birge, W., et al., *Recommendations on numerical values for regulating iron and chloride concentrations for the purpose of protecting warm water species of aquatic life in the Commonwealth of Kentucky*. Memorandum of Agreement, 1985. **5429**.
47. Evans, M. and C. Frick, *The effects of road salts on aquatic ecosystems*. 2001, National Water Research Institute, Environmental Canada: Ottawa, Canada.
48. Richburg, J., W. Patterson, and F. Lowenstein, *Effects of road salt and Phragmites australis invasion on the vegetation of a Western Massachusetts calcareous lake-basin fen*. Wetlands, 2001. **21**(2): p. 247-255.
49. Foos, A., *Spatial distribution of road salt contamination of natural springs and seeps, Cuyahoga Falls, Ohio, USA*. Environmental Geology, 2003. **44**(1): p. 14-19.
50. Fraser, D. and E.R. Thomas, *Moose-Vehicle Accidents in Ontario: Relation to Highway Salt*. Wildlife Society Bulletin (1973-2006), 1982. **10**(3): p. 261-265.
51. Bollinger, T.K., P. Mineau, and M.L. Wickstrom, *Toxicity of sodium chloride to house sparrows (Passer domesticus)*. Journal of Wildlife Diseases, 2005. **41**(2): p. 363-370.
52. Wilcox, D.A., *The effects of deicing salts on vegetation in Pinhook Bog, Indiana*. Canadian Journal of Botany, 1986. **64**(4): p. 865-874.
53. United States Environmental Protection Agency. *National recommended water quality criteria - aquatic life criteria table*. [cited 2017; Available from: <https://www.epa.gov/wqc/national-recommended-water-quality-criteria-aquatic-life-criteria-table>].
54. Findlay, S.E.G. and V.R. Kelly, *Emerging indirect and long-term road salt effects on ecosystems*. Annals of the New York Academy of Sciences, 2011. **1223**(1): p. 58-68.
55. U.S. Census Bureau. *State and County QuickFacts*. 2015 [cited 2015; Available from: <http://quickfacts.census.gov/qfd/states/17/1706613.html>].
56. Illinois State Water Survey, *Illinois Water and Climate Summary*. 2004.
57. Beach, V. and E.W. Peterson, *Variation of hyporheic temperature profiles in a low gradient third-order agricultural stream – A statistical approach*. Open Journal of Modern Hydrology, 2013. **3**(2): p. 55-66.
58. Peterson, E.W. and C. Benning, *Factors influencing nitrate within a low-gradient agricultural stream*. Environmental Earth Sciences, 2013. **68**(5): p. 1233-1245.
59. Peterson, E.W. and T.B. Sickbert, *Stream water bypass through a meander neck, laterally extending the hyporheic zone*. Hydrogeology Journal, 2006. **14**(8): p. 1443-1451.
60. Peterson, E.W., T.B. Sickbert, and S.L. Moore, *High frequency stream bed mobility of a low-gradient agricultural stream with implications on the hyporheic zone*. Hydrological Processes, 2008. **22**(21): p. 4239-4248.
61. Sickbert, T.B. and E.W. Peterson, *The effect of surface water velocity on hyporheic interchange*. Journal of Water Resource and Protection, 2014. **6**(4): p. 327-336.
62. Van der Hoven, S.J., N.J. Fromm, and E.W. Peterson, *Quantifying nitrogen cycling beneath a meander of a low gradient, N-impacted, agricultural stream using tracers and numerical modelling*. Hydrological Processes, 2008. **22**(8): p. 1206-1215.

63. Bastola, H. and E.W. Peterson, *Heat tracing to examine seasonal groundwater flow beneath a low-gradient stream*. Hydrogeology Journal, 2016. **24**(1): p. 181-194.
64. Mosley, M.P. and A.I. McKerchar, *Streamflow*, in *Handbook of Hydrology*, D.R. Maidment, Editor. 1993, McGraw Hill: New York. p. 8.1-8.39.
65. Harbaugh, A.W., et al., *MODFLOW-2000, The U. S. Geological Survey Modular Ground-Water Model-User Guide to Modularization Concepts and the Ground-Water Flow Process*, in *Open-File Report 00-92*, U. S. Geological Survey, Editor. 2000, U. S. Geological Survey, Reston, VA. p. 134.
66. Zheng, C. and P.P. Wang, *MT3DMS: A Modular Three-Dimensional Multispecies Transport Model for Simulation of Advection, Dispersion, and Chemical Reactions of Contaminants in Groundwater Systems; Documentation and User's Guide*. Vol. Contract Report SERDP-99-1. 1999, Vicksburg, MS: U.S. Army Engineer Research and Development Center.
67. U.S. Geological Survey, *National Geospatial Technical Operations Center*. 2014, U.S. Geological Survey,.
68. Ackerman, J.R., et al., *Quantifying nutrient removal from groundwater seepage out of constructed wetlands receiving treated wastewater effluent*. Environmental Earth Sciences, 2015. **74**(2): p. 1633-1645.
69. Giadom, F.D., E.G. Akpokodje, and A.C. Tse, *Determination of migration rates of contaminants in a hydrocarbon-polluted site using non-reactive tracer test in the Niger Delta, Nigeria*. Environmental Earth Sciences, 2015. **74**(1): p. 879-888.
70. Kelly, W.R., *Long-term trends in chloride concentrations in shallow aquifers near Chicago*. Ground Water, 2008. **46**(5): p. 772-781.
71. Craun, K.J., et al., *The National Geospatial Technical Operations Center*, in *Fact Sheet*. 2009.
72. Kelly, W.R. and G.S. Roadcap. *Shallow ground-water chemistry in the Lake Calumet area, Chicago, Illinois*. in *of the National Symposium on Water Quality*. 1994. American Water Resources Association, .
73. Dingman, S.L., *Physical Hydrology*. Second ed. 2002, Upper Saddle River: Prentice Hall. 646.
74. Bester, M.L., et al., *Numerical Investigation of Road Salt Impact on an Urban Wellfield*. Ground Water, 2006. **44**(2): p. 165-175.
75. Kelly, W.R., S.V. Panno, and K.C. Hackley, *Impacts of Road Salt Runoff on Water Quality of the Chicago, Illinois, Region*. Environmental & Engineering Geoscience, 2012. **18**(1): p. 65-81.
76. Panno, S.V., et al., *Database for the Characterization and Identification of the Sources of Sodium and Chloride in Natural Waters of Illinois*, I.S.G. Survey, Editor. 2005, Illinois State Geological Survey: Champaign, Illinois. p. 21.
77. Boutt, D.F., et al., *Identifying potential land use-derived solute sources to stream baseflow using ground water models and GIS*. Ground Water, 2001. **39**(1): p. 24-34.
78. Corsi, S.R., et al., *River chloride trends in snow-affected urban watersheds: increasing concentrations outpace urban growth rate and are common among all seasons*. Science of The Total Environment, 2015. **508**: p. 488-497.
79. Lax, S.M., *Estimating stream chloride concentrations as a function of land use change for two small watersheds in central Illinois*, in *Geography-Geology*. 2007, Illinois State University: Normal, IL. p. 44.
80. Kelly, W.R., et al., *Using chloride and other ions to trace sewage and road salt in the Illinois Waterway*. Applied Geochemistry, 2010. **25**(5): p. 661-673.
81. Panno, S.V., et al., *Estimating background and threshold nitrate concentrations using probability graphs*. Ground Water, 2006. **44**(5): p. 697-709.
82. Roadcap, G.S. and W.R. Kelly, *Shallow ground-water quality and hydrogeology of the Lake Calumet area, Chicago, Illinois*. 1994: Illinois State Water Survey.
83. Eggert, M., R. Rowley, and E.W. Peterson, *Chloride Levels in Illinois Rivers and Streams*, in *AAG Annual Meeting*. 2015: Chicago, IL.

Title: Supplement Report—Spatial and temporal modeling of road salts in a watershed with urban and agricultural land use

Research Category: Water quality

Keywords: Deicers; Road Salts; Transport & Fate; Modeling

Principal Investigator: Eric W. Peterson

Academic Rank: Professor

University: Illinois State University

Email: ewpeter@ilstu.edu

Phone: 309-438-7865

Congressional District: 105th

I. Follow Up Activities since May 2017

Since May 2017, the project has been picked up by an incoming MS student, Andrew Oberhelman. Mr. Oberhelman is building off of the earlier work, but has changed the watershed of interest to explore questions raised from the previous work and to better address the questions he has developed. Upon examining earlier work, a question concerning the role of agriculture in introducing chloride to a system in non-urban areas was posited. It is also unclear why salinization is observed in rural basins where salt application is minimal compared to heavily urbanized ones. Road salt contributes a portion, but no study has considered the role of agricultural Cl^- sources in salinization. To assess the role of agriculture, Cl^- sources must be identifiable and the importance of their contribution assessed in multi-use basins. Ratios of Cl^- to other ions like bromide⁻ and sodium show potential for such evaluations. Andrew is examining that question with his work. Additionally, Andrew will explore the importance of storm events to Cl^- load dynamics at basin scales. Specifically, his thesis explores the role of storm events and source in Cl^- dynamics is warranted. His thesis will:

- (1) Investigate the contribution of storm events to Cl^- transport in multi-land use watershed
 - a. What is the role of storm events in chloride load?
 - b. What is the contribution of storm events to Cl^- load among the seasons?
- (2) Differentiate the signature of urban and agricultural Cl^- with chemical ratios in a multi-land use watershed.
 - a. Do waters from urban and agricultural sources will have different Cl^- ratios?
 - b. Can Cl^- sources be identified?

II. Students supported - Update

A total of five students were involved in the project: Graduate students Jessica Ludwikowski and Lucas Chabela; Undergraduate students Kyagaba David Lwanga, Alan Jensen; and Clint Updike. Direct support was provided to Mr. Chabela, Mr. Jensen, and Mr. Updike. Ms. Ludwikowski and Mr. Lwanga were involved through independent research. Below, I provide an update on their status.

Jessica Ludwikowski – MS 2016, Ms. Ludwikowski is still employed as an **Environmental Control Engineer with the** Cook County Department of Environmental Control.

Lucas Chabela – MS 2017, Mr. Chabela took a position with Terracon, in Milwaukee, WI.

Kyagaba David Lwanga – BS 2016, Mr. Lwanga took a position as a GIS analyst at ExteNet Systems in Lisle, IL. He has seeking to begin a graduate degree.

Alan Jensen – BS 2016, Mr. Jensen continues to work for Mostardi Platt, an environmental consulting firm in Chicago.

Clint Updike – BS expected 2019

III. Publications

a. Peer-Reviewed Academic Journals

Ludwikowski, J.*, and **Peterson, E. W.**, *in press*, Transport and accumulation of chloride in a urban-rural watershed.: Hydrogeology Journal, doi:10.1007/s10040-018-1732-3

A second manuscript drawing from the thesis by Lucas Chabela is drafted and is being reviewed by Mr. Chabela. The manuscript will be submitted this summer

b. Presentations

Peterson, E.W., Ludwikowski, J.*, and Chabela, L.*, (2018) Transport and fate of chloride within the groundwater of a mixed urban and agricultural watershed, Illinois Lake Management Association, 33rd Annual Conference, March 22,201

Modeling the integration of green infrastructure into urban landscapes using a reliability-based framework

Basic Information

Title:	Modeling the integration of green infrastructure into urban landscapes using a reliability-based framework
Project Number:	2017IL329B
Start Date:	3/1/2017
End Date:	2/28/2018
Funding Source:	104B
Congressional District:	IL-013
Research Category:	Engineering
Focus Categories:	Management and Planning, Climatological Processes, Floods
Descriptors:	None
Principal Investigators:	Ashlynn S. Stillwell, Reshmina William

Publications

There are no publications.

Modeling and the integration of green infrastructure into urban landscapes using a reliability-based framework

Research category: Engineering

Student category: Graduate

Keywords: green infrastructure; network reliability; stormwater mitigation

Principal Investigator:

Ashlynn S. Stillwell, Ph.D.
Assistant Professor
University of Illinois at Urbana-Champaign
ashlynn@illinois.edu
(217) 244-6507

Co-Principal Investigator:

Reshmina William, E.I.T.
Graduate Research Assistant
University of Illinois at Urbana-Champaign
willi149@illinois.edu

Congressional district: 13th Congressional district of Illinois

Final Report: Modeling the integration of green infrastructure into urban landscapes using a reliability-based framework

WATER RESOURCES CONTEXT

Urbanization has led to a dramatic increase in local flooding and poor water quality. The rapid increase in impervious area has meant less infiltration and more runoff, which often carries with it a range of contaminants, including heavy metals, fertilizers, and pesticides [1]. For cities with combined sewer networks, another challenge is degradation of local receiving waters through combined sewer overflows (CSOs). CSO events typically occur when excess rainfall or snowmelt overwhelms existing conveyance and treatment capacities [2]. During these events, local water bodies are subject to significant loadings of microbial, sediment, nutrient, and heavy metal contamination, often in violation of USEPA water quality standards [2-5]. These effects are exacerbated by climate change, which is predicted to increase the frequency of high-intensity storm events in cities such as Chicago [6].

To meet USEPA water quality standards, cities such as Chicago have historically turned to large-scale grey-infrastructure alternatives to store and treat excess stormwater. However, these projects are often expensive, inflexible, and have long construction timeframes. Green infrastructure, which uses natural elements and processes to provide key ecosystem services [7], has been suggested as a complementary approach to grey infrastructure. In fact, multiple studies indicate that a combination of green and grey infrastructure is crucial to expanding existing sewer services at a reasonable cost without creating adverse environmental impacts [8,9]. Furthermore, green infrastructure has been repeatedly proven to have multiple benefits in terms of ecological function, air and water quality, temperature control, mitigation of the urban heat island effect, runoff reduction, and even public health [10-21]. However, many of these benefits are highly variable. While green infrastructure typically shows great mitigating ability for smaller storms with shorter return periods, this ability is greatly reduced during high-intensity events [21-23]. Antecedent soil moisture conditions, inter-storm duration, soil texture, media depth, and vegetation type also have a significant impact on green infrastructure performance [21-25].

Quantifying the hydrologic performance of green infrastructure remains as an emerging gap in water resources management. We address a key element of green infrastructure variability that was previously unexplored: the impact of green infrastructure placement within an existing network. While many studies have been conducted regarding the spatial optimization of green infrastructure within urban environments, few have investigated the synergy between green infrastructure and existing grey infrastructure in a probabilistic fashion [26,27]. Due to the high levels of uncertainty associated with green infrastructure performance, a reliability-based framework is especially well suited to analyzing the suitability of green infrastructure for different performance objectives. This research quantitatively assesses the impact of the geographic placement of green infrastructure within an existing urban network on the system's ability to reliably mitigate urban flooding challenges.

SUMMARY OF RESEARCH OBJECTIVES

In our work using reliability analysis to quantitatively assess the performance of green infrastructure, we used the following research objectives to guide our work:

1. Characterize modular green infrastructure performance within a reliability framework.

To quantify green infrastructure performance in a reliability context, we created modular fragility curves representing the probability of failure for a model rain garden under different forcing conditions to test the effect of maintenance schedules and antecedent moisture conditions.

2. Probabilistically assess the spatial characterization of green infrastructure placement with respect to the performance of existing sewersheds.

Building on the modular fragility curves, we have introduced this reliability analysis approach into models of a sewershed representative of a U.S. urban area. In future work, this fragility framework will support network-scale assessment of failure.

3. Understand and assess the incorporation of risk-defined paradigms into urban planning policy.

Stormwater policy currently lacks consideration of risk and reliability in its formulation. Using reliability analysis tools, we suggest approaches for introducing risk-defined paradigms into stormwater policy.

MAJOR FINDINGS

Probabilistic approaches are needed to quantify and account for uncertainties in green infrastructure performance. One approach to quantifying performance reliability is through the use of fragility functions. Fragility is defined as the conditional probability of attaining or exceeding a specified standard of performance conditioned on different demand variables (i.e., loading intensity measures). Originally developed in the field of earthquake engineering [28,29], fragility functions have been used in multiple other applications [30,31], including flood control [32,33]. William and Stillwell [34] developed a methodology to generate fragility curves for green stormwater infrastructure (GSI) to study the reliability of a green roof under different storm conditions. While the methodology was illustrated using a green roof case study, it is flexible enough to be extended to many other failure modes and types of green infrastructure.

Rain garden modeling

General methodology

Failure for green infrastructure can be defined in terms of different hydrologic or environmental standards and targets. We define failure as the inability of the green infrastructure, here a rain garden, to reduce runoff volume below a specified percentage of the effluent from a similarly-sized paved area. Following the conventional notation in reliability analysis [30,35], Equation 1 mathematically defines the conditional probability of failure F for a given rainfall magnitude r .

$$F = P(\alpha V_{paved}(\mathbf{x}, r) - V_{GSI}(\mathbf{x}, r) < 0 \mid r) \quad (\text{Eq. 1})$$

where α is a specified fractional “reduction standard”, \mathbf{x} is a vector of state-variables that define the state of the paved area and the green infrastructure, r is the rainfall magnitude, V_{paved} is the runoff volume from the paved area, and V_{GSI} is the runoff volume from the green infrastructure. In the context of reliability analysis, $\alpha V_{paved}(\mathbf{x}, r)$ represents the capacity of the green infrastructure and $V_{GSI}(\mathbf{x}, r)$ represents the demand the green infrastructure is subject to for a given rainfall of magnitude r .

We develop fragility functions for green infrastructure accounting for the changes over time of the state variables due to the increasing clogging. The change in the state variables \mathbf{x} is modeled using stochastic life-cycle analysis (SLCA) [36-38]. SLCA models the deterioration of infrastructure as occurring either “gradually” and/or as a sequence of “shock” events. Gradual deterioration takes place over a span of time, while shocks are essentially instantaneous. At the time scale over which a GSI becomes clogged (i.e., several years), the storm events that wash total suspended sediment (TSS) into the structure leading to clogging can be modeled as shocks. According to SLCA, two components are required to model shock deterioration: 1) the characteristics of the shocks, including frequency and intensity; and 2) the change of the state variables \mathbf{x} due to a shock of a given intensity.

To quantify the effects of shock deterioration on future infrastructure performance, Jia et al. (2017) use a metric called the “instantaneous reliability”. Instantaneous reliability (Q) (given in Equation 2) is defined as

$$Q = 1 - P_f(t) = 1 - \int F[r(t)] f[r(t)] dr \quad (\text{Eq. 2})$$

where P_f is the probability of failure at a future time t defined as the integral of F (defined in Equation 1) at time t multiplied by the probability density function (PDF) of $r(t)$ also at time t , $f[r(t)]$. The instantaneous reliability is a metric for system functionality, since it allows the quantification of future performance over the entire fragility curve based on current deterioration. For a system undergoing clogging, we expect Q to decrease over time, with sharp decreases at shock events (i.e., storms).

Based on a mathematical modeling of $\mathbf{x}(t)$ as the clogging processes progress and the fragility curves in Equation 1 as functions of \mathbf{x} , we determine the time until maintenance is required to restore system functionality due to clogging. The vector \mathbf{x} contains the following variables: the rain garden saturated hydraulic conductivity in mm/hr ($ksat$), the seepage rate into the surrounding soil in mm/hr (*seepage*), soil porosity (*porosity*), soil thickness in mm (*thickness*), and initial saturated fraction (*sat.frac*). The methodology used to determine the time taken to clog a green infrastructure installation follows two main steps, as shown in Figure 1. Step 1, shown in black boxes, involves changing the saturated hydraulic conductivity ($ksat$) to examine how it affects the resulting fragility curves; calculating the instantaneous reliability (Q) for each fragility curve; defining a relationship between Q and $ksat$; and using this relationship to find the acceptable value $ksat_{acc}$ corresponding to a given acceptable value of Q_{acc} . Step 2, shown in grey boxes, is an iterative while loop. Firstly, we determine whether a storm happens in a given month, and if so, how many storms occur, and how large they are, based on the distribution $f[r(t)]$. These results are used to determine the influent volume and the new $ksat$. Mathematical descriptions of these processes are detailed in the following sections. We then use the results from Step 1 to determine how the green infrastructure responds to a given storm, and to ascertain whether or not $ksat_{acc}$ has been reached. If it has, the value of the time step is output. If not, the cycle is repeated. This process is repeated 450 times to create a probability distribution of the time to clogging (t_{final}) for different influent TSS concentrations.

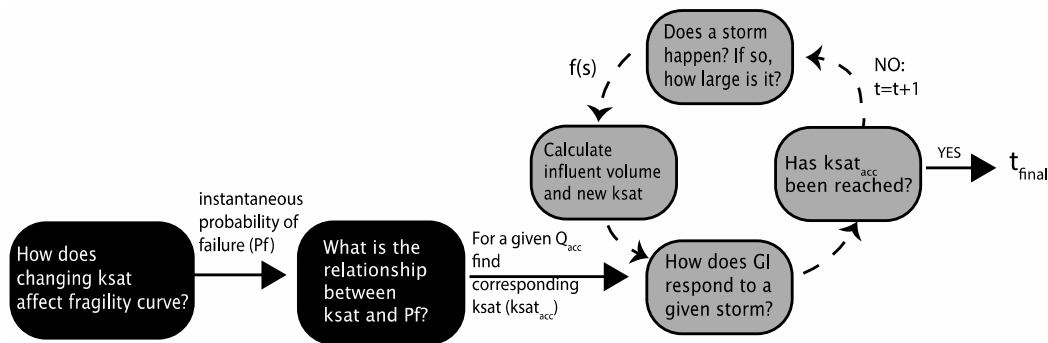


Figure 1. The general methodology for determining the probability distribution of the mean time to clogged is a two-stage process. The process is repeated 450 times to determine the probability distribution for the time to clogging.

Model setup and calibration

Rain gardens, planted areas designed to collect and infiltrate stormwater runoff, are a form of green infrastructure commonly used in urban areas [39]. We create a model “test” rain garden

using EPA-SWMM, and calibrate and validate the model using data provided by the U.S. Geological Survey for a rain garden field site in Madison, WI (William Selbig, personal communication, July 13th 2016). The Madison rain garden was constructed in 2003, and is around 9.3 m² (100 ft²) in area, draining a 46-m² (500-ft²) asphalt shingle roof. The native surrounding soil is a clay loam; the rain garden itself is filled with a sandy loam mixed with screened compost. Hydrological and climate measurements (including rainfall, relative humidity (RH), net radiation, wind speed, temperature, soil moisture, ponding depth, and runoff volume) were taken over the course of five years. In this analysis, data from summer 2006 are used in calibration and validation as an example of a particularly wet season with multiple different-sized rainfall events.

To test the ability of the model to respond accurately to multiple storm events, the model calibration encompasses a 16-day period from July 12th – July 28th. A warm up time of one month of rainfall data is used. Calibration parameters are mainly chosen from the soil layer of the model, although the seepage rate is also a significant calibration parameter. Using calibrated parameters, the calculated Nash-Sutcliffe Efficiency (NSE) for this time period is 0.76, within the bounds of effectiveness set by Moriasi et al. [40]. The chosen parameter values are reasonable based upon literature values taken from the SWMM User Manual. A shorter validation period was chosen on August 24th to test the ability of the model to respond to single, larger storm events. The NSE calculated for this event is 0.71. The SWMM model is thus considered an appropriate representation of the hydrologic responses of the system under real conditions.

Creating the capacity and demand models

We conduct a regression analysis to model the relationship between effluent runoff volume from the calibrated rain garden for two-hour duration storms and five variables related to the garden's vegetation and soil parameters. The probability distributions of each of these variables are based on the calibration or on literature. Thirty-five scenarios randomly sampled from the distributions of the seven variables are batch-processed in SWMM. We calculate regressions for different design storms to illustrate how the rain garden responded hydrologically to different storm conditions.

The regression fits for the demand ($V_{GSI}(x, r)$) are divided into three sections based on the quantity of runoff generated for storms within that section. Section 1 contains storms with less than 30 mm (1.2 in) precipitation, which produce no runoff at most values of $ksat$ and thus have very low probabilities of failure. Section 2 contains storms between 30 mm and 48 mm (1.9 in) of precipitation, which produce a combination of runoff and no runoff, depending on the values of the input variables. The regressions for Section 2 storms follow a two-stage process: a logistic regression to separate outputs into storms producing runoff versus those not producing runoff, and a linear regression between the square root of the volumetric runoff and saturated hydraulic conductivity, porosity, and precipitation. The accuracy of the logistic regression (ratio of the number of true matches over the total number of cases) is 96%. Section 3 contains all storms larger than 48 mm (1.9 in) of precipitation. These storms follow a linear relationship between the volumetric runoff and saturated hydraulic conductivity, seepage rate, porosity, and precipitation. Table 1 contains coefficient values, model form, and adjusted R-squared (representing goodness-of-fit) for each of the three sections. Figure 2 shows a plot of fitted volume versus calculated volume for Sections 2 and 3, along with the respective standard deviations.

Table 1. Model form, coefficient values and R-squared for each of the three sections, for $ksat$ in mm/hr, $seepage$ in mm/hr, and r in mm.

Section	Model form	Coefficient values	Adjusted R-squared
Section 1 ($r < 30$ mm) ($r < 1.2$ in)	$V = 0$	N/A	N/A
Section 2 (30 mm $\leq r < 48$ mm) (1.2 in $\leq r < 1.9$ in)	$h = \frac{1}{1 + e^{25.1 + 0.43ksat + 19.8porosity - 1.02r}}$ $V^{0.5} = \begin{cases} \theta_0 + \theta_1porosity + \theta_2ksat + \theta_3r, & h > 0.5 \\ 0, & otherwise \end{cases}$	θ_0 -9.13	Accuracy= 0.96, R ² = 0.83
		θ_1 -7.02	
		θ_2 -5.26	
		θ_3 0.46	
Section 3 ($r \geq 48$ mm) ($r \geq 1.9$ in)	$V = \theta_0 + \theta_1seepage + \theta_2porosity + \theta_3ksat + \theta_4r$	θ_0 -133	0.97
		θ_1 2.45	
		θ_2 -5.23	
		θ_3 -1.90	
		θ_4 5.19	

Rosner tests are used as appropriate to remove outlier points, while backwards stepwise regression is used to reduce the number of variables and simplify the model. All of the model coefficients are statistically significant ($p < 0.05$). To calculate the capacity ($\alpha V_{paved}(x, r)$), we create a new SWMM model by removing the bioretention LID module and increasing the impervious fraction of the subcatchment to 100%, effectively ‘paving over’ the rain garden surface. The relationship between precipitation (in mm) and runoff volume depth (mm) for a paved surface is linear, as shown in Equation 3.

$$V = 5.35r - 3.56 \quad (R^2 = 1) \quad (\text{Eq. 3})$$

Modeling the clogging process

Based on reporting from the SWMM user manual as well as literature [41], we identify saturated hydraulic conductivity $ksat$ as the primary random variable affected by progressive clogging. While clogging can be based on biochemical as well as physical processes [41], we chose to base our modeling of clogging on sediment deposition, a physical process. TSS is a major source of clogging impairment in bioretention cells and rain gardens, particularly for those without pre-treatment.

In modeling clogging, SWMM uses an empirical ‘clogging factor’ to decrease $ksat$ proportional to the volume of water influent into the bioretention cell. Rather than using this approach, we chose to follow the more precise logistic regression proposed by Viviani and Iovino [41]. We use the logistic regression model because of its mathematical simplicity, but also because it captures the $ksat$ asymptotic decay observed in many field studies of green infrastructure [23,42,43]. The relationship between $ksat$ and the TSS cumulative loading density L_{TSS} (the influent loading in terms of depth multiplied by the influent concentration) can be described as shown in Equation 4, where a and b are empirical parameters dependent on the type of soil in question. In this analysis, we chose a as $0.02 \text{ m}^2/\text{g}$ and b as 0.513 based on Viviani and Iovino’s [41] calculated values for a loam soil loaded with artificial wastewater (containing only suspended solids and no organic matter).

$$ksat(\tau_1) = \frac{ksat(\tau_2)}{1 + aL_{TSS}^b} \quad (\text{Eq. 4})$$

Modeling the shock events

The distribution of rainfall is modeled as a compound (or spiked) Poisson process. Compound Poisson processes are defined as stochastic processes with random jumps that are distributed via a Poisson distribution. If the Poisson rate parameter is denoted by λ and the jump size magnitude has a distribution G , then a compound Poisson process is defined as given in Equation 5, where $N(t)$ is a Poisson process with rate λ , and D_i are independent and identically distributed random variables with distribution G [44]. A similar distribution was used by Ozturk [45] to describe the distribution of monthly rainfall.

$$Y(t) = \sum_{i=1}^{N(t)} D_i \quad (\text{Eq. 5})$$

We model storm frequency and magnitude within a monthly timeframe based on 50 years of daily precipitation data (from 1977-2017) taken from the NOAA gage in northwest Urbana, IL. These precipitation data are used to generate a generic rainfall input as a scenario analysis using the test rain garden model. The best fit probability density function of storm occurrence ($N(t)$) within any given month is a Poisson distribution with rate 9.79. The best fit distribution G of the storm magnitudes is defined as a gamma distribution with shape parameter $\alpha=0.52$ and rate parameter $\beta=1.54$. All events are assumed to be independent and identically distributed.

Modular fragility curves

Results

The fragility curve of the as-built rain garden, shown in Figure 2, highlights the three distinct regions used in the regression analysis. The ± 1 -sigma uncertainty bounds are created using the methodology described in Gardoni et al. [28] to capture the epistemic uncertainty in the model parameters. Storms below 48 mm (1.9 in) of precipitation (Sections 1 and 2) have negligible probabilities of failure. These low values are unsurprising, given that many rain garden design standards specify a minimum volumetric retention depth on the order of 25 mm (1 in) of runoff. Storms above 48 mm show a rapid increase in the probability of failure.

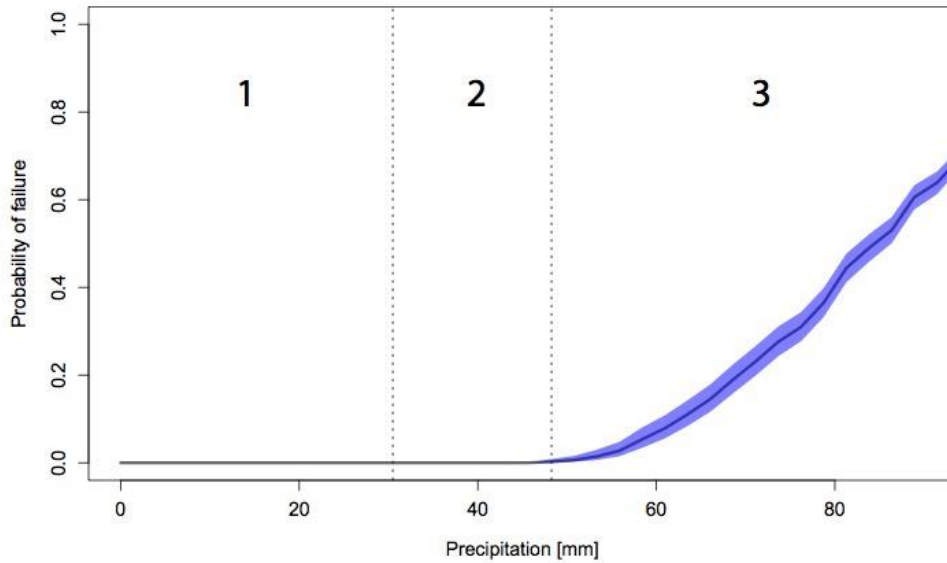


Figure 2. The as-built fragility curve for 80% volume reduction for a two-hour duration storm is divided into three distinct sections.

Figure 3 plots the fragility curves for the rain garden after clogging (i.e., at reduced levels of $ksat$). The impact of $ksat$ on rain garden failure is significant, particularly for larger storms. As the garden becomes more clogged, the curves shift up and to the left; smaller storms begin to generate runoff. The overall shape of the curve also changes, with clogged curves showing steeper slopes in the early portion of the graph compared to the as-built curve. The graphs' curvatures also change as the system becomes more clogged. The unclogged, as-built system is concave, with a large increase in the conditional probability of failure for storms above a certain threshold. At lower $ksat$, the fragility curves tend towards a convex shape, reaching an asymptotic maximum failure at much smaller storm magnitudes.

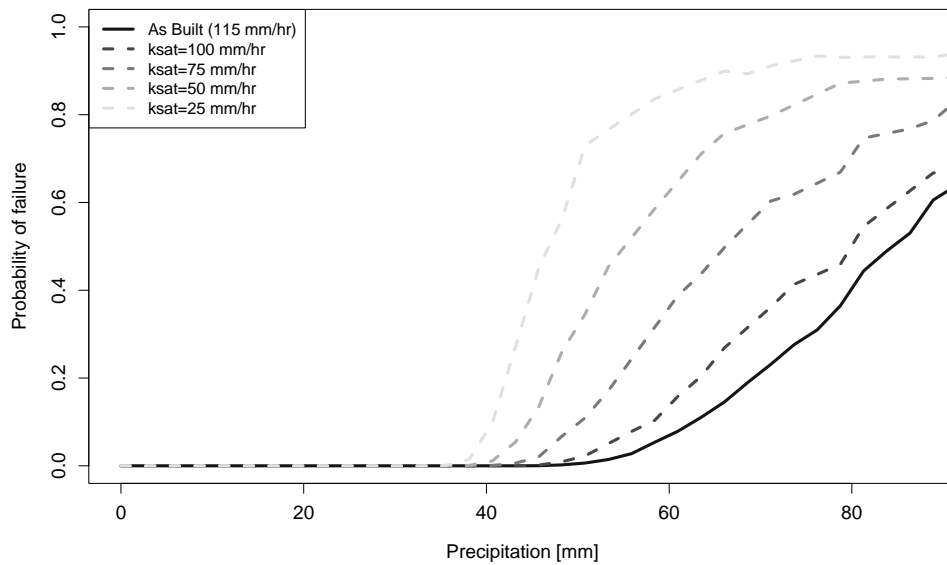


Figure 3. Changing the $ksat$ via clogging significantly alters the shape of the fragility curve.

The rapid increase in the conditional probability of failure as a result of decreasing $ksat$ leads to larger instantaneous probability of failure, and thus lower instantaneous reliability. As shown in Figure 4, instantaneous reliability decreases rapidly over time. Each “step” in the graph represents a storm or series of storms that has taken place in a given month. Months without a decrease in reliability indicate no precipitation. Importantly, because of the probability distribution of the rainfall magnitudes, a large jump in the graph is most likely due to several smaller storms rather than one large storm. As the simulation progresses, reliability asymptotically approaches the limit set by the chosen Q_{acc} (0.9, or a rain garden that performs as expected in nine storm events out of ten). This asymptotic decrease is reflective of the logistic regression used to recursively calculate the $ksat$. The asymptotic decrease in the instantaneous reliability also implies that the rain garden continues to function fairly well, even at low levels of $ksat$.

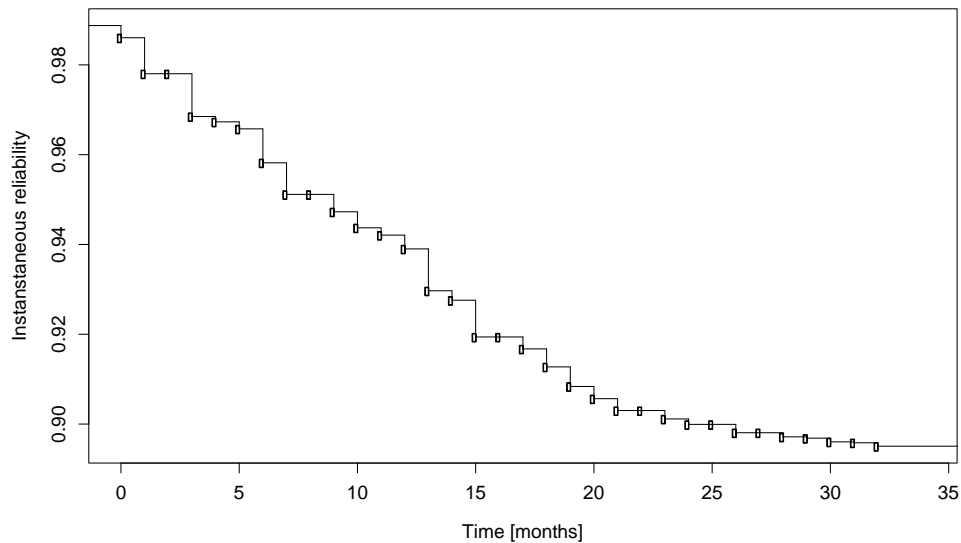


Figure 4. The instantaneous reliability (Q) shows an asymptotic decay towards the chosen threshold reliability (0.9) over time.

Finally, Figure 5 shows the change in the cumulative distribution function (CDF) of the time to clog for different influent concentrations of TSS. The three influent concentrations are chosen as representative of runoff effluent from a roof gutter system (10 mg/L), runoff influent to a typical rain garden with some pre-treatment (40 mg/L), and runoff from a parking lot without pre-treatment (297 mg/L) [46-47]. The 40 mg/L curve has a mean time to clogged of approximately 34 months, in contrast to approximately 66 months for 10 mg/L and approximately 15 months for 297 mg/L. Intuitively, these values make sense, since higher loadings of suspended sediments would tend to clog the system more quickly: many existing rain garden systems use pre-treatment for this reason. Interestingly, the general slope of the CDF decreases with decreasing TSS concentrations: the 10 mg/L CDF has an estimated standard deviation of 7 months, while the 40 mg/L CDF has a standard deviation of 5 months, and the 297 mg/L CDF has a standard deviation of 3 months. The reason for this trend is that the lower concentration CDF is more sensitive to the random distribution of rainfall events; a cluster of large storms tends to clog the system more quickly. In the case of the high concentration CDF, this effect is less pronounced, since every storm already carries a high sediment loading regardless of its size. The error bounds on the CDFs also increase with decreasing TSS concentration, illustrating that the effects of uncertainty in the model parameters are also more pronounced.

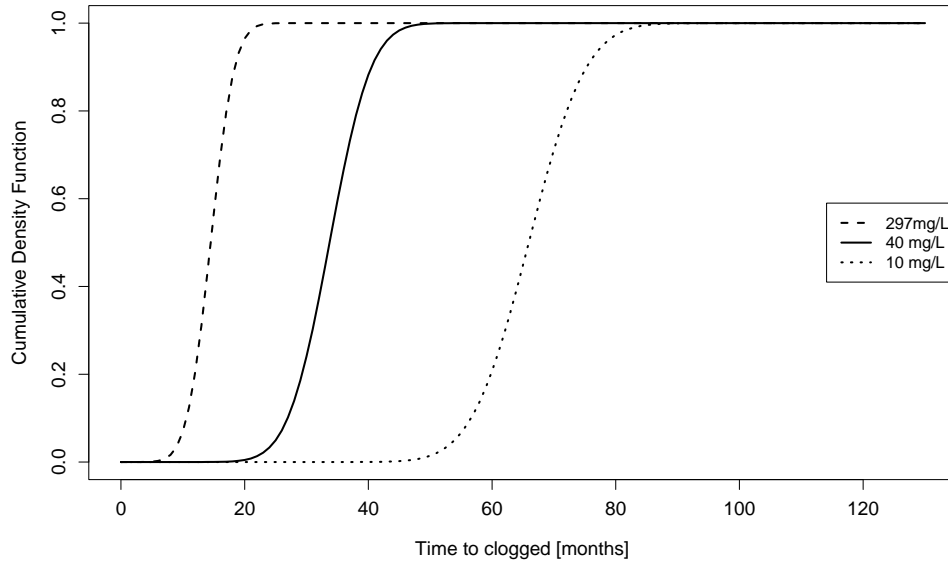


Figure 5. Changing the influent TSS concentration alters the cumulative probability density of the time to clogged. The shaded areas correspond to the error bounds on the CDF.

Discussion

The reliability analysis of rain garden clogging suggests that monitoring and maintenance should ideally be conducted on average every 3 years (based on model results of 34 months to clogged conditions) to ensure optimal performance. Importantly, this analysis assumes a high performance standard for the considered rain garden since the garden was designed to retain and infiltrate the majority of the stormwater that fell on the property. Using a lower performance standard would help to increase the time window for maintenance. The rain garden on which the SWMM model was based is also highly oversized: during the period of study, there were very few events that generated any runoff from the rain garden [48]. The oversized nature of this rain garden correspondingly leads to very low probabilities of failure in the model results.

Rain garden volumetric retention is greatly decreased for larger storm events, which reduces its overall future performance ability. Moreover, clogging increases the probability that smaller storms will begin to generate runoff. As expected, mean clogging time decreases with increasing influent TSS concentration. However, the standard deviation also decreases, implying that while rain garden pre-treatment does improve long-term performance, it also produces high performance variability due to the sensitivity of performance on rainfall distribution. While the methodology is described for a generic rain garden model calibrated with specific empirical data, the method can easily be adapted to other types of infiltration-based green infrastructure and for other forcings, like back-to-back rainfall events.

Although the model presents a first attempt at using a reliability-based approach to evaluate the performance of a rain garden over time, it is still highly simplified. The model assumes a uniform effect of clogging throughout the soil thickness, while literature suggests that clogging typically manifests in the top few inches of the bioretention column [41]. In addition, many other factors impact the change in $ksat$ other than influent TSS. For instance, Le Coustumer et al. [43] indicate that the presence of coarse-root vegetation in the bioretention cell can help decrease the likelihood of clogging. Other studies [49] also showed that while $ksat$ decreases rapidly in bioretention cells within the first six months of planting, cells recovered functionality due to plant macropore processes. In addition, Mehring and Levin [50] suggest that rain garden ecology and

a flourishing macrofauna can have important impacts on maintaining infiltration capacity. Earthworm burrows can increase infiltration rates by factors of 2 to 15 in terrestrial systems. In addition, their burrows create preferential flow paths under wet conditions. Other burrowing invertebrates such as termites and ants can also have the same effect [50]. While rain garden sizing can also be used to mitigate potential clogging [43], field inspections of bioretention cells in North Carolina revealed that over half of the bioretention cells were undersized [51].

Another factor that was not considered was the buildup of sediment in the upstream treated area between storm events, which could alter influent concentrations. However, previous research has found that no correlation exists between first flush and antecedent dry weather period [52]. The phenomenon of a greater proportion of pollutant loads being washed off surfaces early on in the storm, leading to variable influent concentrations, is known as 'first flush'. This study evaluates the effects of long-term clogging on rain garden performance, and so excludes the first flush effect, instead assuming constant concentrations based on average reported concentrations from rainfall collected over several sizes of storms.

Using this reliability analysis framework, we have expanded the approach to consider the impact of antecedent moisture conditions in green infrastructure performance. Analysis of back-to-back rainfall storms is on-going for the same model rain garden.

Sewershed analysis

Modular fragility curves represent the probability of failure of a single green infrastructure installation. Scaling these modular curves, we create a framework for analyzing green infrastructure performance in a network context for a given sewershed. We created an ArcPy script, tested using data from Kennilworth, IL as shown in Figure 6, to find appropriate locations for different types of green infrastructure in each drainage area. These results support a final ArcMap file with all the data needed to import into MIKE URBAN.



Figure 6. An ArcPy script selects appropriate locations for different types of green infrastructure based on existing information about a drainage area.

MIKE URBAN is a 2D urban water modeling software that uses the MOUSE modeling engine and GIS integration for stability and physical soundness. MIKE URBAN has been used in previous studies modeling large scale urban flooding, sewer surcharge, and stormwater

drainage [53,54]. The program uses a low-impact development interface similar to the one used by SWMM.

A sewershed in the Gwynn Falls subwatershed in West Baltimore is selected for this analysis. The area is mostly residential, with several large parking lots and tenement housing. Parts of the sewershed are also comprised of single family residences and parkland. Storm sewer data were collected from the City of Baltimore data archives [55]; digital elevation model (DEM) and orthophoto datasets were collected from the National Map Viewer [56]; and soil data were collected from the NRCS soil survey [57]. Modular fragility curves will be used to estimate the volumetric reduction potential of a given form of green infrastructure added to the MIKE URBAN model. Future work will demonstrate the network fragility framework for this Gwynn Falls subwatershed to clarify what is the lowest amount green infrastructure added to the system that will improve system reliability from the perspective of reduced volumetric discharge.

Stormwater policy analysis

Some important policy topics related to green infrastructure implementation naturally arise out of this research. Most importantly, because of the decentralized nature of green infrastructure, a need exists to consider the implications of using public investment for the private implementation of a distributed solution to a public goods problem. This issue has major repercussions in terms of the efficacy of implementing large-scale non-point pollution protection in the form of a Total Maximum Daily Load (TMDL). We addressed some of these challenges from an economic standpoint, using a collaborative game theory framework to evaluate the effectiveness of three policies commonly used to incentivize green infrastructure implementation [58]; the results were published previously in *Water Resources Research*. Importantly, the results specifically suggest that stormwater fees do not significantly affect urban environmental impacts. Although municipal regulation generally has the largest environmental impact, the consideration of which policy option is “best” needs to be evaluated in context for each individual case.

While game theory is a useful strategy in addressing the issue of public-private investment in green infrastructure, it assumes that human beings are rational actors driven by economic incentives. Although using a game theoretic approach to capture human interactions is a significant step forward from an engineered, optimization-based approach, it does not capture the full complexity of human motivation. We use literature from environmental psychology to expand stormwater policy analysis and suggest some additional approaches to promote green infrastructure implementation in individual communities. Literature suggests that socially-based approaches to motivating sustainability lead to long-lasting positive behavioral change [59]. In particular, the appropriate use of descriptive norms (information on the actions our communities perform regularly) and injunctive norms (information on what behaviors are approved of or frowned upon) can significantly alter behavior [60, 61]. This idea of community-based behavioral change is deeply rooted in the psychological foundation of Self Determination Theory, which postulates that human behavior is motivated by *autonomy*, *competence*, and *relatedness* [62]. Thus, a rain garden incentives program that is grass-roots-driven, uses peer role models, facilitates social interactions, and encourages the development of new personal skills and abilities (e.g., gardening) is likely to be environmentally, economically, and socially sustainable.

PROJECT TEAM

The project team included PI Ashlynn Stillwell, Assistant Professor, and Co-PI Reshmina William, Ph.D. student, both in the Department of Civil and Environmental Engineering at the University of Illinois at Urbana-Champaign. Additional research support came from Undergraduate Research Assistant Gabrielle Bethke, who was funded by the CEE Research Experiences for Undergraduates program.

PUBLICATIONS

One publication based on this work is currently under review at the *Journal of Sustainable Water in the Built Environment* and another manuscript is in preparation to submit to *Water Resources Research*. Results from each of the research objectives will contribute to on-going work by Co-PI Reshmina William and will appear in her Ph.D. dissertation prior to her anticipated graduation May 2019.

REFERENCES

- [1] Water Environment Federation (WEF). (1998). Urban Runoff Quality Management. In *WEF Manual of Practice No. 23* (Chapter 1). WEF: Alexandria, VA.
- [2] Pongmala, K., Autixier, L., Madoux-Humery, A., Fuamba, M., Galarneau, M., Sauvé, S., Prévost, M. & Dorner, S. (2015). Modeling total suspended solids, *E. coli* and carbamezpine, a tracer of wastewater contamination from combined sewer overflows. *Journal of Hydrology*, 531, 830-839.
- [3] Arnone, R. & Walling, J. (2007). Waterborne pathogens in urban watersheds. *Journal of Water and Health*, 5(1), 149-162.
- [4] Chambers, P., Allard, M., Walker, S., Marsalek, J., Lawrence, J., Servos, M., Busnarda, J., Munger, K., Adare, K., Jefferson, C., Kent, R. & Wong, M. (1997). Impacts of municipal wastewater effluents on Canadian waters: A review. *Water Quality Research Journal of Canada*, 32(4), 659-713.
- [5] Ellis, B. & Yu, W. (1995). Bacteriology of urban runoff: The combined sewer as a bacterial reactor and generator. *Water Science and Technology*, 31(7), 303-310.
- [6] Changnon, S. & Westcott, N. (2002). Heavy rainstorms in Chicago: Increasing frequency, altered impacts, and future implications. *Journal of the American Water Resources Association*, 38(5), 1467-1475.
- [7] Benedict, M. & McMahon, E. (2006). *Green infrastructure: Linking landscapes and communities*. Washington, DC: Island Press.
- [8] City of New York Department of Environmental Protection. (2014). *Report for post-construction monitoring green infrastructure neighborhood demonstration areas*. New York: City of New York Bureau of Sustainability.
- [9] Wang, R., Eckelman, M., & Zimmerman, J. (2013). Consequential environmental and economic life cycle assessment of green and gray stormwater infrastructures for combined sewer systems. *Environmental Science and Technology*, 47, 11189-11198.
- [10] Oberdorfer, E. Lundholm, J. Rass, B., Coffman, R., Doshi, H., Dunnett, N., Gaffin, S., Kohler, M., Liu, K. & Rowe, B. (2007). Green roofs as urban ecosystems: Ecological structures, functions and services. *BioScience*, 57 (10), 823-833.
- [11] Rowe, D. (2011). Green roofs as a means of pollution abatement. *Environmental Pollution*, 159 (9), 2100-2110. <http://dx.doi.org/10.1016/j.envpol.2010.10.029>.
- [12] Baik, J., Kwak, K., Park, S. & Ryu, Y. (2012). Effects of building roof greening on air quality in street canyons. *Atmospheric Environment*, 61, 48-55.
- [13] Mentens, J., Raes, D., & Hermy, M. (2005). Green roofs as a tool for solving the rainwater runoff problem in the urbanized 21st century? *Landscape and Urban Planning*, 77, 21–226.
- [14] Moran, A., Hunt, B., & Smith, J. (2005). Hydrologic and water quality performance from green roofs in Goldsboro and Raleigh, North Carolina. *Third Annual Greening Rooftops for Sustainable Communities Conference, Awards and Trade Show* (pp. 4–6). Washington, DC: Green Infrastructure Foundation.
- [15] Getter, K., & Rowe, D. (2006). The role of extensive green roofs in sustainable development. *HortScience*, 41(5), 1276-1285.
- [16] Carter, T., & Rasmussen, T. (2006). Hydrologic behavior of vegetated roofs. *Journal of the American Water Resources Association*, 42(5), 1261-1274.
- [17] Gagliano, A., Detommaso, M., Nocera, F., & Evola, G. (2015). A multi-criteria methodology for comparing the energy and environmental behavior of cool, green and traditional roofs. *Building and Environment*, 90, 71-81.
- [18] Santamouris, M. (2015). Regulating the damaged thermostat of the cities: Status, impacts and mitigation challenges. *Energy and Buildings*, 91, 43-56.
- [19] Niachou, A., Papakonstantinou, K., Santamouris, M., Tsangrassoulis, A., & Mihalakakou, G. (2001). Analysis of the green roof thermal properties and investigation of its energy performance. *Energy and Buildings*, 33, 719-729.

- [20] Virk, G., Jansz, A., Mavrogianni, A., Mylona, A., Stocker, J., and Davies, M. (2015). Microclimatic effects of green and cool roofs in London and their impacts on energy use for a typical office building. *Energy and Buildings*, 88, 214-228.
- [21] William, R., Goodwell, A., Richardson, M., Le, P., Kumar, P., Stillwell, A. (2016). An environmental cost-benefit analysis of alternative green roofing strategies. *Ecological Engineering*, 95, 1-9.
- [22] Holman-Dodds, J., Bradley, A., & Potter, K. (2003). Evaluation of hydrologic benefits of infiltration based urban stormwater management. *Journal of the American Water Resources Association*, 39(1), 205-215.
- [23] Davis, A. (2008). Field performance of bioretention: Hydrology impacts. *Journal of Hydrologic Engineering*, 13(2), 90-95.
- [24] Vanuytrecht, E., Van Mechlen, C., Van Meerbeek, K., Willems, P., Hermy, M., & Raes, D. (2014). Runoff and vegetation stress of green roofs under different climate change scenarios. *Landscape and Urban Planning*, 122, 68-77.
- [25] VanWoert, N., Rowe, D., Andresen, J., Rugh, C., Fernandez, R., & Xiao, L. (2005). Green roof retention: Effects of roof surface, slope and media depth. *Journal of Environmental Quality*, 34, 1036-1044.
- [26] Giacomoni, M. (2015). Low Impact Development Placement Investigation using a Multi-Objective Evolutionary Optimization Algorithm. *Proceedings of the World Environmental and Water Resources Congress: Floods, Droughts and Ecosystems*. Austin, TX: ASCE.
- [27] Damodaram, C. & Zechman, E. (2013). Simulation-Optimization approach to design low impact development for managing peak flow alterations in urbanizing watersheds. *Journal of Water Resources Planning and Management*, 139(3), 290-298.
- [28] Gardoni, P., Der Kiureghian, A., & Mosalam, K. M. (2002). Probabilistic Capacity Models and Fragility Estimates for Reinforced Concrete Columns based on Experimental Observations. *Journal of Engineering Mechanics*, 128(10), 1024–1038. [http://doi.org/10.1061/\(ASCE\)0733-9399\(2002\)128:10\(1024\)](http://doi.org/10.1061/(ASCE)0733-9399(2002)128:10(1024))
- [29] Gardoni, P., Mosalam, K. M., & Der Kiureghian, A. (2003). Probabilistic seismic demand models and fragility estimates for RC bridges. *Journal of Earthquake Engineering*, 7(1), 79–106.
- [30] Gardoni, P. (Ed.). (2017). *Risk and reliability analysis: Theory and applications*. Springer.
- [31] Gardoni, P., & LaFave, J. (Eds.). (2016). *Multi-hazard approaches to civil infrastructure engineering*. Springer.
- [32] Sayers, P., Flickweert, J., & Kortenhaus, A. (2012). Supporting flood risk management through better infrastructure design and management. In P. Sayers (Ed.), *Flood risk: Planning, design and management of flood defense infrastructure* (pp. 73–101). London: ICE Publishing.
- [33] Stewart, D. (2012). Urban drainage systems. In P. Sayers (Ed.), *Flood risk: Planning, design and management of flood defense infrastructure* (pp. 139–171). London: ICE Publishing.
- [34] William, R., & Stillwell, A. S. (2017). Use of fragility curves to evaluate the performance of green roofs. *Journal of Sustainable Water in the Built Environment*, 3(4), 04017010.
- [35] Ditlevsen, O., & Madsen, H. (1996). *Structural reliability methods* (2.3). Wiley.
- [36] Jia, G., Tabandeh, A., & Gardoni, P. (2017). Life cycle analysis of engineering systems: Modeling deterioration, instantaneous reliability, and resilience. In P. Gardoni (Ed.), *Risk and reliability analysis: Theory and applications* (pp. 465–494). Springer International Publishing. <http://doi.org/10.1007/978-3-319-52425-2>
- [37] Kumar, R., & Gardoni, P. (2012). Modeling structural degradation of RC bridge columns subjected to earthquakes and their fragility estimates. *Journal of Structural Engineering*, 138(1), 42–51.
- [38] Kumar, R., Cline, D., & Gardoni, P. (2015). A stochastic framework to model deterioration in engineering systems. *Structural Safety*, 53, 36–43.
- [39] Chini, C., Canning, J., Schreiber, K., Peschel, J., & Stillwell, A. (2017). The Green Experiment: Cities, Green Stormwater Infrastructure, and Sustainability. *Sustainability*, 9(1), 105. <http://doi.org/10.3390/su9010105>
- [40] Moriasi, D. N., Arnold, J. G., Van Liew, M. W., Binger, R. L., Harmel, R. D., & Veith, T. L. (2007). Model evaluation guidelines for systematic quantification of accuracy in watershed simulations. In *Transactions of the ASABE* (Vol. 50, pp. 885–900). <http://doi.org/10.13031/2013.23153>
- [41] Viviani, G., & Iovino, M. (2004). Wastewater reuse effects on soil hydraulic conductivity. *Journal of Irrigation and Drainage Engineering*, 130(6), 476–484. [http://doi.org/10.1061/\(ASCE\)0733-9437\(2004\)130:6\(476\)](http://doi.org/10.1061/(ASCE)0733-9437(2004)130:6(476))
- [42] Li, H., & Davis, A. (2008). Urban Particle Capture in Bioretention Media. II: Theory and Model Development. *Journal of Environmental Engineering*, 134(6), 419–432. [http://doi.org/10.1061/\(ASCE\)0733-9372\(2008\)134:6\(419\)](http://doi.org/10.1061/(ASCE)0733-9372(2008)134:6(419))
- [43] Le Coustumer, S., Fletcher, T. D., Deletic, A., Barraud, S., & Poelsma, P. (2012). The influence of design

- parameters on clogging of stormwater biofilters: A large-scale column study. *Water Research*, 46(20), 6743–6752. <http://doi.org/10.1016/j.watres.2012.01.026>
- [44] Siegrist, K. (2003). Compound Poisson Process. Retrieved from <http://www.math.uah.edu/stat/poisson/Compound.html>
- [45] Ozturk, A. (1981). On the study of a probability distribution for precipitation totals. *Journal of Applied Meteorology*, 20, 1499–1505.
- [46] Fuerhacker, M., Haile, T., Monai, B., & Mentler, A. (2011). Performance of a filtration system with filter media for parking lot runoff treatment. *Desalination*, 275, 118–125.
- [47] Wright Water Engineers and Geosyntec Consultants. (2010). International Stormwater Best Management Practices (BMP) Database User's Guide for BMP Data Entry Spreadsheets, (August).
- [48] Selbig, W., & Balster, N. (2010). *Evaluation of turf-grass and prairie-vegetated rain gardens in a clay and sand soil, Madison, Wisconsin, Water Years 2004-2008*. Reston, VA.
- [49] Hatt, B., Fletcher, T., & Deletic, A. (2009). Hydrologic and pollutant removal performance of stormwater bioinfiltration systems at the field scale. *Journal of Hydrology*, 365(3), 310–321.
- [50] Mehring, A. S., & Levin, L. A. (2015). Potential roles of soil fauna in improving the efficiency of rain gardens used as natural stormwater treatment systems. *Journal of Applied Ecology*, 52(6), 1445–1454. <http://doi.org/10.1111/1365-2664.12525>
- [51] Wardynski, B. J., & Hunt, W. F. (2012). Are Bioretention Cells Being Installed Per Design Standards in North Carolina? A Field Study. *Journal of Environmental Engineering*, 138(12), 1210–1217. [http://doi.org/10.1061/\(ASCE\)EE.1943-7870.0000575](http://doi.org/10.1061/(ASCE)EE.1943-7870.0000575)
- [52] Lee, J., Bang, K., Ketchum, L., Choe, J., & Yu, M. (2002). First flush analysis of urban storm runoff. *Science of The Total Environment*, 293, 163–175.
- [53] D. Bisht, C. Chatterjee, S. Kalakoti, P. Upadhyay, M. Sahoo, and A. Panda, “Modeling urban floods and drainage using SWMM and MIKE URBAN: a case study,” *Nat. Hazards*, vol. 84, pp. 749–776, 2016.
- [54] L. Locatelli *et al.*, “Modelling the impact of retention-detention units on sewer surcharge and peak and annual runoff reduction,” *Water Sci. Technol.*, vol. 1, no. 6, pp. 898–903, 2015.
- [55] C. of Baltimore, “City of Baltimore Geographic Information System data.” City of Baltimore, Baltimore, MD, 2017.
- [56] USGS, “The National Map Viewer,” 2017. [Online]. Available: <https://viewer.nationalmap.gov/advanced-viewer/>.
- [57] NRCS, “Web Soil Survey,” 2017. [Online]. Available: <https://websoilsurvey.sc.egov.usda.gov/App/WebSoilSurvey.aspx>.
- [58] R. William, J. Garg, and A. S. Stillwell, “A game theory analysis of green infrastructure stormwater management policies,” *Water Resour. Res.*, vol. 53, no. 9, pp. 8003–8019, 2017.
- [59] McKenzie-Mohr, D. (2010). *Fostering Sustainable Behavior: Community-Based Social Marketing* [electronic version]. Retrieved from <http://www.cbsm.com/pages/guide/preface/>
- [60] Aronson, E., and O'Leary, M. (1982). The relative effectiveness of models and prompts on energy conservation: A field experiment in shower room. *Journal of Environmental Systems*, 12,219-224.
- [61] Cialdini, R., Demaine, L., Sagarin, B., Barret, D., Rhoads, K., & Winter, P. (2006). Managing social norms for persuasive impact. *Social Influence*, 1(1), 3-15.
- [62] Ryan, R., & Deci, E. (2000). Self determination theory and the facilitation of intrinsic motivation, social development, and well-being. *American Psychologist*, 55, 68-78.

Identifying nitrogen removal limitations in constructed wetlands treating agricultural tile drainage

Basic Information

Title:	Identifying nitrogen removal limitations in constructed wetlands treating agricultural tile drainage
Project Number:	2017IL330B
Start Date:	3/1/2017
End Date:	2/28/2019
Funding Source:	104B
Congressional District:	IL-16
Research Category:	Engineering
Focus Categories:	Agriculture, Nutrients, Wetlands
Descriptors:	None
Principal Investigators:	Karl John Rockne

Publications

There are no publications.

Progress report: Identifying nitrogen removal limitations in constructed wetlands treating agricultural tile drainage

Primary research category: Agriculture and Engineering

Secondary research category: Water Quality and Biological Sciences

Keywords. Agriculture, drain tile, nutrients, water quality, denitrification, wetland

PI: Karl Rockne, PhD, PE, M.ASCE

Professor and Interim Head

University of Illinois at Chicago

842 W. Taylor St., M/C 246

Chicago, IL 60607

krockne@uic.edu

312-413-0391

Student PI: Mahsa Izadmehr

PhD student in Environmental Engineering,

Department of Civil and Materials Engineering

University of Illinois at Chicago

842 W. Taylor St., M/C 246

Chicago, IL 60607

Mizadm2@uic.edu

312-413-7638

Introduction

Aquatic hypoxia results from the depletion of oxygen in the water column due to excessive organic matter loading from photosynthetic algal growth stimulated by high levels of the nutrient elements nitrogen (N) and phosphorus (P). Once the algae die, their cells are oxidized by bacteria that consume oxygen at a rate higher than it can be replenished, resulting in hypoxia that results in fish kills and damage to other aquatic animals that require oxygen.

Water column hypoxia was first discovered on a massive scale in the northern Gulf of Mexico,¹ which was accompanied by large fish kills. Coastal hypoxia has since been found in many estuaries around the world.² Research has demonstrated that nutrient loading to the Gulf of Mexico (the ultimate cause of the hypoxia) comes from the agricultural Midwest through the Mississippi River (Fig. 1). Further, the state of Illinois is the largest single contributor of both N and P loading to the Gulf.^{2,3} To combat this problem, agreements have been made to manage nutrient loading in Midwestern states, and as part of this plan the state of Illinois has pledged to reduce N and P loading to the Mississippi River by 20% by the year 2020, and 45% by 2040.⁴

Given that 80% of N and 50% of P loading is from rural farms in Illinois, a focus of nutrient reduction efforts has been on agriculture. Although source control through reduced usage of fertilizer is a primary solution strategy, nutrient releases are inevitable from farms. Various strategies to capture these releases have been proposed, among which “nutrient farming”⁶ has shown promise. One type of nutrient farming involves the capture of nutrients in a wetland to stimulate the growth of wetland plants that uptake N and P while they grow. Although the biogeochemical cycles of N and P are relatively well-understood at the local scale, reaction processes can frequently be difficult to elucidate at the field scale where heterogeneous phase transformations take place. N has a more complex biogeochemical cycle than P because of the existence of gaseous forms (N₂, N₂O and un-ionized NH₃), as well as its role as an electron

acceptor (NO_3^-) utilized by denitrifying bacteria, or as an electron donor (NH_3) by nitrifying bacteria.

An important aspect of the denitrification process is that the end product is N_2 gas, which is environmentally benign and leaves the system. As such, denitrification can result in significant nutrient removal. A general equation to describe how denitrifying bacteria ("Cells") grow while oxidizing an electron donor (ED) coupled with the complete denitrification of nitrate to dinitrogen gas (N_2) is:



In this case, the electron donor is typically a fermentation product like acetate or H_2 that results naturally from the breakdown of organic matter in the sediment.

Agricultural fields with subsurface tile drainage will have dramatically enhanced subsurface flows, and research clearly demonstrates that tile drainage results in the rapid export of surface-applied N and P fertilizers to receiving waters. In Illinois and the upper Midwest, extensive tile drainage has resulted in high levels nitrate in surface waters contributing to eutrophication and poor water quality. Constructed wetlands hold promise as a treatment option to mitigate these non-point source nutrient loads by capturing P and creating conditions to stimulate denitrification for the removal of N.

Updated Timeline

In February 2018, we had requested and received a 12-month no cost extension on the award due to issues getting started. This report details our progress on the award during the last project period, and our plans for the next period.

Research Hypothesis H1. The results of the 2016 sampling campaign have demonstrated that denitrification/N removal has been quite limited in the wetland. Given that the system has high amounts of electron acceptor (nitrate), equation 1 suggests that either electron donor is limited (organic matter in the sediment), or the system is biologically limited. The latter could occur if denitrifying bacteria ("Cells") cannot utilize the nitrate fast enough because of a short contact time (hydraulically overloaded), or sufficient time has not yet passed for the enrichment of a robust population of denitrifiers in the sediment. Based upon this analysis, I propose the following two hypotheses to guide this research:

H1. *An electron donor limited system will have low levels of biodegradable organic matter present in the sediment.*

C1. *A corollary to H1 is Growth of the wetland plants will increase levels of biodegradable organic matter in the wetland sediment.*

Experimental Methodology for testing H1. Testing H1 will necessitate a characterization of the wetland sediments (the source of electron donors to drive denitrification). For this research, I propose to use the state-of-the art technique of Differential Scanning Calorimetry/Thermogravimetric Analysis (DSC-TG) that has been used in the soil science literature to quantitatively characterize the bioavailability and biodegradability of soil OM. This equipment is available for a contract fee at the Research Resource Center (RRC) at the University of Illinois (UIC).

The results of the DSC-TG analyses on sediment samples early in the season and following a full growing season in 2016 will allow me to assess whether the biodegradability of soil OM was high in the wetland sediment, and whether the extensive growth of wetland plants observed during the year resulted in an increase in soil OM. Comparison of the soil OM characteristics in

samples from early in 2016 to those sampled later will allow me to test whether sufficient biodegradable OM is present in the wetland sediments, and whether biodegradable OM has been enriched by wetland plant growth. The null hypothesis would be that soil OM levels and biodegradability were low/unchanged over time.

Research Hypothesis H2. The second possible explanation for the limited denitrification activity in the wetland is biological. While nitrate levels are high, it is possible that the microbial community in the sediments has not been enriched with denitrifiers to a level that would support active denitrification. Based on this, I propose a second hypothesis as follows.

H2. High levels of nitrate in the inlet water have resulted in increases in the denitrifying bacteria populations in the wetland sediments over time.

Experimental Methodology for testing H2. The molecular biological technique of 16S rRNA sequencing is a common method to quantitatively characterize the microbial communities (“microbiome”) in various environmental niches. To assess H2, I propose to extract DNA from preserved and new sediment samples from the wetland for sequencing and analysis of 16S rRNA using an Illumina HiSeq2000 and MiSeq next generation DNA sequencing. DNA extraction is done routinely in our laboratory at UIC, and the sequencing can be done via contract with the DNA core facility at the RRC at UIC. Phylogenetic alignment of the resulting data will be performed using the Metagenomics Raster Server (MG-RAST) at Argonne National Laboratory for metagenomics analysis¹¹ and microbiome characterization.

Hypothesis Testing. H2 will be tested by performing 16S rRNA sequencing on preserved sediment samples that have been obtained monthly at each 2 cm from water-sediment interface. Characterization of the microbiome and quantification of known denitrifiers in sediment samples at various depths will allow me to assess the presence and development of the denitrifying microbial population over time and with depth in the sediment. In addition to quantifying known denitrifying bacteria, these data will allow me to quantitatively analyze other important microbial communities in the sediment, including fermenters, ANNAMOx, and nitrifying bacteria. The null hypothesis would be that no known denitrifiers are present, and/or their population levels are not enhanced over time during the development of the wetland.

Summary. I have proposed a series of measurements to test two hypotheses I have formulated to help explain the lack of denitrification in the treatment wetland. Successfully identifying limits to denitrification in treatment wetlands will help us to design these low-cost systems to more efficiently remove N and facilitate their widespread use by farmers to help Illinois achieve its mandated nutrient reduction targets

Background

The performance of wetland W_1 in Bureau County has been monitored since Spring 2016, which removed 12% and 35% of influent NO_3^- in 2016 and 2017, respectively, with very high removal (70-80%) observed in summer 2017. Research efforts have focused on addressing the **fundamental hypothesis driving this investigation that a combination of low levels of labile organic electron donor and microbial community structure adaptation limits denitrification in a wetland treating tile drainage.**

Progress

Work has progressed on obtaining data to test the project hypothesis on two fronts: genomic information to characterize the microbial community and geochemical information to characterize the lability of the organic matter in the wetland sediment.

Sediment cores have been obtained throughout wetland W₁ over the course of multiple years. Cores were obtained at nine sites within the wetland on a bi-monthly basis during the ice-free season, as well as from two sites on a more frequent basis. The sediment cores were sectioned at various depths from the sediment-water interface, and the segments were homogenized for analysis.

DNA was extracted from 288 samples using established protocols for soil and sediment analysis. The DNA extracts were sequenced using the DNA core facility at the University of Illinois at Chicago. The large set of genomic data is currently being analyzed with the assistance of a microbiologist from the Department of Biological Sciences at the University of Illinois at Chicago.

The lability of the sediment organic matter is being assessed using differential scanning calorimetry/thermal gravimetric analysis. This technique utilizes detailed measurement of heat flux during precision heating of the samples to determine the energy in the organic matter bonds as they are thermally broken down. These data can be used to determine a ratio of recalcitrant organic matter to labile, easily degradable organic matter. Results so far are strongly supportive of the hypothesis that growth of plants in the wetland has created more degradable organic matter in the sediments in 2017 compared to 2016.

Dissemination

This project will be presented at the American Society of Civil Engineering Environmental Water Resources Institute (ASCE-EWRI) World Congress next month. Mahsa Izadmehr was notified she is a top-three finalist for the best graduate student paper award.

Plans for the next project period

The thermal characterization will be finished and the genomic data analysis will continue during the next project period. It is notable that the size of the dataset is quite large, thus necessitating access to a dedicated genomic data pipeline, thus necessitating our collaboration with Biological Sciences.

With the acquisition of the OM and genomic data, we will be testing our hypotheses. Statistical comparisons will be made between the lability of the OM in different operation years, and the spatial and temporal evolution of the wetland sediment microbiome will be characterized during the two year development of the treatment wetland. We anticipate having all data acquired and analysis nearing completion by the fall meeting.

Evaluating the ability of wetland mitigation banks in the Chicago region to replace plant species lost to impacts to natural wetlands

Basic Information

Title:	Evaluating the ability of wetland mitigation banks in the Chicago region to replace plant species lost to impacts to natural wetlands
Project Number:	2017IL331B
Start Date:	3/1/2017
End Date:	2/28/2019
Funding Source:	104B
Congressional District:	IL-013
Research Category:	Biological Sciences
Focus Categories:	Wetlands, Surface Water, Conservation
Descriptors:	None
Principal Investigators:	Jeffery Matthews

Publications

There are no publications.

Project Title: Evaluating the ability of wetland mitigation banks in the Chicago region to replace plant species lost to impacts to natural wetlands

Student Supported on the Grant:

Stephen C. Tillman, Co-Principal Investigator

M.S. Student and Graduate Research Assistant

Department of Natural Resources and Environmental Sciences

University of Illinois at Urbana-Champaign

stillma2@illinois.edu, (630) 441-8979

Faculty Investigators:

Dr. Jeffrey W. Matthews, Principal Investigator

Assistant Professor

Department of Natural Resources and Environmental Sciences

University of Illinois at Urbana-Champaign

jmatthew@illinois.edu, (217) 244-2168

Proposal Summary

We will use a novel simulation modeling approach to evaluate the ability of wetland mitigation banks to replace the plant species lost in natural wetlands due to permitted impacts. We will test species replacement using plant species lists obtained from wetland banks regulated by the Chicago District of the Army Corps of Engineers and from natural wetlands in the same region, which were surveyed by the Illinois Natural History Survey (INHS) for the Illinois Department of Transportation (IDOT). We will use R software to create a model that simulates impacts to natural wetlands and the resulting transactions that are designed to compensate for these wetland impacts with credits produced by mitigation banks. During each simulation, our model will generate a list of all the plant species lost from natural wetlands due to permitted impacts and a list of the species from the mitigation bank used as compensation. Comparing these lists will allow us to assess the percentage of species from natural wetlands that mitigation banks are able to effectively replace, and to characterize which species tend to be replaced, lost, or gained due to the practice of wetland mitigation banking. We will then manipulate parameters of the model that correspond to real-world policy conditions in order to determine how changes to the policies governing mitigation transactions may affect and improve species replacement by mitigation banks.

Work Completed

We obtained vegetation monitoring reports from the U.S. Environmental Protection Agency for all Chicago District wetland mitigation banks that received final credit release before the summer of 2017. We scanned these documents and copied sitewide plant species lists from each bank, in every year for which data was available. Banks typically undergo final evaluation by regulatory agencies in their fifth year of management and monitoring. We did not have fifth year data from each bank, so we chose to include in our study only those banks for which we have at least one year of data from the bank's fourth through sixth year of monitoring. This left us with 13 banks to include in this study. We acquired sitewide plant species lists from 2,005 natural wetlands from INHS. We transformed species lists from banks and natural wetlands into a common system of plant names so that we will be able to compare them directly to test for species replacement.

Using R software we created a model that can simulate the credit transactions between natural IDOT wetlands that are destroyed and the banks that are used to compensate for these losses. In each trial the model generates a list of the species lost from natural wetlands and gained in the mitigation bank. We can run this model to include each bank in our study, and to replicate trials at each bank. The output of this model is an average species replacement rate at each bank and an average number of new species gained from each bank as a result of the mitigation credit transactions.

We have produced only preliminary quantitative results at this time, but we can provide figures and tables showing the way in which we intend to present our final results, as well as the general trends we expect to find. Figures 1 and 2 show the percentage of species present in natural wetlands that are replaced by banks (Figure 1) and the mean number of species gained in banks (Figure 2) when we vary the mitigation ratio used in the model. Tables 1 and 2 show one way that we intend to examine specific plant species, by presenting the species that are most likely to be gained (Table 1) and lost (Table 2) due to the practice of wetland mitigation banking.

Remaining Work

We will update our model to include, for each plant species, species characteristics obtained from a recently published flora that is specific to the Chicago region (Wilhelm and Rericha 2017). These traits will include native status and a quantitative floristic quality metric. This will allow us to restrict our analysis of species replacement to include only native species and to examine characteristics of the species that are most likely to be lost, replaced, or gained.

We will then run our model under various experimental treatments, manipulating the model parameters to represent real-world mitigation policy conditions. The mitigation policies we will test include geographic restrictions on the area in which transactions can occur and requirements that more mitigation credits be purchased for impacts to natural wetlands of high floristic quality. We will evaluate how the ability of banks to replace the native plant species lost from natural wetlands varies based on these conditions, and we will conduct statistical tests for differences in bank performance based on policy. Once analysis is complete, we will write and submit a final report to the Illinois Water Resources Center. We also intend to submit this report as a manuscript to an academic journal.

References

Wilhelm, G., and L. Rericha. 2017. Flora of the Chicago region: A floristic and ecological synthesis. Indiana Academy of Science, Indianapolis, Indiana, USA.

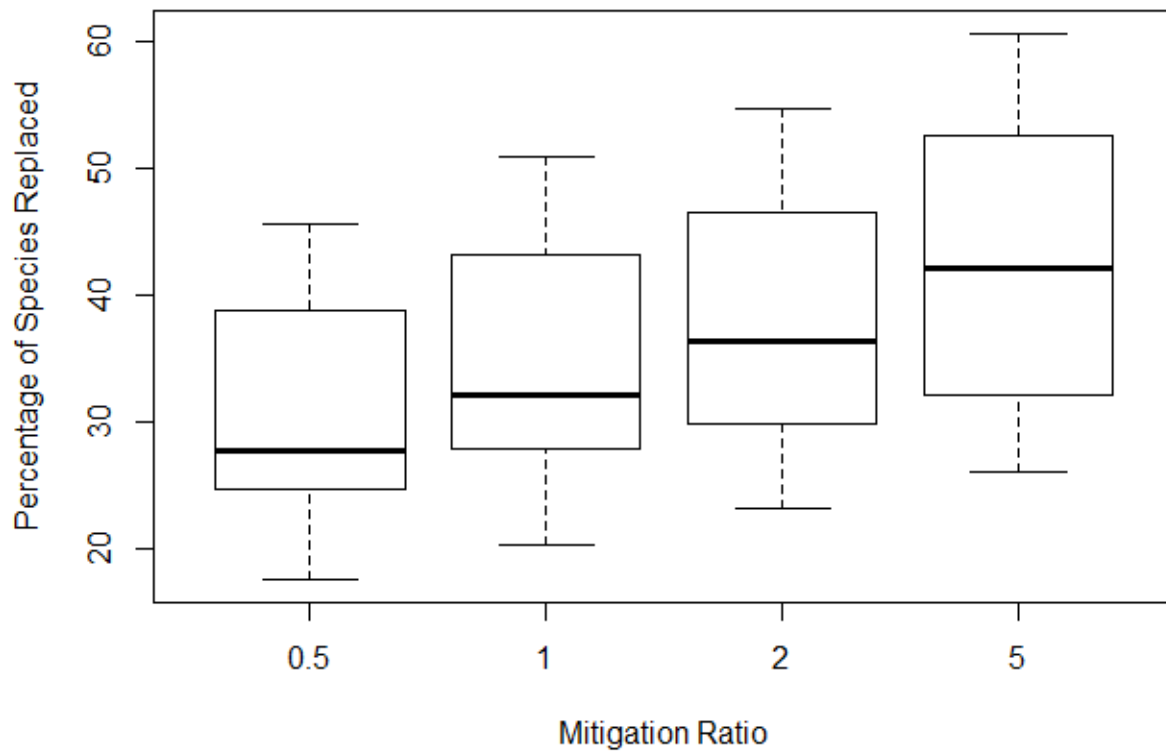


Figure 1. Percentage of species present in natural wetlands that were replaced in mitigation banks during runs of a model simulating credit transactions between natural wetlands and banks. This value was generated at different mitigation ratios. A higher mitigation ratio requires that more credits from a bank be purchased to compensate for each acre of natural wetland lost to permitted impacts. Boxplots show the distribution of percentage of species present values for 13 banks included in the model. The percentage of species present for each individual bank is the mean value of 50 trials.

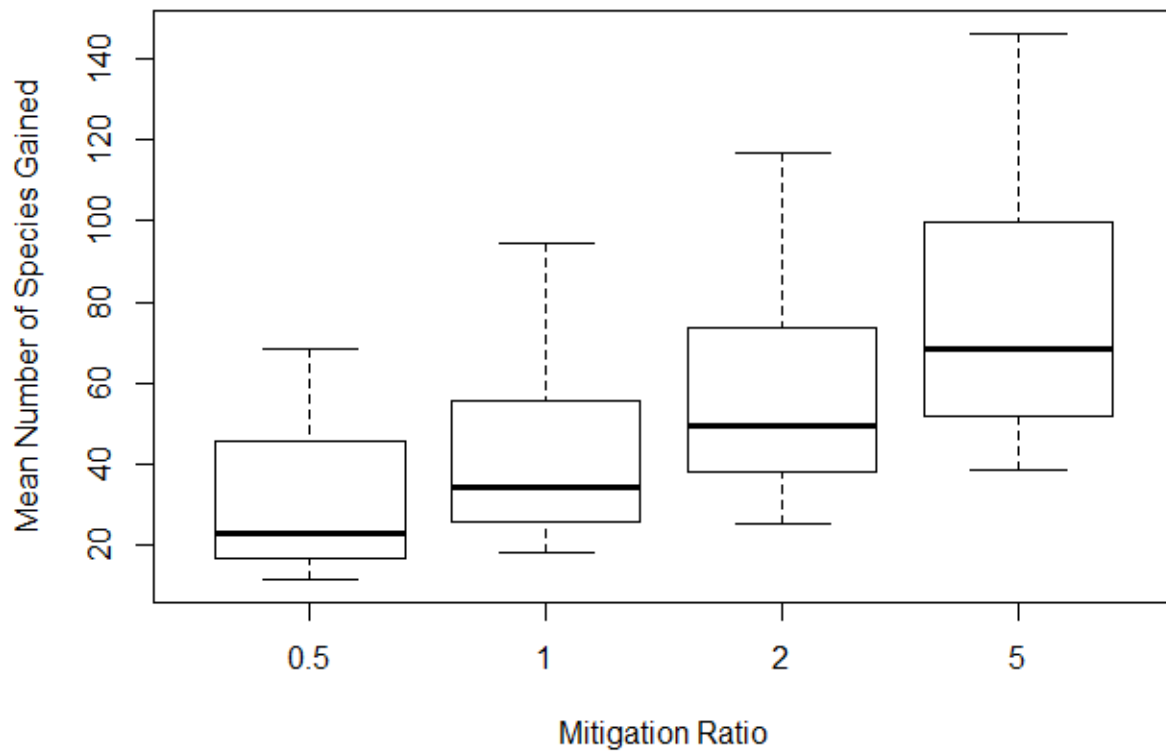


Figure 2. Mean number of plant species present in mitigation banks that were not present in natural wetlands (i.e. species gained) during runs of a model simulating credit transactions between natural wetlands and banks. This value was generated at different mitigation ratios. A higher mitigation ratio requires that more credits from a bank be purchased to compensate for each acre of natural wetland lost to permitted impacts. Boxplots show the distribution of mean number of species gained values for 13 banks included in the model. The mean number of species gained for each individual bank is the mean value of 50 trials.

Table 1. The 25 plant species with the greatest positive difference in frequency between wetland mitigation banks (n=13) and IDOT wetlands (n=2005). This difference is represented by positive values to indicate that these species are likely to be gained through the practice of wetland mitigation banking, since they are more frequent in mitigation banks than in natural IDOT wetlands.

Species	Frequency in Banks	Frequency in IDOT sites	Difference (Bank - IDOT)
<i>Rudbeckia hirta</i>	1.00	0.01	0.99
<i>Silphium perfoliatum</i>	1.00	0.02	0.98
<i>Panicum virgatum</i>	1.00	0.05	0.95
<i>Oenothera biennis</i>	1.00	0.05	0.95
<i>Carex scoparia</i>	0.92	0.00	0.92
<i>Zizia aurea</i>	0.92	0.01	0.91
<i>Juncus effusus</i> var. <i>solutus</i>	0.92	0.01	0.91
<i>Andropogon gerardii</i>	0.92	0.01	0.91
<i>Echinochloa crus-galli</i> *	0.92	0.02	0.90
<i>Potentilla norvegica</i>	0.92	0.02	0.90
<i>Bidens cernua</i>	0.92	0.02	0.90
<i>Penthorum sedoides</i>	0.92	0.04	0.88
<i>Apocynum sibiricum</i>	0.92	0.05	0.88
<i>Helianthus grosseserratus</i>	1.00	0.13	0.87
<i>Juncus torreyi</i>	1.00	0.14	0.86
<i>Daucus carota</i> *	1.00	0.14	0.86
<i>Elymus virginicus</i>	0.92	0.07	0.86
<i>Sagittaria latifolia</i>	0.92	0.07	0.86
<i>Carex vulpinoidea</i>	1.00	0.15	0.85
<i>Aster novae-angliae</i>	0.92	0.07	0.85
<i>Asclepias incarnata</i>	1.00	0.16	0.84
<i>Juncus dudleyi</i>	1.00	0.16	0.84
<i>Elymus canadensis</i>	0.85	0.01	0.84
<i>Ambrosia trifida</i>	1.00	0.17	0.83
<i>Scirpus cyperinus</i>	0.85	0.02	0.83

* Non-native species

Table 2. The 25 plant species with the greatest negative difference in frequency between wetland mitigation banks (n=13) and IDOT wetlands (n=2005). This difference is represented by negative values to indicate that these species are likely to be lost through the practice of wetland mitigation banking, since they are more frequent in natural IDOT wetlands than in mitigation banks.

Species	Frequency in Banks	Frequency in IDOT sites	Difference (Bank - IDOT)
<i>Dipsacus laciniatus</i> *	0.00	0.17	-0.17
<i>Rhamnus cathartica</i> *	0.23	0.37	-0.14
<i>Echinochloa muricata</i>	0.00	0.13	-0.13
<i>Solanum dulcamara</i> *	0.15	0.26	-0.11
<i>Lonicera tatarica</i> *	0.00	0.09	-0.09
<i>Solidago canadensis</i>	0.31	0.39	-0.08
<i>Solidago sempervirens</i>	0.00	0.08	-0.08
<i>Ribes americanum</i>	0.00	0.08	-0.08
<i>Viburnum opulus</i> *	0.00	0.08	-0.08
<i>Parthenocissus quinquefolia</i>	0.15	0.21	-0.06
<i>Atriplex patula</i> *	0.00	0.05	-0.05
<i>Fallopia scandens</i>	0.00	0.05	-0.05
<i>Salix fragilis</i> *	0.00	0.05	-0.05
<i>Rorippa palustris</i> var. <i>palustris</i>	0.00	0.05	-0.05
<i>Fraxinus lanceolata</i>	0.31	0.35	-0.05
<i>Cryptotaenia canadensis</i>	0.00	0.05	-0.05
<i>Sanicula odorata</i>	0.00	0.04	-0.04
<i>Sambucus canadensis</i>	0.15	0.20	-0.04
<i>Antenoron virginianum</i>	0.00	0.04	-0.04
<i>Gleditsia triacanthos</i>	0.00	0.04	-0.04
<i>Agrimonia parviflora</i>	0.00	0.04	-0.04
<i>Aster ontarionis</i>	0.00	0.03	-0.03
<i>Hackelia virginiana</i>	0.00	0.03	-0.03
<i>Ribes missouriense</i>	0.00	0.03	-0.03
<i>Viburnum recognitum</i>	0.00	0.03	-0.03

* Non-native species

Impacts of stormwater-induced road salt runoff on soil and water quality in urban greenspaces

Basic Information

Title:	Impacts of stormwater-induced road salt runoff on soil and water quality in urban greenspaces
Project Number:	2017IL332B
Start Date:	3/1/2017
End Date:	2/28/2018
Funding Source:	104B
Congressional District:	IL-009
Research Category:	Water Quality
Focus Categories:	Climatological Processes, Water Quality, Non Point Pollution
Descriptors:	None
Principal Investigators:	Aaron Packman

Publications

There are no publications.

Impacts of stormwater-induced road salt runoff on soil and water quality in urban greenspaces

Research Category: Water quality

Research Subcategory: Climate and hydrologic processes

Keywords: stormwater, water quality, road salt, urban greenspaces

Congressional District for Northwestern University: IL-009

PIs

1. **Aaron Packman**
Professor of Civil and Environmental Engineering
Northwestern University
a-packman@northwestern.edu
2. **William Miller**
Professor of Chemical and Biological Engineering
Northwestern University
wmmiller@northwestern.edu

Student Co-PIs

1. **Vivien Rivera**
PhD Student
Northwestern University
vivienr@u.northwestern.edu
2. **Liliana Hernandez Gonzalez**
PhD Student
Northwestern University
lilianahernandezgonzalez2014@u.northwestern.edu

Additional students trained as part of this project

1. **Alma Bartholow**
Undergraduate student
Northwestern University
Supported by McCormick Summer Research Grant, Northwestern University
2. **Gabriel Martinez**
Undergraduate student
University of Puerto Rico – Mayaguez
Supported by Summer Research Opportunity Program, Northwestern University
3. **Loren Ayala**
Undergraduate student; MS student
Northwestern University
Supported by Gates Millennium Scholarship

Total students trained through this project: 2 Ph.D., 1 M.S., 3 Undergraduate

Background and Motivation

Deicing, a strategy for improving safety on motorways under freezing conditions, results in a concerning degree of salt accumulation in aquifers in cold regions (Shaw, et al., 2012; Rivett et al., 2016). Large increases in road salt usage in the northern United States in the past 35 years have had a measurable impact on chloride concentrations in glacial aquifers, a drinking water source for a large proportion of the nation (Warner and Ayotte, 2014). Urban planning in areas where deicing is required on a large scale must take the environmental impacts of the practice into account. Contamination of groundwater due to road salt is likely to be a constraint on urban growth, as up to 40% of applied road salt may infiltrate into groundwater (Howard and Maier 2006, Perera et al., 2012). Groundwater storage also constitutes a long-term source of chloride to surface waters, increasing the base concentration of chloride in floodplains even in seasons where salt is not applied (Ledford et al., 2016). These effects can persist for over a century (Shaw et al., 2012). Clearly, there is a critical need to improve deicing to ensure road safety without compromising important natural resources.

Shifts in weather patterns due to climate change require the development of new strategies to manage landscapes and infrastructure for predicted precipitation and temperature regimes. Many climate adaptation strategies incorporate green infrastructure, which serves a vital role in managing stormwater runoff and mitigating the effects of flooding. However, urban greenspaces are sensitive ecosystems, and thus susceptible to degradation by contaminants carried in stormwater and snowmelt runoff, including road salt. It is important that communities are equipped with tools that can inform decisions about precipitation management and road safety measures to ensure that valuable community resources such as green spaces are protected. It is also vital that communities have access to data about the direct effects of such strategies.

This project used a combination of high-frequency sensor data and a dense sampling network to identify pathways of stormwater runoff and road salt transport through an urban prairie. The longterm goal of this work is to develop high-resolution models to understand salt transport to surface water, groundwater, and soil in order to recommend strategies for protection of urban greenspaces. The specific project objectives were: 1) Quantify the impacts of winter deicing salt on soil, surface water, and groundwater in an urban prairie nature preserve; 2) Explore the effects of seasonality, including winter storms, spring snowmelt, and summer flooding events, on salt delivery to and transport within the prairie.

Site Overview

Gensburg Markham Prairie (GMP) is a high-quality Midwestern prairie grassland and ephemeral wetland located in Markham, Illinois. Owned by Northeastern Illinois University (NEIU) and managed by The Nature Conservancy of Illinois (TNC) and NEIU, this site is part of the Indian Boundary Prairies, a larger network of prairie remnants operated by TNC in the Chicago metropolitan area (**Figure 1**). Major roadways Interstate 294 and U.S. Route 57 intersect in the heart of the Indian Boundary Prairie complex and GMP is surrounded on west and east by these two highways. To the north and south, GMP is closely bordered by residential and commercial areas, with major streets associated with roadside drainage ditches.

The major features of the prairie are shown in **Figure 2**. A primary drainage ditch transports runoff from residential areas from west to east at the northern boundary of the prairie. Ditches aligned along parallel north-south lines, remnants of an abandoned residential development project, cut through the prairie. These north-south ditches are disconnected from the main drainage ditch and store surface water in the prairie. In the southern part of the prairie, runoff from residential areas drains into the prairie via an intermittent ditch. Additional surface water storage occurs in a large ephemeral wetland, fed by runoff via a lower swale to the southeast.

Both the ephemeral wetland and the lower swale retain water throughout winter and spring, when both rainfall and snowmelt contribute to surface water. The southwestern part of the prairie is dominated by a higher-elevation beach ridge of medium-grained, well-draining sand, while the low-lying regions of the prairie features silty and clayey soils.

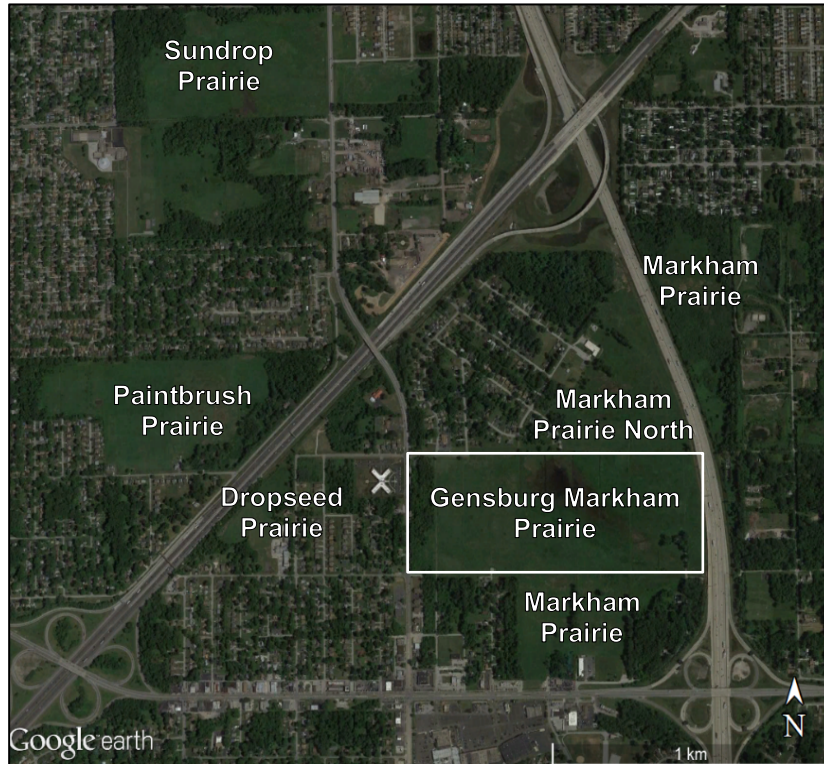


Figure 1: Map of the Indian Boundary Prairies in Markham, IL, including Gensburg Markham Prairie and the surrounding major roadways and residential areas

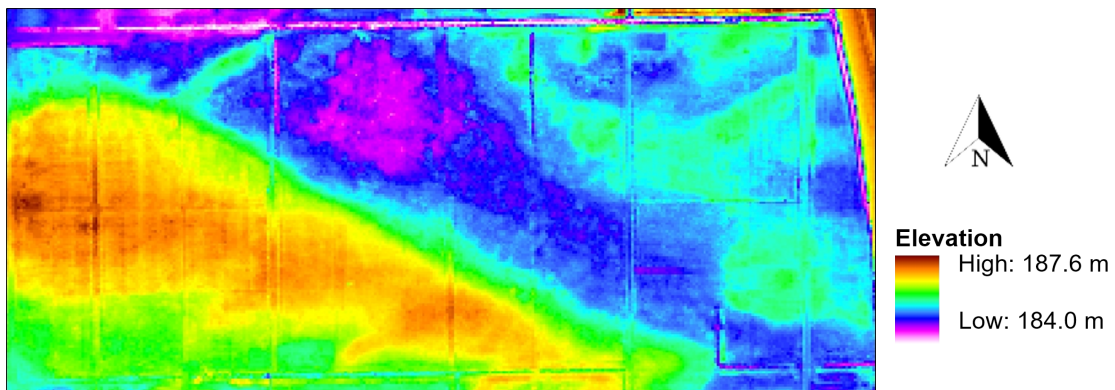


Figure 2: Major features of Gensburg Markham Prairie, including sand ridge, lower swale, drainage ditches, and ephemeral wetland, DEM from 2009 Cook County LiDAR Flyover

Methods

Electrical conductivity (EC) sensors were installed throughout GMP, in soils and in surface waters, and were used in conjunction with a pre-existing sensor network to monitor the influx of road salt components into the site. Sensors implemented as part of prior installation campaigns in 2016 and 2017 include 13 groundwater level sensors in 1-meter wells, 8 surface water level

sensors in surface channels, 2 1-meter soil moisture profile probes with point salinity sensors 20 cm below the ground surface, and a rain gauge. Soil EC sensors, METER GS3 (Meter Group, Inc.) were installed at 15 cm and at 30 cm below the ground surface at each installation location, with two locations near the residential area at the southern edge of the prairie and four locations along the highway at the eastern edge of the prairie. These sensors were aligned along pre-existing transects of water sensors (**Figure 3**). Each transect originates in a surface drainage channel and a water EC sensor, METER ES-2 (Meter Group, Inc.) is installed in each drainage channel, near a surface water level sensor. Water EC sensors are located at the bottom of each channel, as close to the center as possible, and are shielded with open-ended PVC tubing to permit water flow through the sensor head while protecting the sensor from debris. All EC sensors were installed in September 2018. All EC sensors collect data at 30-minute measurement intervals and the data is retrieved monthly.

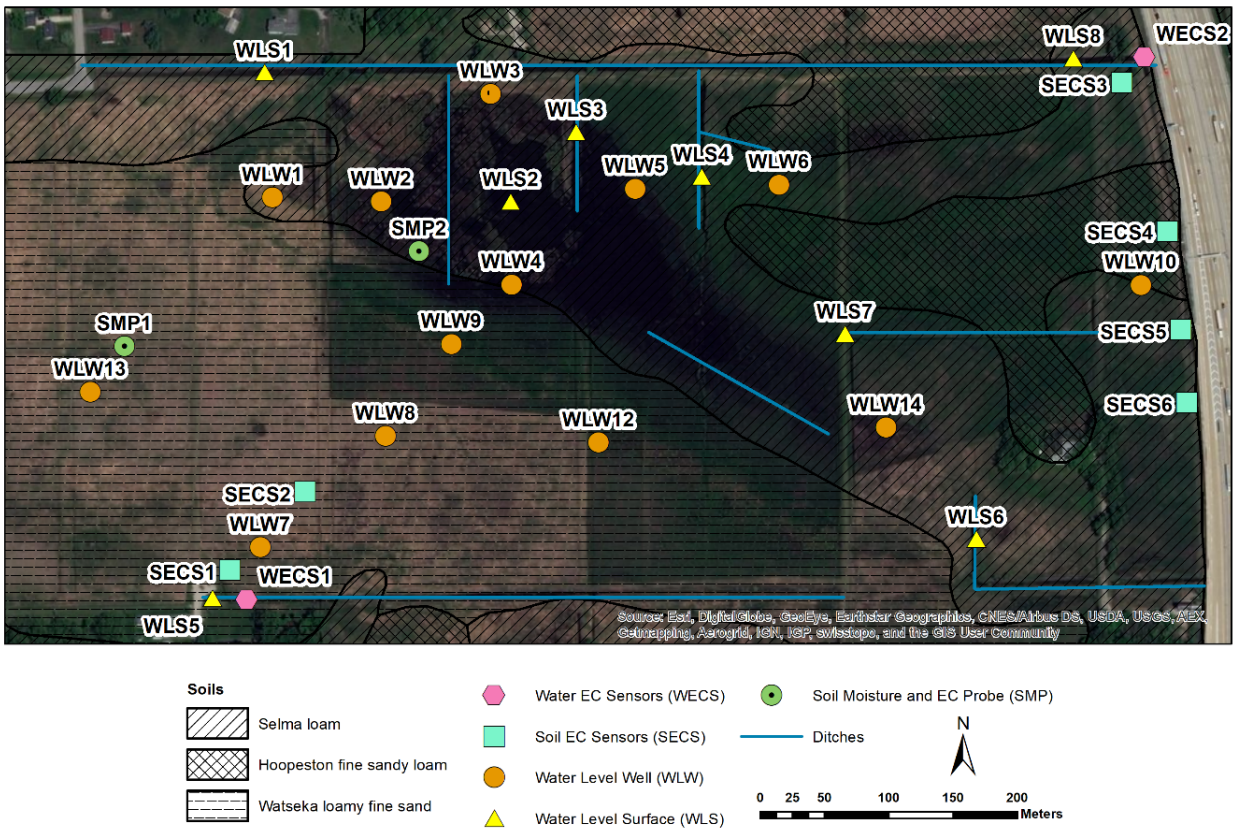


Figure 3: Map of pre-existing sensors and sensors installed as part of this research. Soil EC Sensor (SECS) locations include two sensors at 15 and 30 cm depth. Water EC Sensor (WECS) locations include one sensor on the bottom of the drainage channel.

Soil samples were collected from each location at the time of equipment installation. Water samples were collected monthly from each groundwater well and from surface channels near each surface water level sensor, when possible, as part of an ongoing water quality monitoring campaign. Water samples were collected using polyethylene bailers. The bailers were slowly introduced into the water column to minimize turbidity and disturbances. Water samples were stored in 1L plastic bottles and transferred to Northwestern University in coolers with ice. The samples were preserved and digested with 2% nitric acid, filtered using a 0.45 µm syringe filter, placed in 15 mL conical vials, and kept refrigerated until analyzed. Both soil and water samples were analyzed for total metals concentrations by Inductively Coupled Plasma - Optical Emission

Spectrometry (ICP-OES, Optima 8300, Perkin-Elmer), including common road salt components (e.g., sodium, magnesium, and calcium). In addition, the electrical conductivities of water samples from January, February, March, and April of 2018 were determined using a FieldScout EC Probe soon after sampling, and these samples were analyzed for chloride content by ion chromatography (IC). Samples for IC analyses were passed through 0.2 μm filter and analyzed on a Supp5 column in a Metrohm 930 Compact IC instrument.

In addition to our installed rain gauge, we incorporated precipitation data obtained from NOAA to improve the quality of our data set by including the winter precipitation events that trigger road salting (Huntington, et al., 2017). We are also working to incorporate state and county data on deicing activity for the 2017-2018 winter and spring seasons.

Results

Objective 1: Quantify the impacts of winter deicing salt on soil, surface water, and groundwater in an urban prairie nature preserve. Along our sensor transects, we observed changes in soil and water electrical conductivity with precipitation events and temperature changes. Conductivity in surface waters is generally an order-of-magnitude larger than in soils. Throughout winter, warm periods associated with melting snow and ice were followed by small, temporary increases in EC in deeper soils (30 cm), with a baseline conductivity of approximately 20 $\mu\text{S}/\text{cm}$ along the eastern transect near I-294 and 13 $\mu\text{S}/\text{cm}$ in the southern part of the prairie. It was not possible to obtain a baseline EC for surface waters due to dry conditions in drainage channels during winter. Along the eastern transect, soil EC sensors nearer the northern drainage ditch returned to the baseline EC more quickly after a rain event.

Concentrations of Ca in soil cores (0 to 120 cm) varied between 0 mg/kg to 3898 mg/kg (mean 702 mg/kg). Na ranged from 20 mg/kg to 269 mg/kg (mean 58 mg/kg), and Mg ranged from 3 mg/kg to 8489 mg/kg (mean 1347 mg/kg). Additional surface samples (0 to 10 cm, N=22) were collected from the soils at GMP. Ca was found in concentrations ranging from 0 mg/kg to 1806 mg/kg (mean 627 mg/kg). Concentrations of Mg were between 223 mg/kg and 10177 mg/kg (mean 1864 mg/kg). Two surface samples exceeded the mean background levels in Illinois for Mg of 7231 mg/kg (IEPA 1994). High Mg and Ca concentrations were found in drainage ditches near roads, which may indicate road salt intrusion to the site during winter months.

Water samples collected during the months of February, March, and April, 2018 had EC values in the range of 35 $\mu\text{S}/\text{cm}$ to 1364 $\mu\text{S}/\text{cm}$ (mean 412 $\mu\text{S}/\text{cm}$). In general, EC decreased from February to April in the groundwater wells located in the sand ridge, and increased in the surface channels located in the lower swale (*c.f.*, Figure 2). Concentrations of Ca in water samples from February and March were between 0.25 mg/L and 13.55 mg/L (mean 3.57 mg/L). Concentrations of Mg varied from 0.84 mg/L to 43.67 mg/L (mean 12.08 mg/L). Na had concentrations ranging from 0.65 mg/L to 132.42 mg/L (mean 15.96 mg/L). Highest concentrations of these road salt components were found in groundwater wells (WLW14 and WLW10 near the highway, implying direct impact of deicing chemicals into GMP).

The US EPA does not have regulatory standards for calcium, magnesium and sodium. However, the background level for sodium in shallow aquifers of Illinois is 15 mg/L (Panno et al. 2006). The release of sodium in the environment is known to alter soil chemistry by ion exchange, releasing elements such as calcium and magnesium into the groundwater and surface water, affecting the capacity of water to buffer acid deposition and eventually impacting aquatic life (NHDES 2016).

Objective 2: Explore the effects of seasonality on salt delivery to and transport within the prairie. Initially, we hypothesized that occurrence of road salt components in the prairie would lag

behind frozen precipitation events and we expected to observe little to no change in EC while temperatures remained below freezing. As winter transitions to spring, temperatures fluctuate, resulting in cycles of frozen precipitation and deicing activity interspersed with rainfall and transport events. Sensor measurements generally reflect this pattern for larger weather events.

A representative example of the response of the northern drainage ditch to snowmelt and precipitation in late February, 2018, is shown in **Figure 4**. Two weeks of freezing temperatures, during which multiple precipitation events occurred, led to accumulation of approximately 30 cm of snow in the prairie. Over the course of three days, from February 18 through February 20th, heavy rains and warm temperatures increased water depth in the drainage ditch due to a combination of snowmelt and rainwater runoff. Temperatures above freezing (about 8 °C) and a small amount of rainfall (about 1.2 cm) led to a large increase in water EC as salts applied earlier in the month were mobilized. In the following days, large amounts of rain (> 8 cm in 48 hours) resulted in decreased water EC, most likely due to dilution by fresh water with no additional salt inputs. The most intense rainfall of the event, however, resulted in a spike in water EC, potentially caused by increased runoff mobilizing additional salts from roads or soils. For the following weeks, individual rainfall events consistently produced temporary decreases in EC, indicative of dilution, though with a general seasonal trend of increasing EC as frozen precipitation events were interspersed with rainfall and warmer days.

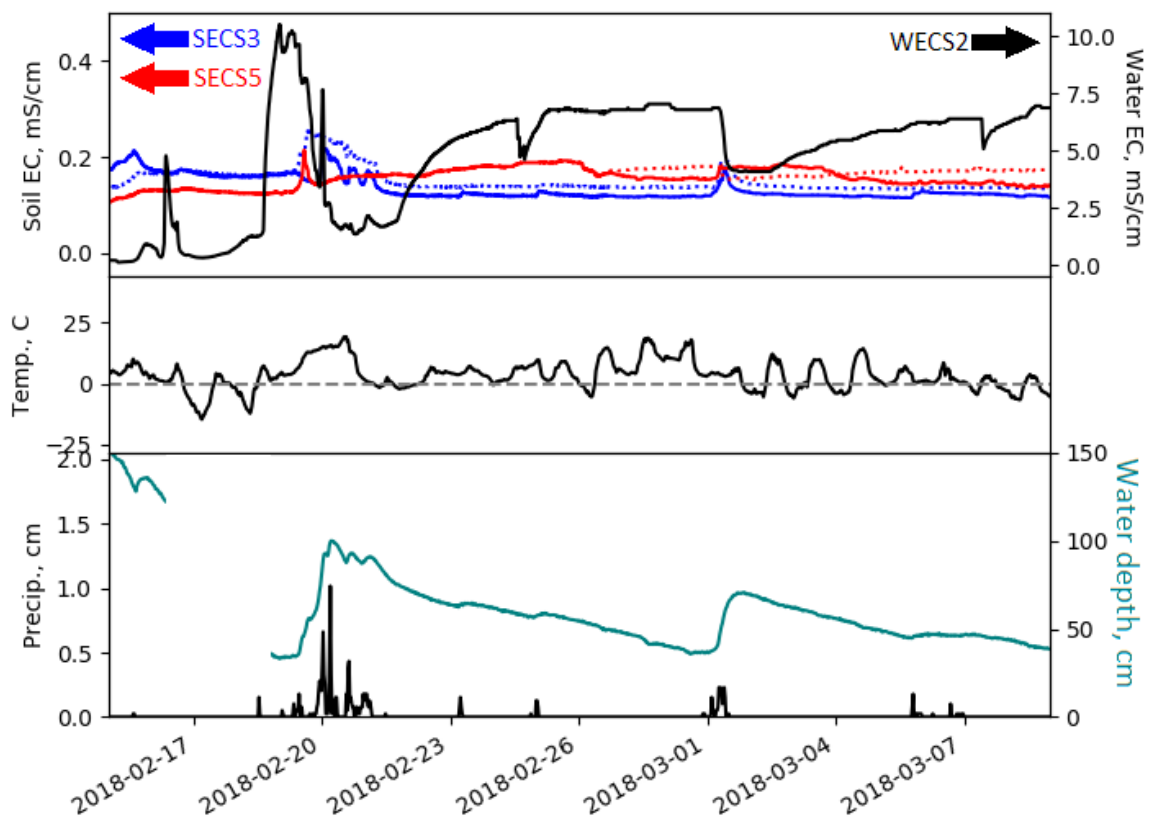


Figure 4: Top: Electrical conductivity in soil (blue, red), and water (black). For soil, solid lines indicate the upper sensor (15 cm), while dashed lines indicate the lower sensor (30 cm); Middle: Air temperature, measured by built-in temperature sensor in local rain gauge; Bottom: Water depth in drainage ditch (teal) superimposed on 30-minute summed local precipitation. Gap in depth data record indicates time when the ditch was frozen and depth measurements of depth are unreliable;

The connection between precipitation, temperature, and salt occurrence in the prairie during the transition from winter to spring was not as straightforward as we originally expected. Precipitation events did not consistently result in an intrusion of salt in the prairie along the pathways that we monitored. For example, the precipitation and warming event portrayed in **Figure 4** resulted in increased soil moisture in the southern part of the prairie, but no significant coincident increased electrical conductivity in soils in the sand ridge.

Concentrations of Ca, Mg and Na in samples collected monthly from August 2016 to March 2018 from the northern ditch of the site (WLS1) are compared with rainfall in **Figure 5**. The occurrence of increased Mg, Ca, and Na in surface waters during months with no deicing activity suggests that salts are stored in the prairie during very wet periods with slow flow and are flushed out by flashier rain events during dry periods. We did not predict that heavy rains in summer months when there is little antecedent moisture and no salting would result in sharp increases in road salt constituents. As a result, we did not monitor EC in waters in the prairie during the summer. We will continue to monitor surface and groundwater quality year-round at GMP in order to capture these complex dynamics.

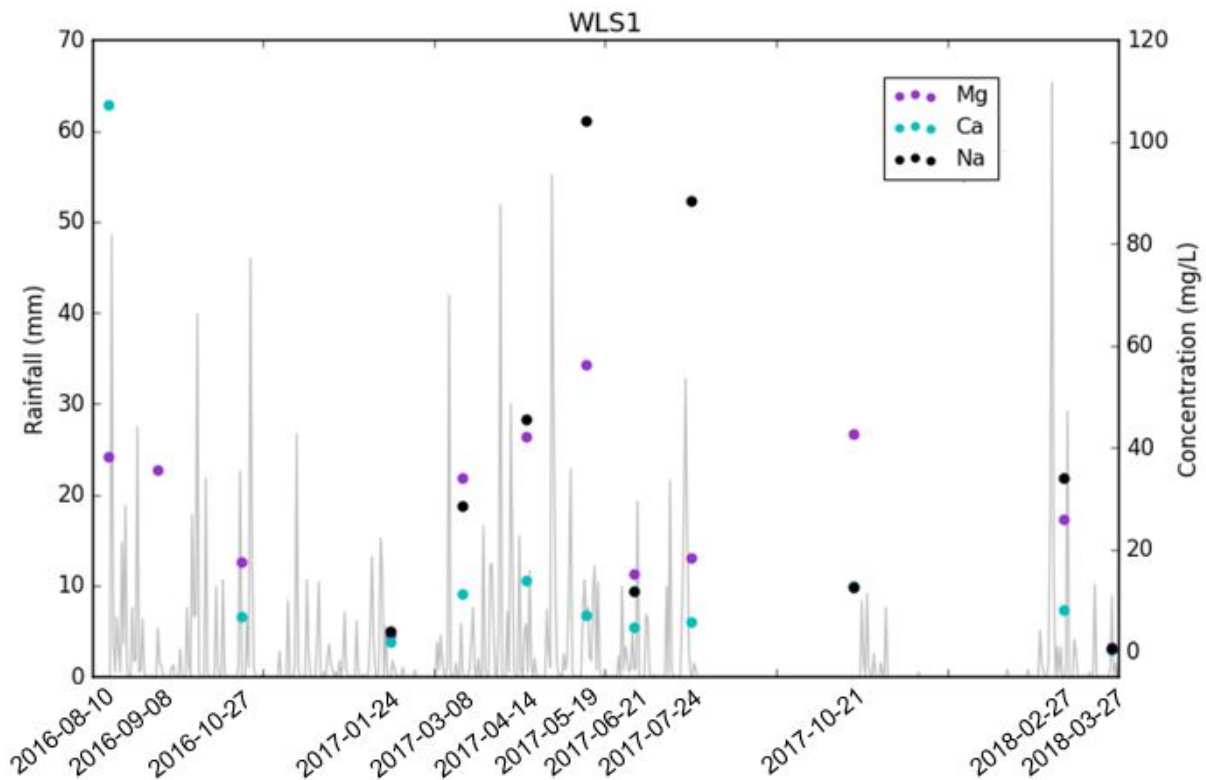


Figure 5: Concentrations of metals in the north drainage channel through one year and 7 months of surface water sampling. Increased concentrations of cations associated with deicing salt are observed in warm, wet months August, May, and July. Water was collected when ditches were neither dry nor frozen over. Local rain gauge data is not available for June 27 through October 6, 2017.

Ongoing Work and Dissemination of Findings

We are collaborating with TNC and NEIU to evaluate the anthropogenic effects of runoff on this urban prairie nature preserve. The results of this work were presented to the TNC Science Advisory Council in March 2018. This work constitutes a resource for TNC in managing GMP and the other prairies in the Indian Boundary Prairies to preserve biodiversity and maintain valuable ecosystem services. These results are also in preparation for publication. Continuing work at Gensburg Markham Prairie includes sampling of surface soils from the bottom of ditches during the dry season to evaluate deposition of metals and road salt constituents from water that infiltrates into the subsurface. Additional methods of estimating soil EC are also being explored to permit separation of intrinsic soil properties from anthropogenic effects on EC.

As part of an ongoing partnership with Argonne National Laboratory, we are working to integrate the EC sensors installed as part of this research with larger-scale environmental sensing infrastructure via the Waggle platform (Beckman et al., 2016). This integration will permit open data dissemination in real time, allowing these measurements to inform site management decisions and be available to the public to facilitate discussion of alternative deicing strategies.

References

- Beckman, P., Sankaran, R., Catlett, C., Ferrier, N., Jacob, R., Papka, M. "Waggle: An open sensor platform for edge computing." IEEE SENSORS 2016. Oct 30, 2016 - Nov 2, 2016. Orlando, Florida, USA.
- Howard, KWF and H Maier. 2007. "Road de-icing salt as a potential constraint on urban growth in the Greater Toronto Area, Canada." *J. Contam. Hydrol.* 91:146–170.
- Huntington, J., Hegewisch, K., Daudert, B., Morton, C., Abatzoglou, J., McEvoy, D., and T., Erickson. (2017). *Climate Engine: Cloud Computing of Climate and Remote Sensing Data for Advanced Natural Resource Monitoring and Process Understanding*. Bulletin of the American Meteorological Society.
- IEPA. 1994. *A Summary of Selected Background Conditions for Inorganics in Soil*, Illinois Environmental Protection Agency report IEPA/EVN/94-161.
- Ledford SH, LK Lautz, JC Stella. 2016. "Hydrogeologic Processes Impacting Storage, Fate, and Transport of Chloride from Road Salt in Urban Riparian Aquifers." *Environ. Sci. Technol.*, 50:4979-4988.
- NHDES, 2016, *Road Salt and Water Quality*, New Hampshire Department of Environmental Services, Report WD-WMB-4.
- Panno, S. V. et al. 2006. "Characterization and Identification of Na-Cl Sources in Ground Water." *Ground Water* 44(2): 176–87.
- Perera N, B Gharabaghi, and K Howard. 2012. "Groundwater chloride response in the Highland Creek watershed due to road salt application: A re-assessment after 20 years." *Journal of Hydrology*, 479:159-168.
- Rivett MO, MO Cuthbert, R Gamble, LE Connon, A Pearson, MG Sheply, J Davis. 2016. "Highway deicing salt dynamic runoff to surface water and subsequent infiltration to groundwater during severe UK winters." *Science of the Total Environment*, 565:324-338.
- Shaw SB, RD Marjerison, DR Bouldin, JY Parlange, MT Walter. 2012. "Simple Model of Changes in Stream Chloride Levels Attributable to Road Salt Applications." *J. Environ Eng.* 138(1):112-118.
- Warner KL and JD Ayotte. 2014. "The Quality of Our Nation's Waters; Water Quality in the Glacial Aquifer System, Northern United States, 1993-2009." U.S. Geological Survey Circular 1352, p. 73-76.

Diurnal and Seasonal Variation in Groundwater Nitrate-N Concentration in a Riparian Buffer Zone

Basic Information

Title:	Diurnal and Seasonal Variation in Groundwater Nitrate-N Concentration in a Riparian Buffer Zone
Project Number:	2017IL333B
Start Date:	3/1/2017
End Date:	2/28/2019
Funding Source:	104B
Congressional District:	IL-105
Research Category:	Water Quality
Focus Categories:	Agriculture, Non Point Pollution, Nutrients
Descriptors:	None
Principal Investigators:	Eric Wade Peterson

Publications

There are no publications.

Final Report: Diurnal and Seasonal Variation in Groundwater Nitrate-N Concentration in a Riparian Buffer Zone

Principal Investigator: Eric W. Peterson

Academic Rank: Professor

University: Illinois State University

Email: ewpeter@ilstu.edu

Phone: 309-438-7865

Research Category: Water quality

Secondary Research Category: Agriculture

Keywords: Nitrate, denitrification, riparian buffer, tile water, groundwater

For Period: March 1, 2017 to February 28, 2018

Submitted: May 12, 2017

Table of Contents

I. Introduction.....	4
II. Research Objectives.....	5
III. Site Description	5
IV. Methodology	6
V. Principle Findings.....	7
a. Nitrate-N data.....	7
b. Statistical Analyses of Nitrate-N Data	11
c. Environmental Factors	13
d. Discussion	15
VI. Significance.....	18
VII. Students supported.....	19
VIII. Publications	20
a. MS Thesis.....	20
b. Peer-Reviewed Academic Journals	20
c. Presentations.....	20
d. Media recognition.....	20
IX. References	21

Table of Tables

Table 1. Descriptive statistics for NO ₃ ⁻ -N concentration among the seasons, values represent mean ± standard deviation.	7
Table 2. <i>t</i> -test results for the stated comparisons. Results in bold signify a statistically significant difference.	12
Table 3. <i>t</i> -test Results for statistically significant difference between $\mu_{\text{daily [NO}_3^- \text{-N] season}}$ & $\mu_{\text{daily [NO}_3^- \text{-N] season}}$	13
Table 4. Seasonal means ± standard deviation for environmental factors	15

Table of Figures

Figure 1: Visual of field site A) general site location in Illinois, B) local site location. Well of interest is yellow. The stream flows north and groundwater flows from the southeast to northwest, c) east to west cross-section illustrating the surficial geology. 5

Figure 2. Conceptual model of subsurface flow. Groundwater flows in the sandy gravelly clay unit from southeast to northwest. Organic topsoil is overlain by a sandy gravelly clay unit, which is underlain by tight clay. The unconfined aquifer occupies the sandy gravelly clay unit. 6

Figure 3. NO_3^- -N concentrations and environmental factors observed during the 24-hour collection periods. A) mean air temperature and mean groundwater temperature; B) mean solar intensity and dissolved oxygen; C) NO_3^- -N concentration and mean water column height. The ends of the boxes represent the 25th and 75th percentiles with the solid line at the median and the dashed line at the mean; the error bars depict the 10th and 90th percentiles and the points represent the 5th and 95th percentiles. 8

Figure 4. Time series trends for normalized $[\text{NO}_3^-$ -N] (circle) and $[\text{Cl}^-]$ (triangle) over the course of the study. Grey area indicates the dark period and white area indicates the photoperiod. Points are the mean and error bars are one standard deviation. A) Sinusoidal trend B) Increase trend C) Decrease trend..... 9

Figure 5. Frequency of NO_3^- -N concentration patterns (sinusoidal, increase, and decrease) by season.... 10

Figure 6. a) Frequency of maximum NO_3^- -N concentration by time-of-day for increase, decrease, and sinusoidal trends. B) Frequency of minimum NO_3^- -N concentration by time-of-day for increase, decrease, and sinusoidal trends. C) Frequency of maximum NO_3^- -N concentration by time-of-day for sinusoidal trends. D) Frequency of minimum NO_3^- -N concentration by time-of-day for sinusoidal trends. 11

Figure 7. Box and whisker plots for the seasonal $\mu_{\text{difference}[\text{NO}_3^-$ -N]}. No statistically significant differences in $\mu_{\text{difference}[\text{NO}_3^-$ -N]} are present among seasons. The ends of the boxes represent the 25th and 75th percentiles with the solid line at the median and the dashed line at the mean; the error bars depict the 10th and 90th percentiles; the points depict the outliers. 12

Figure 8. Daily NO_3^- -N concentration by season. Letters above the boxes identify seasons with statistically significant difference between seasonal $\mu_{\text{daily}[\text{NO}_3^-$ -N]}. The ends of the boxes represent the 25th and 75th percentiles with the solid line at the median and the dashed lined at the mean; the error bars depict the 10th and 90th percentiles. 13

Figure 9. Daily $\mu_{\text{max}[\text{NO}_3^-$ -N]} and $\mu_{\text{min}[\text{NO}_3^-$ -N]} for each season. Statistically significantly different $\mu_{\text{max}[\text{NO}_3^-$ -N]} and $\mu_{\text{min}[\text{NO}_3^-$ -N]} occur in each season. The ends of the boxes represent the 25th and 75th percentiles with the solid line at the median and the dashed line at the mean; the error bars depict the 10th and 90th percentiles. 13

Figure 10. Environmental factor correlations for sinusoidal, increase, and decrease trends by season. Difference between 24-hour maximum and minimum on Y axis A) daily air temperature B) daily water temperature, range: 1.4-31.4°C C) daily average solar intensity D) daily dissolved oxygen E) water column height F) 24-hour water temperature difference..... 14

Figure 11. $\mu_{\text{daily}[\text{NO}_3^-$ -N]} concentrations versus $\mu_{\text{difference}[\text{NO}_3^-$ -N]} for sinusoidal pattern. Despite a range of 5.4 mg/L in $\mu_{\text{daily}[\text{NO}_3^-$ -N]}, the majority of $\mu_{\text{difference}[\text{NO}_3^-$ -N]} exhibits minimal variation, a range of 0.4 mg/L..... 18

I. Introduction

Agriculture is acknowledged as a leading cause of surface water pollution (Anderson *et al.*, 2014, Galloway *et al.*, 2003), serving as the principal source of nitrogen (N), primarily nitrate (NO_3^-), to aquatic environments (Dick *et al.*, 2000, Turlan *et al.*, 2007, Delgado, 2002, David *et al.*, 1997). Hypoxia, eutrophication, and biodiversity changes within surface waters, specifically the Gulf of Mexico, are attributed to excess NO_3^- loading (Turner *et al.*, 2006, Turner *et al.*, 2012, Scavia *et al.*, 2003, Rabalais *et al.*, 2002). On an annual basis in the US Midwest, an estimated 1 million metric tons of N is leached from the agricultural fields into waters of the Mississippi River (Kovacic *et al.*, 2006). Since 1950, the NO_3^- -N load discharged into the Gulf of Mexico has tripled (Scavia *et al.*, 2003, Goolsby *et al.*, 2001), with the Illinois River identified as the second leading contributor of NO_3^- to the Mississippi River (Scott *et al.*, 2007). As a whole, agricultural activity in Illinois contributes 19% of the NO_3^- load delivered to the Gulf of Mexico by the Mississippi River (Keeney & Hatfield, 2001, David & Gentry, 2000, David *et al.*, 2006).

The upper Mississippi River Basin, which includes Illinois, has some of the most fertile soils and experiences intensive agricultural practices. In Illinois, 23 million acres or nearly 80% of land use is agriculture (Illinois Department of Agriculture, 2014), but excess water and a shallow water table limits crop yield (Urban & Rhoads, 2003). Prior to settlement, wetlands were prevalent in Illinois, with an estimated 50% of Illinois believed to be wetlands (Rhoads & Herricks, 1996). Upon passage of both the Farm Drainage Act and the Farm Levee Act in 1879, extensive channelization and installation of subsurface draining within watersheds of Illinois was initiated to maximize yields, avert planting delays, and prevent water stress on crops (Sands *et al.*, 2008, David *et al.*, 2010, Urban & Rhoads, 2003, Davis *et al.*, 2000, Fausey *et al.*, 1995).

Installation of tile drains circumvents the natural attenuation by draining NO_3^- rich waters from the fields directly into surface waters (Royer *et al.*, 2004, Randall *et al.*, 1997, Dinnes *et al.*, 2002). While the installation of tile drains has been highly successful in opening up additional lands for agricultural development, the short-circuiting of natural processes (Mohanty *et al.*, 1998) directly contributes to 52% of N entering the Gulf of Mexico (Alexander *et al.*, 2008). Headwater stream basins play a primary role in the mitigation of NO_3^- (Alexander *et al.*, 2000, Peterson *et al.*, 2001), but these watersheds are often the subject of tile-drainage systems. Limiting the export of NO_3^- to surface water will aid in the efficiency of headwater streams to remediate NO_3^- , preventing export further downstream.

NO_3^- removal in riparian buffer zones occurs through denitrification and assimilation. Denitrification, the process where NO_3^- is converted to dinitrogen (N_2) through microbial metabolism (Zumft, 1997), results in the permanent removal of NO_3^- due to the loss of N as N_2 to the atmosphere. Assimilation occurs by incorporation of nitrogen into biomass through vegetation uptake (Kuusemets *et al.*, 2001). The cyclic nature of assimilation makes it a temporary storage mechanism for nitrogen. Although assimilated nitrogen may cycle back into the environment as NO_3^- , its temporary storage represents a substantial ecological relief from NO_3^- burden (Beaulieu *et al.*, 2014).

Diurnal and seasonal changes in solar radiation not only govern air and groundwater temperature but also influence growth of terrestrial plants directly by controlling photosynthesis, the mechanism by which plants capture photons to produce energy. Local diurnal and seasonal cycles of increased and decreased solar intensity result in seasonal and diurnal cycles of photon availability, air temperature, and groundwater temperature. Plants are therefore subject to cyclic patterns of energy availability for nitrogen uptake and biomass growth (Delhon *et al.*, 1996).

Several studies performed under laboratory conditions offer evidence for NO_3^- uptake variation on the diurnal scale, which may be expanded to explain variation on a seasonal scale (Delhon *et al.*, 1996, Pearson & Steer, 1977, Scaife & Schloemer, 1994, Bot & Kirkby, 1992). Delhon *et al.* (1996) and Pearson and Steer (1977) reasoned that diurnal changes in NO_3^- uptake are due to decreased phloem transport of photosynthetically manufactured sugars and metabolic products down to root tissue (Delhon *et al.*, 1996). The lack of activity in darkness leaves root tissue lacking energy for uptake (Delhon *et al.*,

1996). If NO_3^- uptake is influenced by light available on the diurnal scale, then NO_3^- uptake variation can be expected to display a similar relationship on the seasonal scale as solar intensity varies.

The relative importance of plant uptake when compared to denitrification is disputed. Gilliam (1994) found NO_3^- loss to be greatest in the winter months when plants are dormant, and Sabater *et al.* (2003) found no seasonal difference in NO_3^- removal. However, other research suggests NO_3^- uptake by vegetation is important and the resulting observed seasonal variation is significant (Hill, 1996). Haycock and Pinay (1993) found riparian vegetation uptake to be a major NO_3^- attenuation mechanism in summer. Haycock and Pinay (1993) and Simmons *et al.* (1992) reasoned that vegetation uptake dominates when the water table is high enough for roots to reach it but low enough for overlying soil to become aerated.

II. Research Objectives

This work examined the variability of NO_3^- concentrations in a saturated buffer zone on a diurnal scale within and among seasons. Specifically, the research addressed the following questions and hypotheses. “Does riparian zone shallow groundwater NO_3^- concentration vary temporally?” This question was broken into the following questions and hypotheses: 1) Does NO_3^- -N concentration vary over a 24-hour period in each season? H_0 : There will be no significant difference between the mean daily maximum ($\mu_{\max} [\text{NO}_3^- \text{-N}]$) and minimum ($\mu_{\min} [\text{NO}_3^- \text{-N}]$) NO_3^- -N concentration in each season; 2) Does mean daily NO_3^- -N concentration vary seasonally? H_0 : There will be no significant difference in mean daily NO_3^- -N concentration ($\mu_{\text{daily}} [\text{NO}_3^- \text{-N}]$) seasonally; 3) Does the daily timing of maximum and minimum NO_3^- -N concentration vary seasonally? H_0 : There will be no difference in the time-of-day when the maximum and minimum NO_3^- -N concentration occurs among seasons; 4) Does the mean difference between daily maximum and minimum NO_3^- -N concentration vary seasonally? H_0 : There will be no significant difference between the mean daily maximum and minimum NO_3^- -N concentration difference ($\mu_{\text{difference}} [\text{NO}_3^- \text{-N}]$) among seasons. In addition to addressing the above hypotheses, environmental factors were used to investigate processes responsible for statistically significant differences

III. Site Description

The study centers on a reclaimed saturated buffer zone along a stream, T3, located within central Illinois (40.614382°N, -89.023542°W) (Figure 1). Historically, the site was farmed but has since been fully converted to a switchgrass prairie. The site receives agricultural tile-water from a farm located approximately 120m upgradient to the east. A tile diversion system has been installed within the buffer diverting tile water into the subsurface of the buffer zone 20-35 m upgradient from the stream. This saturated zone allows tile discharge to infiltrate into the unconfined aquifer rather than directly entering

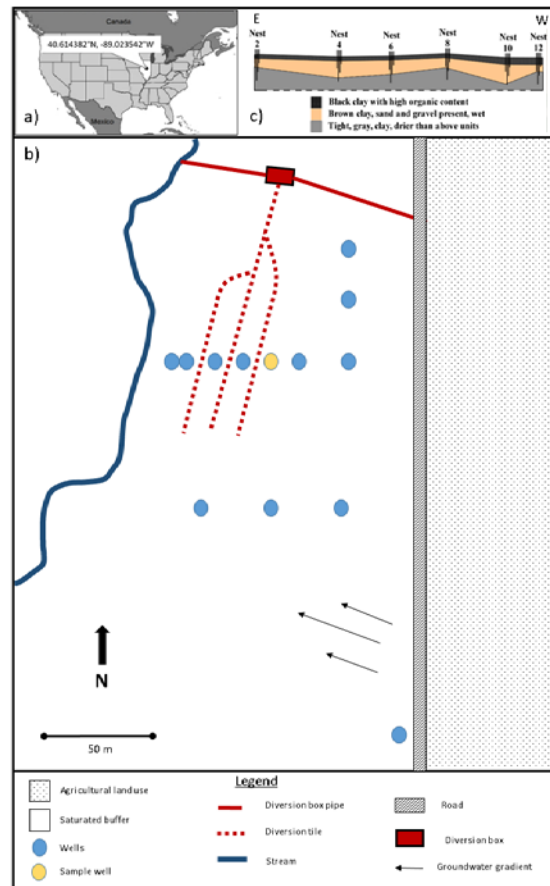


Figure 1: Visual of field site A) general site location in Illinois, B) local site location. Well of interest is yellow. The stream flows north and groundwater flows from the southeast to northwest, c) east to west cross-section illustrating the surficial geology.

the stream. Seven water table wells (1.5 m) and six nests of wells have been installed to monitor water chemistry. Each nest includes wells screened at depths of at 4.5m, 3m, 2.3m, and 1.5m.

Site geology at the surface (0-0.63m) is dark organic rich topsoil (Figure 2). The organic rich topsoil is underlain (0.66-1.5m) by a firm clay loam with an increasing sand and gravel percent composition with depth. The clay loam transitions into coarse-grained lense, silty sand to silty-sandy pebbles from 1.5m to 2m depth. The coarse grained lense is underlain (>2m) by mud-matrix diamicton (Weedman *et al.*, 2014). The diamicton is thought to have an average thickness of 30-45 m terminating at Silurian dolomite bedrock (Wickham *et al.*, 1988). The diamicton belongs to the Tiskilwa Till member of the Wedron Formation and was deposited during the Wisconsin glaciation. Horizontal groundwater flow is primarily in the coarse sandy/gravelly clay unit, with limited penetration into the underlying tight clay (Figure 2). Hydraulic head and groundwater chemistry data (unreported) suggests upwelling from the underlying clay into the coarse sandy/gravelly clay unit.

This study site has a temperate climate with a 60-year average annual air temperature of 11.2°C and a monthly average variance of 30°C depending on season (Changnon *et al.*, 2004, Beach, 2008). Yearly average precipitation is 950 mm ± 100 mm (Changnon *et al.*, 2004), with 40-year monthly averages showing greatest precipitation in the spring and lowest precipitation in the winter (Changnon *et al.*, 2004).

IV. Methodology

Sample events occurred weekly in well 4D for a year. Well 4D is 1.5 m deep and located near the perforated diversion pipes at site T3 (Figure 1). Each sampling event included the collection of a water sample every hour for 24-hours by an ISCO autosampler. Samples were stored in a refrigerator less than 24 hours before analysis. A DIONEX ICS-1100 ion chromatography system was employed to analyze samples for nitrate as nitrogen (NO₃⁻-N) and chloride (Cl⁻); a conservative tracer, Cl⁻ served as a proxy for dilution. Samples were filtered using a 0.45 μm pore space fiberglass filter to remove large particles before analysis by ion chromatography. Ion chromatography quality assurance and quality control techniques included blanks, duplicates, and standard replicates. Error was found to be <1% with a relative standard deviation of 0.005 mg/L. A Decagon groundwater depth, temperature, and conductance (DTC) sensor housed in the sampled well recorded measurements every 15 minutes over the entire 24-hour sampling period. A HOBO Pendant® temperature/light logger (UA-002-08) mounted on a metal stake collected air temperature (-20°-70°C) and light intensity (0-30,000 lumens/ft²). Air temperature accuracy is +/- 0.53°C from 0°-50°C and drifts less than 0.1°C/year. Dissolved oxygen concentration was measured before and after the sampling event with a YSI 85.

Data analysis included t-tests for null hypotheses, and a Pearson correlation analysis for environmental factors. Seasons were defined by the 2017 solstices and equinoxes: Spring: March, 20 – June, 20; Summer: June, 21 – September, 21; Fall: September, 22 – December, 20; Winter: December, 21 – March, 19. For hypothesis 1, H₀: There will be no significant difference between μ_{max} [NO₃⁻-N] and μ_{min} [NO₃⁻-N] in each season was tested by a 1-tailed dependent groups t-test, α=0.05. A one tailed t-test was used, as the alternative hypothesis is restricted to μ_{max} [NO₃⁻-N] > μ_{min} [NO₃⁻-N] (Ramsey & Schafer, 2002). For hypothesis 2 and 3, H₀: There will be no significant difference in μ_{daily} [NO₃⁻-N] seasonally and H₀: There

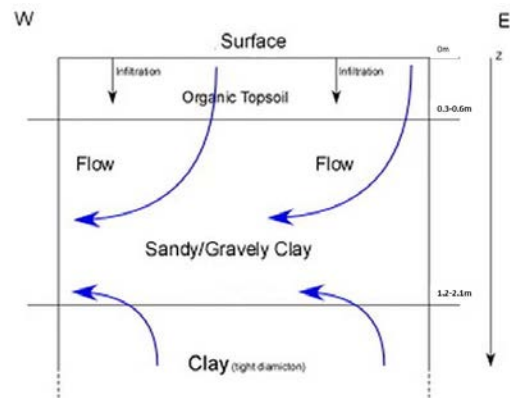


Figure 2. Conceptual model of subsurface flow. Groundwater flows in the sandy gravelly clay unit from southeast to northwest. Organic topsoil is overlain by a sandy gravelly clay unit, which is underlain by tight clay. The unconfined aquifer occupies the sandy gravelly clay unit.

will be no significant difference between $\mu_{\text{difference [NO}_3^- \text{-N}]}$ among seasons were tested using a 2-tailed independent groups t-test, $\alpha=0.05$. A 2-tailed t-test was used here, as the alternative hypothesis is not restricted ($\mu_1 \neq \mu_2$) (Ramsey & Schafer, 2002). For hypothesis 4, H_0 : There will be no difference in the time-of-day when the maximum and minimum $\text{NO}_3^- \text{-N}$ concentration occurs among seasons was analyzed qualitatively by grouping hours into bins: hour 1-6 = bin 1, hour 7-12 = bin 2, hour 13-18 = bin 3, hour 19-24 = bin 4. These bins were selected because bin 1 and 4 hold hours of darkness while bins 2 and 3 hold the photoperiod. Pearson correlations were 2-tailed, $\alpha=0.05$ (Ramsey & Schafer, 2002).

V. Principle Findings

a. Nitrate-N data

Thirty-three collection events were distributed over a year as follows: spring-13, summer-9, fall-5, winter-6. Fewer samples were collected in fall due to a low water table and winter due to autosampler malfunction in low temperatures. From August 2016 to February 2017, $\text{NO}_3^- \text{-N}$ concentrations remained between 1.5 and 3 mg/L, then increased from February 2017 to late March 2017 where a peak of 6mg/L was reached (Figure 3). From March 2017 to May 2017 $\text{NO}_3^- \text{-N}$ concentrations decreased back down to between 1.5 and 3 mg/L, but then again increased to 6 mg/L from June 2017 to August 2017 (Figure 3). Times of maximum and minimum $\text{NO}_3^- \text{-N}$ concentration were divided into 4 groups of 6-hour intervals on a 24-hour scale (1=1:00am, 24=12:00am): hours 1-6, hours 7-12, hours 13-18, and hours 19-24. $\text{NO}_3^- \text{-N}$ concentration behavior over 24 hours followed 3 trends: 11 sinusoidal, 19 increase, and 2 decrease (Figure 4, Figure 5).

Over the entire duration of the study, the sampled waters had a mean daily $\text{NO}_3^- \text{-N}$ concentration ($\mu_{\text{daily [NO}_3^- \text{-N] All}}$) of 3.52 mg/L, a mean daily maximum $\text{NO}_3^- \text{-N}$ concentration ($\mu_{\text{max [NO}_3^- \text{-N] All}}$) of 3.67 mg/L, and a mean daily minimum $\text{NO}_3^- \text{-N}$ concentration ($\mu_{\text{min [NO}_3^- \text{-N] All}}$) of 3.15 mg/L (Table 1). The difference between maximum and minimum $\text{NO}_3^- \text{-N}$ concentration ($\mu_{\text{difference [NO}_3^- \text{-N]}}$) was 0.52 mg/L (Table 1). The time of maximum $\text{NO}_3^- \text{-N}$ concentration occurred most frequently in the hours 7-12, and the daily timing of minimum $\text{NO}_3^- \text{-N}$ concentration occurred most frequently between the hours 1-6 (Figure 6). When only days with a sinusoidal trend are considered, daily time of maximum $\text{NO}_3^- \text{-N}$ concentration occurred most frequently hours 1-6 (n=6), and the daily timing of minimum $\text{NO}_3^- \text{-N}$ concentration occurred most frequently hours 13-18 (n=8) (Figure 6).

Table 1. Descriptive statistics for $\text{NO}_3^- \text{-N}$ concentration among the seasons, values represent mean \pm standard deviation.

Season	$\mu_{\text{daily[NO}_3^- \text{-N]}}$ (mg/L)	$\mu_{\text{max[NO}_3^- \text{-N]}}$ (mg/L)	$\mu_{\text{min[NO}_3^- \text{-N]}}$ (mg/L)	$\mu_{\text{difference[NO}_3^- \text{-N]}}$ (mg/L)
Spring (n=13)	3.45 \pm 1.50	3.59 \pm 1.54	2.98 \pm 1.52	0.61 \pm 0.79
Summer (n=9)	4.63 \pm 1.38	4.81 \pm 1.41	4.25 \pm 1.34	0.56 \pm 0.25
Fall (n=5)	2.18 \pm 0.49	2.33 \pm 0.47	1.93 \pm 0.57	0.41 \pm 0.21
Winter (n=6)	3.11 \pm 1.37	3.25 \pm 1.45	2.87 \pm 1.19	0.38 \pm 0.28
All Seasons (n=33)	3.52 \pm 1.52	3.67 \pm 1.55	3.15 \pm 1.47	0.52 \pm 0.53

Note. $\mu_{\text{daily [NO}_3^- \text{-N]}}$ represents mean daily concentration for the season. $\mu_{\text{max [NO}_3^- \text{-N]}}$ represents the mean maximum concentration for the season. $\mu_{\text{min [NO}_3^- \text{-N]}}$ represents the mean minimum concentration for the season. $\mu_{\text{difference [NO}_3^- \text{-N]}}$ represents the mean difference between the 24-hour maximum and minimum for the season.

Spring had a mean daily $\text{NO}_3^- \text{-N}$ concentration ($\mu_{\text{daily [NO}_3^- \text{-N] Spring}}$) of 3.45 mg/L, a mean daily maximum $\text{NO}_3^- \text{-N}$ concentration ($\mu_{\text{max [NO}_3^- \text{-N] Spring}}$) of 3.59 mg/L, and a mean daily minimum $\text{NO}_3^- \text{-N}$ concentration ($\mu_{\text{min [NO}_3^- \text{-N] Spring}}$) of 2.98 mg/L (Figure 3, Figure 4) (Table 1). The difference between maximum and minimum $\text{NO}_3^- \text{-N}$ concentration ($\mu_{\text{difference [NO}_3^- \text{-N] Spring}}$) was 0.61 mg/L (Figure 9, Table 1). The daily time of maximum $\text{NO}_3^- \text{-N}$ concentration occurred most frequently in hours 1-6 (n=4) and in hours 7-12 (n=4), and the daily timing of minimum $\text{NO}_3^- \text{-N}$ concentration occurred most frequently

Diurnal and Seasonal Variation in Groundwater Nitrate-N Concentration in a Riparian Buffer Zone

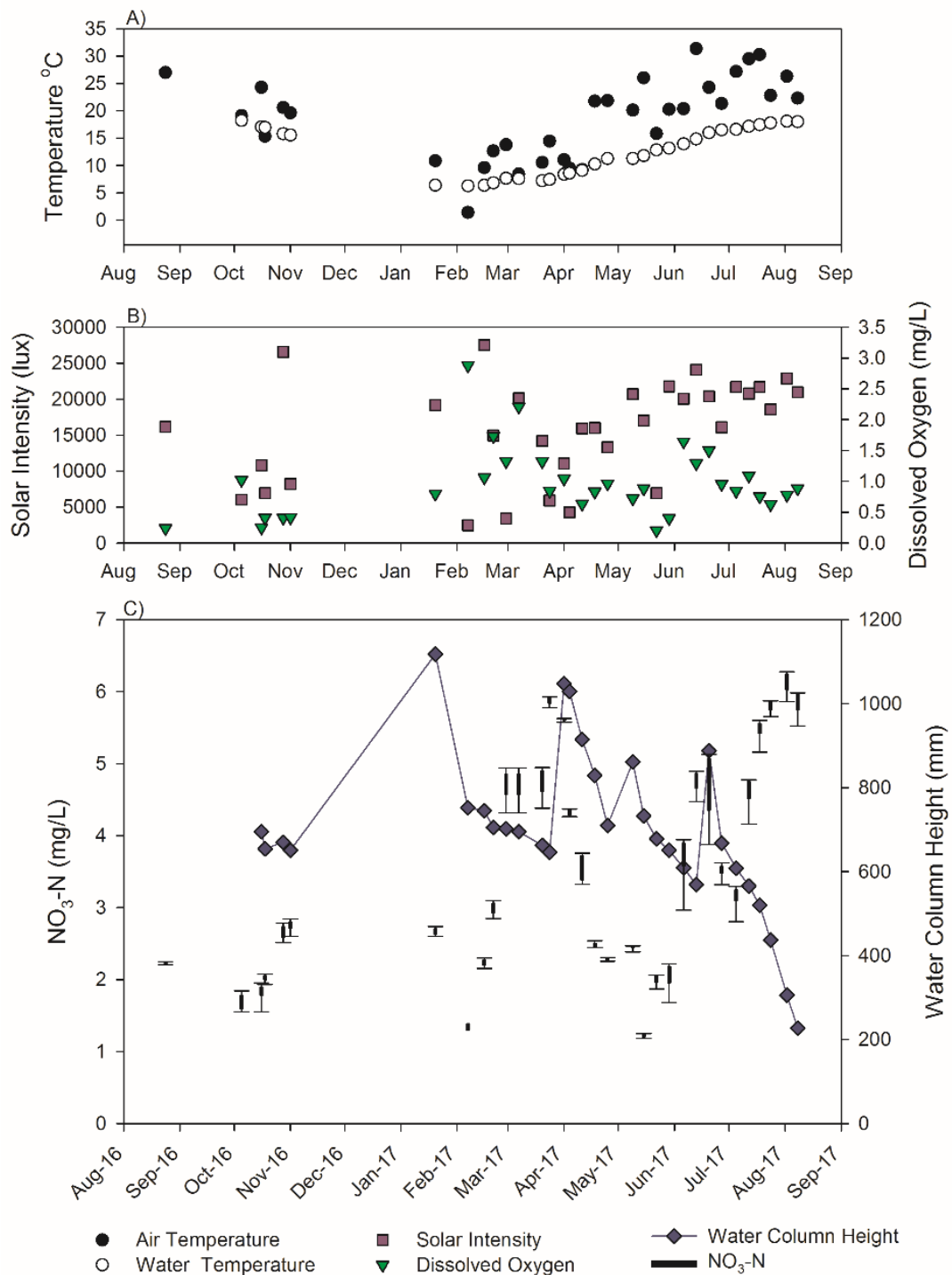


Figure 3. NO_3^- -N concentrations and environmental factors observed during the 24-hour collection periods. A) mean air temperature and mean groundwater temperature; B) mean solar intensity and dissolved oxygen; C) NO_3^- -N concentration and mean water column height. The ends of the boxes represent the 25th and 75th percentiles with the solid line at the median and the dashed line at the mean; the error bars depict the 10th and 90th percentiles and the points represent the 5th and 95th percentiles.

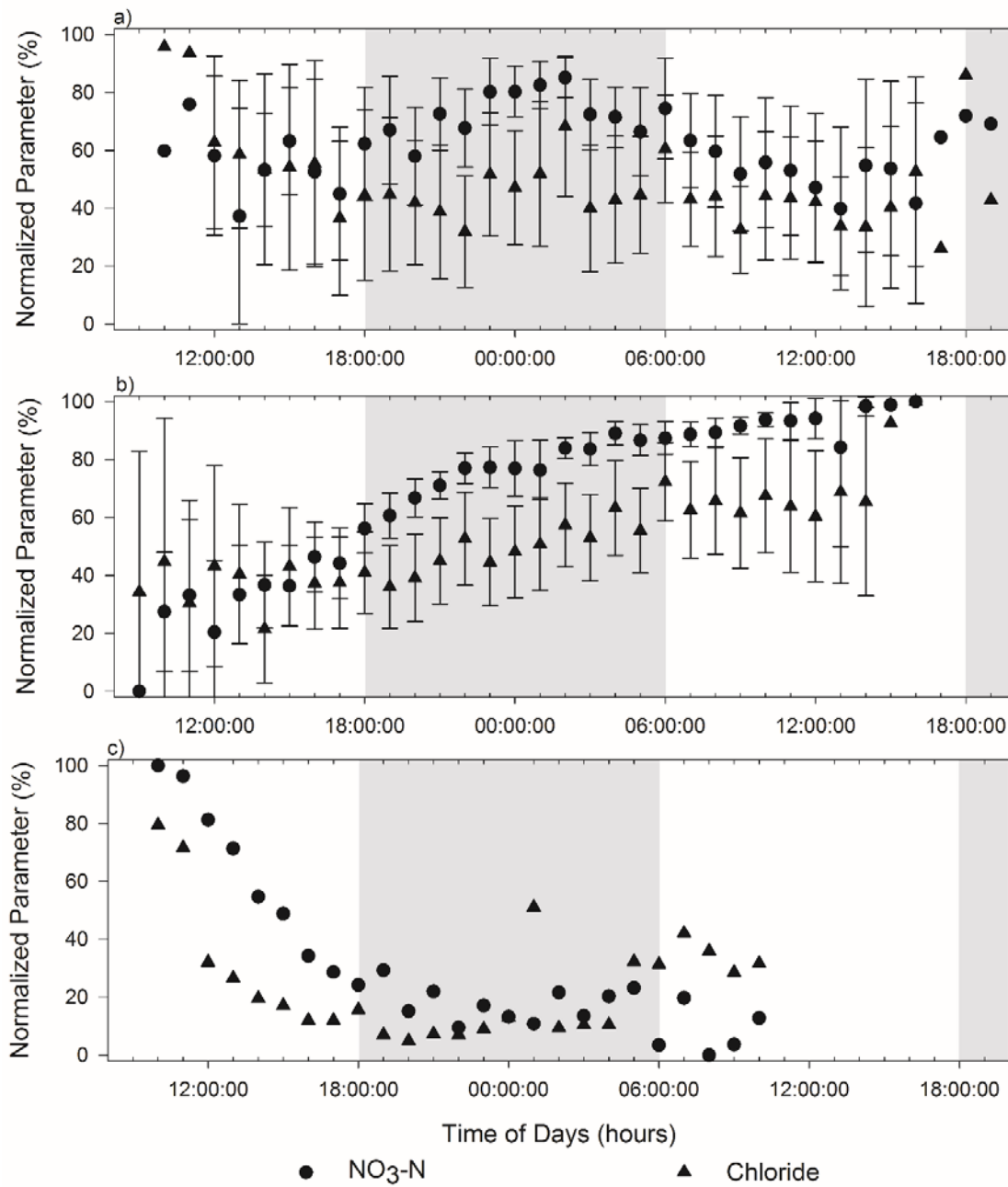


Figure 4. Time series trends for normalized [NO₃⁻-N] (circle) and [Cl⁻] (triangle) over the course of the study. Grey area indicates the dark period and white area indicates the photoperiod. Points are the mean and error bars are one standard deviation. A) Sinusoidal trend B) Increase trend C) Decrease trend.

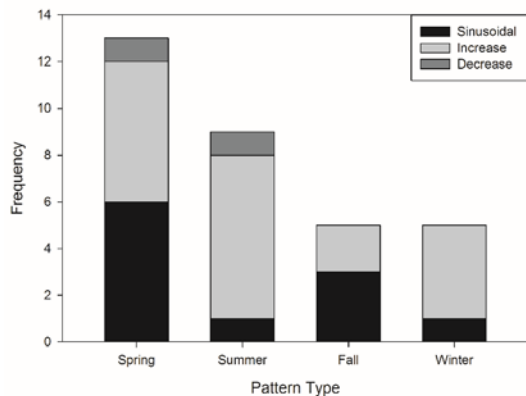


Figure 5. Frequency of NO₃⁻-N concentration patterns (sinusoidal, increase, and decrease) by season.

difference between maximum and minimum NO₃⁻-N concentration ($\mu_{\text{difference [NO}_3^- \text{-N] Summer}}$) was 0.56 mg/L (Figure 9, Table 1). The daily time of maximum NO₃⁻-N concentration occurred most frequently in the hours 7-12 (n=6), and the daily timing of minimum NO₃⁻-N concentration occurred most frequently in the hours 7-12 (n=5) (Figure 8). NO₃⁻-N concentration behavioral trends included 1 sinusoidal, 7 increase, and 1 decrease (Figure 7). When only days with a sinusoidal trend are considered, daily time of maximum NO₃⁻-N concentration occurred hours 1-6 (n=1), and the daily timing of minimum NO₃⁻-N concentration occurred hours 19-24 (n=1) (Figure 8).

Fall had a mean daily NO₃⁻-N concentration ($\mu_{\text{daily [NO}_3^- \text{-N] Fall}}$) of 2.18 mg/L, a mean daily maximum NO₃⁻-N concentration ($\mu_{\text{max [NO}_3^- \text{-N] Fall}}$) of 2.33 mg/L, and a mean daily minimum NO₃⁻-N concentration ($\mu_{\text{min [NO}_3^- \text{-N] Fall}}$) of 1.93 mg/L (Figure 3, Figure 4, Table 1). The difference between maximum and minimum NO₃⁻-N concentration ($\mu_{\text{difference [NO}_3^- \text{-N] Fall}}$) was 0.41 mg/L (Figure 9, Table 1). The daily time of maximum NO₃⁻-N concentration occurred most frequently in the hours 1-6 (n=2) and 13-18 (n=2), and the daily timing of minimum NO₃⁻-N concentration occurred most frequently during hours 13-18 (n=4) (Figure 8). NO₃⁻-N concentration behavioral trends included 3 sinusoidal, 2 increase, and no decreases (Figure 7). When only days with a sinusoidal trend are considered, daily time of maximum NO₃⁻-N concentration occurred most frequently hours 1-6 (n=2), and the daily timing of minimum NO₃⁻-N concentration occurred most frequently hours 13-18 (n=2) (Figure 8).

Winter had a mean daily NO₃⁻-N concentration ($\mu_{\text{daily [NO}_3^- \text{-N] Winter}}$) of 3.11 mg/L, a mean daily maximum NO₃⁻-N concentration ($\mu_{\text{max [NO}_3^- \text{-N] Winter}}$) of 3.25 mg/L, and a mean daily minimum NO₃⁻-N concentration ($\mu_{\text{min [NO}_3^- \text{-N] Winter}}$) of 2.87 mg/L (Figure 3, Figure 4, Table 1). The difference between maximum and minimum NO₃⁻-N concentration ($\mu_{\text{difference [NO}_3^- \text{-N] Winter}}$) was 0.38 mg/L (Figure 9, Table 1). The daily time of maximum NO₃⁻-N concentration occurred most frequently during hours 1-6 (n=3), and the daily timing of minimum NO₃⁻-N concentration occurred most frequently in the hours 13-18 (n=3) (Figure 8). NO₃⁻-N concentration behavioral trends included 1 sinusoidal, 4 increases, and no decreases (Figure 7). When only days with a sinusoidal trend are considered, daily time of maximum NO₃⁻-N concentration occurred most frequently hours 1-6 (n=1), and the daily timing of minimum NO₃⁻-N concentration occurred most frequently hours 13-18 (n=1) (Figure 8).

between hours 13-18 (n=9) (Figure 8). NO₃⁻-N concentration behavioral trends included 6 sinusoidal, 6 increase, and 1 decrease (Figure 7). When only days with a sinusoidal trend are considered, daily time of maximum NO₃⁻-N concentration occurred most frequently hours 1-6 (n=2) and 19-24 (n=3), and the daily timing of minimum NO₃⁻-N concentration occurred most frequently hours 13-18 (n=5) (Figure 8).

Summer had a mean daily NO₃⁻-N concentration ($\mu_{\text{daily [NO}_3^- \text{-N] Summer}}$) of 4.63 mg/L, a mean daily maximum NO₃⁻-N concentration ($\mu_{\text{max [NO}_3^- \text{-N] Summer}}$) of 4.81 mg/L, and a mean daily minimum NO₃⁻-N concentration ($\mu_{\text{min [NO}_3^- \text{-N] Summer}}$) of 4.25 mg/L (Figure 3, Figure 4, Table 1). The

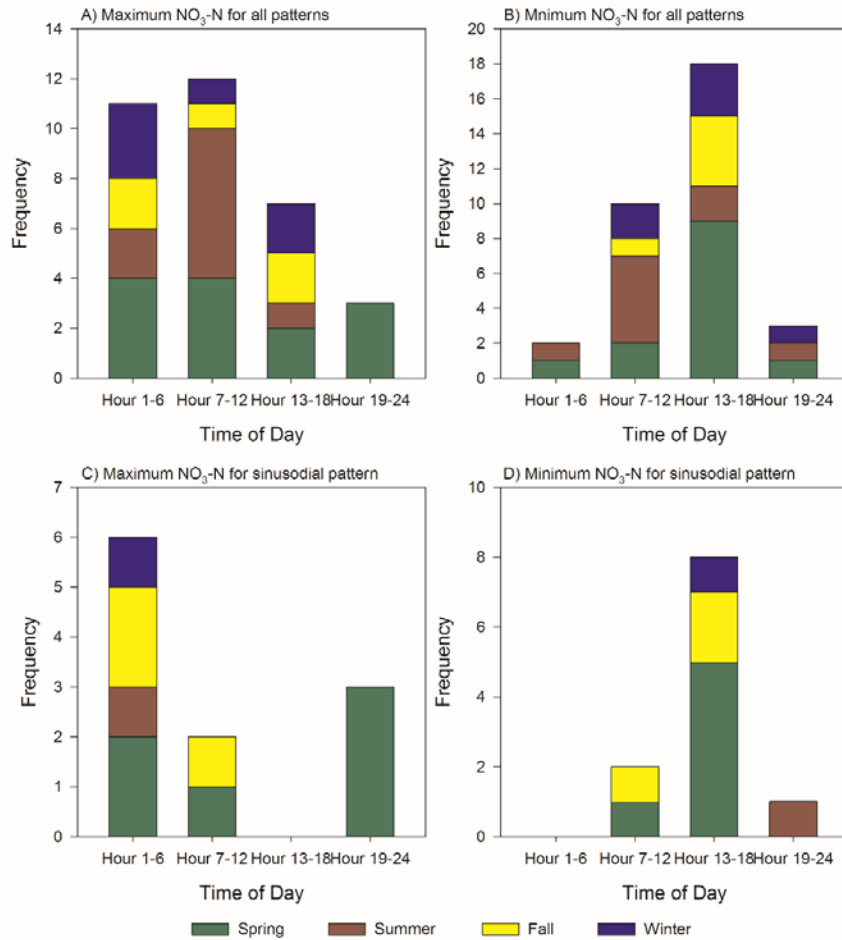


Figure 6. a) Frequency of maximum NO₃⁻-N concentration by time-of-day for increase, decrease, and sinusoidal trends. B) Frequency of minimum NO₃⁻-N concentration by time-of-day for increase, decrease, and sinusoidal trends. C) Frequency of maximum NO₃⁻-N concentration by time-of-day for sinusoidal trends. D) Frequency of minimum NO₃⁻-N concentration by time-of-day for sinusoidal trends.

b. Statistical Analyses of Nitrate-N Data

All seasons showed a statistically significant difference between their respective $\mu_{\max} [\text{NO}_3^- \text{-N}]$ and $\mu_{\min} [\text{NO}_3^- \text{-N}]$ (Figure 8, Table 2). The difference between $\mu_{\max} [\text{NO}_3^- \text{-N}]_{\text{All}}$ (3.67 mg/L) and $\mu_{\min} [\text{NO}_3^- \text{-N}]_{\text{All}}$ (3.15 mg/L) was also statistically significant. The $\mu_{\text{difference}} [\text{NO}_3^- \text{-N}]$ was greatest in the summer (0.61 mg/L) and lowest in the winter (0.38 mg/L) (Figure 7). However, there were no statistically significant differences between any season combinations (Figure 7, Table 2).

Two seasonal comparisons show a statistically significant difference between the mean daily NO₃⁻-N concentration (Figure 8, Table 3). The concentration difference between $\mu_{\text{daily}} [\text{NO}_3^- \text{-N}]_{\text{Fall}}$ was statistically significant to both $\mu_{\text{daily}} [\text{NO}_3^- \text{-N}]_{\text{Summer}}$ and $\mu_{\text{daily}} [\text{NO}_3^- \text{-N}]_{\text{Spring}}$. Spring-Summer, Spring-Winter, Summer-Winter, and Fall-Winter combinations are not statistically different (Figure 8, Table 3).

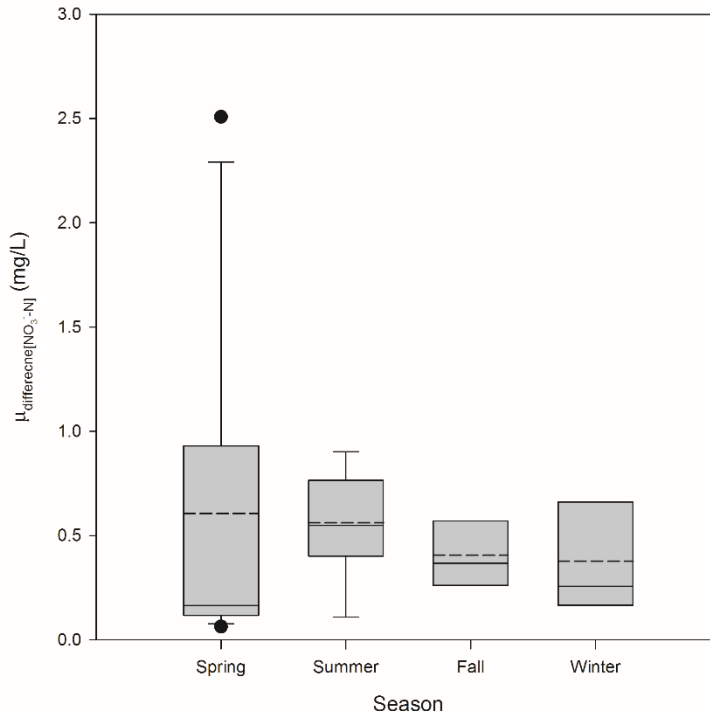


Figure 7. Box and whisker plots for the seasonal $\mu_{\text{difference}[\text{NO}_3\text{-N}]}$. No statistically significant differences in $\mu_{\text{difference}[\text{NO}_3\text{-N}]}$ are present among seasons. The ends of the boxes represent the 25th and 75th percentiles with the solid line at the median and the dashed line at the mean; the error bars depict the 10th and 90th percentiles; the points depict the outliers.

Table 2. *t*-test results for the stated comparisons. Results in bold signify a statistically significant difference.

Scenario	Outcome
Hypothesis 1	
$\mu_{\text{max}[\text{NO}_3\text{-N}] \text{ Spring}} > \mu_{\text{min}[\text{NO}_3\text{-N}] \text{ Spring}}$	$(t(12)=2.76, p=0.01)$
$\mu_{\text{max}[\text{NO}_3\text{-N}] \text{ Summer}} > \mu_{\text{min}[\text{NO}_3\text{-N}] \text{ Summer}}$	$(t(8)=6.83, p<0.01)$
$\mu_{\text{max}[\text{NO}_3\text{-N}] \text{ Fall}} > \mu_{\text{min}[\text{NO}_3\text{-N}] \text{ Fall}}$	$(t(4)=4.34, p=0.01)$
$\mu_{\text{max}[\text{NO}_3\text{-N}] \text{ Winter}} > \mu_{\text{min}[\text{NO}_3\text{-N}] \text{ Winter}}$	$(t(5)=3.33, p=0.01)$
$\mu_{\text{max}[\text{NO}_3\text{-N}] \text{ All}} > \mu_{\text{min}[\text{NO}_3\text{-N}] \text{ All}}$	$(t(32)=5.69, p<0.01)$
Hypothesis 2	
$\mu_{\text{difference} [\text{NO}_3\text{-N}] \text{ Spring}} \neq \mu_{\text{difference} [\text{NO}_3\text{-N}] \text{ Summer}}$	$(t(15.14)=0.19, p=0.85)$
$\mu_{\text{difference} [\text{NO}_3\text{-N}] \text{ Spring}} \neq \mu_{\text{difference} [\text{NO}_3\text{-N}] \text{ Fall}}$	$(t(16)=0.55, p=0.59)$
$\mu_{\text{difference} [\text{NO}_3\text{-N}] \text{ Spring}} \neq \mu_{\text{difference} [\text{NO}_3\text{-N}] \text{ Winter}}$	$(t(17)=0.68, p=0.51)$
$\mu_{\text{difference} [\text{NO}_3\text{-N}] \text{ Summer}} \neq \mu_{\text{difference} [\text{NO}_3\text{-N}] \text{ Fall}}$	$(t(12)=0.19, p=0.26)$
$\mu_{\text{difference} [\text{NO}_3\text{-N}] \text{ Summer}} \neq \mu_{\text{difference} [\text{NO}_3\text{-N}] \text{ Winter}}$	$(t(13)=1.35, p=0.20)$
$\mu_{\text{difference} [\text{NO}_3\text{-N}] \text{ Fall}} \neq \mu_{\text{difference} [\text{NO}_3\text{-N}] \text{ Winter}}$	$(t(9)=0.19, p=0.85)$

Table 3. *t*-test Results for statistically significant difference between $\mu_{\text{daily}}[\text{NO}_3^--\text{N}]_{\text{season}}$ & $\mu_{\text{daily}}[\text{NO}_3^--\text{N}]_{\text{season}}$

	$\mu_{\text{daily}}[\text{NO}_3^--\text{N}]_{\text{Spring}}$	$\mu_{\text{daily}}[\text{NO}_3^--\text{N}]_{\text{Summer}}$	$\mu_{\text{daily}}[\text{NO}_3^--\text{N}]_{\text{Fall}}$	$\mu_{\text{daily}}[\text{NO}_3^--\text{N}]_{\text{Winter}}$
$\mu_{\text{daily}}[\text{NO}_3^--\text{N}]_{\text{Spring}}$	-	$(t(20)=-1.89, p=0.07)$	$(t(15.90)=2.70, p=0.02)$	$(t(17)=0.46, p=0.65)$
$\mu_{\text{daily}}[\text{NO}_3^--\text{N}]_{\text{Summer}}$	-	-	$(t(10.91)=4.83, p<0.01)$	$(t(13)=2.10, p=0.06)$
$\mu_{\text{daily}}[\text{NO}_3^--\text{N}]_{\text{Fall}}$	-	-	-	$(t(9)=-1.44, p=0.19)$
$\mu_{\text{daily}}[\text{NO}_3^--\text{N}]_{\text{Winter}}$	-	-	-	-

Note. Significance indicated in bold.

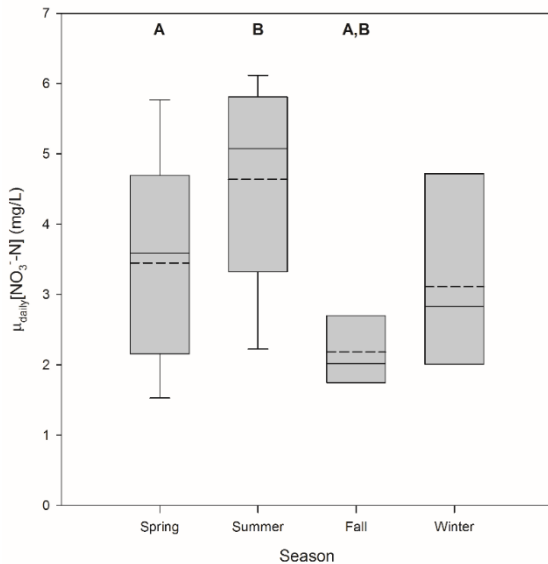


Figure 8. Daily NO_3^--N concentration by season. Letters above the boxes identify seasons with statistically significant difference between seasonal $\mu_{\text{daily}}[\text{NO}_3^--\text{N}]$. The ends of the boxes represent the 25th and 75th percentiles with the solid line at the median and the dashed lined at the mean; the error bars depict the 10th and 90th percentiles.

c. Environmental Factors

Environmental factor data were analyzed by grouping sinusoidal trend, increase trend, decrease trend, and all data. Groundwater temperature changed by an average of 0.14°C over 24-hours and followed air temperature seasonally increasing in summer and decreasing in winter (Figure 3, Table 4). DO remained below the 4.5mg/L threshold identified by Gómez *et al.* (2002) throughout the entire study (Table 4). Water column height peaked at >1,000 mm in January but then decreased to 600 to 700 mm from February to April (Figure 3). Another peak in water column height occurred in April from which it decreased with minor variation until August (Figure 3). Solar intensity in August 2016 was ~15,000 lux but decreased to < 5,000 lux in February 2017 (Figure 3). From February 2017 solar intensity increased steadily to 20,000 to 25,000 lux in June 2017 (Figure 3). Overall, no significant correlations existed among the environmental factors and the NO_3^--N concentration difference. Water temperature did not display a significant correlation with NO_3^--N concentration difference (Pearson correlation $r=0.31, p=0.08$) (Figure 15). Water temperature change over 24-hours did not display a significant correlation with NO_3^--N concentration difference (Pearson correlation $r=-0.25, p=0.20$) (Figure 10). When all data

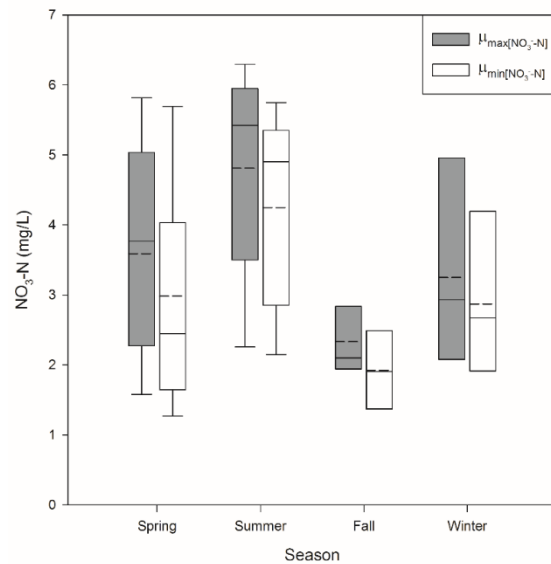


Figure 9. Daily $\mu_{\text{max}}[\text{NO}_3^--\text{N}]$ and $\mu_{\text{min}}[\text{NO}_3^--\text{N}]$ for each season. Statistically significantly different $\mu_{\text{max}}[\text{NO}_3^--\text{N}]$ and $\mu_{\text{min}}[\text{NO}_3^--\text{N}]$ occur in each season. The ends of the boxes represent the 25th and 75th percentiles with the solid line at the median and the dashed line at the mean; the error bars depict the 10th and 90th percentiles.

are analyzed together, other environmental factors including air temperature, average solar value, water column height, and dissolved oxygen did not display a correlation with NO_3^- -N concentration difference (Figure 10). When data were grouped as diurnal sinusoidal and increase/decrease trends, environmental factors including water temperature, air temperature, average solar value, water column height, and dissolved oxygen did not display a significant correlation with NO_3^- -N concentration difference (Figure 10).

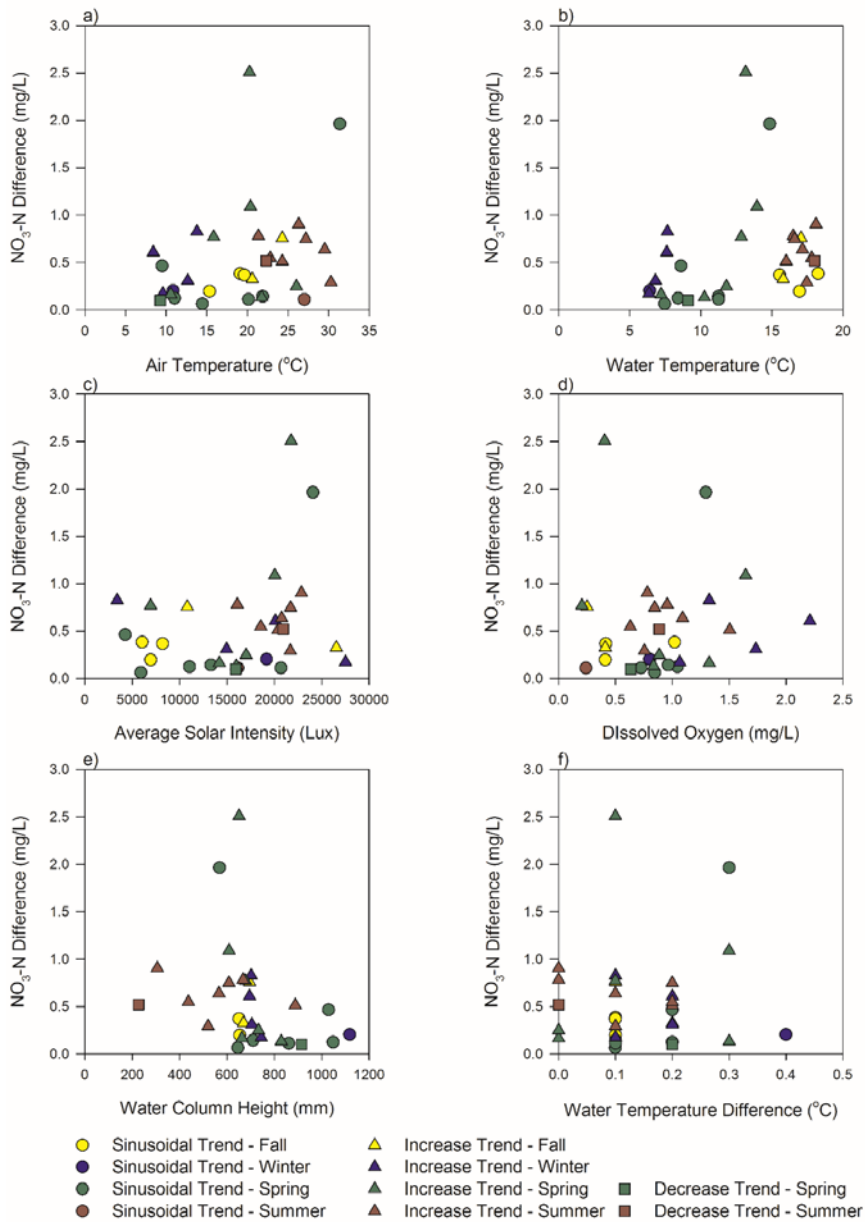


Figure 10. Environmental factor correlations for sinusoidal, increase, and decrease trends by season. Difference between 24-hour maximum and minimum on Y axis A) daily air temperature B) daily water temperature, range: 1.4-31.4°C C) daily average solar intensity D) daily dissolved oxygen E) water column height F) 24-hour water temperature difference.

Table 4. Seasonal means \pm standard deviation for environmental factors

Season	Water Column Height (mm)	Dissolved Oxygen (mg/L)	Groundwater Temperature (°C)	Air Temperature (°C)	Average Solar Value (lux) *	Temperature Difference over 24-hours (°C)
Spring	764 \pm 157	0.90 \pm 0.40	12.27 \pm 5.35	17.88 \pm 6.82	14,707 \pm 6,276	0.15 \pm 0.11
Summer	527 \pm 209	0.85 \pm 0.34	18.02 \pm 1.58	25.68 \pm 3.17	19,907 \pm 2,440	0.10 \pm 0.09
Fall	667 \pm 20	0.50 \pm 0.30	16.73 \pm 1.08	19.79 \pm 3.21	11,710 \pm 8,481	0.12 \pm 0.04
Winter	786 \pm 164	1.67 \pm 0.77	6.96 \pm 0.76	9.45 \pm 4.40	14,606 \pm 9,905	0.18 \pm 0.12
All Seasons	695 \pm 190	0.97 \pm 0.58	13.36 \pm 5.33	18.77 \pm 7.38	15,652 \pm 6,976	0.14 \pm 0.10

Note. * average solar value = $\frac{\sum \text{hourly solar intensity}}{24 \text{ hours}}$; lux = lumen/m²

d. Discussion

Over the duration of the study, statistically significant variation in NO₃⁻-N concentration was observed on the seasonal scale (Figure 3, Table 3). Seasonally, both spring and summer had significantly greater $\mu_{\text{daily}}[\text{NO}_3^- \text{-N}]$ than fall, while spring, summer, and winter combinations are similar (Figure 3, Table 3). Therefore, the hypothesis that there will be no significant difference in $\mu_{\text{daily}}[\text{NO}_3^- \text{-N}]$ seasonally was rejected. Spring (3.45 mg/L) and summer (4.63 mg/L) display high $\mu_{\text{daily}}[\text{NO}_3^- \text{-N}]$ and can be described as enriched compared to fall (2.18 mg/L), while fall can be described as depleted. The enriched spring and summer $\mu_{\text{daily}}[\text{NO}_3^- \text{-N}]$ coincided with routine fertilizer application for this area in March and May (Lamb, 2004). Although additional fertilizer is typically applied post-harvest, the use of N-Serve with a fall fertilizer application would result in the delay of NO₃⁻ generation, accounting for the depleted $\mu_{\text{daily}}[\text{NO}_3^- \text{-N}]$ observed in fall and enriched $\mu_{\text{daily}}[\text{NO}_3^- \text{-N}]$ in winter. N-Serve delays NO₃⁻ generation by slowing bacterial nitrification of anhydrous ammonia, the form of nitrogen fertilizer used in Central Illinois (Lamb, 2004).

Within each season, the 24-hour $\mu_{\text{max}}[\text{NO}_3^- \text{-N}]$ is significantly greater than the 24-hour $\mu_{\text{min}}[\text{NO}_3^- \text{-N}]$ (Figure 9, Table 2). Therefore, the hypothesis that there will be no significant difference between $\mu_{\text{max}}[\text{NO}_3^- \text{-N}]$ and $\mu_{\text{min}}[\text{NO}_3^- \text{-N}]$ in each season was rejected (Figure 4). Change in NO₃⁻-N concentration over a 24-hour period was the result of both physical and biological processes such as vegetation uptake, nitrification, dilution, and NO₃⁻ transport. The source of diurnal change in NO₃⁻-N concentration were identified through examination of the high resolution 24-hour time-series NO₃⁻-N concentration data. Specific processes manifest as a specific trend in groundwater NO₃⁻-N concentration over time. Time-series data followed three trends of hourly change over 24-hours: increase, decrease, and sinusoidal (Figure 4).

Summer and winter diurnal changes in NO₃⁻-N concentration are primarily caused by three processes of NO₃⁻-N concentration increase, as the increase trend produced by these three processes comprises >50% of sampling days in these seasons (Figure 5). The three processes of NO₃⁻-N concentration increase include: input of NO₃⁻ to the system by transport from outside the saturated buffer, concentration of solute by evapotranspiration, and nitrification.

Input of NO₃⁻ to the system by transport from outside the saturated buffer is possible by advection-dispersion. Moore and Peterson, 2007 found NO₃⁻ transport by advection-dispersion in glacial till, the material of this study site, to be related to fertilizer application and unrelated to precipitation events. The upgradient agricultural land-use area would serve as a NO₃⁻ source with potential for transport downgradient to the saturated buffer. This explanation fits observed 24-hour scale NO₃⁻-N and Cl⁻ data. Data show NO₃⁻-N and Cl⁻ concentration increase together but do not increase in parallel (Figure 3). Downgradient transport of NO₃⁻ from fertilizer application could include Cl⁻, because Cl⁻ is a degradation product of N-serve, a nitrogen stabilizer, known to be applied with fertilizer in this area (Lamb, 2004). Degradation of N-Serve to Cl⁻ provides a source of Cl⁻ that is transported alongside NO₃⁻ in similar but non-parallel amounts, accounting for the observed NO₃⁻-N and Cl⁻ concentration changes.

Evapotranspiration (ET) may play a role by concentrating solute in the shallow subsurface. McIsaac *et al.* (2010) estimated the May-November 2005-2008 average evapotranspiration total for switchgrass plots in Central Illinois to be 291-308 mm based on soil moisture measurements. Water table fluctuations

related to ET have been observed on the seasonal and diurnal scales (Satchithanatham *et al.*, 2017) and even used to estimate vegetation water demands (Nachabe *et al.*, 2005, Loheide II, 2008). It is conceivable that switchgrass ET concentrated NO_3^- in the shallow aquifer by removing water from the system on the seasonal scale. Across the field site, diurnal changes in head correspond with long term increases or decreases and do not exhibit cyclic diurnal fluctuation (unreported data). Evaporation removes water from the system directly, by vaporizing water from the land surface and soil. Transpiration is a process where vegetation transmits water from root tissue to leaves and the atmosphere. NO_3^- uptake by vegetation operates independently of transpiration (Hopmans & Bristow, 2002), meaning NO_3^- concentration by ET is possible if the rate of ET is greater than the rate of NO_3^- uptake. Water column height data supports ET as a mechanism, as water column height generally dropped over periods of NO_3^- -N concentration increase. The substantial drop in water column height observed from June 2017 to August 2017 (Figure 3) indicates a lack of rain that would drive vegetation to extract water from the aquifer. The 24-hour time-series increase trend NO_3^- -N and Cl^- data taken in conjunction with water column height data support ET as a contributor to NO_3^- -N and Cl^- concentration increases, as NO_3^- -N and Cl^- concentration increases are loosely coupled (Figure 6). ET cannot be the only cause of NO_3^- -N concentration increases, because NO_3^- -N concentration increases faster than Cl^- concentration.

Nitrification is another mechanism that may contribute to the observed increase in NO_3^- -N. Nitrification produces NO_3^- independent of Cl^- and can account for the minor divergence in NO_3^- -N and Cl^- concentration, where NO_3^- increases faster than Cl^- (Figure 6). Nitrification is a nitrogen transformation process where ammonium (NH_4^+) is converted to NO_3^- via aerobic microbial metabolism (Hefting *et al.*, 2004). Nitrification is not possible in anoxic conditions, leaving ammonium to accumulate until nitrification can occur (Hefting *et al.*, 2004). Ammonium could have accumulated in the saturated zone pore space until the water table dropped enough for pore space to become aerated and support the conversion of NH_4^+ to NO_3^- by nitrification in the unsaturated zone. No data was collected in the unsaturated zone, but saturated zone average DO concentration remained below the 1.0 mg/L threshold, below which nitrification remains arrested allowing NH_4^+ accumulation, identified by Garrido *et al.* (1997) in spring, summer, and fall (Table 4). Further supporting this speculation, water column height decreased over periods where NO_3^- -N concentration increased (Figure 3). Similar to this study, Hefting *et al.* (2004) found nitrification to increase as water table level dropped. NO_3^- produced by nitrification in the unsaturated zone could be transported to the saturated zone by percolating soil water. Soil water is known to be a conduit by which solutes can be transported through unsaturated flow (Nielsen *et al.*, 1986).

A multi-mechanism process of NO_3^- -N concentration increase is the best supported explanation, given the similar but slightly faster increase in NO_3^- -N compared to Cl^- . The multi mechanism process includes ET driven concentration of solute and water table drop, nitrification stimulated by water table drop and aeration, and transported NO_3^- from upgradient agricultural land use. The primary mechanism, or mechanism producing the greatest change, likely varies through the year as environmental conditions change favoring one over another. For example, increases during the winter are more likely driven by NO_3^- transport than ET or nitrification. Evaporation is decreased during winter months in Central Illinois, and transpiration is limited as vegetation goes dormant. Data averaged over 35 years in Central Illinois, obtained from Angel (2017), displays total pan evaporation for October to be <50% of July. Although a precise range for optimal nitrification is disputed, several studies agree that bacterial nitrification rates in soil decreases with temperature and steeply declines below 10°C (Frederick, 1956, Saad & Conrad, 1993, Sabey *et al.*, 1956).

The decrease trend was observed in spring and summer, but did not occur often and is not characteristic of any season. The two decrease trends observed display a parallel decrease in NO_3^- -N and Cl^- , indicative of dilution (Figure 4). Further providing evidence of dilution, precipitation events of ~12 mm occurred 4-5 days before the sampling periods that generated the 24-hour decreasing NO_3^- -N concentration trends (Angel, 2017). Precipitation takes days to infiltrate and may contribute to dilution of solute in the aquifer several days later.

Spring and fall changes in NO_3^- -N concentration on the 24-hour scale is primarily caused by vegetation uptake, as the sinusoidal trend produced by vegetation uptake comprises $\geq 50\%$ of trends observed in these seasons. Vegetation uptake produces the sinusoidal trend by extraction of NO_3^- from the surficial aquifer during the photoperiod and a lack of vegetation extraction during the dark period. Delhon *et al.* (1996) observed a similar sinusoidal trend in NO_3^- uptake rate that displayed a relationship to photoperiod in soybean. Spring and fall environmental conditions support vegetation growth, as air and groundwater temperature data remain well above the 10°C threshold for plant growth (Mitchell *et al.*, 1997) (Figure 3, Table 4). Well-developed root systems of vegetation like switchgrass, the dominant species on the study site, are known to have a great capacity for NO_3^- uptake (Schimel, 1986), capable of recovering 66% of applied nitrogen (Bransby *et al.*, 1998). Switchgrass is not known to be a substantial nitrifier, and recent studies have found nitrogen fertilization to increase biomass yield (Lemus *et al.*, 2008, Guretzky *et al.*, 2011). An increase in biomass yield from fertilization confirms the responsiveness of switchgrass to NO_3^- inputs. This study site was not fertilized and external NO_3^- inputs are limited to NO_3^- import from upgradient fields.

Time of maximum and minimum NO_3^- -N concentration further indicates the process responsible for the sinusoidal trend is vegetation uptake. Time of maximum and minimum NO_3^- -N concentration varies by season for all data combined (Figure 9). However, sinusoidal trend days displayed a pronounced pattern of minimum NO_3^- -N concentration at the end of the photoperiod and maximum NO_3^- -N concentration near the beginning (Figure 6). During the summer, when days are longer, the time of minimum shifted to later in the day (Figure 6). Therefore, the hypothesis that there will be no difference in the time-of-day when the maximum and minimum NO_3^- -N concentration occurs for all seasons is rejected. Although the duration of the photoperiod differs between spring and summer, the observed relationship between photoperiod and NO_3^- -N concentration is the same (Figure 6). This is consistent with the findings of Delhon *et al.* (1996) that NO_3^- uptake in soybean coincided with photoperiod. Delhon *et al.* (1996) and Pearson and Steer (1977) reasoned that photoperiod controlled energy availability in plant vascular tissue through photosynthesis, and that NO_3^- uptake is limited in dark conditions.

Relevant environmental factors such as water column height, groundwater temperature, air temperature, and solar intensity did not display a significant relationship with the magnitude of difference in NO_3^- -N concentration when grouped by trend or combined data (Figure 10). This is surprising, as an increase in vegetation uptake was expected with greater solar intensity and warmer temperatures. The lack of a strong relationship between environmental factors and vegetation uptake indicates that vegetation uptake is unaffected by changes beyond a threshold for photosynthesis, or that competing processes mask relationships that may exist. Samples taken during this study measured net NO_3^- -N concentration, meaning measured NO_3^- -N concentration is the product of combined processes such as vegetation uptake, ET, nitrification, dilution, leaching, and denitrification. A process or group of related processes can only be identified by net NO_3^- -N concentration trends when sufficiently isolated from background.

An alternate process with the potential to produce a sinusoidal trend is microbial denitrification. If microbial denitrification rate changed within a 24-hour period, that change could produce a sinusoidal trend. Denitrification rate is controlled by temperature, dissolved oxygen, and dissolved organic carbon. If any of these factors varied on the 24-hour scale, then a change in denitrification rate would be expected. However, temperature and dissolved oxygen data do not support microbial denitrification as the mechanism for the sinusoidal trend. Groundwater temperature varied by an average of $0.14 \pm$ the standard deviation of 0.01°C over a 24-hour period for all seasons, and dissolved oxygen remained well below the 4.5mg/L threshold for denitrification for all seasons (Table 4). Additionally, 24-hour water temperature difference displays no correlation with NO_3^- -N concentration difference for days with sinusoidal trend or comprehensive data (Figure 10). Dissolved organic carbon samples were not collected in this study and is a topic for future research.

A higher frequency of sinusoidal trends was expected in summer, as the potential for photosynthesis is high during summer. However, competing processes overwhelmed the vegetation uptake signal. The vegetation uptake signal appears and disappears throughout the study period and is only observed once in

summer. The presence or absence of a vegetation uptake signal requires the magnitude of hourly background variation to be lower than that of vegetation uptake. This observation is confirmed by other riparian zone studies which found NO_3^- processing mechanisms to operate independently or simultaneously depending on environmental conditions (Sabater *et al.*, 2003, Haycock & Pinay, 1993, Simmons *et al.*, 1992). Winter displaying a sinusoidal trend once during the season was also surprising (Figure 5). However, this is explained by the unusually warm $>10^\circ\text{C}$ average air temperature for the day, which would have allowed for vegetation uptake (Figure 3). Overall, winter NO_3^- concentrations are likely controlled by NO_3^- transport from upgradient sources.

A statistically significant difference in $\mu_{\text{difference}}[\text{NO}_3^-\text{-N}]$ was expected among seasons, as some seasons are more heavily influenced by one process than another. This is evident in the frequency of each trend throughout the year, and the underlying mechanisms responsible for the trend i.e. vegetation uptake, ET, leaching, nitrification, and dilution. However, no statistically significant differences in $\mu_{\text{difference}}[\text{NO}_3^-\text{-N}]$ were found between any season combinations (Figure 10, Table 2).

Therefore, the hypothesis that there will be no significant difference between $\mu_{\text{difference}}[\text{NO}_3^-\text{-N}]$ among the four seasons is accepted. This means the magnitude of difference in NO_3^- concentration that occurred over 24-hours due to vegetation uptake, nitrification, dilution, NO_3^- transport, and ET is similar. This may be due to a dampening effect from competing processes within one day or averaged over a season. Additionally, a lack of significant differences in $\mu_{\text{difference}}[\text{NO}_3^-\text{-N}]$ across seasons that have a significantly different $\mu_{\text{daily}}[\text{NO}_3^-\text{-N}]$ suggests $\mu_{\text{daily}}[\text{NO}_3^-\text{-N}]$ did not influence $\mu_{\text{difference}}[\text{NO}_3^-\text{-N}]$. In other words, the amount of NO_3^- available did not affect the magnitude of 24-hour change observed in this study (Figure 11). Ultimately, this study has demonstrated that variation in NO_3^- concentration exists on both the seasonal and diurnal scale, multiple processes produce variation i.e. vegetation uptake, ET, nitrification, and NO_3^- transport, and that variation over 24-hours is consistent across processes.

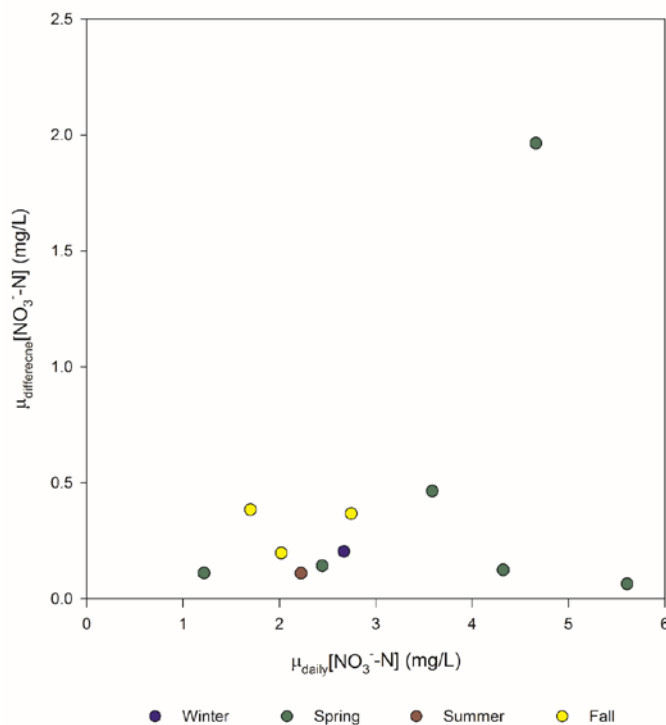


Figure 11. $\mu_{\text{daily}}[\text{NO}_3^-\text{-N}]$ concentrations versus $\mu_{\text{difference}}[\text{NO}_3^-\text{-N}]$ for sinusoidal pattern. Despite a range of 5.4 mg/L in $\mu_{\text{daily}}[\text{NO}_3^-\text{-N}]$, the majority of $\mu_{\text{difference}}[\text{NO}_3^-\text{-N}]$ exhibits minimal variation, a range of 0.4 mg/L.

VI. Significance

Seasonally, both spring and summer average significantly greater daily NO_3^- -N concentrations than fall (Figure 3). Therefore, the hypothesis that there will be no significant difference in $\mu_{\text{daily}}[\text{NO}_3^-\text{-N}]$ seasonally is rejected. Within each season, average daily maximum NO_3^- -N concentration is significantly greater than average daily minimum (Figure 4). Therefore, the hypothesis that there will be no significant

difference between the $\mu_{\max} [\text{NO}_3^- \text{-N}]$ and $\mu_{\min} [\text{NO}_3^- \text{-N}]$ $\text{NO}_3^- \text{-N}$ concentration in each season is rejected (Figure 4). Time of maximum and minimum $\text{NO}_3^- \text{-N}$ concentration varies by season (Figure 7, Figure 8). Therefore, the hypothesis that there will be no difference in the time-of-day when the maximum and minimum $\text{NO}_3^- \text{-N}$ concentration occurs for all seasons is rejected. No statistically significant differences in $\mu_{\text{difference}} [\text{NO}_3^- \text{-N}]$ were found between any season combinations (Figure 9). Therefore, the hypothesis that there will be no significant difference between $\mu_{\text{difference}} [\text{NO}_3^- \text{-N}]$ among the four seasons is accepted.

The most notable observations in this study are the 24-hour time series vegetation uptake and multi-process increase signals. Time of maximum and minimum $\text{NO}_3^- \text{-N}$ concentration data indicate vegetation uptake generates the sinusoidal trend. Time of maximum and minimum $\text{NO}_3^- \text{-N}$ concentration occurs when it would be expected for a photosynthetically controlled process. Maximum $\text{NO}_3^- \text{-N}$ concentration occurs during the dark period, while minimum $\text{NO}_3^- \text{-N}$ concentration occurs at the end of the photoperiod (Figure 4, Figure 6). Vegetation uptake is observed under conditions where vegetation growth is possible and sufficiently isolated from competing processes by environmental conditions. The alternate explanation for the sinusoidal trend, denitrification, is not supported by these data. If denitrification were the process responsible for the time of maximum and time of minimum $\text{NO}_3^- \text{-N}$ concentration, then the denitrification rate would need to change and would have to be driven by water temperature changes. No relationship exists between 24-hour water temperature difference and $\text{NO}_3^- \text{-N}$ concentration difference (Figure 15). Additionally, these data indicate multiple processes are responsible for the increase trend. Anoxic conditions in the saturated zone coupled with water column height drops from ET provide ideal conditions for conversion of accumulated NH_4^+ to NO_3^- in the unsaturated zone. NO_3^- produced by nitrification in the unsaturated zone was then transported to the saturated zone by unsaturated flow. NO_3^- transport from the upgradient agricultural land use are best accounts for increases during the winter.

As an area that is intensively farmed, Illinois fields receive a large amount of NO_3^- fertilizer yearly [46]. Tile drains make many forms of NO_3^- management ineffective, exporting NO_3^- through soil into streams, bypassing riparian zones and making best management practices such as riparian buffers less effective [47]. The results of this study reinforce the importance of vegetation NO_3^- uptake. The results presented here provide evidence for a measurable contribution of NO_3^- removal by vegetation. Seasons that have a significantly different $\mu_{\text{daily}} [\text{NO}_3^- \text{-N}]$ do not have a significantly different $\mu_{\text{difference}} [\text{NO}_3^- \text{-N}]$. This means the amount of NO_3^- available does not influence the magnitude of change over 24-hours. If implemented, conservation practices that intercept and increase residence times of water will reduce NO_3^- loads. Future research could focus on quantification of total nitrogen captured by vegetation, NO_3^- flux in the unsaturated zone, and stable isotope methods for NO_3^- source and fate. This study focused on $\text{NO}_3^- \text{-N}$ in the saturated zone, but other forms of nitrogen such as ammonium and nitrite in the unsaturated zone may be of interest.

VII. Students supported

A total of three students were directly involved in the project: Graduate student Joseph Miller; Undergraduate students Linnea Johnson and Clint Updike. Direct support was provided to Mr. Miller and Mr. Updike. Ms. Johnson was involved through independent research. Below, I provide a more detailed description of the students' role and status.

Joseph Miller – MS 2017, Mr. Miller served as the lead student on the project. Mr. Miller conducted the weekly sampling events and analyzed all of the samples. In addition to coordinating and collecting the water samples, Mr. Miller conducted the statistical analyses under the guidance of PI Peterson. Mr. Miller presented his work at two conference: the Geological Society of America annual meeting in Seattle, WA and at the Illinois Groundwater Association meeting at Argonne National Laboratory. An article in Redbird Scholar focused on Mr. Miller's work. Mr. Miller graduated in December 2017 and is actively seeking employment.

Linnea Johnson – BS expected 2019, Ms. Johnson was involved in data management and reduction. Using this data set and additional data collected from the T3 site, she developed an independent project
.....

Clint Updike – BS expected 2019, Mr. Updike provided field support for Mr. Miller. Mr. Updike was involved with sample preparation, sample collection, and data entry.

GEO 444 – Applied Groundwater Modeling: The data collected during the project was incorporated into the curriculum of the Applied Groundwater Modeling course in the Fall 2017. Students used the data in a solute transport model of the T3 site. Model development is ongoing. .

VIII. Publications

a. *MS Thesis*

Miller, J., 2018, Diurnal and seasonal variation in nitrate-nitrogen concentrations of groundwater in a saturated buffer zone.: Normal, IL, Illinois State University, 79 p.

b. *Peer-Reviewed Academic Journals*

Miller, J.*, and **Peterson, E.W.**, *in review*, Diurnal and seasonal variation in nitrate-nitrogen concentrations of groundwater in a saturated buffer zone: Hydrological Processes

A second publication is being drafted that details the role of the saturated buffer in the removal of nitrate from the system. The paper relies heavily on the work of Mr. Miller and Ms. Johnson.

c. *Presentations*

Miller, J. *, and **Peterson, E.W.**, (2018) Diurnal and seasonal variation in groundwater nitrate-N concentration in a saturated buffer zone, Illinois Lake Management Association, 33rd Annual Conference, March 22,2018

Miller, J. *, and **Peterson, E.W.**, (2017) Diurnal and seasonal variation in groundwater nitrate-N concentration in a saturated buffer zone, Illinois Groundwater Association, October 27, 2017.

Johnson, L.L.**, O'Reilly, C.M., **Peterson, E.W.**, Heath, V.E., Miller, J.J.*, Gregorich, H.G.***, and Twait, R., (2017) Field drain tile diversion into a riparian buffer zone effects on spatial dispersion of nitrate in groundwater, Abstract with Programs - Geological Society of America, October 2017, Vol. 49, No. 6, doi: 10.1130/abs/2017AM-308134

Miller, J. *, **Peterson, E.W.**, and Twait, R, (2017) Diurnal and seasonal variation in groundwater nitrate-N concentration in a saturated buffer zone, Abstract with Programs - Geological Society of America, October 2017, Vol. 49, No. 6, doi: 10.1130/abs/2017AM-305004

d. *Media recognition*

“Aspiring hydrogeologist offers a fresh take on water quality” *Redbird Scholar*, September 14, 2017, <https://news.illinoisstate.edu/2017/09/aspiring-hydrogeologist-offers-fresh-take-water-quality/> The article details the relevance of the Joe Miller’s project and impact on the drinking water reservoirs in the area.

IX. References

- Alexander, R.B., Smith, R.A. & Schwarz, G.E. (2000) Effect of stream channel size on the delivery of nitrogen to the Gulf of Mexico. *Nature* 403, 758-761.
- Alexander, R.B., Smith, R.A., Schwarz, G.E., Boyer, E.W., Nolan, J.V. & Brakebill, J.W. (2008) Differences in phosphorus and nitrogen delivery to the Gulf of Mexico from the Mississippi River Basin. *Environmental Science & Technology* 42, 822-830.
- Anderson, T.R., Groffman, P.M., Kaushal, S.S. & Walter, M.T. (2014) Shallow groundwater denitrification in riparian zones of a headwater agricultural landscape. *Journal of Environmental Quality* 43, 732-744.
- Angel, J. (2017) Weather Observations for Champaign-Urbana. Illinois State Water Survey.
- Beach, V. (2008) The impact of streambed sediment size on hyporheic temperature profiles in a low gradient third-order agricultural stream. Illinois State University, Normal.
- Beaulieu, J.J., Mayer, P.M., Kaushal, S.S., Pennino, M.J., Arango, C.P., Balz, D.A., Canfield, T.J., Elonen, C.M., Fritz, K.M., Hill, B.H., Ryu, H. & Domingo, J.W.S. (2014) Effects of urban stream burial on organic matter dynamics and reach scale nitrate retention. *Biogeochemistry* 121, 107-126.
- Bot, J.L. & Kirkby, E.A. (1992) Diurnal uptake of nitrate and potassium during the vegetative growth of tomato plants. *Journal of Plant Nutrition* 15, 247-264.
- Bransby, D.I., Mclaughlin, S.B. & Parrish, D.J. (1998) A review of carbon and nitrogen balances in switchgrass grown for energy. *Biomass and Bioenergy* 14, 379-384.
- Changnon, S.A., Angel, J.R., Kunkel, K.E. & Lehmann, C.M.B. (2004) *Climate atlas of Illinois*. Illinois State Water Survey.
- David, M.B., Drinkwater, L.E. & Mcisaac, G.F. (2010) Sources of nitrate yields in the Mississippi River Basin. *Journal of Environmental Quality* 39, 1657-1667.
- David, M.B. & Gentry, L.E. (2000) Anthropogenic inputs of nitrogen and phosphorus and riverine export for Illinois, USA. *Journal of Environmental Quality* 29, 494-508.
- David, M.B., Gentry, L.E., Kovacic, D.A. & Smith, K.M. (1997) Nitrogen balance in and export from an agricultural watershed. *Journal of Environmental Quality* 26, 1038-1048.
- David, M.B., Wall, L.G., Royer, T.V. & Tank, J.L. (2006) Denitrification and the nitrogen budget of a reservoir in an agricultural landscape. *Ecological Applications* 16, 2177-2190.
- Davis, D.M., Gowda, P.H., Mulla, D.J. & Randall, G.W. (2000) Modeling nitrate nitrogen leaching in response to nitrogen fertilizer rate and tile drain depth or spacing for southern Minnesota, USA. *Journal of Environmental Quality* 29, 1568-1581.
- Delgado, J.A. (2002) Quantifying the loss mechanisms of nitrogen. *Journal of Soil and Water Conservation* 57, 389-398.
- Delhon, P., Gojon, A., Tillard, P. & Passama, L. (1996) Diurnal regulation of NO_3^- uptake in soybean plants IV. Dependence on current photosynthesis and sugar availability to the roots. *Journal of Experimental Botany* 47, 893-900.
- Dick, R.P., Christ, R.A., Istok, J.D. & Iyamuremye, F. (2000) Nitrogen fractions and transformations of vadose zone sediments under intensive agriculture in Oregon. *Soil Science* 165, 505-515.
- Dinnes, D.L., Karlen, D.L., Jaynes, D.B., Kaspar, T.C., Hatfield, J.L., Colvin, T.S. & Cambardella, C.A. (2002) Nitrogen management strategies to reduce nitrate leaching in tile-drained Midwestern soils. *Agronomy Journal* 94, 153-171.
- Eggert, M., Rowley, R. & Peterson, E.W. (2015) Chloride Levels in Illinois Rivers and Streams. AAG Annual Meeting. Chicago, IL.
- Fausey, N.R., Brown, L.C., Belcher, H.W. & Kanwar, R.S. (1995) Drainage and Water Quality in Great Lakes and Cornbelt States. *Journal of Irrigation and Drainage Engineering* 121, 283-288.
- Frederick, L.R. (1956) The Formation of Nitrate from Ammonium Nitrogen in Soils: I. Effect of Temperature. *Soil Science Society of America Journal* 20, 496-500.

- Galloway, J.N., Aber, J.D., Erisman, J.W., Seitzinger, S.P., Howarth, R.W., Cowling, E.B. & Cosby, B.J. (2003) The nitrogen cascade. *BioScience* 53, 341-356.
- Garrido, J.M., Van Benthum, W.a.J., Van Loosdrecht, M.C.M. & Heijnen, J.J. (1997) Influence of dissolved oxygen concentration on nitrite accumulation in a biofilm airlift suspension reactor. *Biotechnology and Bioengineering* 53, 168-178.
- Gilliam, J.W. (1994) Riparian Wetlands and Water Quality. *Journal of Environmental Quality* 23, 896-900.
- Gómez, M., Hontoria, E. & González-López, J. (2002) Effect of dissolved oxygen concentration on nitrate removal from groundwater using a denitrifying submerged filter. *Journal of hazardous materials* 90, 267-278.
- Goolsby, D.A., Battaglin, W.A., Aulenbach, B.T. & Hooper, R.P. (2001) Nitrogen input to the Gulf of Mexico. *Journal of Environmental Quality* 30, 329-336.
- Guretzky, J.A., Biermacher, J.T., Cook, B.J., Kering, M.K. & Mosali, J. (2011) Switchgrass for forage and bioenergy: harvest and nitrogen rate effects on biomass yields and nutrient composition. *Plant and Soil* 339, 69-81.
- Haycock, N.E. & Pinay, G. (1993) Groundwater nitrate dynamics in grass and poplar vegetated riparian buffer strips during the winter. *Journal of Environmental Quality* 22, 273-278.
- Hefting, M., Clément, J.C., Dowrick, D., Cosandey, A.C., Bernal, S., Cimpian, C., Tatur, A., Burt, T.P. & Pinay, G. (2004) Water table elevation controls on soil nitrogen cycling in riparian wetlands along a European climatic gradient. *Biogeochemistry* 67, 113-134.
- Hill, A.R. (1996) Nitrate removal in stream riparian zones. *Journal of Environmental Quality* 25, 743-755.
- Hopmans, J.W. & Bristow, K.L. (2002) Current Capabilities and Future Needs of Root Water and Nutrient Uptake Modeling. *Advances in Agronomy* (ed D.L. Sparks), pp. 103-183. Academic Press.
- Illinois Department of Agriculture (2014) Facts About Illinois Agriculture.
- Keeney, D.R. & Hatfield, J.L. (2001) The nitrogen cycle: Historical perspective, and current and potential future concerns. *Nitrogen in the environment: Sources, problems, and solutions* (eds R. Follett & J.L. Hatfield), pp. 3-16. Elsevier, Amsterdam.
- Kelly, W.R. (2008) Long-term trends in chloride concentrations in shallow aquifers near Chicago. *Ground Water* 46, 772-781.
- Kelly, W.R., Panno, S.V. & Hackley, K.C. (2009) Impacts of road salt on water resources in the Chicago region. 2009 UCOWR conference. Southern Illinois University, Carbondale, IL.
- Kelly, W.R., Panno, S.V., Hackley, K.C., Hwang, H.H., Martinsek, A.T. & Markus, M. (2010) Using chloride and other ions to trace sewage and road salt in the Illinois Waterway. *Applied Geochemistry* 25, 661-673.
- Kovacic, D.A., Twait, R.M., Wallace, M.P. & Bowling, J.M. (2006) Use of created wetlands to improve water quality in the Midwest-Lake Bloomington case study. *Ecological Engineering* 28, 258-270.
- Kuusemets, V., Mander, Ü., Lõhmus, K. & Ivask, M. (2001) Nitrogen and phosphorus variation in shallow groundwater and assimilation in plants in complex riparian buffer zones. *Water Science and Technology* 44, 615-622.
- Lamb, D. (2004) *Vadose and Shallow Saturated Nitrate Transport at Lake Bloomington, Illinois*. MS, Illinois State University, Normal, IL.
- Lemus, R., Charles Brummer, E., Lee Burras, C., Moore, K.J., Barker, M.F. & Molstad, N.E. (2008) Effects of nitrogen fertilization on biomass yield and quality in large fields of established switchgrass in southern Iowa, USA. *Biomass and Bioenergy* 32, 1187-1194.
- Loheide II, S.P. (2008) A method for estimating subdaily evapotranspiration of shallow groundwater using diurnal water table fluctuations. *Ecohydrology* 1, 59-66.
- Mcisaac, G.F., David, M.B. & Mitchell, C.A. (2010) Miscanthus and Switchgrass Production in Central Illinois: Impacts on Hydrology and Inorganic Nitrogen Leaching All rights reserved. No part of this periodical may be reproduced or transmitted in any form or by any means, electronic or mechanical, including photocopying, recording, or any information storage and retrieval system,

- without permission in writing from the publisher. *Journal of Environmental Quality* 39, 1790-1799.
- Mitchell, R.B., Moore, K.J., Moser, L.E., Fritz, J.O. & Redfearn, D.D. (1997) Predicting developmental morphology in switchgrass and big bluestem. *Agronomy Journal* 89, 827-832.
- Mohanty, B.P., Bowman, R.S., Hendrickx, J.M.H., Simunek, J. & Van Genuchten, M.T. (1998) Preferential transport of nitrate to a tile drain in an intermittent-flood-irrigated field: Model development and experimental evaluation. *Water Resources Research* 34, 1061-1076.
- Nachabe, M., Shah, N., Ross, M. & Vomacka, J. (2005) Evapotranspiration of two vegetation covers in a shallow water table environment. *Soil Science Society of America Journal* 69, 492-499.
- Nielsen, D.R., Th. Van Genuchten, M. & Biggar, J.W. (1986) Water flow and solute transport processes in the unsaturated zone. *Water Resources Research* 22, 89S-108S.
- Panno, S.V., Hackley, K.C., Hwang, H.H., Greenberg, S.E., Krapac, I.G., Landsberger, S. & O'Kelly, D.J. (2006a) Characterization and identification of Na-Cl sources in ground water. *Ground Water* 44, 176-187.
- Panno, S.V., Kelly, W.R., Martinsek, A.T. & Hackley, K.C. (2006b) Estimating background and threshold nitrate concentrations using probability graphs. *Ground Water* 44, 697-709.
- Panno, S.V., Nuzzo, V.A., Cartwright, K., Hensel, B.R. & Krapac, I.G. (1999) Impact of urban development on the chemical composition of ground water in a fen-wetland complex. *Wetlands* 19, 236-245.
- Pearson, C.J. & Steer, B.T. (1977) Daily changes in nitrate uptake and metabolism in *Capsicum annuum*. *Planta* 137, 107-112.
- Peterson, B.J., Wollheim, W.M., Mulholland, P.J., Webster, J.R., Meyer, J.L., Tank, J.L., Martí, E., Bowden, W.B., Valett, H.M., Hershey, A.E., McDowell, W.H., Dodds, W.K., Hamilton, S.K., Gregory, S. & Morrall, D.D. (2001) Control of nitrogen export from watersheds by headwater streams. *Science* 292, 86-90.
- Rabalais, N., Turner, R.E., Dortch, Q., Justic, D., Bierman, V., Jr. & Wiseman, W., Jr. (2002) Nutrient-enhanced productivity in the northern Gulf of Mexico: past, present and future. *Nutrients and Eutrophication in Estuaries and Coastal Waters* (eds E. Orive, M. Elliott & V. De Jonge), pp. 39-63. Springer Netherlands.
- Ramsey, F.L. & Schafer, D.W. (2002) *The Statistical Sleuth: A Course in Methods of Data Analysis*. Duxbury/Thomson Learning, Pacific Grove, CA.
- Randall, G.W., Huggins, D.R., Russelle, M.P., Fuchs, D.J., Nelson, W.W. & Anderson, J.L. (1997) Nitrate losses through subsurface tile drainage in conservation reserve program, alfalfa, and row crop systems. *Journal of Environmental Quality* 26, 1240-1247.
- Rhoads, B. & Herricks, E. (1996) Naturalization of headwater streams in Illinois: Challenges and possibilities. *River channel restoration: Guiding principles for sustainable projects* (eds A. Brooks & F.D. Shields Jr.), pp. 331-367. John Wiley & Sons, New York.
- Roadcap, G.S. & Kelly, W.R. (1994) *Shallow ground-water quality and hydrogeology of the Lake Calumet area, Chicago, Illinois*. Illinois State Water Survey.
- Royer, T.V., Tank, J.L. & David, M.B. (2004) Transport and fate of nitrate in headwater agricultural streams in Illinois. *Journal of Environmental Quality* 33, 1296-1304.
- Saad, O.a.L.O. & Conrad, R. (1993) Temperature dependence of nitrification, denitrification, and turnover of nitric oxide in different soils. *Biology and Fertility of Soils* 15, 21-27.
- Sabater, S., Butturini, A., Clement, J.-C., Burt, T., Dowrick, D., Hefting, M., Matre, V., Pinay, G., Postolache, C., Rzepecki, M. & Sabater, F. (2003) Nitrogen removal by riparian buffers along a European climatic gradient: Patterns and factors of variation. *Ecosystems* 6, 0020-0030.
- Sabey, B.R., Bartholomew, W.V., Shaw, R. & Pesek, J. (1956) Influence of Temperature on Nitrification in Soils. *Soil Science Society of America Journal* 20, 357-360.
- Sands, G., Song, I., Busman, L. & Hansen, B. (2008) The effects of subsurface drainage depth and intensity on nitrate loads in the northern cornbelt. *Transactions of the Asabe* 51, 937-946.

- Satchithanatham, S., Wilson, H.F. & Glenn, A.J. (2017) Contrasting patterns of groundwater evapotranspiration in grass and tree dominated riparian zones of a temperate agricultural catchment. *Journal of Hydrology* 549, 654-666.
- Scaife, A. & Schloemer, S. (1994) The diurnal pattern of nitrate uptake and reduction by spinach (*Spinacia oleracea* L.). *Annals of Botany* 73, 337-343.
- Scavia, D., Rabalais, N.N., Turner, R.E., Justić, D. & William J. Wiseman, J. (2003) Predicting the response of Gulf of Mexico hypoxia to variations in Mississippi River nitrogen load. *Limnology and Oceanography* 48, 951-956.
- Schimel, D.S. (1986) Carbon and nitrogen turnover in adjacent grassland and cropland ecosystems. *Biogeochemistry* 2, 345-357.
- Scott, D., Harvey, J., Alexander, R. & Schwarz, G. (2007) Dominance of organic nitrogen from headwater streams to large rivers across the conterminous United States. *Global Biogeochemical Cycles* 21.
- Simmons, R.C., Gold, A.J. & Groffman, P.M. (1992) Nitrate dynamics in riparian forests: Groundwater studies. *Journal of Environmental Quality* 21, 659-665.
- Turlan, T., Birgand, F. & Marmonier, P. (2007) Comparative use of field and laboratory mesocosms for in-stream nitrate uptake measurement. *Annales de Limnologie* 43, 41-51.
- Turner, R.E., Rabalais, N.N. & Justic, D. (2006) Predicting summer hypoxia in the northern Gulf of Mexico: Riverine N, P, and Si loading. *Marine Pollution Bulletin* 52, 139-148.
- Turner, R.E., Rabalais, N.N. & Justić, D. (2012) Predicting summer hypoxia in the northern Gulf of Mexico: Redux. *Marine Pollution Bulletin* 64, 319-324.
- United States Environmental Protection Agency National recommended water quality criteria - aquatic life criteria table. United States Environmental Protection Agency,.
- Urban, M.A. & Rhoads, B.L. (2003) Catastrophic Human-Induced Change in Stream-Channel Planform and Geometry in an Agricultural Watershed, Illinois, USA. *Annals of the Association of American Geographers* 93, 783-796.
- Weedman, N.R., Malone, D.H. & Shields, W.E. (2014) Surficial Geologic Map of the Normal West 7.5 Minute Quadrangle, McLean County, Illinois. (ed Illinois State Geological Survey). Illinois State Geological Survey, <http://isgs.illinois.edu/maps/isgs-quads/surficial-geology/student-map/normal-west>.
- Wickham, S.S., Johnson, W.H. & Glass, H.D. (1988) Regional geology of the Tiskilwa Till Member, Wedron Formation, northeastern Illinois. Circular no. 543.
- Zumft, W.G. (1997) Cell biology and molecular basis of denitrification. *Microbiology and Molecular Biology Reviews* 61, 533-616.

Are Current Sediment Bioassays Being Biased by Collecting and Holding Time Procedures?

Are Current Sediment Bioassays Being Biased by Collecting and Holding Time Procedures?

Basic Information

Title:	Are Current Sediment Bioassays Being Biased by Collecting and Holding Time Procedures?
Project Number:	2017IL337S
USGS Grant Number:	G17AP00056
Sponsoring Agency:	U.S. Geological Survey
Start Date:	5/1/2017
End Date:	2/1/2017
Funding Source:	104S
Congressional District:	None
Research Category:	None
Focus Categories:	
Descriptors:	None
Principal Investigators:	

Publications

There are no publications.

Effect of Sample Holding Time on Pyrethroid- and Polychlorinated Biphenyl-Contaminated Sediment Assessments: Application of Single-Point Tenax Extractions

Kara E. Huff Hartz,^a Federico L. Sinche,^a Samuel A. Nutile,^{a,1} Courtney Y. Fung,^a Patrick W. Moran,^b Peter C. Van Metre,^c Lisa H. Nowell,^d Marc Mills,^e Michael J. Lydy^{a,*}

^a Center for Fisheries, Aquaculture and Aquatic Sciences and Department of Zoology, Southern Illinois University, Carbondale, IL 62901, USA

^b Washington Water Science Center, U.S. Geological Survey, Tacoma, WA 98402 United States

^c Texas Water Science Center, U.S. Geological Survey, Austin, TX 78754, United States

^d California Water Science Center, U.S. Geological Survey, Sacramento, CA 95819, United States

^e U.S. Environmental Protection Agency, National Risk Management Research Laboratory, Office of Research and Development, Cincinnati, OH 45268, United States

Highlights

- Sediment holding time was assessed using Tenax extraction and bioassays
- Bioaccessible pyrethroids were related to amphipod lethality and growth
- Bioaccessible polychlorinated biphenyls were related to oligochaete bioaccumulation
- Holding time caused 1st-order loss for bioaccessible pyrethroids in some sediments
- Declines with holding time may occur for recently applied compounds

Abstract

The adverse effects of hydrophobic organic compound (HOC) contamination in sediment are often assessed using laboratory exposures of cultured invertebrates to field-collected sediment. The use of a sediment holding time (storage at 4 °C) between field sampling and the beginning of the bioassay is common practice, yet the effect of holding time on the reliability of bioassay results is largely unknown, especially for current-use HOCs, such as pyrethroid insecticides. Single-point Tenax extraction can be used to estimate HOC concentrations in the rapidly desorbing phase of the organic carbon fraction of sediment (i.e., bioaccessible concentrations), which relate to sediment toxicity and bioaccumulation in invertebrates. In this study, repeated measurements of bioaccessible concentrations (via Tenax), and *Hyalella azteca* 10-d survival and growth were made as a function of sediment holding time using pyrethroid-contaminated field sediment. Similarly, bioaccessible concentrations and 14-d bioaccumulation were measured in *Lumbriculus variegatus* as a comparison using the legacy HOCs, polychlorinated biphenyls (PCBs). While the bioaccessible and bioaccumulated PCB concentrations did not change significantly through 244 d of holding time, the bioaccessible pyrethroid concentrations were more varied. Depending on when pyrethroid-contaminated sediments were sampled, the

bioaccessible pyrethroid concentrations showed first-order loss with half-lives ranging from 3 to 45 d of holding, or slower, linear decreases in concentrations up to 14% decrease over 180 d. These findings suggest that at least in some field sediments, holding the sediments prior to bioassays can bias toxicity estimates.

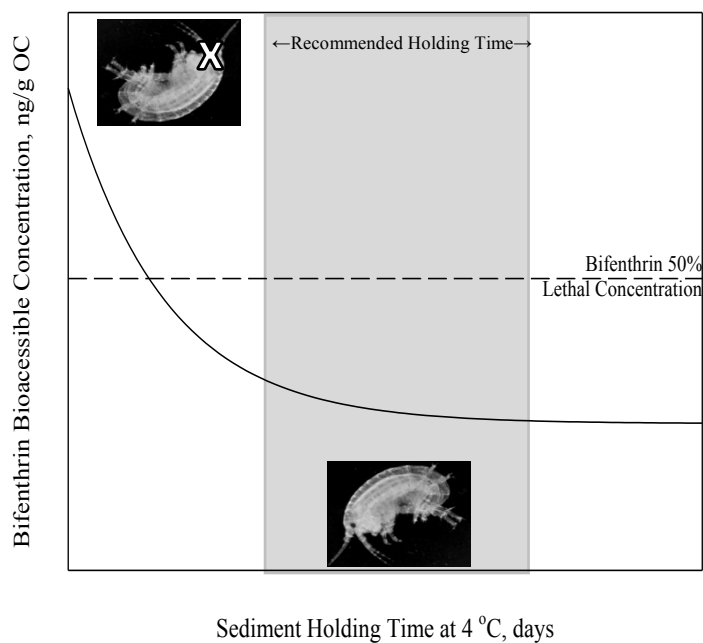
Keywords

Pyrethroids; Sediment; Holding time; Tenax; Bioassays

¹Current address: School of Science, Penn State Behrend, Erie, Pennsylvania 16563, USA

*Corresponding author

Graphical abstract



1. Introduction

Sediment testing is an important component of ecological risk assessments because it estimates the effects of contaminated sediments to the health of the ecosystem and provides feedback for contaminated sites undergoing remediation (Suter, 1996; USEPA, 1997). Sediment is a repository for persistent and/or hydrophobic chemicals and can be a source of exposure of HOCs to benthic species. The potential effects of this exposure can be assessed using standard bioaccumulation and toxicity bioassays conducted in the laboratory using field-collected sediments (USEPA, 2000; ASTM, 2005). However, these tests have limitations, including the potential to alter sediment-contaminant interactions with sediment removal from the field, transport, storage, and homogenization of the sediment samples.

Holding sediment prior to testing is common practice because it reduces the number of native invertebrates in the sample that may prey on test animals (United States Environmental Protection Agency (USEPA), 2000 and Defoe and Ankley, 1998). Furthermore, it may be necessary for logistical reasons when extensive sampling campaigns require coordination of bioassays for samples collected over multiple days or weeks (Moran et al. 2017). Typically, a sediment holding time of at least 30 d, but no more than 56 d, at 4 °C under dark conditions is recommended (Becker and Ginn, 1990). Other agencies recommend at least 14 d at 0-6 °C (no freezing) and restrict holding times to no more than 56 d (SWAMP, 2017; ASTM, 2005).

Although HOCs are inherently persistent because they are resistant to chemical and microbial degradation, holding sediment prior to testing may affect toxicity and bioaccumulation results. For example, Becker and Ginn (1995) found that amphipod survival in Puget Sound sediment increased after a holding time of 112 d at 4 °C, and that the increase was more important for sediment with low and intermediate toxicity. Defoe and Ankley (2003) found that for polychlorinated biphenyl (PCB)-contaminated sediment sampled from the Raisin River, MI, storage time (up to 273 d at 4 °C) decreased toxicity to *Chironomus tentans* using a time-to-death assay that showed subtle changes in toxicity in comparison to a fixed-time endpoint. In addition, an inter-laboratory assessment of marine sediment toxicity to six crustacean species showed that storage time was an important factor in bioassay results, where sediments assessed prior to 28 d of storage were classified as moderately toxic and all but one of the sediment assessed after 28 d were classified as non-toxic (Casado-Martínez et al. 2006). Other studies have examined the effect of sediment holding time on HOC concentrations in sediment. For example, Lyytikäinen et al. (2003) showed that sediment stored for 28 d at 3 °C caused little change in the concentrations of the pyrethroid insecticide esfenvalerate, triazine herbicides, and most organochlorine pesticides, while γ -chlordane and organophosphate insecticides degraded during storage, showing a 10% loss within 6-13 d. In 2005, the USEPA re-evaluated sediment holding times for PCBs at two temperatures (4 °C and -20 °C) and determined that a 168-d holding time had no effect on the concentrations of three Aroclors or seven individual PCB congeners, however, they did not evaluate the effect of holding time on toxicity or bioavailability (USEPA, 2005). Federal guidance is available for PCBs and some HOC classes (USEPA, 2000, 2005; ASTM, 2005), but less guidance is given on pyrethroids (SWAMP, 2017; CFR, 2003). The available guidance for pyrethroids is limited to aqueous samples and pyrethroids in sediment stored by freezing (-20 °C)

slated for exhaustive extraction (Hladik et al. 2009), and no guidance for pyrethroids based on toxicity to organisms is available.

The rate of HOC partitioning between sediment and overlying water is affected by the presence of different fractions of HOCs in the sediment (Cornelissen et al. 2000). Desorption of contaminants from sediment follows a kinetic continuum, with the desorption rates dependent on the distribution of the chemical within different compartments of the sediment matrix. Contaminant desorption from sediments can be described as a triphasic process with rapidly desorbing, slowly desorbing, and very slowly desorbing fractions. The rapidly desorbing fraction represents the most bioaccessible portion of HOCs in the sediment, that is, the portion that is readily available for uptake by sediment-dwelling organisms (Cornelissen et al. 2001; ten Hulscher et al. 2003).

Single-point Tenax extraction (SPTE) is a method that measures bioaccessible HOC concentrations, where HOCs extracted by Tenax sorbent in direct contact with sediment correspond to the HOC concentrations in the rapidly desorbing or bioaccessible fraction (Cornelissen et al. 2001). The SPTE concentrations have been directly correlated to bioaccumulation and toxicity (Harwood et al. 2015; Lydy et al. 2015). A useful feature of SPTEs is that Tenax extraction requires only 24 h of contact with sediment, so bioaccessible concentrations can be measured within about 2 d of sediment collection. The SPTEs also can be repeated at multiple time points during a sediment holding period or during a toxicity bioassay (typically 10 d to 42 d, depending on the species and endpoint). In addition, obtaining a rapid estimate of the bioaccessible fraction of HOCs in a sediment is important because it better represents the ambient conditions in the stream and it allows one to distinguish the effects of abiotic and microbial degradation that may occur in longer (10 d or more) bioassays.

The objective of this study was to determine if sediment holding applied after collection, but prior to testing, changes the Tenax extractable concentrations or sediment toxicity (to *Hyalella azteca*) from a current-use class of insecticides, pyrethroids. Ten pyrethroid-contaminated sediment samples were collected from urban and suburban areas in California during two different years, and SPTE was used as a direct measure of pyrethroid bioaccessibility as a function of sediment holding time. For comparison, two sediments contaminated with legacy pollutants, PCBs, were collected from the Manistique River in Michigan, and PCB bioaccessibility was measured as a function of holding time. Bioaccessible pyrethroids and PCBs were compared to total concentrations as determined by exhaustive chemical extraction. Bioaccessible pyrethroid concentrations were related to toxicity, as assessed in sediment bioassays with the amphipod, *Hyalella azteca*, and bioaccessible PCB concentrations were related to bioaccumulation using sediment exposure to the oligochaete, *Lumbriculus variegatus*.

2. Materials and Methods

2.1 Chemicals

A custom pyrethroid mixture containing 10 target pyrethroids (10 µg/mL in acetone, see SM) and a PCB mixture (WHO/NIST/NOAA congener list, 10 µg/mL in isooctane) containing 28 congeners were purchased from AccuStandard, Inc. (New Haven, CT, USA). Recovery

surrogates 4,4'-dibromooctafluorobiphenyl (DBOFB, 250 µg/mL in acetone) and PCB-209 (200 µg/mL in acetone) were purchased from Supelco Inc. (Bellefonte, PA, USA) and PCB-186 (35 µg/mL in isooctane) was purchased from AccuStandard. The octachlorobiphenyl (PCB-204, 35 µg/mL in isooctane) internal standard was purchased from AccuStandard. Stable isotope labeled pyrethroid internal standards were donated by Kalexsyn, Inc. (Kalamazoo, MI, USA), and ¹³C₁₂-PCB-15, ¹³C₁₂-PCB-52, ¹³C₁₂-PCB-141, and ¹³C₁₂-PCB-209 (each 40 µg/mL in nonane) were purchased from Cambridge Isotope Laboratory (Andover, MA, USA). The sources of additional materials can be found in Supplemental Material (SM).

2.2 Sample Collection, Storage, and Physical Characterization

Sites were selected in urban- and suburban-influenced streams in northern and southern California with prior histories of pyrethroid contamination. Sediments were collected from six sites on April 6, 2016 and four sites on May 30, 2017 (**Table 1**). Fine-grained fluvial sediment (2-4 L) was sampled from depositional zones in each stream by pressing a stainless steel cup with drain holes into soft sediment and removing the top 2 cm sediment with a stainless steel spatula (Moran et al. 2012). Multiple samples were composited, homogenized by hand with a stainless steel ladle, and passed through a 2 mm stainless steel sieve in the field (Shelton and Capel 1994). Sediment was placed in a 7.6 L Uline (Pleasant Prairie, WI) high density polyethylene pail, sealed with Uline lid, and shipped on ice overnight to Southern Illinois University (SIU). Upon receipt, sediment was homogenized by hand using a long-handled stainless steel spoon and then stored in an environmental chamber (BioCold Environmental, St. Louis, MO, USA) at 4 °C in the dark. Hourly temperature measurements were collected using a ThermoData Series 1 TempLogger (ThermoWorks, Salt Lake City, UT, USA) placed near the sample containers and the temperatures did not deviate by more than 0.5 °C from 4 °C during the study.

Two sites with known PCB contamination were selected along the Manistique River near Manistique, MI. Surficial sediment (approximately 2 kg) was sampled to a depth of no more than 15 cm using a petite ponar. Two to three grab samples were composited, placed in 950 mL and 1900 mL plastic containers with lids (United Solutions, Leominster, MA, US), and shipped on ice to SIU. Sediment samples contained rocks and sawdust debris from a paper mill near the sampling site that was removed by sieving with a 2 mm stainless steel sieve. The sieved sediment was homogenized using a stainless steel spoon in a stainless steel bowl, split into two 900 mL glass jars (Jarden Home Brands, Fishers, IN, US), and stored in the environmental chamber.

Subsamples of each sediment were analyzed at successive holding times with holding time defined as the as time difference between sediment sampling and the beginning of the Tenax extraction. At each time point, subsamples were obtained after rehomogenizing the sediment by hand in the storage container using a stainless steel scoop and spoon and then storing at 4 °C for 18-48 prior to Tenax extraction. In 2017, the first subsample was analyzed as soon after sample collection as was logistically possible (2 days). Subsamples for exhaustive chemical extraction and dry weight (dw) analysis were collected at the same time point as the Tenax samples. Holding times for Tenax extractions of pyrethroids in California sediments (shown in Table S1)

were 2, 5, 10, 21, 49 and 105 d in 2017 and were 14, 29, 62, 125, and 222 d in 2016. Holding times for Michigan sediments analyzed for PCBs were 7, 14, 38, 64, 123, 184 and 244 d. Subsamples for organic carbon (OC) and particle size analysis for all sediments were taken at approximately 14 d after sample collection. The physical properties of the sediments were characterized by dw fraction, OC fraction, and particle size distribution. Details of these procedures can be found in SM.

2.3 Single-Point Tenax Extractions of Sediment

To determine if bioaccessible pyrethroid and PCB concentrations change with sediment holding time, Tenax extractions were conducted using methods adapted from Nutile et al. (2017a) and Sinche et al. (2017). Briefly, wet sediment (3 g on a dw basis from wet to dry ratios determined on separate aliquots) was placed in a 50 mL screw-top centrifuge tube, along with 0.500 g Tenax, 1.5 mL 3 mg/mL aqueous HgCl₂, and 45 mL of reconstituted moderately hard water (RMHW) (Smith et al. 1997). The sediment was rotated for 24 h on a rotator (Scientific Equipment, Baltimore, MD, USA) at a rate of 24 rotations per minute (rpm). After rotation, the tubes were removed and then centrifuged at 2000 rpm (IEC Clinical Centrifuge, Needham, MA, USA) to separate the Tenax beads from the sediment. The Tenax was removed, placed in a vial containing 5 mL of acetone and the target analytes were extracted from the Tenax by sonicating for 5 min. This extraction step was repeated with an additional 5 mL of acetone and by using two 5 mL washes with 1:1 acetone:hexane. The extracts were combined and solvent exchanged to hexane. Additional extract cleanup details and quality control procedures are provided in SM.

2.4 Bioassays

To evaluate changes in pyrethroid and PCB bioaccessible concentrations with sediment holding time, toxicity, and bioaccumulation, bioassays were conducted during the holding time studies. Pyrethroids tend to show acute toxicity to amphipods and tend to be biotransformed, thus a 10-d *H. azteca* acute toxicity bioassay was selected. Conversely, PCBs have significant bioaccumulation potential, thus a *L. variegatus* bioaccumulation bioassay was selected for PCB-contaminated sediments. Two bioassays for 2017 pyrethroid samples were conducted, and day zero of the bioassay coincided with holding times of 11 d and 49 d. Three bioassays for the PCB sediments were conducted, and day zero of the bioassays coincided with holding times of 7 d, 14 d, and 244 d.

The *H. azteca* 10-d toxicity bioassay followed protocols outlined by the USEPA (2000). The sediment was rehomogenized and subsamples (100 mL) were distributed into each of four replicate 300-mL glass jars, RMHW (Ivey and Ingersoll 2016) was added (175 mL), and the contents were allowed to settle for 24 h at 23°C. After the sediment settled, ten 7- to 8-d old *H. azteca* were added to each of the four replicate jars. Sand and LaRue Pine Hills (LPH, Wolf Lake, IL) reference sediment were used as negative controls (Nutile et al. 2017a; Sinche et al. 2017). Three reference sediments from the northeastern United States (Beaver Brook at North Pelham, NH, Sugar Run near Wilmot, PA, and Canajoharie Creek near Canajoharie, NY) were used, and these sediments met minimum acceptable growth requirements (Ivey et al. 2016). Test chambers were housed in an automated water renewal system maintained at 23°C with four

automatic water renewals (100 mL/test vessel/renewal) performed daily for the duration of the test. Organisms were fed a diet consisting of a Tetramin suspension with diatoms (*Thalassiosira weissflogii* 1200TM (Reed Mariculture, Inc. Campbell, CA, USA) (Ivey et al. 2016). After 10 d, the *H. azteca* were removed from the test beakers, and survival and dry biomass (60 °C, 48 h) were recorded.

The *L. variegatus* 14-d bioaccumulation bioassay followed protocols outlined by the USEPA (2000). Approximately 100 mL of each sediment, sand, and LPH sediment was placed into four replicate 600 mL beakers and covered with 500 mL overlying RMHW. After allowing the sediment to settle for 24 h, 50 *L. variegatus* were added to each beaker and the beakers placed in an automated water renewal system, which conducted 100 mL automated water changes three times daily. The *L. variegatus* were allowed to reside in the sediment for 14 d at 23 ± 1 °C with a light cycle of 16:8 h light:dark. After 14 d, the *L. variegatus* were removed from the beakers, rinsed with RMHW, placed in new beakers containing RMHW, and allowed to deplete their gut contents for 6 h.

2.5 Exhaustive Chemical Extraction of Sediment and *L. variegatus*

The total concentration of pyrethroids and PCBs in sediment was determined by exhaustive chemical extraction. Upon subsamples, sediments were stored in a -20 °C freezer (Frigidaire, Charlotte, NC, USA) for no more than 130 d for pyrethroids and 152 d for PCBs until extraction. Prior to extraction, samples were freeze dried (Labconco, Kansas City, MO, USA). Analytes were extracted from sediment by pressurized liquid extraction using a Dionex 200 Accelerated Solvent Extraction (ASE) System (Waltham, MA, USA). Freeze-dried sediment (3 g) was placed in an ASE cell equipped with a filter and 5 g of silica gel (activated at 130 °C for 12 h) and filled with sea sand. Sediments were extracted using a 1:1 dichloromethane:acetone solution at 100 °C and 1500 pounds per square inch (psi) which was held for two heat-static cycles of 10 min each. After extraction, extracts were solvent exchanged with 20 mL of hexane, and concentrated to 1 mL (Nutile et al. 2017b). Additional extract cleanup details and quality control procedures are provided in SM.

Lumbriculus variegatus tissue was prepared for PCB analysis following similar methods (see Sinche et al. 2017). Briefly, *L. variegatus* tissue from the bioaccumulation assay was extracted with a high-intensity sonicator (Sonics & Materials VCX400, Newtown, CT, USA) using three 20 s pulses with 10 mL of acetone. Next, 10 mL of hexane was added to the vial and the samples were incubated in a bath sonicator (Branson 3510, Branson Ultrasonic Corporation, Danbury, CT, USA) for 30 minutes. Sodium sulfate columns were used to remove remaining tissue and water, and then the extracts were concentrated to 2 mL using a Reactivap. The extracts were cleaned with sulfuric acid and transferred to vials using hexane. Additional extract cleanup details and quality control procedures are provided in SM.

2.6 Pyrethroid and PCB Analysis

Pyrethroid concentrations in Tenax and ASE extracts were determined by gas chromatography/mass spectrometry (GC/MS) in negative chemical ionization mode (Nutile et al. 2017b). The PCB concentrations in Tenax, ASE, and *L. variegatus* extracts were determined by

GC/MS in electron ionization mode (Sinche et al. 2017). The instrumental details, separation method, and quantification procedures can be found in SM. Pyrethroid and PCB concentrations in Tenax extracts and ASE extracts were normalized by the OC per gram dw sediment. Bioaccumulated PCB concentrations in *L. variegatus* were reported as normalized for lipid fraction on a wet weight basis, where lipid fraction was determined using extraction and spectrophotometry (Lu et al. 2008).

2.7 Data and Statistical Analysis

The pyrethroid and PCB concentrations (C_t) were measured as a function of holding time (t) and were fit to one of two equations that represent their observed loss in bioaccessible concentration (for pyrethroid and PCB concentrations in Tenax extracts) and total concentration (for pyrethroids and PCBs measured in ASE extracts). The holding time was defined as time difference between sediment sampling and the beginning of the Tenax extraction. Equation 1 represents a linear equation where the slope of the regression represents the initial rate of loss of compound and the intercept represents the initial concentration of compound.

$$C_t = \text{slope} \times t + \text{intercept} \quad (1)$$

Equation 2 represents kinetics for the first-order exponential loss of compound as follows:

$$C_t = C_f + \Delta C e^{-kt} \quad (2)$$

where C_f = final concentration, ΔC = difference between final and initial concentration, and k = first-order rate constant. SigmaPlot (version 10.0, Systat Software, Inc. San Jose, CA, USA) was used to perform linear least-squares regression analyses. The linear equation (Equation 1) was used for all total pyrethroid and PCB concentrations. For bioaccessible concentrations, the exponential equation (Equation 2) was selected when the probability value (p) in the analysis of variance calculated by the regression was less than 0.05. When $p > 0.05$, Equation 1 was used. For all statistical tests, confidence levels were set to 95%, and p values greater than or equal to 0.05 indicated non-significant differences.

3. Results

3.1 Sediment Characteristics

The sum of pyrethroid concentrations as determined by exhaustive chemical extraction ranged from 601 ng/g OC to 6870 ng/g OC for the sediments collected from pyrethroid-contaminated sites (Table 1). The sum of PCB concentrations as determined by exhaustive chemical extraction were approximately 10,000 ng/g OC at the two PCB-contaminated sites. None of the pyrethroid-contaminated sediment contained detectable concentrations of PCBs, and neither of the PCB contaminated sediments contained quantifiable levels of pyrethroids. For this reason, simultaneous determination of both classes of analytes was not done. The OC content in the sediment ranged from 0.26% to 3.89%. The particle size distributions were determined for six size classes from <0.0625 mm to 2 mm. The particle size distributions varied from site to site. Three sites were dominated by very fine particles (<0.0625 mm, IC, SR16, and TR), three sites were dominated by fine particles (0.125-0.25 mm, SR17, SRu, M1), one site was dominated by

coarse particles (0.5 - 1 mm, BC), and the remaining sites showed bimodal distributions (GS, DC, M2, KCGG, KCCC). None of the size class percentages were correlated with the dry weight-normalized pyrethroid concentrations, according to Spearman's rank order correlations.

3.2 Pyrethroid-Contaminated Sediment

In Tenax extracts, bifenthrin was detected and quantified in all 10 sediments (**Table S1**), and it was the most abundant bioaccessible pyrethroid in eight out of the 10 sediments (up to 2380 ng/g OC at BC). Bifenthrin and λ -cyhalothrin were the most frequently detected pyrethroids, followed by cyfluthrin, cypermethrin, esfenvalerate, permethrin and deltamethrin. Tefluthrin and fenpropathrin were not detected in any of the sediments.

The pyrethroid-contaminated sediments collected in 2016 showed significant decreases in bioaccessible pyrethroid concentration, so these data were fit to a first-order exponential model (Equation 2). Figure 1c shows the behavior of the bioaccessible bifenthrin concentrations, with decreases in bioaccessible concentrations through 50 d followed by stabilization through 222 d. The half-lives of bioaccessible pyrethroids (Table S2) ranged from 3 d to 45 d. Although the lack of Tenax extractions collected prior to 14 d adds to the uncertainty of these half-life estimates, the kinetic behavior strongly suggests that the bioaccessible pyrethroid concentrations decreased substantially with holding time for the sediments in 2016 (Figure 1c).

In contrast, there was little change in the bioaccessible bifenthrin concentrations measured in sediment collected in 2017 during the holding time period (**Figure 1a**). Because the concentrations collected in 2017 did not fit a first-order exponential loss (Equation 2), a linear model (Equation 1) was used to estimate the rate of change with time (**Table S2**). A negative value for slope suggested a decrease in bioaccessible pyrethroid concentration as a function of holding time, however the p values for slope were greater than 0.05, which indicated that the slope value could not be distinguished from zero. Thus, for the pyrethroid-contaminated sediment collected in 2017, no change in bioaccessible bifenthrin could be detected over the 105 d holding time period.

The total pyrethroid concentrations were measured as a function of holding time to determine if changes in the bulk sediment could explain changes in the bioaccessible fraction for 2016 sediments (**Table S3**). In contrast to the bioaccessible concentrations, little-to-no losses in the total pyrethroid concentrations were observed in sediments (shown for bifenthrin in Figure 1b and 1d); therefore, the data were fit to a linear equation (Equation 1). The slope measured by this analysis represents the initial loss rate and the y-intercept is the interpolated initial total concentration, which represents total concentration present in the sediment directly after sampling. However, none of the negative slope values (Table S2) were significantly different than zero ($p > 0.05$). Thus, decreases in bioaccessible pyrethroid concentrations could not be due to changes during the holding time in total pyrethroid concentrations in sediments.

3.3 Effect of Holding Time on the *Hyalella azteca* Toxicity Bioassay Results

Ten-day toxicity bioassays were conducted by exposing *H. azteca* to the 2017 pyrethroid-contaminated sediments. Bioassays were not conducted on 2016 sediments. The effect of holding

time on sediment bioassay results was assessed by conducting each bioassay twice: near the beginning of the holding time, when time zero of the bioassay coincided with the day 11 of the holding time, and near the end of the holding time, when time zero of the bioassay coincided with day 49 of the holding time (**Figure 2**). A two-sample homoscedastic t-test was used to compare the average percent survival and percent biomass reduction for the day 11 and day 49 bioassay for each sediment, and no significant differences were observed ($p > 0.05$). In addition, an analysis of variance (ANOVA) was used to compare the overall effect of holding time on sediment, and no significant differences ($p > 0.05$) were found between day 11 and day 49 for average percent survival and for average percent biomass reduction. These results indicate that for the 2017 pyrethroid-contaminated sediment, the bioassay results were similar regardless of the holding time.

3.4 PCB-Contaminated Sediment

The PCB-contaminated sediment collected from the Manistique River showed very little change in either bioaccessible or total PCB concentrations as a function of holding time over the 244 d (**Figure 3a and 3b**). Only one PCB in the bioaccessible concentrations (PCB-28 in sediment M1) two PCBs in the total concentrations (PCB-28 and PCB-187 in sediment M1) had slope values that were significantly different from zero (p -value in the slope < 0.05) out of 24 PCBs monitored in the two sediments. The largest decrease relative to the initial concentration calculated at 180 d of holding was -10% for PCB-187. Thus, little-to-no change in bioaccessible and total concentrations was found as a function of sediment holding time.

3.5 Effect of Sediment Holding Time on *Lumbriculus variegatus* PCB Bioaccumulation Bioassay Results

Lumbriculus variegatus bioaccumulation bioassays were conducted three times, where day zero of the bioassay coincided with 7 d, 14 d, and 244 d of holding time. No changes in the sum of bioaccumulated PCB concentrations were observed as a function of sediment holding time for any of the congeners monitored for either sediment (**Figure 4**). One-way ANOVAs indicated that no significant differences in the sum of PCB congeners could be detected as a function of holding time ($p > 0.05$); however, a few individual congeners were significantly different (Figure S1): in M1, PCB-8 ($p = 0.039$), PCB-52 ($p = 0.010$), PCB-66 ($p = 0.0026$), PCB-101 (0.0082), PCB-118 (0.00057), PCB-153 ($p < 0.0001$), and in M2, PCB-8 ($p = 0.0392$), PCB-28 ($p = 0.0044$).

4. Discussion

The bioaccessible pyrethroid concentrations as function of holding time showed different behaviors between the two years of sample collection. Sediments collected in 2017 showed no significant change in bioaccessible pyrethroid concentrations as a function of holding time. Furthermore, the stability of bioaccessible pyrethroids in 2017 sediments was consistent with the 10-d *H. azteca* bioassay results. No changes in sediment toxicity, measured as percent survival and biomass reduction, were observed in 2017 by exposure of *H. azteca* to sediment held for 11 d and for 49 d after sampling. Pyrethroid insecticides, especially bifenthrin, are often the most important causal factors for *H. azteca* toxicity from sediments collected across a large range of

sites (Kuivila et al. 2012 and Kemble et al. 2013; Moran et al. 2017). Assuming that pyrethroid contamination drove sediment toxicity to *H. azteca* in the 2017 sediments, then the lack of change in the *H. azteca* survival and biomass as a function of sediment holding time may reflect a lack of change in bioaccessible pyrethroid concentrations. Similarly, the Tenax extraction results suggest that for pyrethroid-contaminated sediments collected in 2017, consistent bioassay results would have been expected at any of the recommended holding times.

In contrast, the 2016 sediments showed significant losses in pyrethroid bioaccessible concentrations in all six sediments, and the bioaccessible concentrations were well predicted by using a first-order exponential equation (Equation 2). The half-lives of loss in bioaccessible pyrethroids ranged from 3 d to 45 d after sampling, and these half-lives coincided with the range of typically-used holding times (28 - 56 d) (SWAMP, 2017; ASTM, 2005). The observed decreases in bioaccessible pyrethroid concentrations could not be explained by pyrethroid degradation during sediment storage, as the total pyrethroid concentrations were generally consistent when held at 4 °C for 105 d (for 2017 sediments) and for 222 d (for 2016 sediments). Previous work has shown that the half-lives for degradation of bifenthrin in runoff sediments stored under anaerobic conditions at 4 °C ranged from 764 d to 1950 d, and half-lives for aerobic degradation ranged from 277 d to 470 d (Gan et al. 2005). In addition, the range of half-lives for degradation of permethrin isomers is more variable than bifenthrin, with aerobic half-lives at 4 °C ranging from 151 d to 2150 d and anaerobic degradation half-lives ranging from 148 d to 450 d (Gan et al. 2005). Thus, pyrethroid degradation at 4 °C is slower than the changes in bioaccessible pyrethroid concentrations observed in 2016 sediments.

Identical sediment collection and preparation procedures were used for pyrethroid-contaminated sediment in 2016 and 2017, thus we can rule out differences due to sampling and homogenization in the effects of holding time. We cannot, however, rule out that a decrease in bioaccessible pyrethroid concentration occurred too quickly in 2017 (<2 d after sampling) to observe. One difference between sediments from the two years is that the 2017 samples were collected 56 d later in the spring season (May 30) in comparison to 2016 (April 6). The year 2017 was a wet year following the 2012-2016 drought in California (USGS, 2017). Monthly runoff data compiled from CA gaged stream sites indicate higher flows and peak flows earlier in 2017 than in 2016 (Figure S2a). Peak monthly runoff in 2016 occurred in March (about 21 d prior to sample collection); whereas, peak 2017 runoff occurred in Feb (over 3 months prior to sample collection) and was almost twice as high as the maximum 2016 runoff. A similar pattern was observed in monthly discharge observed at Whittier Narrows Dam (Figure S2b), located upstream from SR16, SR17, and SRu sites. We hypothesize that sediment collected in 2017 had received pyrethroid-contaminated runoff earlier in the season, and that the pyrethroids in the 2017 sediments were already sequestered into sediment OC, whereas the pyrethroids in the 2016 sediments had not been in contact with sediment OC long enough to reach equilibrium. Support for this hypothesis can be found in the range of the bioaccessible fraction of pyrethroids in sediments, which tended to be higher in 2016 (5%-54%) than in 2017 (6-16%) (Table S1).

Decreases in the amount HOCs available in sediment OC for assimilation with potential for toxicity have been previously related to longer contact times with sediment (Alexander, 2000).

Similarly, longer contact times may cause a decrease in the fraction of pyrethroids in rapidly desorbing sites and an increase in the fraction of pyrethroids in slowly and very slowly desorbing sites in sediment OC. Furthermore, laboratory experiments using spiked sediment showed that the rapidly desorbing concentrations of bifenthrin, cyfluthrin, fenpropathrin, and λ -cyhalothrin decreased during incubation at 21 °C with half-lives that ranged from 24 d to 50 d after addition of pyrethroids (Xu et al. 2008). It is possible that pyrethroids with longer contact times in field sediment have already established equilibrium (sequestration is effectively complete) which resulted in little change to bioaccessible concentration with sediment holding time. Thus, sediments with more recent additions of pyrethroids are likely to show decreases in bioaccessible pyrethroid concentrations with holding time, and more pronounced decreases would occur closer in time to pyrethroid application.

Particle size distributions did not affect the HOC concentrations as a function of holding time, yet the bioaccessible pyrethroid half-lives were smaller for sediment samples with larger OC fractions. In particular, the bifenthrin first-order rate constant (k) directly increased with increasing OC (**Figure S3**). Although the OC content was directly related to the rate constant of decrease for sediments collected in 2016, the OC fractions for sediments collected in 2017 (2.04%-3.20%) were within the range of sediment collected in 2016 (0.26%-3.54%). Thus, sediment OC content cannot explain the differences in the observed decreases from 2016 and 2017 samples.

Although *H. azteca* bioassays were not conducted on the 2016 sediments, the observed decrease in the bioaccessible pyrethroids in sediment may have led to a reduction in sediment toxicity. This notion is supported by the observation that bioavailable concentrations reported in Figure 1 (hundreds to a few thousand ng pyrethroids /g OC) are within the range of expected sediment toxicity thresholds from a review of spiked-sediment bioassay data recently summarized by Nowell et al. (2016). If sampling the sediment disrupts the equilibrium between pyrethroids and rapidly and slowly desorbing sites, then a holding time prior to bioassays may allow for re-equilibration and prevent potential overestimation of bioaccessible pyrethroids. Bioassays conducted prior to re-equilibration may give false positive results due to artificially high bioaccessible pyrethroid concentrations. On the other hand, it is possible that the field exposures to pyrethroids are best estimated by bioaccessible concentrations measured as soon as possible after sampling. As an example, the estimated bioaccessible bifenthrin concentration at Ingram Creek at time of collection was 864 ng/g OC (calculated as $(\Delta C + C_f)$ from Equation 2). This initial bioaccessible concentration was greater than the reported median lethal concentration (LC50) for *H. azteca* exposed for 10 d in spiked sediment, 523 ng/g OC, suggesting that the sediment would cause lethality in a *H. azteca* bioassay (Amweg et al. 2005). Due to sediment holding, the bioaccessible bifenthrin concentration decreased from 478 ng/g OC at 14 d to 341 ng/g OC at 29 d, and stabilized at 263 ng/g OC after 60 d. These bifenthrin concentrations were below the LC50, thus the sediment would be expected to cause less mortality in a *H. azteca* bioassay and appear less toxic in comparison to a bioassay conducted immediately after sample collection. Therefore, using a sediment holding time of 30-60 d prior to bioassay may underestimate the sediment toxicity in comparison to a prompt assessment directly after sampling.

Both bioaccessible and total PCB concentrations showed only negligible changes as a function of holding time from 7 d through 244 d after sampling. These results are consistent with previous work (USEPA, 2005), in which three Aroclors and seven PCB congeners, determined by exhaustive chemical extraction, showed < 20% decrease within 260 d for holding at 4 °C and 281 d for holding at -20 °C. Furthermore, the lack of change in bioaccessible PCB concentrations was reflected in the stability of the bioaccumulation results for *L. variegatus* as a function of holding time. This finding suggests that PCBs have stable bioaccessible concentrations as well as stable total concentrations in sediment stored at 4 °C, and that PCB bioaccumulation bioassays conducted between 7 d and 200 d after sampling would give similar results. The stability of PCBs in the bioaccessible fraction may be a consequence of their historical contamination; the majority of sediment contamination of sediment by PCBs likely occurred over 30 years ago prior to manufacture bans. As a consequence, the equilibria between PCBs and the rapidly, slowly, and very slowly desorbing sites within the organic carbon of sediment were well-established. As long as the organic carbon binding sites are not altered in the field or by sampling methods, the concentration of PCBs in the bioaccessible portion should be stable.

5. Conclusions

The potential effect of holding time at 4 °C on pyrethroid toxicity and PCB bioaccumulation was tested using sediment-dwelling invertebrates. Repeated Tenax extractions were conducted through the holding time, which enabled monitoring of the bioaccessible concentrations. Because toxicological endpoints and bioaccessibility are important for assessment of sediment toxicity (Ehlers and Luthy, 2003), techniques, such as single-point Tenax extraction, that can capture rapid changes in bioaccessible concentrations with a smaller time resolution (24 h) relative to typical sediment holding times (28-56 d) are useful to understand how and when holding time affects sediment assessments.

Pyrethroid insecticides showed different rates of loss of bioaccessible concentrations as a function of 4 °C holding time, ranging from no significant loss through 105 d of holding to losses with half-lives ranging from 3 d to 45 d. The cause of these differences is hypothesized to depend on the contact time of pyrethroids with sediment, where sediments with longer contact times have a greater degree of pyrethroid sequestration and show little if any changes in bioaccessible pyrethroid concentrations. This difference is especially important for current-use HOCs, such as pyrethroids, because they are more likely to be recently applied.

This work demonstrates that holding times can affect current-use HOC bioaccessibility, and as a consequence, may cause inconsistencies between lab bioassay results and the actual toxicity in the field. Additional work is needed to investigate the role of contact time in the field, especially quantification of pyrethroid bioaccessibility. If holding a sediment prior to conducting a bioassay increases the contact time and subsequently the degree of pyrethroid sequestration, then holding a sediment prior to testing would cause an underestimation of sediment toxicity relative to field toxicity.

6. Acknowledgements

The authors thank J. Orlando, B. Phillips, and D. Weston for assistance in site selection; C. Burton, C. Brilmyer, T. Davis, J. Domagalski, A. Egler, L. Kammel, R. Kent, J. Orlando, M. Peterson, and E. Pietrzak for their technical support in sample collection; A. Derby, J. Gray, A. Harwood, B. Hamilton, S. Kahil, V. Lydy, and H. Sever for technical support in sample preparation; Kalexsyn, Inc and D. Koch for supplying deuterated pyrethroid standards. This work was supported by the National Institute of Water Research (G15AS00019) and supplemental funding by US Geological Service and University of Illinois (G17AP00056).

7. References

- Alexander, M., 2000. Aging, bioavailability, and overestimation of risk from environmental pollutants. *Environmental Science and Technology* 34(20), 4259-4264.
- ASTM International 2005. E 1706-05. Standard Test Method for Measuring the Toxicity of Sediment-Associated Contaminants with Freshwater Invertebrates. ASTM International, West Conshohocken, PA. 118 p.
- Amweg, E.L., Weston, D.P., Ureda, N.M., 2005. Use and toxicity of pyrethroid pesticides in the Central Valley, California, USA. *Environmental Toxicology and Chemistry* 24(5), 1300-1.
- Becker, D.S., Ginn, T.C., 1990. Effects of sediment holding time on sediment toxicity. EPA 910/9-90-009, U.S. Environmental Protection Agency, Washington, DC.
- Becker, D.S., Ginn T.C., 1995. Effects of storage time on toxicity of sediments from Puget Sound, Washington. *Environmental Toxicology and Chemistry* 14(5), 829-835.
- Casado-Martínez, M.C., Beiras, R., Belzunce, M.J., González-Castromil, M.A., Marín-Guirao, L., Postma, J.F., Riba, I., DelValls, T.A., 2006. Interlaboratory assessment of marine bioassays to evaluate the environmental quality of coastal sediments in Spain. IV. Whole sediment toxicity test using crustacean amphipods. *Ciencias Marinas* 32(1B), 149–157. doi: 10.7773/cm.v32i12.1039
- [CFR] Code of Federal Regulations, 2003. Guidelines Establishing Test Procedures for the Analysis of Pollutants, Title 40 Protection of the Environment, Section 136. U.S. Environmental Protection Agency, Washington, DC.
- Cornelissen G., Rigterink, H., Van Noort, P.C.M., Govers, H.A.J., 2000. Slowly and very slowly desorbing organic compounds in sediments exhibit Langmuir-type sorption. *Environmental Toxicology and Chemistry* 19(6), 1532-1539. doi: 10.1002/etc.5620190609
- Cornelissen, G., Rigterink, H., ten Hulscher, D.E.M., Vrind, B.A., Van Noort, P.C.M., 2001. A simple Tenax extraction method to determine the available of sediment-sorbed organic compounds. *Environmental Toxicology and Chemistry* 20(4), 706–711. doi: 10.1002/etc.5620200403
- Defoe, D.L., Ankley, G.T., 1998. Influence of storage time on toxicity of sediment to benthic invertebrates. *Environmental Pollution* 199, 123-131.

- Defoe, D.L., Ankley, G.T., 2003. Evaluation of time-to-effects as a basis for quantifying the toxicity of contaminated sediments. *Chemosphere* 51, 1–5. doi: 10.1016/S0045-6535(02)00768-3
- Ehlers, L.J., Luthy, R.G., 2003. Contaminant bioavailability in soil and sediment. *Environmental Science and Technology* 37(15), 295A-302A. doi: 10.1021/es032524f
- Gan, J., Lee, S.J., Liu, W.P., Haver, D.L., Kabashima, J.N., 2005. Distribution and persistence of pyrethroids in runoff sediments. *Journal of Environmental Quality* 34, 836-841. doi: 10.2134/jeq2004.0240
- Harwood, A.D., Nutile, S.A., Landrum, P.F., Lydy, M.J., 2015. Tenax extraction as a simple approach to improve environmental risk assessments. *Environmental Toxicology and Chemistry* 34(7), 1445-53. doi: 10.1002/etc.2960
- Hladik, M.L., Orlando, J.L. Kuivila, K.M., 2009. Collection of Pyrethroids in Water and Sediment Matrices: Development and Validation of a Standard Operating Procedure. Scientific Investigations Report 2009–5012. U.S. Geological Survey, Reston, Virginia.
- Ivey, C.D., Ingersoll, C.G., 2016. Influence of bromide on the performance of the amphipod *Hyalella azteca* in reconstituted waters, *Environmental Toxicology and Chemistry* 35(10), 2425-2429. doi: 10.1002/etc.3421
- Ivey, C.D., Ingersoll, C.G., Brumbaugh, W.G., Hammer, E.J., Mount, D.R., Hockett, J.R., Norberg-King, T.J., Soucek, D., Taylor, L., 2016. Using an interlaboratory study to revise methods for conducting 10-d to 42-d water or sediment toxicity tests with *Hyalella azteca*. *Environmental Toxicology and Chemistry* 35(10), 2439–2447. doi: 10.1002/etc.3417
- Kemble, N.E., Hardesty, D.K., Ingersoll, C.G., Kunz, J.L., Sibley, P.K., Calhoun, D.L., Gilliom, R.J., Kuivila, K.M., Nowell, L.H, Moran, P.W. 2013. Contaminants in stream sediments from seven United States metropolitan Areas: Part II—Sediment toxicity to the amphipod *Hyalella azteca* and the midge *Chironomus dilutus*. *Archives of Environmental Contamination and Toxicology*, 64:52-64. doi: 10.1007/s00244-012-9815-y
- Kuivila, K.M., Hladik, M.L., Ingersoll, C.G., Kemble, N.E., Moran, P.W., Calhoun, D.L., Nowell, L.H., Gilliom, R.J., 2012. Occurrence and potential sources of pyrethroid insecticides in stream sediments from seven U.S. metropolitan areas. *Environmental Science and Technology* 46(8), 4297–4303. doi: 10.1021/es2044882
- Lu, Y., Ludsin, S.A., Fanslow, D.L., Pothoven, S.A., 2008. Comparison of three microquantity techniques for measuring total lipids in fish. *Canadian Journal of Fisheries and Aquatic Sciences* 65 (10), 2233–2241. doi:10.1139/F08-135
- Lydy, M.J., Harwood, A.D., Nutile, S.A., Landrum, P.F., 2015. Tenax extraction of sediments to estimate desorption and bioavailability of hydrophobic contaminants: A literature review. *Integrated Environmental Assessment and Management* 11(2), 208-220. doi: 10.1002/ieam.1603

- Lyytikäinen, M., Kukkonen, J.V.K., Lydy, M.J., 2003. Analysis of pesticides in water and sediment under different storage conditions using gas chromatography. *Archives of Environmental Contamination and Toxicology* 44, 437–444. doi: 10.1007/s00244-002-2168-1
- Moran, P.W., Calhoun, D.L., Nowell, L.H., Kemble, N.E., Ingersoll, C.G., Hladik, M.L., Kuivila, K.M., Falcone, J.A., Gilliom, R.J., 2012. Contaminants in stream sediments from seven U.S. metropolitan areas—Data summary of a National Pilot Study: U.S. Geological Survey Scientific Investigations Report 2011–5092, 66 p.
- Moran P.W., Nowell, L.H., Kemble, N.E., Mahler, B.J., Waite, I.R., Van Metre, P.C., 2017. Influence of sediment chemistry and sediment toxicity on macroinvertebrate communities across 99 wadable streams of the Midwestern USA. *Science of the Total Environment* 599–600, 1469–1478. doi: 10.1016/j.scitotenv.2017.05.035.
- Nowell, L.H., Norman, J.E., Ingersoll, C.G., Moran, P.W., 2016. Development and application of freshwater sediment-toxicity benchmarks for currently used pesticides. *Science of the Total Environment* 550, 835-850. doi: 10.1016/j.scitotenv.2016.01.081
- Nutile, S.A., Harwood, A.D., Sinche, F.L., Huff Hartz, K.E., Landrum, P.F., Lydy, M.J., 2017a. The robustness of single-point Tenax extractions of pyrethroids: Effects of the Tenax to organic carbon mass ratio on exposure estimates. *Chemosphere* 171, 308-317. doi: 10.1016/j.chemosphere.2016.12.045
- Nutile, S.A., Harwood, A.D., Sinche, F.L., Huff Hartz, K.E., Landrum, P.F., Lydy, M.J., 2017b. Methodological and environmental impacts on bioaccessibility estimates provided by single-point Tenax extractions. *Archives of Environmental Contamination and Toxicology* 72(4), 612-621. doi: 10.1007/s00244-017-0395-8
- Shelton, L.R., Capel, P.D. 1994. Guidelines for collecting and processing samples of stream bed sediment for analysis of trace elements and organic contaminants for the National Water Quality Assessment Program. U.S. Geological Survey, Open-File Report, 94-458. 20 p.
- Sinche, F.L. Nutile, S.A., Landrum, P.F., Lydy, M.J., 2017. Optimization of Tenax extraction parameters for polychlorinated biphenyls in contaminated sediments. *Talanta* 164, 386-395. doi: 10.1016/j.talanta.2016.11.061
- Smith, M.E., Lazorchak, J.M., Herrin, L.E., Brewer-Swartz, S., Thoeny, W.T., 1997. A reformulated, reconstituted water for testing the freshwater amphipod, *Hyalella azteca*. *Environmental Toxicology and Chemistry* 16(6), 1229-1233. doi: 10.1002/etc.5620160618
- [SWAMP] Surface Water Ambient Monitoring Program, 2017. Quality Assurance Program Plan. https://www.waterboards.ca.gov/water_issues/programs/swamp/qapp/swamp_QAPrP_2017_Final.pdf, accessed 7 Dec. 2017. Direct link to relevant guidance: https://www.waterboards.ca.gov/water_issues/programs/swamp/docs/mqo/18_fresh_sed_tox.pdf

Suter, G. W. II. 1996. Toxicological benchmarks for screening contaminants of potential concern for effects on freshwater biota. *Environmental Toxicology and Chemistry* 15, 1232-1241. doi: 10.1002/etc.5620150731

ten Hulscher, T.E.M., Postma, J., den Besten, P.J., Stroomberg, G.J., Belfroid, A., Wegener, J.W., Faber, J.H., van der Pol, J.J.C., Hendriks, A.J. van Noort, P.C.M., 2003. Tenax extraction mimics benthic and terrestrial bioavailability of organic compounds. *Environmental Toxicology and Chemistry* 22, 2258–2265. doi:10.1897/02-488.

USEPA, 1997. Ecological risk assessment guidance for superfund: Process for designing and conducting ecological risk assessments - interim final. EPA 540/R-97.006, U.S. Environmental Protection Agency, Washington, DC.

USEPA, 2000. Methods for measuring the toxicity and bioaccumulation of sediment-associated contaminants with freshwater invertebrates. EPA/600/R-99/064. U.S. Environmental Protection Agency, Washington, DC.

USEPA, 2005. Sample holding time reevaluation. EPA/600/R-05/124. U.S. Environmental Protection Agency, Washington, DC.

USGS, 2017. 2012-2016 California Drought: Historical Perspective. <https://ca.water.usgs.gov/california-drought/california-drought-comparisons.html> accessed 1 February 2018.

Xu, Y., Gan, J., Wang, Z., Spurlock, F., 2008. Effect of aging on desorption kinetics of sediment-associated pyrethroids. *Environmental Toxicology and Chemistry* 27(16) 1293-1301. doi: 10.1897/07-382.1

Table 1: Summary of Sediment Characteristics

Site Name and Description (abbreviation)	Sample Date	Latitude, Longitude	% OC ^a	%Fraction in Particle Sizes						Sum of Pyrethroids (ng/g OC) ^b	Sum of PCBs (ng/g OC) ^c
				<0.062 mm	0.12 - 0.062 mm	0.25 - 0.12 mm	0.5 - 0.25 mm	1 - 0.5 mm	2 - 1 mm		
Ingram Creek at River Road near Patterson, CA (IC)	6Apr16	37.60020, -121.22508	1.05	83.4	11.5	4.1	0.9	0.1	0.0	1195	nd
Dry Creek at Regional Park at Modesto, CA (DC)	6Apr16	37.64568, -120.98081	1.08	18.6	7.8	16.2	35.9	19.9	1.5	1946	nd
Gilsizer Slough at Bogue Road near Yuba City, CA CA6 (GS)	6Apr16	39.09829, -121.63870	0.88	33.9	9.7	16.1	26.8	11.8	1.8	1717	nd
Bouquet Canyon Creek at the mouth of the Santa Clara River near Saugus, CA (BC)	6Apr16	34.42750, -118.54110	0.26	2.7	0.4	2.1	19.5	48.4	26.9	6867	nd
San Gabriel River at College Park Drive near Los Alamitos, CA (SR16)	6Apr16	33.77494, -118.09736	3.50	50.0	28.1	18.1	2.7	0.6	0.5	1952	nd
Tijuana River at Hollister Street near Nestor, CA (TR)	6Apr16	32.55142, -117.08394	3.54	78.1	12.6	5.9	2.4	0.6	0.3	1878	nd
Manistique River at Manistique, MI (M1)	29Nov16	45.9478, -86.2452 ^d	3.89	20.7	20.7	42.8	11.0	4.0	0.8	nd	9250
Manistique River at Manistique, MI (M2)	29Nov16	45.9478, -86.2452 ^d	3.09	18.0	11.1	26.0	38.7	5.5	0.7	BRL	10720
Kaseberg Creek at Country Club and McAnally in Roseville, CA (KCCC)	30May17	38.76415, -121.32280	2.20	10.1	3.1	7.5	29.0	32.1	18.2	2566	nd
Kaseberg Creek at Green Grove Road in Roseville, CA (KCGG)	30May17	38.77529, -121.34203	3.20	35.7	6.8	7.2	13.8	20.3	16.2	1220	nd
San Gabriel River at College Park Drive near Los Alamitos, CA (SR17)	30May17	33.77528, -118.09736	2.04	19.9	23.0	45.4	10.8	0.7	0.1	678	nd
San Gabriel River at College Park Drive near Los Alamitos, CA upstream from SR17 (SRu)	30May17	33.77639, -118.09733	2.88	19.1	21.4	49.2	10.1	0.2	0.1	601	nd

^a% organic carbon

^b Sum of pyrethroids measured by exhaustive extraction of the sample immediately after sampling. nd = none detected and BRL = below reporting limit (See Table S4 for detection and reporting limits).

^c Sum of polychlorinated biphenyls (PCBs) measured by exhaustive extraction of the sample immediately after sampling. nd = none detected.

^dCoordinates are approximate.

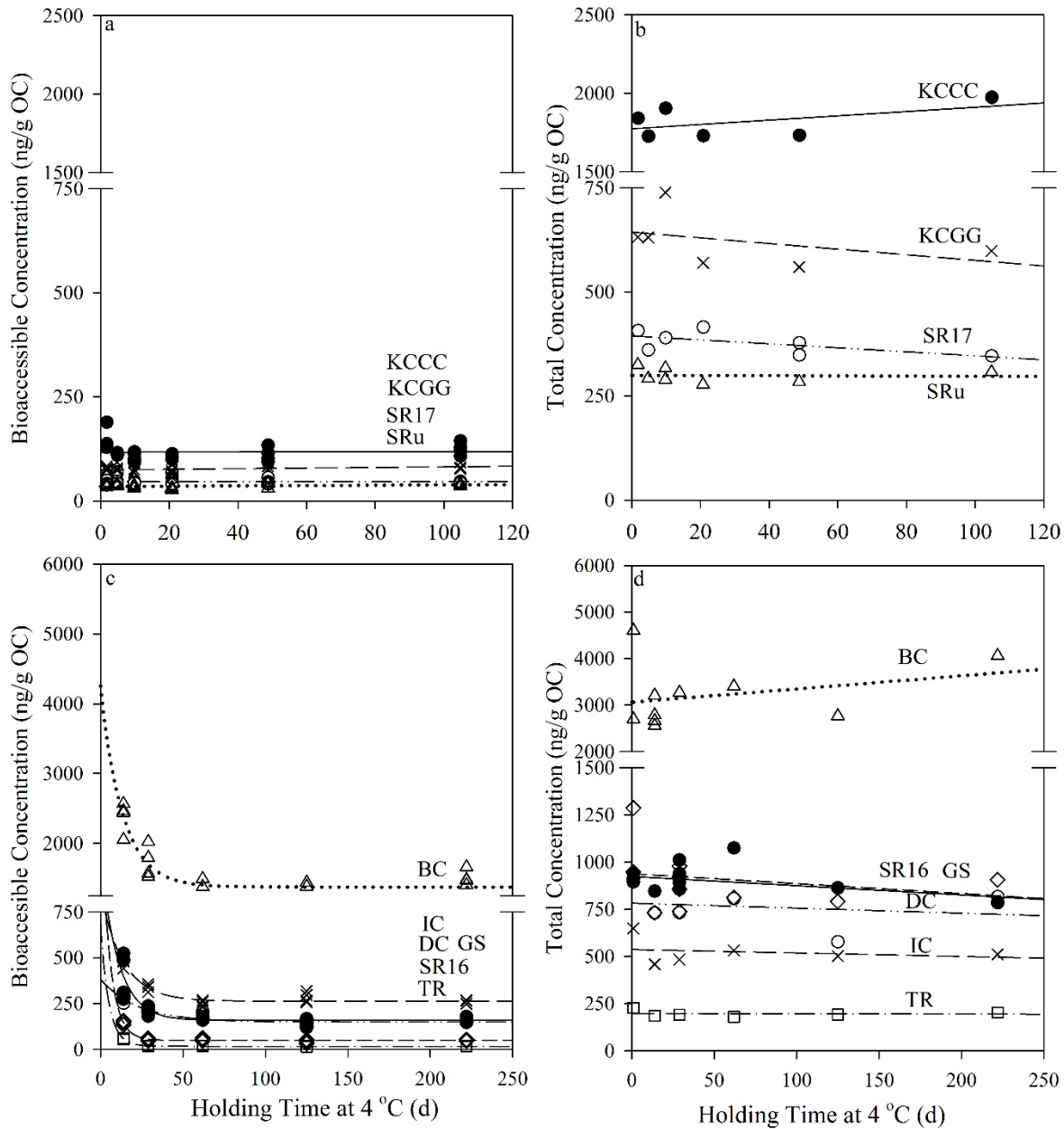


Figure 1: Bifenthrin bioaccessible and total concentrations as a function of sediment holding time at 4 °C. Bioaccessible (a) and total (b) concentrations in sediment sampled 30 May 2017 from Kaseberg Creek at Country Club (KCCC) and at Green Grove Road (KCGG), and San Gabriel River (SR17) and San Gabriel River upstream (SRu). Concentrations fit to a linear equation $C_t = \text{slope} \times t + \text{intercept}$, where C_t is the bioaccessible concentration (a, c) or total concentration (b,d) at any time t , see SI Table 2 for parameters. Bioaccessible (c) and total (d) concentrations in sediment sampled 6 April 2016 from Ingram Creek (IC), Dry Creek (DC), Gilsizer Slough (GS), Bouquet Canyon Creek (BC), San Gabriel River (SR16), and Tijuana River (TR). Bioaccessible concentrations fit to a first-order kinetics equation $C_t = \Delta C e^{-kt} + C_f$, where ΔC is the difference between the initial and equilibrium bioaccessible concentration, k is the first-order rate constant, and C_f is bioaccessible concentration at equilibrium. Total concentrations fit to linear equation, see Table S2 for parameters.

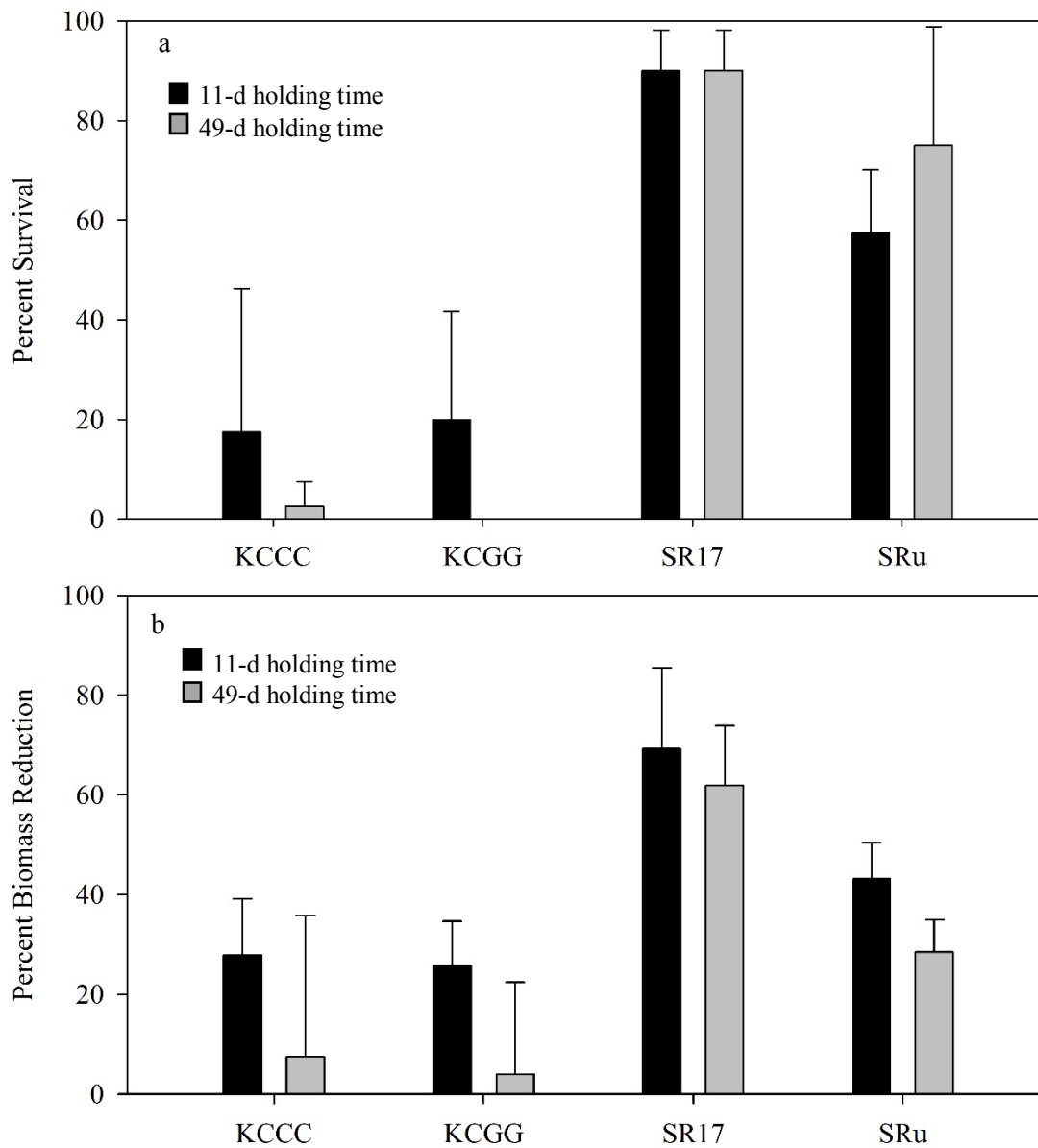


Figure 2. *Hyalella azteca* 10-d toxicity bioassay comparing sediment held at 4 °C for 11 d and 49 d. Bar height indicates average of four replicates and error bars indicate one standard deviation. Endpoints included (a) percent survival and (b) percent reduction in dry biomass relative to reference sediments. No statistical differences were found between 11 d and 49 d for average percent survival and for percent biomass reduction.

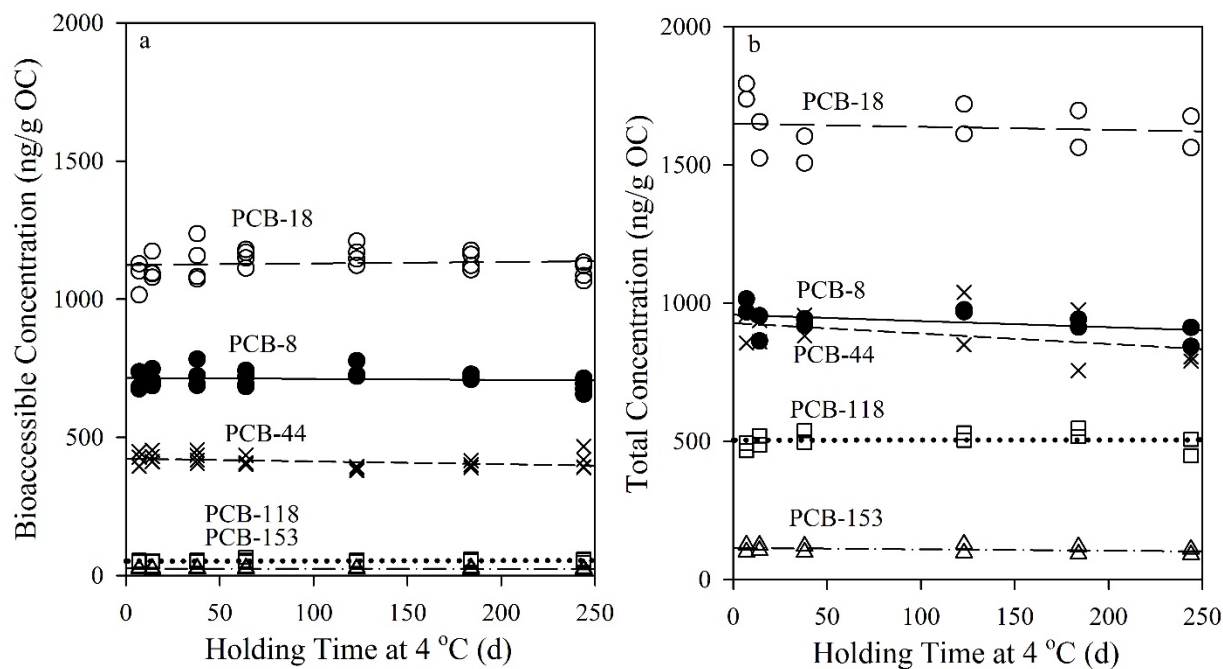


Figure 3. Bioaccessible extraction (a) and total (b) concentrations for selected polychlorinated biphenyl (PCB) congeners as a function of sediment holding time at 4 °C. The PCB-contaminated sediment was sampled on 29 Nov 2016 from the Manistique River near Manistique, MI (M1). Tenax and ASE concentrations were fit to the linear equation: $C_t = \text{slope} \times t + \text{intercept}$, where C_t is the bioaccessible (a) or total (b) concentration at any time t , see Table S2 for parameters.

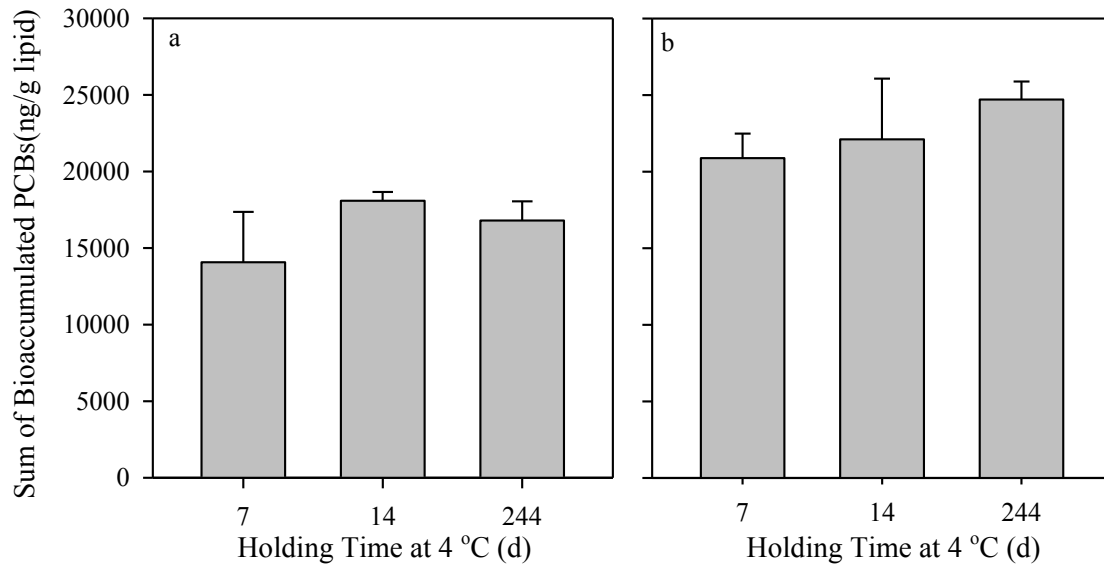


Figure 4. Bioaccumulated polychlorinated biphenyls (PCB) concentrations in *Lumbriculus variegatus* after a 14-d exposure to PCB-contaminated sediment collected from the Manistique River site M1 (a) and M2 (b) that was held at 4 °C for 7 d, 14 d, and 244 d. The height of the bar represents the average of the sum of bioaccumulated PCB concentration normalized for tissue lipid mass in four replicates, and error bars represent one standard deviation. No statistical differences in the averages of bioaccumulated PCBs were found between holding time points.

Supplemental Material

Effect of Sample Holding Time on Pyrethroid- and Polychlorinated Biphenyl-Contaminated Sediment Assessments: Application of Single-Point Tenax Extractions

Kara E. Huff Hartz,^a Federico L. Sinche,^a Samuel A. Nutile,^{a,1} Courtney Y. Fung,^a Patrick W. Moran,^b Peter C. Van Metre,^c Lisa H. Nowell,^d Marc Mills,^e Michael J. Lydy^{a,*}

^a Center for Fisheries, Aquaculture and Aquatic Sciences and Department of Zoology, Southern Illinois University, Carbondale, IL 62901, USA

^b Washington Water Science Center, U.S. Geological Survey, Tacoma, WA 98402 United States

^c Texas Water Science Center, U.S. Geological Survey, Austin, TX 78754, United States

^d California Water Science Center, U.S. Geological Survey, Sacramento, CA 95819, United States

^e U.S. Environmental Protection Agency, National Risk Management Research Laboratory, Office of Research and Development, Cincinnati, OH 45268, United States

1. Method details

1.1 Additional Chemical Sources

Optima grade solvents (hexane, acetone, and methylene chloride), silica gel (60-200 mesh, grade 60), sea sand (washed), ACS grade concentrated sulfuric acid, anhydrous sodium sulfate, glacial acetic acid, and mercury (II) chloride were purchased from Fisher Scientific (Hampton, NH, USA). Nitrogen (purity: 99.998%) and helium (99.999%) were supplied by Airgas Inc. (Marion, IL, USA). Tenax-TA beads (60/80 mesh) were purchased from Scientific Instrument Services Inc. (Ringoes, NJ, USA). Supelco ENVI™-Carb II/primary secondary amine 300/600 mg solid-phase extraction (SPE) cartridges were purchased from Sigma Aldrich (St. Louis, MO, USA).

1.2 Sediment Characterization Methods

The dw fractions were determined gravimetrically by drying a 2-3 g subsample of wet sediment in a 60 °C oven (Precision Scientific Thelco 130D, ThermoFisher Scientific, Waltham, MA, USA) for 48 h. The OC fractions were determined by thermogravimetric analysis using American and Society for Testing and Materials method D5373 (ASTM, 2016) by Midwest Laboratories (Omaha, NE, USA). The particle size distributions were determined by a wet sieve method (Guy, 1969) by the Illinois State Geological Survey for the 2016 pyrethroid sediments and by the Illinois State Water Survey for 2017 pyrethroid and PCB sediments.

1.3 Single-Point Tenax Extractions of Sediment Extract Clean-up Methods

For samples containing pyrethroids, the extracts were cleaned up using a sodium sulfate column (1 g, previously dried at 400 °C for 4 h), evaporated to 0.5 mL using a Pierce Reactivap (Rockford, IL, USA) and acidified to 0.1% with acetic acid. For samples containing PCBs, the Tenax extracts were cleaned up with the addition of 2 mL of concentrated sulfuric acid to each extract (Trimble et al. 2008). Extracts were vortexed (Fisher vortex mixer, ThermoFisher

Scientific) for 5 min at 2000 rpm, centrifuged (Eppendorf centrifuge 5810, Hamburg, Germany), for 5 min at 2000g, and the hexane layer was passed through a Na₂SO₄ (1 g) column to reduce residual water. The remaining sulfuric acid was washed with hexane (2 mL), vortexed, centrifuged, and filtered as described above two additional times. The combined filtered extract was concentrated to 1 mL.

To assess recovery, 40 ng of DBOFB and PCB-209 surrogates were added to each sample for pyrethroids and 50 ng of DBOFB and PCB-186 was added to each sample for PCBs. In addition, four samples of pyrethroid- and PCB-free LaRue Pine Hills (LPH) reference sediment spiked with 40 ng of analytes were extracted with each batch of samples to check for contamination and accurate recovery of analytes.

1.4 Exhaustive Chemical Extraction of Sediment and *L. variegatus* Clean-up Methods

Following bioaccumulation and depuration, the *L. variegatus* were patted dry and massed, and the tissues were stored at -40 °C until extraction and PCB analysis. For accelerated solvent extraction (ASE) extracts analyzed for pyrethroids, potential interferences were reduced by SPE and 1 g of sodium sulfate (previously dried at 400 °C for 4 h). The SPE cartridges were primed using 3 mL of hexane, and after loading onto the cartridge, analytes were eluted with 7 mL of a 7:3 hexane:dichloromethane solution. Extracts were solvent exchanged to hexane, transferred to a GC vial, evaporated to a final volume of 1 mL, and acidified to 0.1 % using acetic acid (Nutile, et al. 2017b). For ASE extracts analyzed for PCBs, potential interferences were reduced using sulfuric acid as described for Tenax extracts.

To assess recovery, 40 ng of DBOFB and PCB-209 surrogates (for pyrethroids) and 50 ng of DBOFB and PCB-186 (for PCBs) were added to each sample prior to ASE and *L. variegatus* extraction. In addition, for every batch of 19 samples extracted, a set of four quality assurance samples were prepared and analyzed along with the samples, and these consisted of one to two blanks (negative controls: sea sand and LaRue Pine Hills (LPH) sediment), a lab control spike (lab sand spiked with pyrethroids), a matrix and matrix spike duplicate (either a LPH or a duplicate sample from the batch).

1.5 Gas Chromatography/Mass Spectrometry Analysis Methods

Pyrethroid insecticides (tefluthrin, fenpropathrin, bifenthrin, λ-cyhalothrin, cis- and trans-permethrin, cyfluthrin, cypermethrin, esfenvalerate, and deltamethrin) were quantified by gas chromatography/mass spectrometry (GC/MS) using an Agilent 7890A GC equipped with an Agilent 5975A inert XL MS (Santa Clara, CA, USA). Samples were injected (1 μL) in pulsed splitless mode at 260 °C and separated using an Agilent HP5ms column (30 m × 250 μm, 0.25 μm film thickness). The oven temperature was initially 50 °C, and ramped to 200 °C at a rate of 20 °C/min, followed by a ramp to 295 °C at 10 °C/min, and held for 10 min. The analytes were separated using He carrier gas with a 1.0 mL/min flow rate and detected in negative chemical ionization (NCI) mode using methane as the reagent gas, and the MS temperatures were as follows: transfer line: 300 °C, ion source: 150 °C, quadrupole: 150 °C.

Polychlorinated biphenyls were quantified by GC/MS using an Agilent 6890 gas chromatograph 5973N mass spectrometer. Samples were injected (2 μ L) in pulsed splitless mode at 265 °C and separated using an Agilent DB-XLB column (30 m \times 180 μ m, 0.18- μ m film thickness). The oven temperature was initially set at 100 °C for 1 minute, and ramped to 255 °C at a rate of 1.2 °C/min, followed by a ramp to 280 °C at 25 °C/min, and held for 3.33 min. The analytes were separated using He carrier gas with a 0.9 mL/min flow rate and detected in electron impact ionization (EI) mode, and the MS temperatures were as follows: transfer line: 280 °C, ion source: 230 °C, quadrupole: 150 °C.

Pyrethroids concentrations in Tenax and ASE extracts were determined by gas chromatography/mass spectrometry (GC/MS) in negative chemical ionization mode (Natile et al. 2017). Analytes were detected in selected ion mode and identified by comparison to standards using retention time (<0.05% agreement), the presence of one target ion and one to two qualifier ions, and with at least one target/qualifier ratio (<20% agreement) (for ions see **Table S5**). Each sample and standard were spiked at 20 ng/mL with an internal standard mixture consisting of deuterated (D₆) tefluthrin, fenpropathrin, bifenthrin, λ -cyhalothrin, cis- and trans-permethrin, cyfluthrin, cypermethrin, esfenvalerate, and deltamethrin, and 2,2',3,4,4',5,6,6'-octachlorobiphenyl, and ¹³C₁₂-decachlorobiphenyl. Analytes were quantified with an eight-point quadratic calibration curve (1 ng/mL – 200 ng/mL) using a custom pyrethroid standard mixture (AccuStandard). Two stereoisomers were observed for permethrin, λ -cyhalothrin, and esfenvalerate, and four stereoisomers were observed for cyfluthrin and cypermethrin (Koch et al. 2013), and concentrations were determined as the sum of isomers. All pyrethroid concentrations were reported normalized by the OC per gram dw sediment. Batch-to-batch reproducibility was verified by injection of a standard subsample and/or by reinjection and quantification of selected samples from prior batches.

The PCB concentrations in Tenax, ASE, and *L. variegatus* extracts were determined by GC/MS in electron ionization mode (Sinche et al. 2017). Analytes were identified by comparison to standards using retention time (<0.05% agreement), using selected ion monitoring with the molecular ion (M⁺) as the target ion and qualified using at least one target ion/qualifier ion ((M+2)⁺ and (M-70)⁺) ratio (<20% agreement). Each sample and standard were spiked at 20 ng/mL with an internal standard mixture consisting of ¹³C₁₂-4,4'-dichlorobiphenyl, ¹³C₁₂-2,2',5,5'-tetrachlorobiphenyl, ¹³C₁₂-2,2',3,4,5,5'-hexachlorobiphenyl, and ¹³C₁₂-decachlorobiphenyl. Analytes were quantified using internal standard calibration with an eight-point quadratic calibration curve (1 ng/mL – 400 ng/mL) using the C-WNN 28-congener PCB standard mixture (AccuStandard). PCB concentrations in Tenax and ASE extracts were reported as normalized by the OC per gram dw sediment.

Lipid content in *L. variegatus* was analyzed using individuals from each bioaccumulation test. Two individuals from each experimental replicate were randomly chosen, blotted dry, weighed (\approx 0.025 g), placed in a glass culture tube, and extracted with chloroform and methanol (1:1, v/v) as previously described (Lu et al. 2008). A vanillin/phosphoric acid reagent was added and transmittance was read at 525 nm using a spectrophotometer (Spectronic 20 Genesys™; Spectronic Instruments, ThermoFisher Scientific, Waltham, MA, USA). A five-point calibration

curve was constructed using dilutions of vegetable oil and treated the same as tissue samples. The transmittance readings were conducted in triplicate to obtain a mean and standard deviation for each sample. Bioaccumulated PCB concentrations in *L. variegatus* were reported as normalized for lipid fraction on a wet weight basis.

Method detection limits (MDLs) and method reporting limits (MRL) applied in the holding time study are shown in Table S4. For pyrethroid Tenax concentrations, MDL was calculated from the extraction and analysis of seven replicate La Rue Pine Hills (3.4 g dry weight) spiked with 2 ng of each pyrethroid and 40 ng of surrogates to verify recovery. The MDLs were calculated as the product of the standard deviation of the dry weight-normalized Tenax concentration and the one-sided Student t-value (99% confidence interval), while MRLs were estimated to be 3×MDL. For accelerated solvent extraction pyrethroid concentrations, the MDL was assumed to be the lowest quantifiable calibration standard and the MRL was assumed to be 3×MDL. For pyrethroids, the reporting limit filter was applied to the dry weight normalized concentrations, where values below the MDL were reported as nd and values above the MDL, but below MRL were reported as below reporting limit (BRL). For the purposes of plotting and averaging, values BRL were applied as MRL/2, but BRL values were omitted from regression analysis. For PCB concentrations, the MRL was assumed to be the lowest value in the calibration curve and the reporting limit was applied to the extract concentration (ng/mL). All concentrations below the MRL were reported as nd.

Additional statistical tests were conducted using Microsoft Excel (version 2013, Redmond, WA, USA) and IBM SPSS Statistics software (version 22, Armonk, NY, USA).

2. Effect of sample storage container on pyrethroid stability in sediment

In order to test the effect of storage container material on bioaccessible pyrethroid concentration, one sediment sample (SR17) was subsampled and stored upon receipt in a 1 L glass jar with Teflon-lined screw-top lid. The single-point Tenax extracts were collected from this glass subsample from the first four time points. The slope of the Tenax concentrations as a function of holding time was slightly positive ($0.015 \text{ ng/g OC d}^{-1}$), but smaller than the standard error in the estimate ($0.198 \text{ ng/g OC d}^{-1}$), and thus no significant change in concentration was observed over the 21 d holding time in glass storage. The Tenax extractable concentrations measured in glass storage were also compared to the storage in the high-density polyethylene (HDPE) pail (Figure S4). The Tenax extractable concentrations of the sediment stored in glass were similar to Tenax extractable concentration of sediment stored in the HDPE pail, and bifenthrin was the only reportable pyrethroid in each set of samples. The paired Student t-tests comparing the averages between each storage container showed no significant difference (probability, $p > 0.05$) at the 95% confidence interval (CI). Furthermore, a two-factor analysis of variance showed no significant difference between the glass and HDPE storage containers ($p > 0.05$, 95% CI). For these reasons, no change in bioaccessible bifenthrin concentration could be detected for 21 d when either glass or HDPE storage containers were used.

3. Quality assurance/quality control results

Recoveries of surrogate compounds were measured relative to spike check standards. The percent recovery of PCB surrogates in Tenax extracts, ASE extracts, and *L. variegatus* samples generally fell within 70-130% acceptability limits (**Table S6**). Although the average percent recovery of surrogates fell within the 70-130% acceptability limits for Tenax and ASE extracts, the range tended to be more variable, falling as low as 37% for DBOFB in an ASE extract and as high as 155% in a Tenax extract. This variability can be attributed to two factors: volatility of the DBOFB surrogate and the matrix effects on DCBP quantification. The DBOFB surrogate is a factor of 100 more volatile (vapor pressure 2.7×10^{-3} mm Hg, Scifinder, 2017) than the pyrethroid in the target analytes with the highest volatility (tefluthrin vapor pressure 6×10^{-5} mm Hg, USEPA, 2017) and a factor of 10,000 more volatile than the pyrethroid detected in samples (bifenthrin 1.8×10^{-7} mm Hg, USEPA, 2017). Low DBOFB values tended to suggest evaporation of analytes, yet the low DBOFB always coincided with good DCBP recovery values (vapor pressure 1.1×10^{-7} mm Hg, USEPA, 2017), thus the low DBOFB recovery values represent worst-case scenario, while the DCBP recovery is a better reflection of the recoveries of pyrethroids in samples. In addition, the sample matrix tended to enhance the ionization and detection of DCBP in the initial samples (first batch of ASE samples and Tenax samples), due to the fact that the internal standard PCB-204 demonstrated incomplete correction of matrix enhancement. In all subsequent batches, the $^{13}\text{C}_{12}$ -DCBP was used as the internal standard, and DCBP recoveries fell within the acceptability limits. The surrogate recoveries of DBOFB and DCBP in the QA/QC samples (blanks, lab control, and matrix spike samples) were also within acceptability limits of 70%-130%, with the exception of a few DBOFB recoveries in *L. variegatus* and ASE extracts and one PCB-186 in a Tenax extract that fell slightly outside of this range (no greater than 133%). However, because DBOFB recoveries were within the acceptable range for these samples, this is likely due to matrix effects rather than sample preparation. Samples that did not meet either surrogate recovery acceptability limits were considered outliers and not included in calculations; this was limited to three Tenax pyrethroid sample replicates, one Tenax PCB sample replicate, one Tenax pyrethroid blank, and one Tenax pyrethroid matrix spike.

The target analytes were also quantified in matrix spike and lab control spiked samples relative to a spike check, and the target analyte recoveries generally fell within the acceptability limits of 50-150% (Table S6). No target analytes were detected in blank PCB samples. In blank pyrethroid samples, peaks corresponding to tefluthrin and esfenvalerate were detected, but the concentrations were below the MDL. The reproducibility of target analyte determination in ASE extracts of PCB and pyrethroid samples, *L. variegatus* samples, and Tenax extracts of PCB samples was assessed by calculating percent relative difference between duplicate matrix-spiked samples, and the average was less than 10%, with the highest percent relative difference as 34%. Because there were four replicates in Tenax extracts of pyrethroids samples, percent relative standard error was calculated, and the average 3% and the highest value was 11%.

Within batch and batch-to-batch quality assurance was monitored for quantification accuracy by several methods depending on the compound class and sample type and how the samples were

batched for analysis. For ASE and *L. variegatus* extracts, samples were batched together and quantified as part of the same sequence. Repeated injection of a check standard (once every 8 or fewer samples) through the sequence demonstrated that the difference between the check standard concentration in comparison to concentrations determined during calibration was <20%. Pyrethroid quantification accuracy between batches was also monitored either by quantifying a prior spike check and comparing to the previous quantification result or sample in subsequent batches or by quantifying an aliquot of an external standard. For comparison to prior spike check or sample, the difference between analyses was <25%. For comparison to an external standard, the difference between the quantified and standard value was <10% over all batches. PCB quantification accuracy was not monitored because with the exception of the first two time points for Tenax extracts, samples were batched together and quantified as part of the same sequence. Regardless, no changes in bioaccessible concentrations were observed.

Hyalella azteca initial biomasses of 7-d old animals were 0.022 mg/ animal for the day 11 test and 0.025 mg/animal for the day 49 test, and these values met the 0.02 to 0.035 mg/animal acceptability limits as defined in Ivey et al. (2016). The *H. azteca* dry biomasses and percent survival upon test completion were 0.078 mg/animal and 97.5% for sand day 11 test, 0.100 mg/ animal and 93% for day 49 test, 0.101 mg/animal and 93%% for sand day 11 test, 0.098 mg/ animal and 95% for day 49 test, 0.112 mg/animal and 96% for the reference sediments day 11 test, and 0.105 mg/animal and 98% survival for the reference sediments day 49 test, which met the minimum survival (>80%) and average dry biomass (>0.05 mg/ animal) acceptability limits determined by Ivey et al. (2016).

Water quality parameters including dissolved oxygen, pH, conductivity, ammonia, and temperature all remained within acceptable ranges during the assays (USEPA, 2000). Water quality was monitored for *H. azteca* bioassays by randomly selecting two to three samples each day for analysis. pH was measured using an Oakton pH/Con 10 Series meter and the average (+1 standard deviation, SD) for all samples was 7.44 (0.28). Dissolved oxygen was measured with Yellow Springs Incorporated 55 dissolved oxygen probe (Yellow Springs, OH, USA) and the average (+1SD) for all samples was 7.54 (0.35) mg/L, and the minimum measured concentration was 6.72 mg/L. Temperature was also measured with the YSI meter (and the average (+1SD) was 23.7 °C (0.7 °C), and the values ranged from 22.7°C to 24.8 °C. Conductivity was monitored using an Oakton Acorn CON 5 meter (Vernon Hills, IL, USA), and the average value (+1SD) was 426 (141) µS. Ammonia was monitored using an API kit (Mars Fishcare, Chalfont, PA, US), and the average value was 0.14 mg/L, and no values were greater than 1.5 ppm. Water quality for *L. variegatus* bioaccumulation tests was measured at the end of bioassay by sampling the overlying water in each replicate. The average (+1SD) pH was 6.99 (0.06) and 6.95 (0.09) for sediment M2 and M1, respectively. The average (+1SD) temperature was 24.4 °C (0.8 °C) and 24.7 °C (0.5 °C) for sediment M2 and M1, respectively. The average (+1SD) dissolved oxygen was 4.1(0.1) mg/L and 4.0 (0.2) mg/L for sediment M2 and M1 respectively. The ammonia concentration was less than 1 mg/L in all samples. Conductivity was not measured in *L. variegatus* tests.

4. Additional Results and Discussion

The pyrethroid-contaminated sediments were also extracted using exhaustive chemical methods to provide total chemical concentrations in the sediment at each holding time point. Similar to the Tenax extracts, bifenthrin was found in all ASE extracts of sediment, and bifenthrin was the most abundant pyrethroid (up to 3650 ng/g OC at Bouquet Canyon Creek) in all sediments except one (Tijuana River). All ASE extracts of sediment contained detectable or quantifiable concentrations of cyfluthrin and cypermethrin, and nine out of 10 sediments contained λ -cyhalothrin, permethrin, and deltamethrin. Esfenvalerate was detected in seven of the sediments, while neither tefluthrin nor fenpropathrin were detected in any of the sediments. The pattern for total pyrethroids tended to be similar to the bioaccessible pyrethroid concentration pattern for sediments and at each time point. The exhaustive chemical concentrations were always greater than the bioaccessible concentrations for each pyrethroid because bioaccessible concentrations represent a fraction of the total concentrations.

Although KCCC contained twice the sum of total pyrethroids (2566 ng/g OC) measured by exhaustive chemical extraction as KCGG (1220 ng/g OC), both sites contained similar concentrations of bioaccessible bifenthrin (117 ng/g OC and 77 ng/g OC, respectively). The KCGG site also contained bioaccessible concentrations of cyfluthrin (13 ng/g OC) and cypermethrin (27 ng/g OC), and it is likely that the additive effects of these three pyrethroids contributed to the sediment toxicity noted for *H. azteca*. San Gabriel River (SR17) was the least toxic to *H. azteca* of the sediments assayed both in terms of survival and biomass reduction. SRu showed greater toxicity than SR17, and although SR17 had a similar bioaccessible bifenthrin concentration (45 ng/g OC) as SRu (36 ng/g OC), SRu also contained detectable concentrations of bioaccessible cyfluthrin and cypermethrin, which contributed to the increased toxicity of SRu relative to SR17.

The results from 10-d toxicity bioassay comparing sediment held at 4 °C for 11 d and 49 d prior to beginning the bioassays are shown in **Table S8**. Two endpoints are shown: dry mass per animal and % survival. Three of the four sediments caused reduced survival (**Figure 2a**), and all four sediments caused a decrease in the *H. azteca* biomass relative to reference sediments at the end of the bioassay (**Figure 2b**). Kaseberg Creek at Country Club, McAnally (KCCC) and KCGG were the most toxic sediments to *H. azteca*, where survival ranged from 0% to 20% and the biomass reduction ranged from 4% to 28%.

We could only resample one of the 2016 sites in 2017 (San Gabriel), and we observed a significant decrease in bioaccessible pyrethroids with holding time in 2016, but little change in 2017. This difference suggests that the OC/pyrethroid equilibrium was more resistant to perturbation in 2017, although we cannot rule out a change in OC characteristics from 2016 to 2017.

Bioaccessible PCB concentrations ranged from 10 ng/g OC to 1940 ng/g OC for individual congeners (Table S1), and the total PCB concentrations ranged from 23 ng/g OC to 3890 ng/g OC for individual congeners (Table S3). Similar to pyrethroids, each bioaccessible PCB concentration was a fraction of each total PCB concentration. Detectable PCBs tended to belong

to the lower-chlorinated congener groups (dichloro through hexachloro), while no PCB congeners were detected from the heptachloro congener groups or higher. This pattern is likely due to the site history, which included receiving effluent from a paper mill plant followed by dredging activities, and the PCB pattern is similar to prior analyses (Gustavson, 2014).

Lipid-normalized bioaccumulated PCB concentrations in *L. variegatus* after 14-d exposure to sediment M1 and M2 are shown in **Table S9**. One application that uses bioaccessible concentrations is the prediction of the bioaccumulated PCB concentrations according to the Bioaccumulation-Tenax Model (BTM; Harwood et al., 2015). In the current project, we measured the PCB bioaccumulation in *L. variegatus* and compared it to the bioaccessible concentrations determined by Tenax (Figure S5). All data fit within the 95% confidence intervals of the BTM, which demonstrates excellent agreement between the bioaccessible concentration and PCB concentrations in *L. variegatus*.

Sediment-associated PCBs have half-lives that range from 1080 d to 13,800 d at 7 °C (Sinkkonen and Paasivirta, 2000). Our results were similar, where all but two PCBs showed a significant decrease. No more than 10% decrease in PCB concentration was observed over 180 d.

The 2017 sediments, which showed negligible change in bioaccessible pyrethroids or *H. azteca* toxicity, were rehomogenized before each stage of sampling, suggesting that this processing step did not disrupt organic carbon and release sequestered HOCs into the bioaccessible and bioavailable phase (Burgess and McKinney, 1997). It is possible that other sample preparation practices, such as mechanical mixing prior to analysis, could disrupt organic carbon and release sequestered HOCs into bioaccessible and bioavailable phase (Burgess and McKinney, 1997). If the process of sampling and homogenization disrupts HOC/organic carbon equilibria, then this would suggest that holding times are necessary in order to allow time for sediment to return equilibrium in order to prevent overestimation of toxicity.

A map of the sites is included (**Figure S6**).

4. References

- [ASTM] American Society for Testing and Materials, 2005. Standard Test Method for Measuring the Toxicity of Sediment-Associated Contaminants with Freshwater Invertebrates, Method E1706, ASTM International, West Conshohocken, PA, USA.
- [ASTM] American Society for Testing and Materials, 2016. Standard Test Methods for Determination of Carbon, Hydrogen and Nitrogen in Analysis Samples of Coal and Carbon in Analysis Samples of Coal and Coke, Method D5373, ASTM International, West Conshohocken, PA, USA.
- Burgess, R.M., McKinney, R.A., 1997. Effects of sediment homogenization on interstitial water PCB geochemistry. *Archives of Environmental Contamination and Toxicology* 33, 125–129.
- Gustavson, K. 2014. PCB content of sediments collected at the Manistique Harbor, Michigan. ERDC Technical Notes Collection (ERDC/EL TN-14-2). Vicksburg, MS: U.S. Army Engineer Research and Development Center.

Guy, H.P. 1969. Laboratory theory and methods for sediment analysis in Techniques of Water Resources Investigations of the United States Geological Survey, Chapter C1, Book 5. U.S. Government Printing Office, Washington, DC, US.

Ivey, C.D., Ingersoll, C.G., Brumbaugh, W.G., Hammer, E.J., Mount, D.R., Hockett, J.R., Norberg-King, T.J., Soucek, D., Taylor, L., 2016. Using an interlaboratory study to revise methods for conducting 10-d to 42-d water or sediment toxicity tests with *Hyaella azteca*. Environmental Toxicology and Chemistry 35(10), 2439–2447. doi: 10.1002/etc.3417

Koch, D.A., Clark, D., Tessier, D.M., 2013. Quantification of pyrethroids in environmental samples using NCIGC-MS with stable isotope analogue standards. Journal of Agricultural and Food Chemistry 61, 2330–2339. doi: 10.1021/jf3048912

Lu, Y., Ludsin, S.A., Fanslow, D.L., Pothoven, S.A., 2008. Comparison of three microquantity techniques for measuring total lipids in fish. Canadian Journal of Fisheries and Aquatic Sciences 65 (10), 2233–2241. doi:10.1139/F08-135

Nutile, S.A., Harwood, A.D., Sinche, F.L., Huff Hartz, K.E., Landrum, P.F., Lydy, M.J., 2017. The robustness of single-point Tenax extractions of pyrethroids: Effects of the Tenax to organic carbon mass ratio on exposure estimates. Chemosphere 171, 308-317. doi: 10.1016/j.chemosphere.2016.12.045

SciFinder, version 2017; Chemical Abstracts Service: Columbus, OH, 2017; Vapor pressure value for RN 10386-84-2 (accessed December 7, 2017); calculated using ACD/Labs Software V11.02 © 1994-2017.

Sinche, F.L. Nutile, S.A., Landrum, P.F., Lydy, M.J., 2017. Optimization of Tenax extraction parameters for polychlorinated biphenyls in contaminated sediments. Talanta 164, 386-395. doi: 10.1016/j.talanta.2016.11.061

Sinkkonen, S., Paasivirta, J., 2000. Degradation half-life times of PCDDs, PCDFs and PCBs for environmental fate modeling. Chemosphere 40(9-11), 943-949. doi: 10.1016/S0045-6535(99)00337-9

Trimble, T.A., You, J. Lydy, M.J., 2008. Bioavailability of PCBs from field-collected sediments: application of Tenax extraction and Matrix-SPME techniques. Chemosphere 71(2), 337–344. doi: 10.1016/j.chemosphere.2007.09.001

U.S. Environmental Protection Agency. Chemistry Dashboard.
<https://comptox.epa.gov/dashboard/DTXSID9020160> (accessed December 07, 2017), Bifenthrin

U.S. Environmental Protection Agency. Chemistry Dashboard.
<https://comptox.epa.gov/dashboard/DTXSID4047541> (accessed December 07, 2017),
Decachlorobiphenyl.

U.S. Environmental Protection Agency. Chemistry Dashboard.
<https://comptox.epa.gov/dashboard/DTXSID5032577> (accessed December 07, 2017), Tefluthrin.

US Environmental Protection Agency (USEPA), 2000. Methods for measuring the toxicity and bioaccumulation of sediment-associated contaminants with freshwater invertebrates. EPA/600/R-99/064. U.S. Environmental Protection Agency, Washington, DC.

U.S. Geological Survey (USGS), 2017. 2012-2016 California Drought: Historical Perspective. accessed 1 February 2018 at <https://ca.water.usgs.gov/california-drought/california-drought-comparisons.html>

U.S. Geological Survey (USGS), 2018. National Water Information System data available on the World Wide Web (USGS Water Data for the Nation), accessed 22 March, 2018, at <http://waterdata.usgs.gov/nwis>

Table S1. Bioaccessible pyrethroid and polychlorinated biphenyl (PCB) concentrations and percent bioaccessible in sediment as a function of 4 °C holding time, average of n=4 except where indicated.

Kaseberg Creek at County Club and McAnally (ng/g OC) ^a							
Holding time, d	2	5	10	21	49	105	%bioaccessible ^h
Bifenthrin	145 ^b	112 ^b	104 ^b	105	111	125	6
λ-cyhalothrin	BRL ^c	BRL ^c	BRL ^c	BRL ^c	BRL ^c	BRL ^c	BRL ^c
Permethrin	nd	nd	nd	nd	nd	nd	nd
Cyfluthrin	BRL ^c	BRL ^c	BRL ^c	BRL ^c	BRL ^c	BRL ^c	BRL ^c
Cypermethrin	BRL ^c	BRL ^c	BRL ^c	BRL ^c	BRL ^c	BRL ^c	BRL ^c
Esfenvalerate	nd	nd	nd	nd	nd	nd	nd
Deltamethrin	nd	nd	nd	nd	nd	nd	nd
Kaseberg Creek at Green Grove Road (ng/g OC) ^a							
Holding time, d	2	5	10	21	49	105	%bioaccessible ^h
Bifenthrin	77.1 ^b	78.2 ^b	74.2 ^b	65.3	82.5	81.8	12
λ-cyhalothrin	BRL	BRL	BRL	BRL	BRL	BRL	BRL
Permethrin	nd	nd	nd	nd	nd	nd	nd
Cyfluthrin	13.1 ^b	13.4 ^b	14.1 ^b	13.5	13.9	12.2	12
Cypermethrin	26.0 ^b	30.1 ^b	27.9 ^b	26.0	28.7	25.1	16
Esfenvalerate	nd	nd	nd	nd	nd	nd	nd
Deltamethrin	nd	nd	nd	nd	nd	nd	nd
San Gabriel River at College Park Drive, sampled 2017 (ng/g OC) ^a							
Holding time, d	2	5	10	21	49	105	%bioaccessible ^h
Bifenthrin	42.0 ^b	48.1 ^b	42.6 ^b	51.1	45.8	44.6	13
λ-cyhalothrin	BRL ^c	BRL ^c	BRL ^c	BRL ^c	BRL ^c	BRL ^c	BRL ^c
Permethrin	nd	nd	nd	nd	nd	nd	nd
Cyfluthrin	nd	nd	nd	nd	nd	nd	nd
Cypermethrin	nd	nd	nd	nd	nd	nd	nd
Esfenvalerate	nd	nd	nd	nd	nd	nd	nd
Deltamethrin	nd	nd	nd	nd	nd	nd	nd
San Gabriel River at College Park Drive, sampled 2017 upstream (ng/g OC) ^a							
Holding time, d	2	5	10	21	49	105	%bioaccessible ^h
Bifenthrin	36.4 ^b	37.4 ^b	33.1 ^b	29.1	39.6	38.2	12
λ-cyhalothrin	BRL ^c	BRL ^c	BRL ^c	BRL ^c	BRL ^c	BRL ^c	BRL ^c
Permethrin	nd	nd	nd	nd	nd	nd	nd
Cyfluthrin	BRL ^c	BRL ^c	BRL ^c	BRL ^c	BRL ^c	BRL ^c	BRL ^c
Cypermethrin	BRL ^c	BRL ^c	BRL ^c	BRL ^c	BRL ^c	BRL ^c	BRL ^c
Esfenvalerate	nd	nd	nd	nd	nd	nd	nd
Deltamethrin	nd	nd	nd	nd	nd	nd	nd
San Gabriel River at College Park Drive, sampled 2016 (ng/g OC) ^a							
Holding time, d	14	29	62	125	222	%bioaccessible ^h	
Bifenthrin	147	55.5	54.4	44.6	49.6	5	
λ-cyhalothrin	23.6	BRL	BRL	BRL	BRL	BRL	
Permethrin	189	66.0	63.2	61.3	57.7	12	
Cyfluthrin	53.8	19.8	22.8	14.9	16.0	11	
Cypermethrin	36.6	12.6 ^g	14.7	8.4 ^g	11.4 ^g	12	
Esfenvalerate	BRL	BRL	BRL	BRL	nd	nd	
Deltamethrin	nd	nd	nd	nd	nd	nd	

Ingram Creek (ng/g OC) ^a						
Holding time, d	14	29	62	125	222	%bioaccessible ^h
Bifenthrin	478	341	249	285	257	50
λ -cyhalothrin	104	77.0	64.8	59.2	45.7	54
Permethrin	nd	nd	nd	nd	nd	nd
Cyfluthrin	nd	BRL	BRL	nd	nd	nd
Cypermethrin	BRL	BRL	BRL	nd	BRL	BRL
Esfenvalerate	154	115	83.7	83.9	67.5	7
Deltamethrin	nd	nd	nd	nd	nd	nd
Dry Creek (ng/g OC) ^a						
Holding time, d	14	29	62	125	222	%bioaccessible ^h
Bifenthrin	398	216	166	148	164	18
λ -cyhalothrin	nd	nd	BRL	BRL	nd	nd
Permethrin	nd	nd	nd	nd	nd	nd
Cyfluthrin	BRL	BRL	BRL	BRL	nd	nd
Cypermethrin	BRL	BRL	BRL	BRL	BRL	BRL
Esfenvalerate	BRL	BRL	BRL	BRL	nd	nd
Deltamethrin	BRL	BRL	nd	nd	BRL	BRL
Gilsizer Slough (ng/g OC) ^a						
Holding time, d	14	29	62	125	222	%bioaccessible ^h
Bifenthrin	278	206	177	138	155	20
λ -cyhalothrin	BRL	BRL	BRL	BRL	BRL	BRL
Permethrin	nd	nd	nd	nd	nd	nd
Cyfluthrin	BRL	nd	nd	nd	nd	nd
Cypermethrin	BRL	BRL	BRL	BRL	BRL	BRL
Esfenvalerate	BRL	BRL	BRL	BRL	nd	nd
Deltamethrin	BRL	BRL	nd	nd	nd	nd
Bouquet Canyon (ng/g OC) ^a						
Holding time, d	14	29	62	125	222	%bioaccessible ^h
Bifenthrin	2380	1730	1320	1310	1500	45
λ -cyhalothrin	266	225	221	182 ^g	172 ^g	36
Permethrin	963	653	707	556	565	51
Cyfluthrin	141 ^g	98.0 ^g	124 ^g	67.9 ^g	93.7 ^g	27
Cypermethrin	BRL	BRL	BRL	BRL	BRL	BRL
Esfenvalerate	BRL	BRL	BRL	BRL	BRL	BRL
Deltamethrin	nd	nd	nd	nd	nd	nd
Tijuana River (ng/g OC) ^a						
Holding time, d	14	29	62	125	222	%bioaccessible ^h
Bifenthrin	58.3	18.8	18.9	14.2	16.5	9
λ -cyhalothrin	BRL	BRL	BRL	BRL	nd	nd
Permethrin	306	96.4	83.5	65.9	65.1	17
Cyfluthrin	BRL	BRL	BRL	nd	nd	nd
Cypermethrin	494	166	141	124	97.3	16
Esfenvalerate	17.9	7.3 ^g	8.8 ^g	4.5 ^g	6.3 ^g	19
Deltamethrin	nd	nd	nd	nd	nd	nd

Manistique River (M1) ^{b,d} (ng/g OC)								
Holding time, d	7	14	38	64	123	184	244	%bioaccessible ^h
PCB-8	681 ^c	711	721	709	737	719	685	76
PCB-18	1070 ^c	1110	1140	1150	1160	1140	1100	69
PCB-28	619 ^c	658	661	672	622	620	580	67
PCB-52	1240 ^c	1300	1290	1330	1300	1290	1360	50
PCB-44	407 ^c	427	428	413	386	402	418	47
PCB-66	96.3 ^c	112	115	110	115	109	107	29
PCB-101	93.3 ^c	91.1	96.7	96.9	97.6	100.9	99.4	22
PCB-123	9.8 ^{c,g}	9.7 ^g	17.6	18.4	18.3	19.0	18.3	25
PCB-118	51.2 ^c	50.8	53.0	54.5	53.3	55.3	52.2	10
PCB-153	22.5 ^c	21.9	25.3	24.9	25.0	25.5	21.3	23
PCB-105	15.3 ^{c,g}	17.0	19.7	19.2	19.5	19.2	22.3	7
PCB-138	13.2 ^{c,g}	14.6 ^g	18.7	18.5	18.6	19.3	12.8 ^g	17

Manistique River (M2) ^{b,e} (ng/g OC)								
Holding time, d	7	14	38	64	123	184	244	%bioaccessible ^h
PCB-8	452	462	457	451	466	445	427	75
PCB-18	1450	1470	1460	1460	1480	1460	1540	70
PCB-28	412	417	409	412	431	430	390	54
PCB-52	1940	1900	1820	1770	1830	1750	1920	51
PCB-44	393	403	418	417	411	399	421	45
PCB-66	172	176	172	168	175	174	183	34
PCB-101	148	141	139	128	141	140	153	24
PCB-123	26.2	26.7	25.9	25.1	26.4	27.1	30.6	16
PCB-118	79.4	74.0	73.0	70.2	75.9	75.3	78.7	14
PCB-153	36.6	36.9	37.5	36.4	35.1	35.9	36.5	23
PCB-105	30.7	30.4	31.3	28.6	30.9	31.3	33.1	11
PCB-138	28.7	28.6	28.7	27.5	28.2	27.6	30.2	16

^a nd = none detected) for tefluthrin and fenpropathrin at all holding time points. BRL = below reporting limit (See Table S4 for detection and reporting limits).

^b average of n =5

^c average of n=3

^d nd for PCB-81, PCB-77, PCB-114, PCB-187, PCB-126, PCB-128, PCB-167, PCB-156, PCB-157, PCB-180, PCB-170, PCB-169, PCB-189, PCB-195, PCB-205, PCB-209 at all time points.

^e nd for PCB-81, PCB-77, PCB-114, PCB-187, PCB-126, PCB-128, PCB-167, PCB-156, PCB-157, PCB-180, PCB-170, PCB-169, PCB-189, PCB-195, PCB-205, PCB-209 at all time points.

^f reported as below reporting limit (BRL) although below detection limit

^g reported value although below reporting limit

^h% bioaccessible calculated as the average of the ratio of the bioaccessible concentration to the total concentration

Table S2. Kinetic parameters (standard error, SE) for bioaccessible concentrations (in Tenax extraction) and total concentrations (in exhaustive chemical extracts) of pyrethroid and polychlorinated biphenyls (PCBs) as a function of holding time at 4 °C.^a

Sediment	Compound	Bioaccessible (Tenax)			Total (exhaustive)		
		Slope (SE) ng/g OC/d	p-value in slope	Intercept (SE) ng/g OC	Slope (SE) ng/g OC/d	p-value in slope	Intercept (SE) ng/g OC
KCCC	Bifenthrin	0.013 (0.113)	0.910	117 (5)	1.4 (1.1)	0.296	1770 (55)
	λ-cyhalothrin	na	na	na	0.11 (0.04)	0.061	31.7 (2.0)
	Permethrin	na	na	na	1.1 (0.5)	0.087	471 (22)
	Cyfluthrin	na	na	na	0.090 (0.102)	0.425	59.2 (4.9)
	Cypermethrin	na	na	na	0.13 (0.06)	0.116	71.0 (3.1)
	Deltamethrin	na	na	na	1.2 (0.3)	0.018*	18.0 (15.4)
KCGG	Bifenthrin	0.072 (0.047)	0.140	74.4 (2.1)	-0.68 (0.75)	0.415	643 (36)
	λ-cyhalothrin	na	na	na	-0.088 (0.119)	0.503	37.4 (5.7)
	Permethrin	na	na	na	-2.8 (3.6)	0.482	403 (172)
	Cyfluthrin	-0.0103 (0.0079)	0.205	13.7 (0.4)	3.9 (0.9)	0.011	45.4 (42.2)
	Cypermethrin	-0.0214 (0.0208)	0.313	28.0 (1.0)	-0.40 (0.37)	0.338	181 (18)
	Deltamethrin	na	na	na	-0.24 (0.29)	0.457	135 (14)

Sediment	Compound	Bioaccessible (Tenax)			Total (exhaustive)				
		Slope (SE)	p-value in slope	Intercept (SE)	Slope (SE)	p-value in slope	Intercept (SE)		
		ng/g OC/d		ng/g OC	ng/g OC/d		ng/g OC		
SR17	Bifenthrin	0.015 (0.198)	0.942	45.7 (2.3)	-0.48 (0.26)	0.122	394 (12)		
	Permethrin	na	na	na	0.17 (0.92)	0.338	182 (44)		
	Cyfluthrin	na	na	na	-0.26 (0.10)	0.060	35.5 (5.1)		
	Cypermethrin	na	na	na	-0.017 (0.146)	0.911	30.0 (7.0)		
	Deltamethrin	na	na	na	-0.045 (0.099)	0.665	20.8 (4.8)		
SRu	Bifenthrin	0.037 (0.025)	0.154	34.5 (1.1)	-0.022 (0.213)	0.922	300 (10)		
	λ -cyhalothrin	na	na	na	-0.065 (0.031)	0.091	15.2 (1.4)		
	Permethrin	na	na	na	-0.085 (0.096)	0.413	175 (4.3)		
	Cyfluthrin	na	na	na	0.11 (0.14)	0.457	36.3 (6.1)		
	Cypermethrin	na	na	na	0.057 (0.061)	0.391	26.1 (2.7)		
	Deltamethrin	na	na	na	0.010 (0.092)	0.913	22.0 (4.1)		
Sediment	Compound	Bioaccessible (Tenax)				Total (exhaustive)			
		k (SE)	ΔC (SE)	C_f (SE)	p-value in fit	Half- life, d	Slope (SE)	p-value in slope	Intercept (SE)
		d ⁻¹	ng/g OC	ng/g OC			ng/g OC/d		ng/g OC
Ingram Creek	Bifenthrin	0.0730 (0.0134)	601 (119)	263 (8)	<0.0001	9.5	-0.018 (0.038)	0.662	536 (41)
	λ -cyhalothrin	0.0346 (0.0090)	52 (3)	81 (12)	<0.0001	20.0	-0.24 (0.11)	0.083	167 (11)
	Esfenvalerate	0.0445 (0.0122)	147 (29)	75 (5)	<0.0001	15.6	-0.35 (0.15)	0.0737	264 (16)

Sediment	Compound	Bioaccessible (Tenax)					Total (exhaustive)			
		k (SE) d ⁻¹	ΔC (SE) ng/g OC	C _f (SE) ng/g OC	p-value in fit	Half- life, d	Slope (SE) ng/g OC/d	p-value in slope	Intercept (SE) ng/g OC	
Dry Creek	Bifenthrin	0.0942 (0.0359)	896 (460)	158 (16)	<0.0001	7.4	-0.49 (0.81)	0.559	924 (69)	
	Permethrin	na	na	na	na	na	-0.90 (0.42)	0.063	231 (35)	
	Cyfluthrin	na	na	na	na	na	-0.093 (0.101)	0.395	59.4 (9.6)	
	Cypermethrin	na	na	na	na	na	-0.041 (0.64)	0.591	66.4 (5.5)	
	Deltamethrin	na	na	na	na	na	1.7 (0.6)	0.034	202 (55)	
Gilsizer	Bifenthrin	0.0444 (0.0098)	233 (37)	150 (6)	0.0003	15.6	-0.27 (0.65)	0.703	783 (70)	
	Permethrin	na	na	na	na	na	-0.25 (0.51)	0.646	353 (55)	
	Cypermethrin	na	na	na	na	na	0.10 (0.18)	0.617	102 (20)	
	Esfenvalerate	na	na	na	na	na	-0.062 (0.039)	0.183	126 (4)	
Bouquet	Bifenthrin	0.0748 (0.0212)	2878 (902)	1380 (56)	<0.0001	9.3	2.8 (3.2)	0.399	3060 (3)	
	λ-cyhalothrin	0.0152 (0.0101)	111 (23)	168 (20)	0.0006	45.6	-2.0 (2.5)	0.448	687 (198)	
	Permethrin	0.132 (0.075)	2263 (2350)	608 (28)	<0.0001	5.2	-0.10 (0.76)	0.894	1220 (64)	
	Cyfluthrin	0.0230 (0.0206)	67 (26)	84 (12)	0.0183	30.1	-0.68 (0.31)	0.062	351 (64)	

Sediment	Compound	Bioaccessible (Tenax)				Total (exhaustive)			
		k (SE) d ⁻¹	ΔC (SE) ng/g OC	C _f (SE) ng/g OC	p-value in fit	Half- life, d	Slope (SE) ng/g OC/d	p-value in slope	Intercept (SE) ng/g OC
San Gabriel	Bifenthrin	0.185 (0.052)	1294 (936)	49.5 (2.6)	<0.0001	3.7	-0.53 (0.39)	0.213	939 (33)
	λ-cyhalothrin	na	na	na	na	na	-2.1 (2.6)	0.438	702 (206)
	Permethrin	0.221 (0.074)	2808 (2864)	61.3 (2.8)	<0.0001	3.1	0.11 (0.71)	0.878	517 (60)
	Cyfluthrin	0.207 (0.090)	644 (805)	18.2 (1.2)	<0.0001	3.3	-0.41 (0.48)	0.934	171 (41)
	Cypermethrin	0.210 (0.096)	473 (630)	11.5 (0.84)	<0.0001	3.3	-0.048 (0.100)	0.639	95.3 (8.5)
	Esfenvalerate	na	na	na	na	na	-0.038 (0.11)	0.741	40.3 (9.8)
	Deltamethrin	na	na	na	na	na	0.059 (0.152)	0.705	72.5 (12.9)
Tijuana	Bifenthrin	0.199 (0.042)	675 (397)	16.8 (0.7)	<0.0001	3.5	-0.013 (0.099)	0.901	198 (11)
	Permethrin	0.144 (0.054)	1782 (1327)	69.6 (11.2)	<0.0001	4.8	-0.25 (0.28)	0.423	423 (30)
	Cypermethrin	0.135 (0.017)	2496 (596)	118 (7)	<0.0001	5.1	-0.19 (0.89)	0.845	741 (96)
	Esfenvalerate	0.197 (0.159)	174 (384)	6.7 (0.7)	<0.0001	3.5	0.0091 (0.0395)	0.829	34.6 (4.2)
	Deltamethrin	na	na	na	na	na	0.034 (0.070)	0.651	47.6 (7.5)

Sediment	Compound	Bioaccessible (Tenax)			Total (exhaustive)		
		Slope (SE) ng/g OC/d	p-value in slope	Intercept (SE) ng/g OC	Slope (SE) ng/g OC/d	p-value in slope	Intercept (SE) ng/g OC
M1	PCB-8 (di)	-0.046 (0.070)	0.513	716 (9)	-0.22 (0.15)	0.157	957 (20)
	PCB-18 (tri)	0.031 (0.114)	0.791	1120 (15)	-0.11 (0.30)	0.719	1650 (41)
	PCB-28 (tri)	-0.28* (0.08)	0.002	661 (10)	-0.33* (0.15)	0.049	974 (20)
	PCB-52 (tetra)	0.21 (0.12)	0.096	1290 (16)	0.14 (0.75)	0.860	2580 (102)
	PCB-44 (tetra)	-0.080 (0.053)	0.147	426 (7)	-0.38 (0.26)	0.180	927 (35)
	PCB-66 (tetra)	-0.018 (0.015)	0.256	113 (2)	0.11 (0.14)	0.452	373 (20)
	PCB-101 (penta)	0.031 (0.012)	0.013	93.6 (1.5)	-0.033 (0.127)	0.798	437 (17)
	PCB-77 (tetra)	na	na	na	0.014 (0.039)	0.731	86.9 (5.3)
	PCB-123 (penta)	0.0301 (0.0071)	0.032	13.1 (0.9)	0.048 (0.040)	0.255	72.2 (5.4)
	PCB-118 (penta)	0.0075 (0.0101)	0.465	52.2 (1.3)	0.0073 (0.0975)	0.942	503 (13)
	PCB-153 (hexa)	-0.0080 (0.0044)	0.082	24.0 (0.7)	-0.048 (0.043)	0.292	114 (6)
	PCB-105 (penta)	0.0187 (0.0041)	0.847	17.1 (0.5)	0.138 (0.097)	0.187	257 (13)
	PCB-138 (hexa)	-0.0013 (0.0069)	0.227	16.8 (0.9)	-0.015 (0.045)	0.741	111 (6)
	PCB-187 (hepta)	na	na	na	-0.016* (0.007)	0.048	29.1 (1.0)
	PCB-128 (hexa)	na	na	na	0.016 (0.014)	0.273	31.8 (1.9)
	PCB-180 (hepta)	na	na	na	-0.0050 (0.0028)	0.107	30.6 (0.4)

Sediment	Compound	Bioaccessible (Tenax)			Total (exhaustive)		
		Slope (SE) ng/g OC/d	p-value in slope	Intercept (SE) ng/g OC	Slope (SE) ng/g OC/d	p-value in slope	Intercept (SE) ng/g OC
M1, continued	PCB-169 (hexa)	nd	nd	nd	-0.0066 (0.0037)	0.107	31.9 (0.5)
M2	PCB-8 (di)	-0.10 (0.07)	0.187	461 (9)	0.097 (0.138)	0.704	594 (19)
	PCB-18 (tri)	0.27 (0.18)	0.148	1450 (23)	-0.53 (0.80)	0.528	2180 (109)
	PCB-28 (tri)	-0.029 (0.054)	0.601	417 (7)	0.17 (0.19)	0.393	754 (25)
	PCB-52 (tetra)	-0.13 (0.22)	0.557	1860 (29)	1.3 (1.0)	0.224	3510 (134)
	PCB-44 (tetra)	0.043 (0.059)	0.472	405 (8)	0.24 (0.26)	0.389	873 (35)
	PCB-66 (tetra)	0.036 (0.021)	0.097	171 (3)	0.15 (0.21)	0.796	507 (29)
	PCB-101 (penta)	0.034 (0.028)	0.226	138 (4)	-0.18 (0.15)	0.241	620 (20)
	PCB-81 (tetra)	na	na	na	-0.0025 (0.0055)	0.663	24.4 (0.8)
	PCB-77 (tetra)	na	na	na	0.0045 (0.0447)	0.922	103 (6)
	PCB-123 (penta)	0.015 (0.009)	0.114	25.4 (1.1)	0.0094 (0.0470)	0.845	163 (6)
	PCB-118 (penta)	0.011 (0.014)	0.433	74.1 (1.8)	0.11 (0.22)	0.638	539 (30)
	PCB-153 (hexa)	-0.0038 (0.0045)	0.409	36.7 (0.6)	-0.021 (0.091)	0.821	161 (12)
	PCB-105 (penta)	0.0096 (0.0078)	0.231	30.0 (1.0)	-0.031 (0.169)	0.859	285 (23)
	PCB-138 (hexa)	0.0032 (0.0054)	0.564	28.2 (0.7)	-0.045 (0.063)	0.484	186 (8)
	PCB-187 (hepta)	na	na	na	0.022 (0.018)	0.244	41.1 (2.4)

Sediment	Compound	Bioaccessible (Tenax)			Total (exhaustive)		
		Slope (SE) ng/g OC/d	p-value in slope	Intercept (SE) ng/g OC	Slope (SE) ng/g OC/d	p-value in slope	Intercept (SE) ng/g OC
M2, continued	PCB-128 (hexa)	na	na	na	-0.0025 (0.0337)	0.941	54.2 (4.6)
	PCB-156 (hexa)	na	na	na	-0.002 (0.026)	0.934	48.3 (3.5)
	PCB-180 (hepta)	na	na	na	-0.013 (0.032)	0.692	95.5 (4.4)
	PCB-170 (hepta)	na	na	na	0.026 (0.021)	0.251	45.6 (2.8)
	PCB-169 (hexa)	na	na	na	-0.0071 (0.0104)	0.507	43.4 (1.4)

^aSlope and intercept refer to Equation 1. k (first order rate constant), ΔC (change in bioaccessible concentration), and C_f (final bioaccessible concentration) refer to Equation 2. Half-life calculated as $\ln(2)/k$. See Table 1 for sediment site abbreviations. p-values refer to probability values calculated in the slope coefficient from the linear regression and probability values calculated in the analysis of variance of the nonlinear regression of the data to the exponential equation (Eq 2). na = not analyzed, indicating compounds that were not detected or below reporting limits.

*Indicates negative slopes values which are significantly different from zero (where $p < 0.05$ in the slope coefficient)

Table S3. Total pyrethroid and polychlorinated biphenyl (PCB) concentrations in sediment as determined in exhaustive chemical exhaustive extracts as a function of 4 °C holding time

Kaseberg Creek at Country Club and McAnally ^a (ng/g OC)						
Holding time, d	2	5	10	21	49	105
Bifenthrin	1840	1720	1900	1730	1730	1970
λ-cyhalothrin	34.9	35.6	30.9	31.2	32.9	45.5
Permethrin	515	483	490	461	467	612
Cyfluthrin group	56.7	58.3	58.9	74.7	52.6	71.3
Cypermethrin group	77.8	69.1	65.4	73.0	82.8	82.8
Esfenvalerate	nd	nd	nd	nd	nd	nd
Deltamethrin	42.2	31.4	34.3	33.6	32.7	169
Kaseberg Creek at Green Grove Road ^a (ng/g OC)						
Holding time, d	2	5	10	21	49	105
Bifenthrin	632	631	739	570	560	598
λ-cyhalothrin	29.8	43.8	29.9	50.1	24.0	30.0
Permethrin	189	935	241	162	180	180
Cyfluthrin group	92.9	122	87.6	82.5	120	515
Cypermethrin group	150	165	212	208	136	143
Esfenvalerate	BRL	BRL	BRL	BRL	BRL	BRL
Deltamethrin	127	130	173	116	99.4	121
San Gabriel River at College Park Drive, sampled 2017 ^a (ng/g OC)						
Holding time, d	2	5	10	21	49	105
Bifenthrin	407	361	390	415	363 ^b	346
λ-cyhalothrin	nd	nd	nd	nd	nd ^b	nd
Permethrin	209	158	141	155	249 ^b	157
Cyfluthrin group	22.8	48.8	31.8	33.8	19.2 ^b	24.7
Cypermethrin group	18.5	25.8	31.2	54.6	22.4 ^b	28.9
Esfenvalerate	nd	nd	nd	nd	nd ^b	nd
Deltamethrin	21.1	27.4	28.7	BRL	18 ^b	21.7
San Gabriel River at College Park Drive, sampled 2017 upstream ^a (ng/g OC)						
Holding time, d	2	5	10	21	49	105
Bifenthrin	325	292	303 ^b	277	284	307
λ-cyhalothrin	13.9	12.8	17.9 ^b	12.0	9.3 ^f	9.5 ^f
Permethrin	182	178	166 ^b	174	174	165
Cyfluthrin group	36.4	24.6	32.1 ^b	57.6	52.5	40.4
Cypermethrin group	27.3	36.3	22.7 ^b	25.4	25.4	34.3
Esfenvalerate	nd	nd	nd ^b	nd	nd	nd
Deltamethrin	16.6	16.1	21.8 ^b	38.4	19.7	21.6
San Gabriel River at College Park Drive sampled 2016 ^a (ng/g OC)						
Holding time, d	1	14	29	62	125	222
Bifenthrin	918 ^b	924	1010 ^c	1075	863	785
λ-cyhalothrin	52.9 ^b	27.8	48.5 ^c	20.3	46.7	53.3
Permethrin	584 ^b	414	492 ^c	707	379	597
Cyfluthrin group	183 ^b	33.3	211 ^c	90.4	211	146
Cypermethrin group	114 ^b	71.7	93.3 ^c	79.2	82.0	93.9
Esfenvalerate	27.4 ^b	BRL	51.9 ^c	18.4	25.1	36.8
Deltamethrin	73.6 ^b	21.5	92.5 ^c	36.3	107	75.2

Ingram Creek ^a (ng/g OC)						
Holding time, d	1	14	29	62	125	222
Bifenthrin	648	459	484	532	502	512
λ-cyhalothrin	175	154	150	181	115	120
Permethrin	nd	nd	nd	nd	nd	nd
Cyfluthrin group	BRL	BRL	BRL	BRL	BRL	BRL
Cypermethrin group	68.9	BRL	BRL	BRL	40.3	32.3
Esfenvalerate	303	241	229	251	202	197
Deltamethrin	nd	nd	nd	nd	nd	nd
Dry Creek ^a (ng/g OC)						
Holding time, d	1	14	29	62	125	222
Bifenthrin	1120 ^b	732	875 ^c	812	792	906
λ-cyhalothrin	BRL ^b	BRL	BRL ^c	BRL	21.1334	BRL
Permethrin	338 ^b	153	166 ^c	185	65.4	82.7
Cyfluthrin group	60.4 ^b	BRL	37.4 ^c	92.8	49.7	31.5
Cypermethrin group	68.5 ^b	88.9	62.6 ^c	78.6	47.7	63.9
Esfenvalerate	BRL ^b	BRL	BRL ^c	BRL	36.1	40.5
Deltamethrin	323 ^b	172	166 ^c	337	187	705
Gilsizer Slough ^a (ng/g OC)						
Holding time, d	1	14	29	62	125	222
Bifenthrin	912	730	732	806	578	817
λ-cyhalothrin	BRL	BRL	BRL	BRL	BRL	BRL
Permethrin	364	297	481	287	222	353
Cyfluthrin group	74.3	BRL	BRL	BRL	BRL	43.2
Cypermethrin group	156	89.0	90.6	74.9	105	141
Esfenvalerate	138	119	121	120	115	116
Deltamethrin	72.3	nd	82.6	nd	71.9	83.5
Bouquet Canyon ^a (ng/g OC)						
Holding time, d	1	14	29	62	125	222
Bifenthrin	3650 ^b	2800 ^c	3270	3400	2660	2560
λ-cyhalothrin	1050 ^b	553 ^c	394	378	BRL	341
Permethrin	1250 ^b	1150 ^c	1380	1300	1190	1180
Cyfluthrin group	310 ^b	364 ^c	417	268	146	262
Cypermethrin group	260 ^b	BRL ^c	BRL	BRL	478	130
Esfenvalerate	550 ^b	BRL ^c	231	411	391	158
Deltamethrin	326 ^b	476 ^c	BRL	271	282	321
Tijuana River ^a (ng/g OC)						
Holding time, d	1	14	29	62	125	222
Bifenthrin	227	186	191	181	192	203
λ-cyhalothrin	17.3	BRL	BRL	BRL	BRL	BRL
Permethrin	507	380	396	385	362	395
Cyfluthrin group	33.4	BRL	BRL	BRL	15.0	16.5
Cypermethrin group	984	589	764	567	692	763
Esfenvalerate	45.9	27.7	34.8	28.9	35.0	39.1
Deltamethrin	62.9	29.5	47.5	57.6	45.8	57.5

Manistique River (M1) ^{b,d} (ng/g OC)						
Holding time, d	7	14	38	123	184	244
PCB-8	991	908	931	972	927	877
PCB-18	1770	1590	1560	1670	1630	1620
PCB-28	996	956	941	937	936	878
PCB-52	2600	2590	2490	2740	2480	2640
PCB-44	907	899	919	944	865	798
PCB-66	362	370	375	398	442	359
PCB-101	407	451	447	443	434	419
PCB-77	83.8	89.0	83.7	94.1	95.6	83.3
PCB-153	112	114	109	112	105	100
PCB-105	241	248	294	257	319	268
PCB-138	111	115	100	111	122	97
PCB-187	29	30	27	26	26	26
PCB-128	31	32	32	35	39	32
PCB-180	30	31	31	30	29	30
PCB-169	31	33	32	31	31	30
Manistique River (M2) ^{b,e} (ng/g OC)						
Holding time, d	7	14	38	123	184	244
PCB-8	614	578	587	625	600	619
PCB-18	2220	2010	2100	2410	2080	1920
PCB-28	773	737	739	819	767	789
PCB-52	3450	3540	3480	3890	3810	3670
PCB-44	875	859	852	982	922	892
PCB-66	485	492	504	586	537	471
PCB-101	614	593	637	597	611	554
PCB-81	24	25	23	23	25	23
PCB-77	104	98.3	102	115	102	101
PCB-123	154	163	166	173	179	151
PCB-118	505	540	543	617	574	523
PCB-153	158	155	157	178	166	141
PCB-105	254	265	319	296	325	232
PCB-138	174	187	195	182	186	168
PCB-187	40	42	41	45	47	45
PCB-128	50	48	61	63	55	47
PCB-156	48	43	51	57	42	48
PCB-180	96	96	92	98	92	92
PCB-170	44	44	48	52	53	48
PCB-169	44	44	42	42	40	44

^a non-detect (nd) for tefluthrin and fenpropathrin at all time points. BRL = below reporting limit (see Table S4 for detection and reporting limits).

^b average of n =2

^c average of n =4

^d nd for PCB-81, PCB-114, PCB-126, PCB-167, PCB-156, PCB-157, PCB-170, PCB-189, PCB-195, PCB-205, PCB-209 at all time points.

^e nd for PCB-114, PCB-126, PCB-167, PCB-157, PCB-189, PCB-195, PCB-206, PCB-209

^f value reported below method reporting limit (BRL)

Table S4. Method detection limits (MDLs) and method reporting limits (MRLs) and method detection limits (MDLs) for pyrethroids and polychlorinated biphenyls (PCBs) in Tenax extracts, in exhaustive chemical extractions (accelerated solvent extraction, ASE), and in *Lumbriculus variegatus* extracts.

	Tenax MDL ng/g dry weight	Tenax MRL ng/g dry weight	ASE MDL ng/g dry weight	ASE MRL ng/g dry weight
Tefluthrin	0.18	0.54	0.33	1
Bifenthrin	0.16	0.48	0.33	1
Fenpropathrin	0.11	0.34	0.33	1
λ -cyhalothrin	0.17	0.50	0.33	1
Permethrin	0.45	1.30	0.67	2
Cyfluthrin	0.15	0.43	0.33	1
Cypermethrin	0.15	0.45	0.33	1
Esfenvalerate	0.16	0.47	0.33	1
Deltamethrin	0.16	0.48	0.33	1
	Tenax MRL ng/mL	ASE MRL ng/mL	<i>L. variegatus</i> MRL ng/mL	
All PCB congeners	2	2	2	

Table S5. Quantification and qualification ions reported as mass-to-charge ratio (m/z) used in gas chromatography/mass spectrometry negative chemical ionization mode for pyrethroids analytes, recovery surrogates (RS), and internal standards (IS).

Compound	Quantification ion	Qualification ion 1	Qualification ion 2
Tefluthrin	241	243	na
D ₆ -tefluthrin (IS)	247	249	na
Bifenthrin	386	241	387
D ₆ -bifenthrin (IS)	392	247	na
Fenpropathrin	141	142	na
D ₆ -fenpropathrin (IS)	147	na	na
λ-cyhalothrin	241	205	243
D ₆ -λ-cyhalothrin (IS)	247	211	na
Permethrin	207	209	na
D ₆ -permethrin (IS)	213	215	na
Cyfluthrin	207	209	171
D ₆ -cyfluthrin (IS)	213	215	na
Cypermethrin	207	209	171
D ₆ -cypermethrin (IS)	213	215	na
Esfenvalerate	211	213	na
D ₆ -esfenvalerate (IS)	217	219	na
Deltamethrin	297	295	na
d ⁶ -deltamethrin (IS)	303	301	na
Dibromooctofluorobiphenyl (RS)	456	376	na
2,2',3,4,4',5,6,6'-octachlorobiphenyl (PCB-204) (IS)	430	na	na
Decachlorobiphenyl (RS)	498	500	na
¹³ C ₁₂ -decachlorobiphenyl (IS)	510	na	na

na = no additional ion used

Table S6. Surrogate recoveries for Tenax extracts and accelerated solvent extracts (ASE) pyrethroid and polychlorinated biphenyl sediment, and extracts of *Lumbriculus variegatus*, and quality assurance/quality control (QA/QC) samples, and target compound recoveries and reproducibility of matrix spiked samples^a

Pyrethroid Samples		
Sample Type	Dibromooctafluorobipenyl (DBOFB)	Decachlorobiphenyl (DCBP)
ASE extracts of sediment (n=76)	81% (37%-106%)	94% (76%-115%)
Tenax extracts of sediment (n=242)	97% (52%-161%)	92% (57%-155%)
ASE extracts of blank and matrix spiked QA/QA samples (n=10)	80% (64%-123%)	95% (72%-123%)
Tenax extraction of blank and matrix spiked QA/QC samples (n=86)	92% (72%-114%)	91% (75%-149%)
Polychlorinated biphenyls (PCBs) Samples		
Sample Type	DBOFB	PCB-186
ASE extraction of sediment (n=34)	96% (76%-133%)	103% (93%-110%)
Tenax extraction of sediment (n=55)	108% (85%-127%)	104% (78%-131%)
<i>Lumbriculus variegatus</i> tissue (n= 24)	103% (88%-132%)	109% (81%-128%)
ASE extraction of blank and matrix spiked QA/QA samples (n=10)	104% (91%-126%)	103% (95%-114%)
Tenax extraction of blank and matrix spiked QA/QC samples (n=30)	99% (75%-123%)	96% (78%-112%)
Blank and matrix spiked QA/QA samples (<i>Lumbriculus variegatus</i>) (n=12)	92% (80%-102%)	100% (95%-115%)
	Recovery of target compounds	Relative difference ^b
Pyrethroids (ASE) (n=18)	87% (49%-122%)	9% (0.05%-34%)
PCBs (ASE) (n=5)	85% (92%-128%)	8% (0.0%-21%)
PCB (<i>Lumbriculus</i>) (n=7)	106% (81%-137%)	6% (0.2%-15%)
PCBs (Tenax) (n=15)	102% (70%-132%)	7% (0.0%-28%)
	Recovery of target compounds	Relative standard error ^c
Pyrethroids (Tenax) (n=42)	90% (52%-125%)	3% (0.1%-11%)

^a all recoveries calculated relative to spike check and reported as average(range).

^bRelative difference calculated as absolute value of difference between recovery duplicates normalized by average recovery

^cRelative standard error calculated as standard deviation of recoveries normalized by average of recoveries and divided by the number of replicate

Table S7. *Hyalella azteca* 10-d toxicity bioassay comparing sediment held at 4 °C for 11 d and 49 d before beginning the bioassay. Two endpoints: average and standard deviation of day 10 dry mass per animal and % survival at 10 days, four replicates per endpoint.

Sediment Holding Time	Dry mass/animal (mg) (+1 standard deviation)		% Survival (+1 standard deviation)	
	11 d	49 d	11d	49 d
Kaseberg Creek at Country Club and McAnally	0.031 (0.013)	0.027 (0.008)	17.5% (28.7%)	2.5% (5.0%)
Kaseberg Creek at Green Grove Road	0.029 (0.010)	0.024 (0.005)	20.0% (21.6%)	0.0% (0.0%)
San Gabriel River at College Park Drive, sampled 2017	0.077 (0.018)	0.071 (0.009)	90.0% (8.2%)	90.0% (8.2%)
San Gabriel River at College Park Drive, sampled 2017 upstream	0.048 (0.008)	0.041 (0.003)	57.5% (12.6%)	75.0% (23.8%)
Sand negative control	0.079 (0.006)	0.100 (0.007)	97.5% (5.0%)	92.5% (9.6%)
LaRue Pine Hill negative control	0.101 (0.010)	0.097 (0.010)	97.5% (5.0%)	95.0% (10.0%)
Beaver Brook at North Pelham, NH reference sediment	0.122 (0.003)	0.108 (0.006)	95.0% (10.0%)	100.0% (0.0%)
Sugar Run near Wilmot, PA reference sediment	0.105 (0.015)	0.106 (0.012)	97.5% (5.0%)	95.0% (10.0%)
Canajoharie Creek near Canajoharie, NY reference sediment	0.108 (0.004)	0.101 (0.011)	95.0% (5.8%)	100.0% (0.0%)

Table S8. Lipid-normalized polychlorinated biphenyls (PCB) concentrations in *Lumbriculus variegatus* after 14-d exposure to PCB-contaminated Manistique River (M1 and M2) sediment that was held at 4 °C for 7 d, 14 d, and 244 d prior to beginning the bioassay.

Average Bioaccumulated PCB concentration (+1 standard deviation) (ng/ g lipid)			
Sediment M1			
	Day 7	Day 14	Day 244
PCB-8 ^a	1910 (447)	2390 (83)	2350 (187)
PCB-18 ^a	2980 (590)	3340 (166)	3560 (414)
PCB-28	1890 (452)	2100 (69)	2130 (153)
PCB-52 ^a	4480 (1200)	6550 (218)	5580 (307)
PCB-44	1470 (406)	1770 (56)	1540 (95)
PCB-66 ^a	360 (77) ^b	541 (46)	511 (33)
PCB-101 ^a	420 (74) ^b	559 (29)	507 (22)
PCB-118 ^a	316 (50) ^b	561 (35)	468 (76)
PCB-153 ^a	271 (32) ^b	273 (22) ^b	142 (26) ^b
Sum of PCBs	14100(3290)	18100 (566)	16800 (1250)
Sediment M2			
	Day 7	Day 14	Day 244
PCB-8 ^a	1120 (185)	1170 (119)	1390 (32)
PCB-18	4910 (471)	5080 (1120)	5960 (412)
PCB-28 ^a	1500 (49)	1610 (196)	1880 (56)
PCB-52	7420 (660)	8030 (1730)	9150 (424)
PCB-44	1900 (122)	2140 (359)	1980 (155)
PCB-66	874 (77)	891 (72)	929 (50)
PCB-101	842 (45)	883 (215)	941 (67)
PCB-123	402 (12)	359 (51)	392 (25)
PCB-118	683 (38)	758 (103)	782 (45)
PCB-153	429 (31)	416 (77)	459 (35)
PCB-105	400 (21)	400 (99)	440 (23)
PCB-138	394 (15)	375 (68)	407 (16)
Sum of PCBs	20900 (1600)	22100 (3960)	24700 (1180)

^a Indicates congeners with a significant difference ($p < 0.05$) in the bioaccumulated concentration as a function of holding time determined by one-way analysis of variance. ^b Indicates average values analyzed below the 2 ng/mL reporting limit.

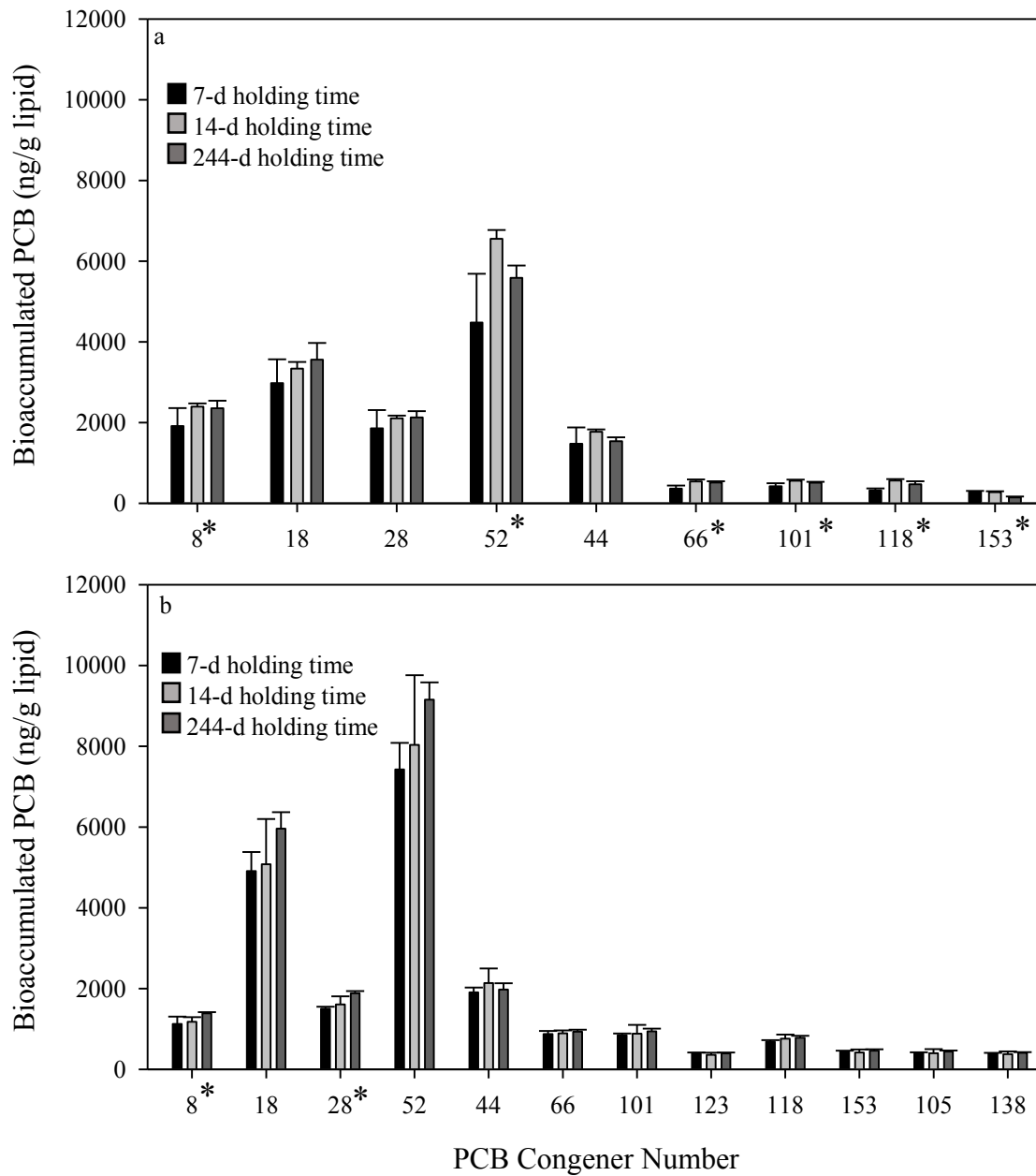


Figure S1. Polychlorinated biphenyls (PCB) concentrations in *Lumbriculus variegatus* after 14-d exposure to PCB-contaminated Manistique River (M1) (a) and Manistique River (M2) sediment (b) that was held at 4 °C for 7 d, 14 d, and 244 d. The height of the bar represents the average bioaccumulated PCB concentration normalized for tissue lipid mass in four replicates, and error bars represent one standard deviation. * Indicates PCB congeners with a significant difference ($p < 0.05$) in the bioaccumulated concentration as a function of holding time determined by one-way analysis of variance.

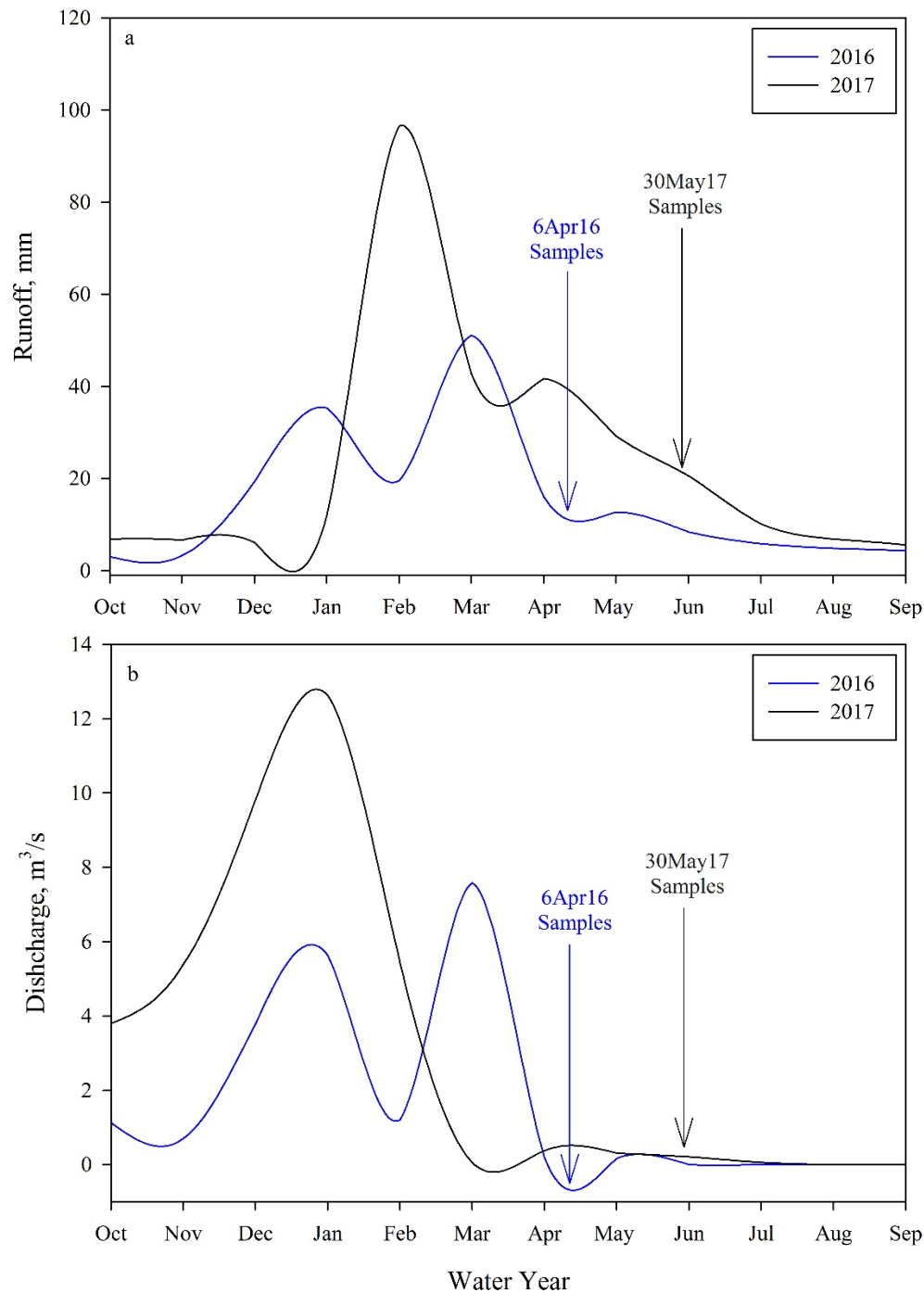


Figure S2. Monthly runoff to California streams and rivers, for 2016 and 2017 compiled from streamflow records at gaged stream sites in California, adapted from USGS (2017). (a) Monthly runoff data during the sampling timeframe were not available near or at the individual sampling sites. However, the monthly average discharge for San Gabriel River at Whittier Narrows Dam (USGS site ID 11087020, USGS (2018)), located 27.6 km north-northeast and upstream from the San Gabriel River sites, has a similar annual pattern (b) to California runoff (a).

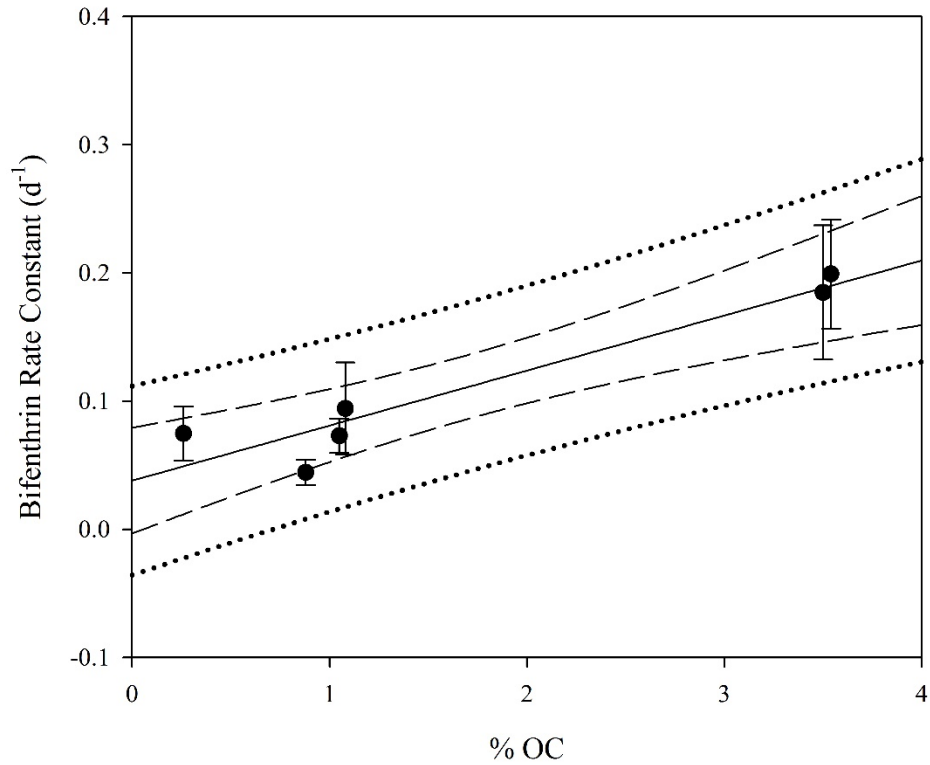


Figure S3. Effect of percent organic carbon (% OC) in sediments on bifenthrin rate constant, k (●). Error bars represent standard error in the rate constants. Solid line represents the best fit line to $k = 0.0429$ (0.0069) % OC + 0.0380 (0.00149), $r^2 = 0.9064$, $F = 38.7294$, $p = 0.0034$, where the value in the parenthesis is the standard error. Dashed lines represent the 95% confidence band and dotted lines represent 95% prediction band.

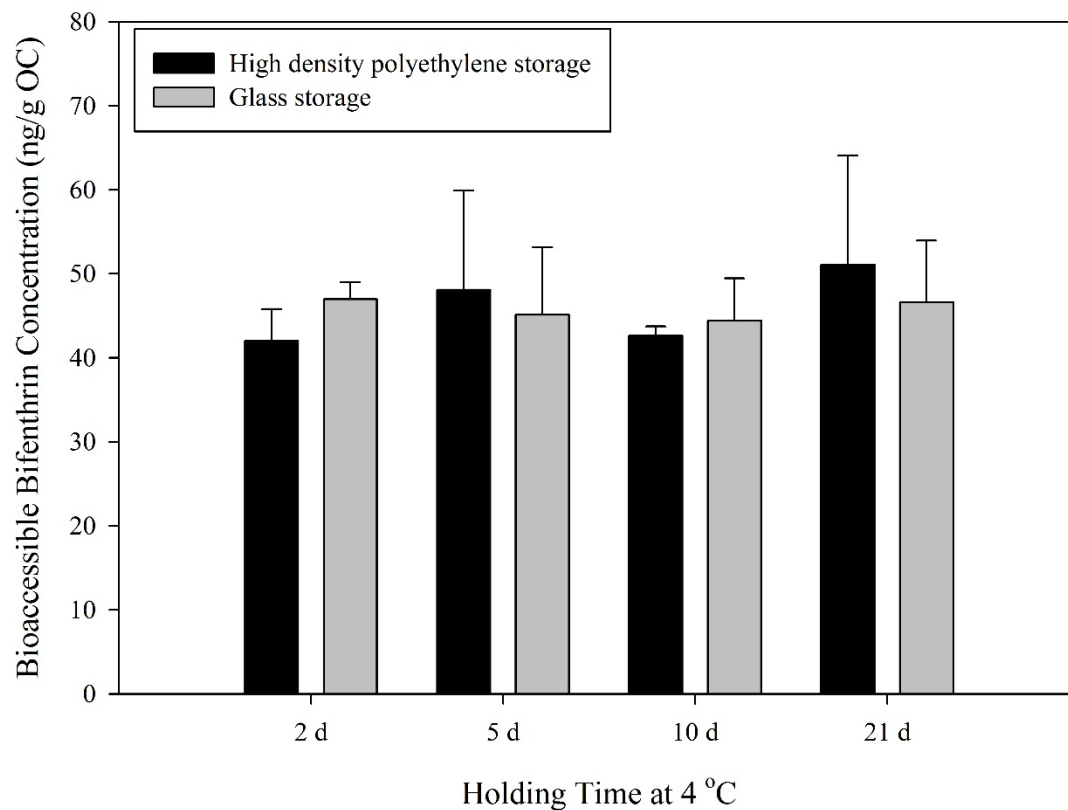


Figure S4. Comparison of storage container material on bioaccessible bifenthrin concentration in San Gabriel River sediments taken from College Park Drive (sampled 2017), where sediment stored in glass was a subsample collected upon receipt of the sediment stored in high density polyethylene (HDPE). The height of the bar represents the average bioaccessible bifenthrin concentration $n=$ four replicates (except for HDPE, $n=$ 5 replicates were measured at 2 d, 5 d, and 10 d), and error bars represent one standard deviation. No statistical differences were found in the averages of the bioaccessible concentrations due to storage container material.

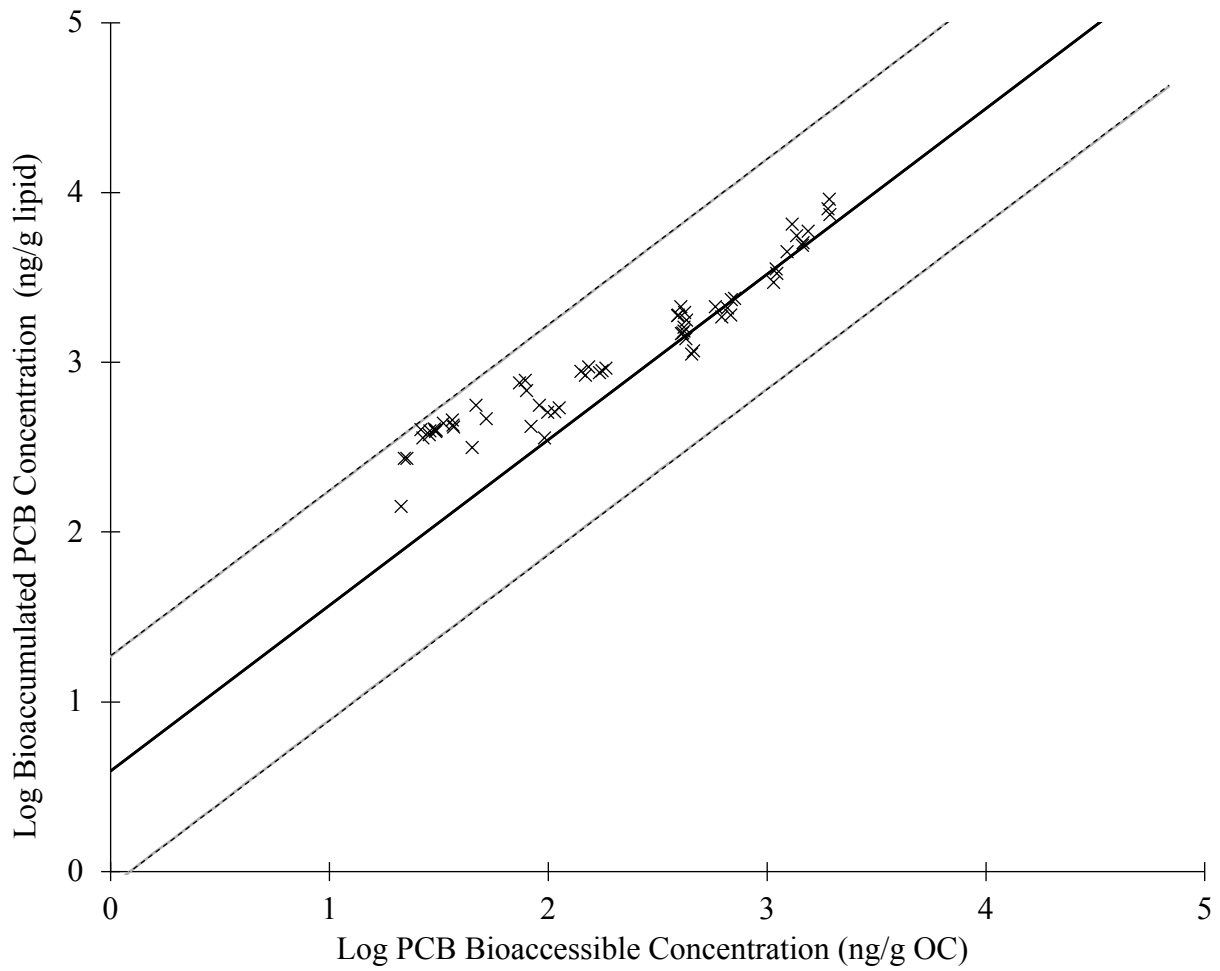


Figure S5. Polychlorinated biphenyl (PCB) concentration bioaccumulated by *Lumbriculus variegatus* and corresponding bioaccessible concentration (×) plotted with the Bioaccumulation Tenax Model (Harwood et al. 2015), where the solid line represents the best fit and the dashed lines are the 95% confidence intervals which predicts the range of uncertainty for a single additional observation.

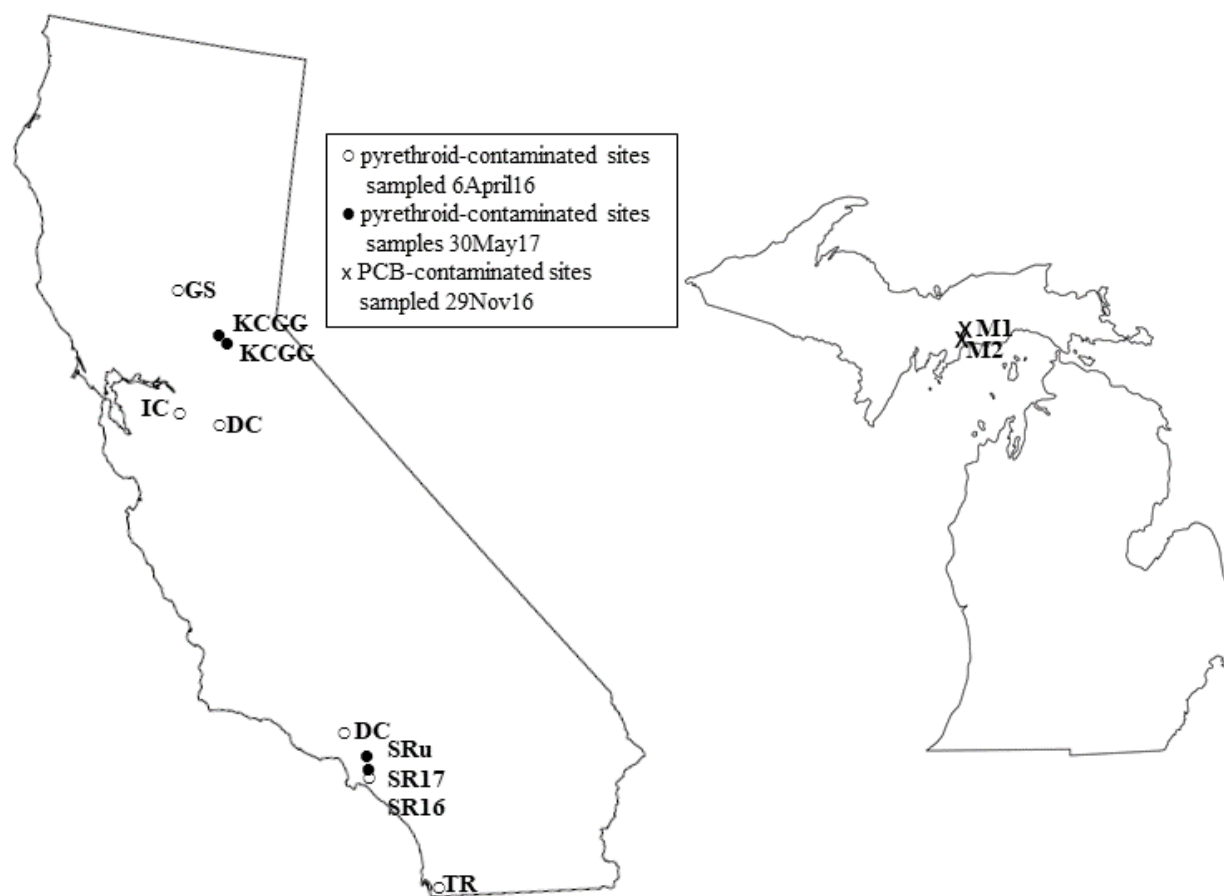


Figure S6. Sampling locations of pyrethroid-contaminated sites located in California, United States (left) and polychlorinated biphenyl (PCB) contaminated sites located in Michigan, United States (right). Maps are not to scale, and locations are approximate. Refer to Table 1 for sample name abbreviations and coordinates.

Information Transfer Program Introduction

Through the outreach efforts of the Illinois Water Resources Center, the people of Illinois will be better informed about the nature of our water resources and the implications of actions.

Transferring Water Resources Information to the People of Illinois

Basic Information

Title:	Transferring Water Resources Information to the People of Illinois
Project Number:	2017IL334B
Start Date:	3/1/2017
End Date:	2/28/2018
Funding Source:	104B
Congressional District:	IL-013
Research Category:	Not Applicable
Focus Categories:	Education, Management and Planning, None
Descriptors:	None
Principal Investigators:	Lisa Merrifield

Publications

There are no publications.

2017-2018 Tech Transfer

In 2017, the Illinois Water Resources Center continued its involvement in the implementation of the Illinois Nutrient Loss Reduction Strategy (INLRS) and maintained its educational and outreach efforts through its social media presence, website, blog, and magazine. Messaging covered topics such as stormwater, nutrient management, and the great outdoors. More details on IWRC's leadership role in the INLRS implementation is outlined below.

Illinois biennial report recognizes positive, voluntary steps to reduce nutrient loss

Relevance: By most estimates, Illinois is the largest contributor of nutrients to the Gulf of Mexico hypoxia. More than 400 million pounds of nitrate-nitrogen and 38 million pounds of phosphorus from Illinois farm fields, city streets, and wastewater treatment plants are carried to the Gulf each year by the Mississippi River system. Every summer, these nutrients spur algal blooms that leave an area roughly the size of Connecticut all but devoid of oxygen and marine life.

Response: Illinois Water Resources Center joined with stakeholders across the board to develop and implement a plan for reducing nutrient pollution from point and non-point sources in priority watersheds. The Illinois Nutrient Loss Reduction Strategy, released in 2015, outlined best management practices to reduce the amount of nitrogen and phosphorus reaching Illinois waterways by 45 percent. In 2017, IWRC coordinated with stakeholders to write the first biennial report summarizing strategy activities since its implementation.

Results: Data gathered for this report revealed that many project partners leveraged resources and retargeted efforts to the nutrient loss goal. In fact, the agricultural sector invested more than \$54 million in nutrient loss reduction for research, outreach, implementation and monitoring. Extensive outreach and other support led to an increase in the adoption of agricultural best management practices to reduce nutrient loss. The strategy update also reported that significant strides have also been made in limiting the amount of phosphorus discharge from wastewater treatment plants in Illinois.

Partners: Illinois Environmental Protection Agency, Illinois Department of Agriculture, Illinois-Indiana Sea Grant, American Bottoms Regional Wastewater Treatment, Urbana-Champaign Sanitary District, Illinois Council on Best Management Practices, University of Illinois at Urbana-Champaign, U.S. Department of Agriculture, Prairie Rivers Network, Illinois Pork Producers Association, Environmental Law and Policy Center, Illinois Farm Bureau, Downers Grove Sanitary District, Illinois Environmental Regulatory Group, Association of Illinois Soil and Water Conservation Districts, Illinois Fertilizer and Chemical Association, Sierra Club, Metropolitan Wastewater Reclamation District of Great Chicago, Illinois Corn Growers Association, The Nature Conservancy, Aqua America, Illinois Association of Drainage Districts, City, Water, Light, and Power, City of Aurora, CMAP, Illinois Department of Natural Resources, DuPage Co.

Inaugural conference checks in with Illinois Nutrient Loss Reduction Strategy stakeholders

Relevance: By most estimates, Illinois is the largest contributor of nutrients to the Gulf of Mexico hypoxia. More than 400 million pounds of nitrate-nitrogen and 38 million pounds of phosphorus from Illinois farm fields, city streets, and wastewater treatment plants are carried to the Gulf each year by the Mississippi River system. Every summer, these nutrients spur algal blooms that leave an area roughly the size of Connecticut all but devoid of oxygen and marine life.

Response: In 2017, Illinois Water Resources Center held the Inaugural Nutrient Loss Reduction Strategy Conference in Springfield for all strategy working group members and others interested in reducing nutrient loss in Illinois. This conference provided an opportunity to assess strategy implementation, including lessons learned and plans for the future. Sessions focused on monitoring, science assessments, and how Illinois compares with other states working to reduce nutrient pollution.

Results: The two-day conference was attended by 105 people representing diverse stakeholder groups, including agricultural commodities, wastewater treatment plants, and state and local governments. At this gathering, an additional working group was established to focus on improving communication with Illinois communities.

Partners: Illinois Environmental Protection Agency, Illinois Department of Agriculture, Illinois-Indiana Sea Grant

USGS Summer Intern Program

None.

Student Support					
Category	Section 104 Base Grant	Section 104 NCGP Award	NIWR-USGS Internship	Supplemental Awards	Total
Undergraduate	15	3	0	0	18
Masters	7	2	0	0	9
Ph.D.	5	0	0	1	6
Post-Doc.	0	0	0	0	0
Total	27	5	0	1	33

Notable Awards and Achievements